

**UNIVERSIDADE FEDERAL DE SANTA CATARINA
PROGRAMA DE PÓS-GRADUAÇÃO EM ENGENHARIA CIVIL**

André Maia Nobre

**SHORT-TERM SOLAR IRRADIANCE FORECASTING AND
PHOTOVOLTAIC SYSTEMS PERFORMANCE IN A
TROPICAL CLIMATE IN SINGAPORE**

Tese submetida ao Programa de Pós-Graduação em Engenharia Civil – PPGEC da Universidade Federal de Santa Catarina para a obtenção do Título de Doutor em Engenharia Civil.

Orientador: Prof. Ricardo Rüther, PhD

Florianópolis
2015

Ficha de identificação da obra elaborada pelo autor,
através do Programa de Geração Automática da Biblioteca Universitária da UFSC.

Nobre, André Maia

SHORT-TERM SOLAR IRRADIANCE FORECASTING AND
PHOTOVOLTAIC SYSTEMS PERFORMANCE IN A TROPICAL CLIMATE IN
SINGAPORE / André Maia Nobre ; orientador, Ricardo Rüther
Florianópolis, SC, 2015.
252 p.

Tese (doutorado) - Universidade Federal de Santa
Catarina, Centro Tecnológico. Programa de Pós-Graduação em
Engenharia Civil.

Inclui referências

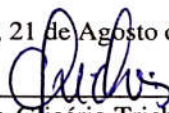
1. Engenharia Civil. 2. irradiação solar. 3. previsão da
irradiação solar. 4. sistemas fotovoltaicos conectados à
rede. 5. simulação e análise de desempenho de sistemas
fotovoltaicos. I. Rüther, Ricardo. II. Universidade
Federal de Santa Catarina. Programa de Pós-Graduação em
Engenharia Civil. III. Título.

André Maia Nobre

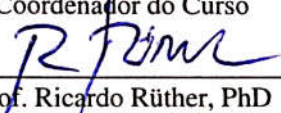
**SHORT-TERM SOLAR IRRADIANCE FORECASTING AND
PHOTOVOLTAIC SYSTEMS PERFORMANCE IN A
TROPICAL CLIMATE IN SINGAPORE**

Esta Tese foi julgada adequada para obtenção do Título de Doutor, e aprovada em sua forma final pelo Programa de Pós-Graduação em Engenharia Civil da Universidade Federal de Santa Catarina.

Florianópolis, 21 de Agosto de 2015.



Prof. Dr. Glicério Trichês
Coordenador do Curso



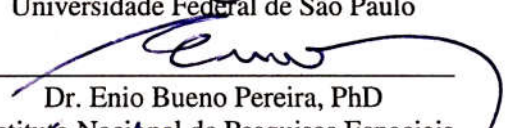
Prof. Ricardo Rüther, PhD
Orientador

Universidade Federal de Santa Catarina

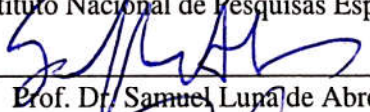
Banca Examinadora:



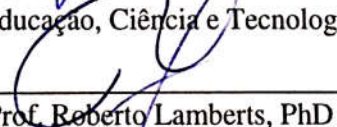
Prof. Dr. Fernando Ramos Martins
Universidade Federal de São Paulo



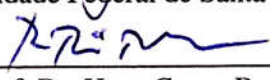
Dr. Enio Bueno Pereira, PhD
Instituto Nacional de Pesquisas Espaciais



Prof. Dr. Samuel Luna de Abreu
Instituto Federal de Educação, Ciência e Tecnologia de Santa Catarina



Prof. Roberto Lamberts, PhD
Universidade Federal de Santa Catarina



Prof. Dr. Hans Georg Beyer
University of Agder, Norway

*To my wife, Delphina, and our son, Luke,
my parents, Eduardo and Luisa,
my sisters, Ana Paula and Myriam
and to family and friends around the world*

ACKNOWLEDGEMENTS

I would like to start by thanking Prof. Ricardo R  ther for accepting me into his team, which allowed me to somehow “return” to Brazil and give back to my country of heart. Thanks for your guidance through the doctorate and your wisdom as one of the pioneers of the photovoltaic scene in Brazil. I would also like to extend my thanks to Universidade Federal de Santa Catarina (UFSC), Laborat  rio de Efici  ncia Energ  tica em Edifica  es (LabEEE), the Solar Research Group Fotovoltaica/UFSC, Tractebel Energia, the ANEEL Research and Development Program through project PE-0403-0027/2011, and the Brazilian Scientific Research Council (CNPq) for the support throughout the past years.

To Dr. Thomas Reindl and Prof. Armin Aberle, my appreciation for being part for the past almost 7 years of a world-class research & development institute at the Solar Energy Research Institute of Singapore (SERIS). I would also like express my appreciation to the National University of Singapore (NUS), the National Research Foundation (NRF) and the Economic Development Board of Singapore (EDB), all of which for funding and supporting a terrific infrastructure that leveraged the R&D initiatives surrounding the work of this thesis.

I would like to extend my deepest gratitude to Prof. Joachim Luther, who trusted in my skills, inviting me in 2009 to be part of SERIS and also for believing in my potential as a researcher and contributor to solar technology for the future of mankind. Thanks also go to Burkhard Holder for introducing me to the world of photovoltaics ten years ago, which led to my arrival in Singapore.

Special thanks go to Mark Kubis for believing in the values of “legacy” and “extra effort”, which we combined together through the years, developing things “from scratch”, which now are and will be part of the world we live in for many generations to come.

Other SERIS colleagues I would like to express my gratitude are Dr. Dazhi Yang, Du Hui, Shravan Karthik, Hansley Cheetamun, Monika Bieri, Stanley Phua, Rupesh Baker, Dr. Wilfred Walsh, Aung Myint Khaing, Dr. Lu Zhao, Dr. Licheng Liu, Haohui Liu, Soe Pyae, Julius Tan, Andrew Nicholls, Janet Goh, Marinel Dungca and Jenny Oh (*in memoriam*).

My appreciation is further extended to the Fotovoltaica/UFSC team, in special Dr. Clarissa Zomer, Alexandre Montenegro, Lucas Nascimento, Elis  ngela Pinheiro, Andr  go Gon  alves, Alice Bittencourt and Dr. Trajano Viana. Likewise, I would like to thank the LabEEE/UFSC colleagues Dr. Deivis Marinoski, Dr. M  rcio Sorgato, Dr.

Miguel Pacheco and Dr. Cláudia Pereira. A special thanks to Dr. Renata De Vecchi for the remote help with the thesis document logistics.

Thanks to collaborators at the Brazilian National Institute for Space Research (INPE), Dr. Enio Bueno Pereira and Prof. Fernando Ramos Martins. A big thank you also goes to other collaborators throughout the past years, namely Dr. Christian Reise at Fraunhofer ISE, Dr. Marius Peters at MIT, Carlos Severiano at UFMG and Dr. Hans Veldhuis at University of Twente.

To the members of the evaluation committee, I express my indebtedness in taking your time to read this work, also in making the trip to Florianópolis (for the ones from out of town) and for your invaluable suggestions for the overall enhancement of my thesis.

A few friends in Brazil I would like to acknowledge who were great companions as I worked on this thesis are Daniel Cima, Micael Duarte, Alessandro Assis, Paulo Dias and Renato Profeta.

Similarly, a few friends based in Singapore who I would like to express my thanks are Dr. Anne Bendt, Peter Pronk and John Cann.

I would like to acknowledge the National Basketball Association (NBA) for being a big part of my entire life and providing me with great joy while writing most of these words. In that same sense, the enjoyment of participating in dragon boating and outrigger canoeing paddling competitions in Singapore with the German Dragons and around the world with the Singapore Paddle Club are memories that will be intertwined with the ones of working towards this degree.

To all my dear family members and old friends in Brazil who I did not spend much time with in the past decade, being on the other side of the planet, my sincere thanks for keeping in touch and helping anyway you could along the way. To new friends in Singapore and elsewhere in the world, thank you for your support.

My parents Eduardo and Luisa have been a lighthouse throughout my life and career, teaching me the important values one should hold dear. Literally and figuratively, I would not be here if it were not for them. Similarly, I would like to acknowledge the loving support from my sisters Ana Paula and Myriam through the years together.

I would like to express my deepest gratitude to my adoring wife Delphina for being there through “thick and thin”, for pushing through this doctorate with all her unwavering support during the past half-decade. Now we get to enjoy our beautiful son Luke even more with the feeling of a job well done! Thanks also are due to my step daughters Kiara and Kyrene, who with their smiles made this entire journey a lot easier.

“With great power comes great responsibility”

Ben Parker

RESUMO

A humanidade usou e continua consumindo em grande quantidade os recursos não-renováveis do planeta como petróleo, gás natural e carvão mineral para suprir suas necessidades energéticas. Somente nas últimas duas décadas que outras fontes de energia renováveis, como a solar fotovoltaica e a eólica, passaram a se tornar relevantes na geração de energia elétrica em nível mundial. Instalações de sistemas fotovoltaicos ao redor do mundo atingiram crescimento da ordem de 40% durante os últimos quinze anos. Entretanto, a grande maioria destes sistemas, (acima de 90%), estão localizados em regiões onde o recurso solar não é tão abundante, ou seja, fora da região dos trópicos do planeta. Devido a este fato, ao tentar incorporar a energia solar fotovoltaica às redes elétricas, uma pergunta que sempre surge está relacionada a variação desta forma de geração de energia elétrica com a produção alternante durante o dia devido ao movimento das nuvens e total ausência no período noturno. Mesmo assim, em alguns países, já se atinge percentuais em torno de 5 a 10% de contribuição da energia elétrica proveniente de energia solar fotovoltaica. Passa a ser desafiador a inserção dessa fonte de energia à rede, de maneira intensiva, em paralelo com os recursos já existentes (em sua maioria ainda de origem fóssil). Nesta tese, foi avaliada a previsão do recurso solar em curtíssimo prazo (como 15-min, 30-min e uma hora) para uma região tropical do planeta, neste caso em Cingapura, ilha que se localiza próxima à linha do equador, no Sudeste Asiático. Esta tese foca em métodos existentes de previsão de irradiância, mas também explora uma nova proposta híbrida, adaptada a uma localidade tropical. Além das previsões de irradiação solar, simulações de sistemas fotovoltaicos e o cálculo de seu desempenho foram estudados e avaliados de modo a se prever quanto de energia elétrica é produzida com a mesma antecedência dada nos produtos de previsão do recurso solar. A influência da gaze de queimada foi um fenômeno particular, comum na Cingapura de hoje, que afeta o desempenho de sistemas fotovoltaicos e que foi investigado em detalhe. Todo o trabalho foi validado por redes detalhadas de estações meteorológicas em solo e também através de monitoramento de sistemas fotovoltaicos por toda Cingapura.

Palavras-chave: irradiação solar, previsão da irradiação solar, sistemas fotovoltaicos conectados à rede, simulação e análise de desempenho de sistemas fotovoltaicos, regiões tropicais.

ABSTRACT

Humanity has used and continues to consume in great proportion non-renewable energy resources of the planet such as oil, natural gas and coal in order to fulfil its energy needs. It was only during the past two decades that other sources of renewable energy such as solar photovoltaics (PV) and wind energy became somewhat relevant towards electricity generation in the world. PV installations worldwide have reached a compound annual growth rate of ~40% for the last fifteen years. However, the great majority of these systems (over 90% of them) are located where the solar energy resource is not the most abundant – outside of the tropical regions of the planet. While trying to incorporate solar energy PV into electrical power grids, one common question which arises is related to the variable aspect of this form of energy generation – with alternating production during the day due to cloud motion, and total absence during night time. Nonetheless, in some countries, contribution ratios of 5 to 10% of electrical energy from solar PV have been achieved. It becomes then challenging to integrate this source of energy into grids in a professional way, in parallel with existing resources (mostly still fossil-fuel-based). In this thesis, short-term forecasting (for time horizons such as 15-min, 30-min and 1-hour) of the solar resource was investigated in a tropical region of the world – in Singapore, 1° North of the Equator, in Southeast Asia. This thesis focuses on existing methods for irradiance forecasting, but also explores a novel Hybrid proposal, tailored to the tropical environment at hand. Beyond the forecast of the solar energy irradiance ahead of time, PV system simulation and performance assessment were studied and evaluated with the goal of predicting how much electricity is produced in the same time frame given by the solar irradiance forecasting products. The influence of haze was a particular phenomenon, common in today's Singapore, which affects PV system performance and which was investigated in detail. All work has been validated by a comprehensive network of ground-based meteorological stations, as well as by various PV system monitoring sites throughout Singapore.

Keywords: solar irradiation, solar irradiation forecasting, grid-connected PV systems, PV systems simulation and performance assessment, tropical regions.

FIGURE LIST

Figure 1: Solar photovoltaics worldwide growth from 2000 to 2014 (SPE, 2015) 38

Figure 2: Annually deployed and cumulative volumes of photovoltaic systems in Brazil (ANTONIOLLI *et al.*, 2014). 40

Figure 3: 1.42 MW_p at the Mineirão Stadium in Belo Horizonte, MG (CEMIG, 2013). 42

Figure 4: 3 MW_p at the UFSC/Tractebel R&D facility in Tubarão, SC (Source: Fotovoltaica/UFSC). 42

Figure 5: Quarterly and cumulatively installed PV capacity in Singapore for the 2012-2014 time period (NSR, 2015c). 43

Figure 6: Annual electricity demand and gross domestic product growth in Singapore for the 2005-2014 period, adapted from (EMA, 2013). ... 44

Figure 7: Electricity generation fuel type in Singapore for the 2009-2015 period, adapted from (EMA, 2013). 45

Figure 8: Daily energy consumption pattern for Singapore during a week in May 2015 (left), as well as progression of peak demand for the period of 2012-2015 (right), adapted from (EMA, 2013). 46

Figure 9: PV systems in Singapore exemplifying the urbanization of solar photovoltaics (NSR, 2015b). 47

Figure 10: Location of the top-ten solar PV markets of the world as of end of 2014, adapted from (IEA, 2014c). 50

Figure 11: A so-called “Sumatra squall” with an approaching storm originating from Indonesia as captured by Doppler radar images in 10-min intervals, adapted from (NEA, 2012). 52

Figure 12: A residential 8.6 kW_p PV system in Singapore with thin-film modules and two inverters (NSR, 2013c). 57

Figure 13: An industrial 300.4 kW_p PV system at the REC facility in Tuas, Singapore with polycrystalline modules (NSR, 2013c). 58

Figure 14: A 3.6 kW_p monocrystalline PV system in a residence in Belo Horizonte, Brazil (SPB, 2012). 58

Figure 15: Desert Sunlight Solar Farm (550 MW_{ac} PV plant), built in California (FIRST_SOLAR, 2013). 59

Figure 16: 1.2 MW_p floating PV system at the Okegawa (left) and 1.7 MW_p Hyogo (right) prefectures in Japan (NIKKEI, 2013; TECHXPLORE, 2015). 60

Figure 17: Relative spectral response of various PV technologies (multicrystalline Si, amorphous Si, CdTe and CIGS), measured under

STC temperature (25°C), with the AM1.5G spectrum (grey) also shown as reference (LIU <i>et al.</i> , 2014b).	61
Figure 18: Price learning curve of photovoltaics (ISE, 2014).	62
Figure 19: Evolution of average price for PV rooftop systems in Germany, including percentage of module cost in final system price (BSW, 2014).	63
Figure 20: Grid parity drivers (LUTHER, 2009).	64
Figure 21: Key countries around the world experiencing grid parity (REUTERS, 2015).	65
Figure 22: Progressive solar PV production peaks in Germany from sunny day examples from 2012 to 2015, adapted from (SMA, 2015a).	67
Figure 23: Variable and low irradiation day examples in Germany in 2015, adapted from (SMA, 2015a).	67
Figure 24: Inverter quality assurance report, highlighting some of the tests which individual units go through (SMA, 2013b).	68
Figure 25: Power flow measured at 110/22 kV substation in Bavaria, South Germany, between 2009 and 2013 (STETZ <i>et al.</i> , 2014).	69
Figure 26: Measured clear sky irradiance day in Singapore (in red) and a day with broken cloud conditions (in blue) (SERIS, 2011).	70
Figure 27: Irradiance variability in Singapore with examples of a) an instant with half of the island covered by rain (left) and b) high peaks of irradiance and cloudy conditions (source: SERIS).	71
Figure 28: Japanese town with high penetration of residential solar PV systems (UEDA, 2010).	72
Figure 29: Future scenarios for the total volume of PV systems deployed worldwide up to 2019 (SPE, 2015).	73
Figure 30: 63 weather stations in Singapore, with the two only government irradiance measuring stations marked in red, adapted from (NEA, 2013a).	75
Figure 31: Solar irradiation components (BADESCU, 2008).	76
Figure 32: Sun path diagrams for the cities of Singapore, Florianópolis and Freiburg (from left to right), adapted from (GAISMA, 2013).	77
Figure 33: Three irradiance devices measuring global horizontal irradiance located at the SERIS meteorological station in Singapore (source: SERIS).	78
Figure 34: GHI and DHI readings on a clear sky day in Singapore measured by several irradiance devices (source: SERIS).	79
Figure 35: Extrapolation of empirical data for the SERIS meteorological station showing highest point of irradiation capture for ~10° of tilt, East oriented (KHOO, NOBRE, <i>et al.</i> , 2014).	81

Figure 36: Module temperature increase versus irradiance on module plane as registered in Singapore and Germany (NOBRE et al., 2015 (under preparation)).....	83
Figure 37: SERIS meteorological station rack, with tilted silicon sensors ranging from 0 to 40 degrees (source: SERIS).....	85
Figure 38: Ambient temperatures in Singapore for the year 2011. The daily averages are plotted in orange (SERIS, 2011).....	85
Figure 39: Global (GHI) and diffuse horizontal irradiance (DHI) in Singapore for the year 2011 (SERIS, 2011).....	86
Figure 40: Relative humidity in Singapore for the year 2011 (SERIS, 2011).	87
Figure 41: Examples of cloud-edge and cloud-enhancement effects, as captured by SERIS' sky cameras and validated by ground-measurement irradiance spikes ($\text{GHI} > 1,000 \text{ W/m}^2$) on sensors (source: SERIS).	88
Figure 42: Irradiance frequency (left) and energy distribution (right) in Singapore for 2011 (SERIS, 2011).....	89
Figure 43: Singapore weather radar located at Changi Airport (FONG, 2012).	89
Figure 44: Average annual global horizontal irradiation profile for South and Southeast Asia (SOLARGIS, 2012).	90
Figure 45: Sequence of sky images during a sudden approaching storm in Singapore, 14:00-15:20, in 5-min intervals (source: SERIS).....	93
Figure 46: Sequence of sky images during a typical irradiance day in Singapore, 12:00-13:20, in 5-min intervals (source: SERIS).....	94
Figure 47: Top – Measured and forecast values for global horizontal irradiance (GHI) at a central meteorological site in Singapore in a day with a sudden storm, and associated errors (NOBRE et al., 2015 (submitted)).	95
Figure 48: Images of the Marina Bay area in downtown Singapore on (a) a day with air quality in the moderate range and (b) on a day with values in the very unhealthy range. Photo courtesy of Monika Bieri-Gmuer. .	96
Figure 49: Five categories of the Pollution Standards Index (PSI) plotted for their annual frequencies and for a period of three months (NOBRE et al., 2015 (accepted)).	98
Figure 50: Measured daily performance ratios of 10 PV systems of two main technologies in Singapore for the period of May to July 2013 (LIU et al., 2014b).	100
Figure 51: Annual global horizontal irradiance (GHI) and diffuse horizontal irradiance (DHI) in the Brazilian territory (PEREIRA, E. B. et al., 2006).	102

Figure 52: Time horizon versus spatial resolution for solar irradiance forecasting and suitable techniques for application. Source: (INMAN <i>et al.</i> , 2013).....	105
Figure 53: Southeast Asia satellite image with Singapore highlighted inside the circle (NEA, 2010).	107
Figure 54: Artificial neural network schematic based on a nonlinear model of a neuron (HAYKIN, 1999).	109
Figure 55: Sky images from cameras with fish-eye lenses (source: UCSD).	110
Figure 56: Deployed network of thirteen sky cameras in Singapore (NSR, 2015e).	111
Figure 57: Silicon sensor installed in the plane of the photovoltaic array, here 10 degrees (source: SERIS).	115
Figure 58: Three sensors measuring global horizontal irradiance under comparison. The CMP11 pyranometer acts as a baseline (source: SERIS).	116
Figure 59: Evolution of performance ratio in Germany through the past 2 decades (REICH <i>et al.</i> , 2012).	117
Figure 60: Progression of soiling accumulation in an unmaintained PV system due to a flat tilt angle (source: SERIS).	121
Figure 61: Wind speed as recorded by the SERIS meteorological station for the year 2011 (SERIS, 2011).....	125
Figure 62: Irradiation on ground level and yield of a PV system on both a clear sky day (PSI = 54) and on a hazy day (PSI = 109) (NOBRE <i>et al.</i> , 2015 (accepted)).....	126
Figure 63: Degradation of a PV system in Singapore after ~1,100 days of operation (NOBRE <i>et al.</i> , 2013).	129
Figure 64: Performance ratio of 11 crystalline wafer-based systems in Singapore (NOBRE, YE, <i>et al.</i> , 2012).	130
Figure 65: The monthly spectrum of variation in the PR losses between a PV system in Singapore and one in Germany (NOBRE <i>et al.</i> , 2015 (in preparation)).....	131
Figure 66: NSR PV system category examples – commercial, industrial, residential and educational systems are categorized in the database (NSR, 2013c).	133
Figure 67: NSR 2013 benchmarking results for PV systems in Singapore (NSR, 2015d).	134
Figure 68: Simulated versus measured loss mechanisms of 11 PV systems in Singapore (NOBRE, YE, <i>et al.</i> , 2012).	137

Figure 69: Module and ambient temperature variations with irradiance for 17 PV systems in Singapore (YE <i>et al.</i> , 2013).	138
Figure 70: Illustration of proposed method: “Irradiance-to-kWh” simulation and validation (adapted for this thesis).	140
Figure 71: Singapore’s 25 ground-based stations of the CERP-04 research (adapted for this thesis).	143
Figure 72: Basic meteorological station #425 (left) and superstation #408 (right, wind sensors not pictured) (source: SERIS).	144
Figure 73: Location of 15 PV sites from the SERIS CERP-02 research in Singapore (adapted for this thesis).	147
Figure 74: Thermography of a monitoring cabinet at around noon (source: SERIS).	150
Figure 75: Map of Singapore presenting the location of the nine meteorological stations used in the proposed Hybrid method (NOBRE <i>et al.</i> , 2015 (submitted)).	156
Figure 76: Typical air pressure variation on a 1-min basis for a clear sky day conditions and during an approaching storm (NOBRE <i>et al.</i> , 2015 (submitted)).	157
Figure 77: Clear sky indices binned in eight time hourly intervals in the day, indicating cloudier afternoons versus mornings (top). ARIMA versus Persistence forecast mean absolute percent errors (MAPEs) plotted against hourly binning through the day (bottom) (NOBRE <i>et al.</i> , 2015 (submitted)).	158
Figure 78: Schematic diagram of the proposed Hybrid algorithm for short-term irradiance forecasting during severe weather events in Singapore (NOBRE <i>et al.</i> , 2015 (submitted)).	160
Figure 79: Global horizontal irradiance during a variable and a cloudy day. The variable day experienced a sudden storm after 15:00, which can be visualized by the sharp increase in relative humidity associated with the presence of rain (NOBRE <i>et al.</i> , 2015 (submitted)).	161
Figure 80: Normalized 1-min AC power output from ten existing PV systems located across Singapore representing different sizes and technologies on a “washout” day and also on a typical day (NOBRE <i>et al.</i> , 2015 (submitted)).	163
Figure 81: Existing (as of November 2013) and proposed stations (by end 2015), as well as perimeter belts of superstations (NOBRE <i>et al.</i> , 2015 (in preparation)).	166
Figure 82: Example sequence of three sky images and associated output cloud motion vectors (NOBRE <i>et al.</i> , 2015 (in preparation)).	169
Figure 83: Simulated versus measured AC power output of a PV system in Singapore under low wind speeds (source: SERIS).	170

Figure 84: Seven categories presented for module temperature variation in Singapore (YE <i>et al.</i> , 2013). Utilization for the method was further validated for PV systems in Brazil (NOBRE, MONTENEGRO, <i>et al.</i> , 2012).	171
Figure 85: Hospital complex in Singapore, home of four PV system sections (A, B, C and D), three of which are unshaded (A, B and C). The glass-glass canopy PV system in section D is heavily shaded by the surrounding hospital wings (source: SERIS, adapted for this thesis). 173	
Figure 86: Daily performance ratios of a high performing PV system (left) and of a poorly maintained one (right), with estimated degradation rates after several years of operations of -0.5% and -3.3% per annum (NOBRE <i>et al.</i> , 2015 (in preparation)).	174
Figure 87: Demonstration of the performance of three filters in three types of days (sunny, rainy and cloudy conditions) to derive the progressive sky conditions for the haze evaluation (NOBRE <i>et al.</i> , 2015 (accepted)).	178
Figure 88: Measured GHI at a central site in Singapore, with the forward ARIMA, Persistence and proposed Hybrid 15-min forecasts (top). The MAPE is given, showing considerable error spikes upon the arrival of the storm for both Persistence and ARIMA methods, but not for the proposed Hybrid model (bottom) (NOBRE <i>et al.</i> , 2015 (submitted)).	182
Figure 89: Mean average percentage errors (MAPE) for ARIMA 15-min forecasts for a sunny and a cloudy month (NOBRE <i>et al.</i> , 2015 (submitted)).	187
Figure 90: Approaching storm originating from E-SE on 30 th May 2015, first captured by new expansion station #426 at Changi Bay (NOBRE <i>et al.</i> , 2015 (in preparation)).	189
Figure 91: Storm progression through Singapore, with resultant vector taking eight sky cameras into account for predominant cloud direction path (NOBRE <i>et al.</i> , 2015 (in preparation)).	191
Figure 92: Storm progression through Singapore, with resultant vectors from eight sky cameras (NOBRE <i>et al.</i> , 2015 (in preparation)).	192
Figure 93: Module temperatures time series at two PV systems ~2 km apart (top left). The modules on a metal rooftop are in average ~15% hotter than the concrete one (bottom left). The temperature difference between module and ambient temperatures on the metal rooftop are compared against a system on a concrete rooftop (right) (NOBRE <i>et al.</i> , 2015 (submitted)).	194
Figure 94: Normalized power AC output sections of a shaded and unshaded PV systems (left). One year data for two irradiance sensors are	

shown for both conditions investigated (NOBRE et al., 2015 (submitted)).	195
Figure 95: 5-year period of a PV system's daily performance ratios (left). The power output of a single typical day five years apart also shows the noticeable system degradation (NOBRE et al., 2015 (submitted)).	196
Figure 96: Recorded 5-year degradation records for the PV system shown in Figure 60, where advanced soiling has been detected (NOBRE et al., 2015 (in preparation)).	197
Figure 97: PV system normalized power AC output on a day with clean skies (PSI < 50) and with polluted skies (PSI > 200) (left). The hazy sky day incurs ~25% power output for the PV system (NOBRE et al., 2015 (submitted)).	198
Figure 98: Simulated versus measured power DC for a 15 kW _p PV system during its first year of operation (top left) and five years later (top right). A larger error was observed for the now older PV system when a simple Persistence forecast was performed (NOBRE et al., 2015 (submitted)).	199
Figure 99: Filter performance progression for three different weather conditions (NOBRE et al., 2015 (accepted)).	201
Figure 100: Post-filtered resulting daily irradiance averages for four varying levels of air pollution (NOBRE et al., 2015 (accepted)).	202
Figure 101: Calculated typical solar irradiation day (in kWh/m ²) using June data for several ranges of the Pollutant Standards Index (PSI). Readings for a pyranometer and from a silicon sensor are shown (NOBRE et al., 2015 (accepted)).	203
Figure 102: Live map (top left of each image sequence, here 15-min), including forecasting (top right), error (bottom left) and Doppler radar (bottom right) developed within the works of this thesis.	210
Figure 103: Doppler radar animation for 6/Jan/2013. Adapted from (NEA, 2013).	215
Figure 104: Geographical distribution of the highest concentrations of PV systems in Singapore in terms of installed capacity in 2014 (source of data: National Solar Repository of Singapore, adapted for this thesis).	216
Figure 105: City of San Francisco, CA, USA (~10x10 km) and ~30 MW _p worth of solar PV systems (adapted for this thesis).	217
Figure 106: Cities of Belo Horizonte (~20x30 km, left) and Florianópolis (~20x50 km, right) (adapted for this thesis).	218
Figure 107: Example of irradiance map, which was developed for Singapore during the course of this thesis.	219

TABLE LIST

Table 1: Ten biggest markets for solar PV in the world at the end of 2014, adapted from (IEA, 2014c)..... 39

Table 2: Potential growth for photovoltaics and associated country metrics in Singapore and Germany, adapted from (EMA, 2014; IEA, 2014b). 47

Table 3: Challenges and solutions to large-scale PV systems integration (AIT, 2012) 69

Table 4: Typical meteorological year averages for Singapore and results for 2011 through 2014 for the SERIS meteorological station. TMY source: (METEOTEST, 2015). Other data source: SERIS. 87

Table 5: Weather statistics for 2013 and 2014 in Singapore including days with sudden storms, total “washout” conditions and with strong air pollution (“haze”) (NOBRE et al., 2015 (submitted)). 91

Table 6: List of countries with tropical climate conditions, adapted from (PEEL *et al.*, 2007)..... 101

Table 7: Key meteorological parameters for PV applications for some capitals in Brazil (NASA, 2013). 103

Table 8: Key meteorological parameters for PV applications for the capitals of the top-6 countries in installed PV capacity in the world (NASA, 2013). 103

Table 9: Measurement uncertainties of super and basic stations of the network (source: adapted from sensor manufacturers)..... 145

Table 10: Basic characteristics of 25 ground-measuring meteorological stations in Singapore (adapted for this thesis)..... 146

Table 11: Basic information for 33 PV sub-systems under monitoring at 15 sites via the SERIS’ CERP-02 research project (adapted for this thesis). 148

Table 12: Measurement uncertainties of the PV system monitoring setup of CERP-02 sites (source: adapted from sensor manufacturers)..... 149

Table 13: Possible combination of time series components in an exponential smoothing model (YANG, SHARMA, *et al.*, 2015). 153

Table 14: Basic characteristics of six ground-measuring meteorological stations for a remote sensing network expansion in Singapore (NOBRE et al., 2015 (in preparation)). 167

Table 15: PV systems basic characteristics used in the detailed up-scaling exercises. Systems’ age are based as of the date of the tests, March 2015 (adapted for this thesis). 179

Table 16: Sudden storm forecasting error improvement when using the novel Hybrid method (NOBRE et al., 2015 (submitted)).	182
Table 17: Case study on washout conditions in Singapore and error avoidance by selection of the Persistence method over ARIMA (NOBRE et al., 2015 (submitted)).	183
Table 18: Case study on hazy days in Singapore and error avoidance by selection of the Persistence method over ARIMA (NOBRE et al., 2015 (submitted)).	184
Table 19: Average monthly 15-min normalized root mean square errors (nRMSEs) for five short-term solar irradiance forecasting methods for a centrally located weather station in Singapore (NOBRE et al., 2015 (submitted)).	185
Table 20: Average monthly 30-min normalized root mean square errors (nRMSEs) for five short-term solar irradiance forecasting methods for a centrally located weather station in Singapore (NOBRE et al., 2015 (submitted)).	186
Table 21: Improvement of the proposed Hybrid method versus the Persistence method (as baseline) on a month-by-month basis, using both absolute errors percentage improvement but also the performance metric “s” (NOBRE et al., 2015 (submitted)).	187
Table 22: Average monthly 1-hr normalized root mean square errors (nRMSEs) for five solar irradiance forecasting methods for a central weather station in Singapore (NOBRE et al., 2015 (submitted)).	188
Table 23: Daily nRMSE results for selected case studies with a storm approaching from E-SE, with and without the use of a new deployed superstation (NOBRE et al., 2015 (in preparation)).	190
Table 24: AC power output conversion model normalized root mean square errors according to the five test sequences proposed in the investigations (NOBRE et al., 2015 (submitted)).	193
Table 25: Power conversion guidelines for a PV system in a tropical environment assuming low wind speeds (NOBRE et al., 2015 (submitted)).	200
Table 26: Daily total irradiation on module plane, PV systems’ yield and performance ratio (PR) for clear sky conditions (“clear”) as per method described in this work (combination of days with PSI < 50) and during a strong hazy conditions day (24 th June 2013, “hazy”). PV systems are located in several parts of Singapore and installed at different tilt angles and azimuths (NOBRE et al., 2015 (accepted)).	204
Table 27: Daily total ambient and module temperature averages for clear sky conditions (NOBRE et al., 2015 (accepted)).	206

Table 28: Preliminary findings on loss of revenue to a future fleet of PV systems in Singapore during a 10-day haze episode which mimics the June 2013 crisis (NOBRE et al., 2015 (in preparation)). 206

Table 29: Up-scaling routine executed for March 2015 (NOBRE et al., 2015 (in preparation))..... 207

Table 30: Cities around the world where remote meteorological sensing networks could be deployed. Singapore is shown as a baseline (adapted for this thesis). 218

LIST OF ABBREVIATIONS

μ c-Si	Microcrystalline Silicon
AC	Alternate Current
AICc	Corrected Akaike Information Criteria
AIST	National Institute of Advanced Industrial Science and Technology, Japan
AIT	Austrian Institute of Technology
AM	Air Mass
AMSL	Above Mean Sea Level
ANEEL	Agência Nacional de Energia Elétrica (Brazilian Electricity Regulatory Agency)
ANN	Artificial Neural Networks
ARIMA	Auto-Regressive Integrated Moving Average
a-Si	Amorphous Silicon
Avg	Average
BEN	Balanço Energético Nacional (Brazilian Energy Balance)
BIPV	Building Integrated Photovoltaics
BMA	Block Matching Algorithm
BOS	Balance of Systems
BSRN	Baseline Surface Radiation Network
CAGR	Compound Annual Growth Rate
CBD	Central Business District (of Singapore)
CCGT	Combined Cycle Gas Turbines
CdTe	Cadmium Telluride
CERP	Clean Energy Research Program
CIGS	Copper Indium Gallium Selenide
CNPq	Conselho Nacional de Desenvolvimento Científico e Tecnológico (Brazilian National Council for Scientific and Technological Development)
CPV	Concentrated Photovoltaics
DC	Direct Current
DHI	Diffuse Horizontal Irradiation
DNI	Direct Normal Irradiation
E	East
E	Error (in ARIMA and ETS algorithms)
EDB	Economic Development Board (of Singapore)
EMA	Energy Market Authority (of Singapore)

EPE	Empresa de Pesquisa Energética (Brazilian Energy Research Office)
EPIA	European Photovoltaic Industry Association
ETS	Common abbreviation for Exponential Smoothing State Space
GHI	Global Horizontal Irradiation
GPS	Global Positioning System
HDB	Housing & Development Board (of Singapore)
HIT	Heterojunction Intrinsic Layer (TM by Panasonic)
IEA	International Energy Agency
IEC	International Electrotechnical Commission
IEEE	Institute of Electrical and Electronics Engineers
INPE	Instituto Nacional de Pesquisas Espaciais (Brazilian National Institute for Space Research)
ISE	Fraunhofer Institute for Solar Energy Systems
KPSS	Kwiatkowski–Phillips–Schmidt–Shin Tests
kWh	Kilowatt-hour
LCOE	Levelized Cost Of Electricity
MAPE	Mean Absolute Percentage Error
MPPT	Maximum Power Point Tracker
m-Si	Monocrystalline Silicon
N	North
NASA	National Aeronautics and Space Administration
NE	Northeast
NEA	National Environment Agency (of Singapore)
NMC	National Metrology Centre (of Singapore)
NREAPs	National Renewable Action Plans
NREL	National Renewable Energy Laboratory
nRMSE	normalized Root Mean Square Error
NRF	National Research Foundation (of Singapore)
NSR	National Solar Repository (of Singapore)
NUS	National University of Singapore
NW	Northwest
NWP	Numerical Weather Prediction
p.a.	per annum
PR	Performance Ratio
p-Si	Polycrystalline Silicon
PSI	Pollutant Standards Index
PUB	Public Utilities Board (of Singapore)
PV	Photovoltaic(s)

PVPS	Photovoltaic Power System Program
REC	Renewable Energy Corporation
R&D	Research & Development
RMSE	Root Mean Square Error
S	Seasonal (in ARIMA and ETS algorithms)
S	South
SE	Southeast
SEIA	Solar Energy Industries Association
SERIS	Solar Energy Research Institute of Singapore
Si	Silicon
SGD	Singapore Dollar
STC	Standard Test Conditions
Std	Standard Deviation
SW	Southwest
T	Trend (in ARIMA and ETS algorithms)
TBD	To Be Deployed
TMY	Typical Meteorological Year
UFSC	Universidade Federal de Santa Catarina
USD	United States Dollar
USP	Universidade de São Paulo
UV	Ultraviolet
W	Watt
W	West
W_p	Watt-peak
WRF	Weather Research and Forecasting Model

LIST OF SYMBOLS

Symbol	Description	Unit
A_{irp}	Air pressure	[hPa]
b	Growth term in (in ARIMA and ETS algorithms)	[dimensionless]
E_{AC}	AC Energy	[kWh]
G	Giga	10^9
G_0	Reference irradiance equal to 1,000	[W/m ²]
G_{mod}	Irradiance in the plane of the array	[W/m ²]
h	Elevation angle	[°]
h	Time period (in ARIMA and ETS algorithms)	[min]
H_{amb}	Relative humidity	[%]
I_{AC}	AC current	[A]
I_{DC}	DC current	[A]
I_{MPP}	Maximum power point current	[A]
I_{SC}	Short-circuit current	[A]
l	Level term (in ARIMA and ETS algorithms)	[dimensionless]
k	kilo	10^3
k_d	Diffuse fraction	[dimensionless]
k_t	Clear sky index	[dimensionless]
M	Mega	10^6
m	milli	10^{-3}
m	meter	[m]
n	nano	10^{-9}
P_0	Rated power of a PV system at STC	[W _p]
P_{AC}	AC power	[W]
P_{DC}	DC power	[W]
PR	Performance ratio	[%]
R	Reflected irradiance	[W/m ²]
R_d	Reduction of the sky view factor and anisotropic scattering	[dimensionless]
T	Tera	10^{12}
T_{amb}	Ambient temperature	[°C]
T_h	Forecast trend (in ARIMA and ETS algorithms)	[dimensionless]
T_{mod}	PV cell temperature	[°C]

V_{AC}	AC voltage	[V]
V_{DC}	DC voltage	[V]
V_{MPP}	Maximum power point voltage	[V]
V_{OC}	Open-circuit voltage	[V]
W	Watt	[W]
Wh	Watt-hour	[Wh]
W_p	Watt-peak	[W _p]
W_D	Wind direction	[°]
W_S	Wind speed	[m/s]
Y	Total PV system annual yield	[kWh/(kW _p .yr)]
Y_f	Final yield of a PV system	[kWh/kW _p]
Y_r	Reference yield of a PV system	[hours]
z	Zenith angle	[°]
μ	Micro	10 ⁻⁶
θ	Incidence angle	[°]
Φ	Damping parameter (in ARIMA and ETS algorithms)	[dimensionless]

INDEX

RESUMO	XI
ABSTRACT	XIII
FIGURE LIST	XV
TABLE LIST	XXIII
LIST OF ABBREVIATIONS	XXVII
LIST OF SYMBOLS	XXXI
INDEX	XXXIII
1. INTRODUCTION	37
1.1 OVERVIEW	37
1.2 MOTIVATION	50
1.3 OBJECTIVES	54
1.3.1 Main Objectives	54
1.3.2 Specific Objectives	54
1.4 STRUCTURE OF THE THESIS	55
2. LITERATURE REVIEW	57
2.1 SOLAR PHOTOVOLTAICS	57
2.1.1 Solar PV systems technology	57
2.1.2 Cost-competitiveness of photovoltaics	62
2.1.3 Grid integration challenges	66
2.1.4 Variability aspect of the PV technology	70
2.1.5 PV market development and future outlook	72
2.2 SOLAR IRRADIANCE AT THE EARTH'S SURFACE	74
2.2.1 Overview on solar irradiance	74
2.2.2 Measuring solar irradiance	78
2.2.3 Irradiance models for PV applications	80
2.2.4 Irradiation data sources and considerations	82
2.3 CHARACTERIZING TROPICAL CLIMATE	83
2.3.1 Preliminary remarks	83
2.3.2 Singapore climate	84
2.3.3 Air quality issues in Southeast Asia	96
2.3.4 Other tropical climates around the globe	101
2.4 SOLAR IRRADIANCE FORECASTING	104
2.4.1 Preliminary notes	104
2.4.2 Stochastic methods	106
2.4.3 Satellite and numeric weather prediction	107
2.4.4 Artificial intelligence methods	108
2.4.5 Sky imagery utilization	110
2.4.6 Research on short-term solar irradiance forecasting	112
2.4.7 Solar irradiance forecasting in the tropics	112

2.5	PV SYSTEMS SIMULATION AND PERFORMANCE.....	114
2.5.1	<i>Yield and performance ratio of PV systems.....</i>	<i>114</i>
2.5.2	<i>Loss mechanisms of PV systems.....</i>	<i>119</i>
2.5.3	<i>Other factors influencing performance</i>	<i>124</i>
2.5.4	<i>PV system performance in warm climates.....</i>	<i>129</i>
2.5.5	<i>National Solar Repository of Singapore.....</i>	<i>132</i>
2.6	PV SYSTEMS MODELING.....	135
2.6.1	<i>Available tools.....</i>	<i>135</i>
2.6.2	<i>Existing research in PV systems modeling</i>	<i>135</i>
2.6.3	<i>Challenges of modeling in tropical conditions</i>	<i>136</i>
3.	METHOD.....	139
3.1	PRELIMINARY REMARKS	139
3.1.1	<i>R&D supporting infrastructure and overview.....</i>	<i>139</i>
3.1.2	<i>Boundary conditions of the investigations.....</i>	<i>142</i>
3.2	SOURCES OF DATA.....	143
3.2.1	<i>Ground-measured irradiance data.....</i>	<i>143</i>
3.2.2	<i>Operational data of PV systems</i>	<i>147</i>
3.2.3	<i>Robustness of the data collection infrastructure</i>	<i>150</i>
3.3	METHODS FOR IRRADIANCE FORECASTING	151
3.3.1	<i>Utilization of existing forecasting techniques.....</i>	<i>151</i>
3.3.2	<i>A Hybrid short-term irradiance forecasting method.....</i>	<i>155</i>
3.3.3	<i>Benchmarking of methods</i>	<i>165</i>
3.3.4	<i>Expanding the Singapore sensing network.....</i>	<i>166</i>
3.3.5	<i>Sky imagery as short-term forecasting support tool.....</i>	<i>168</i>
3.4	METHODS FOR PV SYSTEM POWER CONVERSION	170
3.4.1	<i>Single system modeling opening remarks.....</i>	<i>170</i>
3.4.2	<i>Factors heavily influencing PV system modeling</i>	<i>172</i>
3.4.3	<i>Modeling influences due to haze</i>	<i>175</i>
3.4.4	<i>Country-wide up-scaling routines</i>	<i>179</i>
4.	RESULTS AND DISCUSSIONS.....	181
4.1	SHORT-TERM FORECASTING RESULTS	181
4.1.1	<i>Novel short-term forecasting method findings</i>	<i>181</i>
4.1.2	<i>Benchmarking of various forecasting methods.....</i>	<i>185</i>
4.1.3	<i>Case study when extending the sensing network</i>	<i>189</i>
4.1.4	<i>Cloud vectoring demonstration and functionality</i>	<i>191</i>
4.2	POWER CONVERSION SIMULATION RESULTS.....	193
4.2.1	<i>Results on factors affecting PV power output.....</i>	<i>193</i>
4.2.2	<i>Air pollution investigation findings</i>	<i>201</i>
4.2.3	<i>Results on up-scaling exercises</i>	<i>207</i>

5.	CONCLUSIONS.....	209
5.1	ON THE MAIN FINDINGS OF THIS THESIS	209
5.1.1	<i>On short-term forecasting for the tropics.....</i>	<i>209</i>
5.1.2	<i>On PV systems power conversion</i>	<i>211</i>
5.2	LIMITATIONS OF THE WORK	214
5.3	SUGGESTIONS FOR FUTURE WORKS	215
5.3.1	<i>Hybridization and new forecasting methods</i>	<i>215</i>
5.3.2	<i>Detailed up-scaling exercises and 3D modeling</i>	<i>216</i>
5.3.3	<i>Replication of remote sensing networks</i>	<i>217</i>
5.3.4	<i>Other relevant works</i>	<i>219</i>
6.	PUBLICATIONS.....	221
6.1	THESIS RELATED PUBLICATIONS	221
6.2	OTHER PUBLISHED WORK	224
7.	REFERENCES	229

1. INTRODUCTION

1.1 OVERVIEW

Humanity's modern energy utilization pattern has relied heavily on fossil-fuels. The primary sources consumed through the years were, and are oil, coal and natural gas (IEA, 2014a). Through the past many decades, some countries successfully implemented renewable energy into their energy matrices – primarily hydropower – this being the case for locations with abundant natural resources and privileged terrains. Examples of such nations are Canada, the United States, Brazil, China and Norway. Other types of renewable energy sources used by societies have been vegetable coal, but primarily wood through time. It is only recently that more modern forms of renewable energy such as solar photovoltaics (PV), solar thermal, wind and geothermal have been added as energy generation sources in considerable volumes.

The presence of solar photovoltaics as a contributor to the electric power generation mix around the world has increased substantially during the past two decades. From having crossed the 1 GW_p¹ installed capacity in year 2000, the world's total cumulative solar PV system deployment reached the 178 GW_p-mark at the end of 2014, which is equivalent to a compound annual growth rate (CAGR) of ~40% over the mentioned 15-year period. Figure 1 illustrates this exponential growth in the mentioned time window (SPE, 2015).

Especially in countries with high adoption of photovoltaics, the solar power fed into the electric grid can contribute to a considerable amount of peak demand needs. On 18th August 2014, as an example, ~25% of the peak domestic demand in Germany was met by photovoltaics. Adding its capacities from wind and biomass sources, it was already the case that ~75% of the energy needs of Germany, a country with a population of circa 80 million people, were fully powered by renewables at least for a given moment in time on the mentioned day (RENEWABLES_INTERNATIONAL, 2014).

Germany has led the way in solar photovoltaic implementation worldwide, with 38.2 GW_p of installed PV capacity deployed by 2014 (IEA, 2014c). These installations accounted for 5.7% of the entire country's electricity needs in 2014 (AGEB, 2014). In the Southern state

¹ W_p = Watt-peak. As per International Electrotechnical Commission (IEC) standards (IEC, 2011) for the gauging of photovoltaic modules, the Standard Test Conditions (STC) are the laboratory test conditions of 1,000 W/m² of irradiance, 25°C of PV cell temperature and spectral distribution of light equivalent to 1.5 AM (air mass).

of Bavaria, where solar adoption is stronger due primarily to a more generous solar resource availability, the nearly half a million PV systems (equivalent to $\sim 11 \text{ GW}_p$ of capacity) met circa 12% of the electricity needs of the state in the same year (VBEW, 2014). The German Solar Industry Association (BSW) expects that 10% of the entire electricity needs of Germany will be covered by solar PV by 2020, followed by a 20% contribution by 2030 (BSW, 2013).

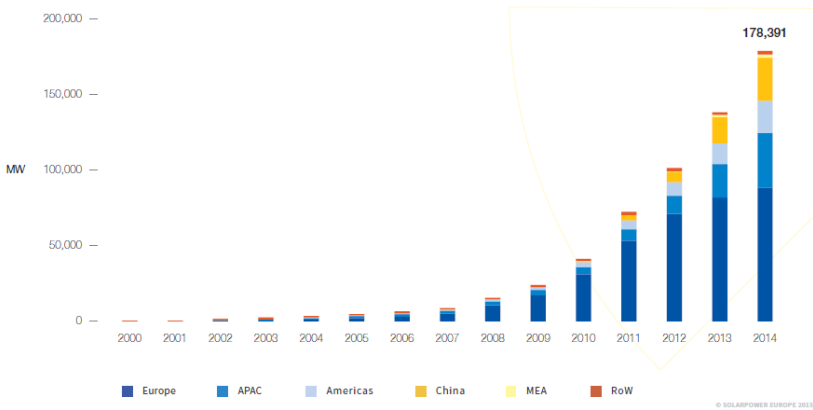


Figure 1: Solar photovoltaics worldwide growth from 2000 to 2014 (SPE, 2015)

Table 1 illustrates where market leaders in solar PV adoption are located in the world, here as shown by a second source in IEA. As of the end of 2014, the top five markets for cumulative installed capacity were Germany, China, Japan, Italy, and the United States, with a considerable installation volume gap between the fifth spot and the remaining countries in the top-ten list – France, Spain, United Kingdom, Australia and Belgium. The entire European continent alone accounts for half of all installed PV power on the planet (IEA, 2014c).

All market leaders except for a portion of Australia are located outside of the tropical regions of the world, the areas between the tropics of Cancer ($\sim 23^\circ\text{N}$) and Capricorn ($\sim 23^\circ\text{S}$), also known as the sun-belt. The tropics have higher levels of annual irradiation and are bound to experience further strong growth rates in PV systems' implementation due to continuing declining costs of the technology. Some of these countries are India (2.94 GW_p installed by 2014), Thailand (1.30 GW_p), Chile (0.60 GW_p), Mexico (0.18 GW_p) and Malaysia (0.16 GW_p) (IEA, 2014c). Chile is experiencing a surge in utility-scale PV installations to

serve the mining industry, with a number of large (upwards of 100 MW_p) power plants installed or in the process of being installed at one of the sunniest sites on Earth, on the Atacama Desert.

Countries which border the tropics have intensified the deployment of PV systems in recent years. Pakistan, which launched a 100 MW_p solar farm in a single location in 2014, will expand the facility to 1 GW_p by 2016 (PV-TECH, 2015). South Africa and Israel had deployed 0.92 and 0.73 GW_p, respectively, by the end of 2014 (IEA, 2014c).

Table 1: Ten biggest markets for solar PV in the world at the end of 2014, adapted from (IEA, 2014c).

Rank	Country	Installed capacity at the end of 2014 [GW _p]	Percentage of solar PV world market
1	Germany	38.2	21.6%
2	China	28.2	15.9%
3	Japan	23.3	13.2%
4	Italy	18.5	10.5%
5	United States	18.3	10.3%
6	France	5.7	3.2%
7	Spain	5.4	3.1%
8	United Kingdom	5.1	2.9%
9	Australia	4.1	2.3%
10	Belgium	3.1	1.8%
	Rest of World	27.1	15.4%
	TOTAL	177.0	100.0%

Notwithstanding the delayed growth for photovoltaic markets in tropical regions in comparison to other well-established, gigawatt-level locations of the world, two countries have shown potential for a rapid PV roll-out – Brazil (in South America) and Singapore (in Southeast Asia).

Brazil is poised to become one of the biggest adopters of the world of photovoltaic system deployment in the tropics. The 5th largest country in the world, both in area as well as in population (8.5 million km² and ~200 million inhabitants respectively), has an infant market in PV. The country has relied for more than half a century on power generated from hydroelectric plants, with the 14-GW power plant at the Itaipu dam as the cornerstone of the electrical generation system.

For Brazil, which possesses a tropical climate in a considerable part of its territory, the PV deployment in absolute numbers is low in

comparison to market leaders, yet with a strong growth experienced in the past four years (CAGR = $\sim 130\%$) as reported in (ANTONIOLLI *et al.*, 2014) and seen in Figure 2. Notwithstanding the low installed capacity of today, the targeted number of deployments for the future is promising (RÜTHER and ZILLES, 2011).

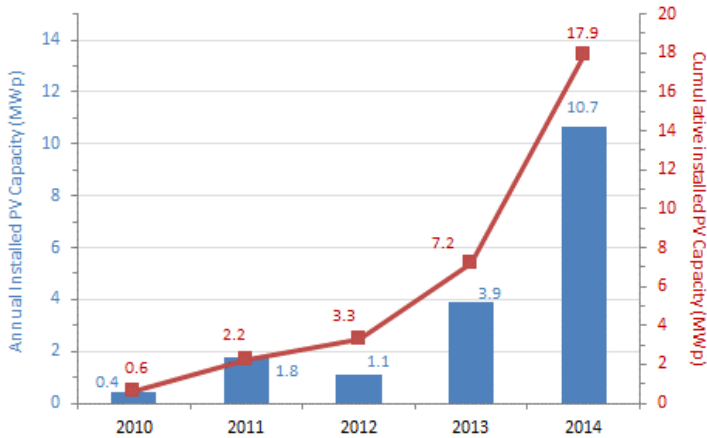


Figure 2: Annually deployed and cumulative volumes of photovoltaic systems in Brazil (ANTONIOLLI *et al.*, 2014).

Most of the existing photovoltaic systems in Brazil until 2011 had been off-grid smaller installations in remote areas where the electricity grid is not available. An approximate volume of 20 MW_p is scattered in many areas of the country, connected to batteries in houses in remote villages. However, this scenario is fast changing, which is already visualized in the country's continuous energy mix transformation.

In its report entitled “Balanço Energético Nacional – Ano Base 2013” (BEN, Brazilian Energy Balance – Year 2013), Empresa de Pesquisa Energética (EPE, Brazilian Energy Research Company) computed that $\sim 46\%$ of the entire Brazilian energy mix (primary matrix, including all energy sources) was met by renewable energy sources, which represents a much higher contribution than the world's average of $\sim 13\%$. If taking only electricity production into account, this ratio goes up to $\sim 80\%$, one of the highest in the world (EPE, 2014).

The overall contribution from renewables in electricity generation in Brazil has reduced from previous years though, as the usage of coal in thermoelectric power plants has increased, due to extended drought

periods in the country. This aspect has generated momentum for solar PV deployment.

Hydropower has provided ~70% of the electricity in Brazil and wind power has contributed enough to appear as a player – 6.6 TWh (~1.1% of the total electricity production for the country of 570 TWh) (EPE, 2014). From 2005 to 2014, wind energy has had a decade run of CAGR of nearly 40%, reaching 2.2 GW of installed capacity at the end of 2014.

In order to produce 1 TWh of electricity, Brazil produces 8 times less greenhouse gas emissions than the United States, 5 times less than Europe and 12 times less than China (EPE, 2014). With such a clean energy matrix, it is understandable why the PV market in the country has taken longer to gain traction. Nonetheless, Brazil currently experiences a late entrance in the solar PV game. On 17 April 2012, the Agência Nacional de Energia Elétrica (ANEEL, Brazilian Electricity Regulatory Agency) approved a new regulation allowing the connection to the grid of PV systems up to 100 kW_p (named “micro-generation” in the law) and between 100 kW_p and 1 MW_p (“mini-generation”) (ANEEL, 2012). In this net-metering scheme, the extra energy generated on site and fed into the grid is kept as a credit and can be used by the producer within a 36-month period. Alternatively, the credit can be transferred to another electricity bill belonging to the same system owner.

3.9 MW_p and 10.7 MW_p newly added PV volumes were connected to the grid in Brazil in 2013 and 2014, respectively, for a total market size of 17 MW_p (ANTONIOLLI *et al.*, 2014). With the push for renewables taking a worldwide stance, together with falling system prices and the newly approved regulation in Brazil, the first MW-level systems started to come online. Some of these MW-level were commissioned on top of stadiums prior to the 2014 Soccer World Cup, such as a 1.42 MW_p installation at the Mineirão Stadium in Belo Horizonte, MG (CEMIG, 2013), see Figure 3, a 400 kW_p system at the Maracanã Stadium in Rio de Janeiro, RJ, a 400 kW_p supporting arena for the World Cup at the Pituacu Stadium in Salvador, BA (AMERICA_DO_SOL, 2012), among others.

Several systems were also installed under R&D grants from ANEEL, such as the 3 MW_p test facility by the Universidade Federal de Santa Catarina (UFSC) and Tractebel in Santa Catarina (see Figure 4). Many years of healthy growth rates are expected, especially with excellent solar resource throughout the country (1,400-2,400 kWh/(m².year) (PEREIRA, E. B. *et al.*, 2006).



Figure 3: 1.42 MW_p at the Mineirão Stadium in Belo Horizonte, MG (CEMIG, 2013).



Figure 4: 3 MW_p at the UFSC/Tractebel R&D facility in Tubarão, SC (Source: Fotovoltaica/UFSC).

Singapore, located just North of the Equator (1.37° N, 103.75° E), although only a small city-state (land area = ~ 718 km², population = 5.47 million as of 2014 (SDS, 2014)), possesses an expanding PV scene taking place within a heavily-built environment. Even though it has only a small fraction of photovoltaics in its energy mix, this Asian tiger nation is a demonstration on how PV is growing in nearby regions around the

tropics. At the end of 2008, not even 1 MW_p of PV systems were installed. However, within the following six years, the volume of installations shot up, with a CAGR of ~80%, with total installations currently at 33 MW_p (see Figure 5). Many locations around the world have reached grid parity, the moment in time when investing on a PV system is cheaper than purchasing electricity from the grid. This was also the case for tropical Singapore in 2012 (CHUA, 2012).

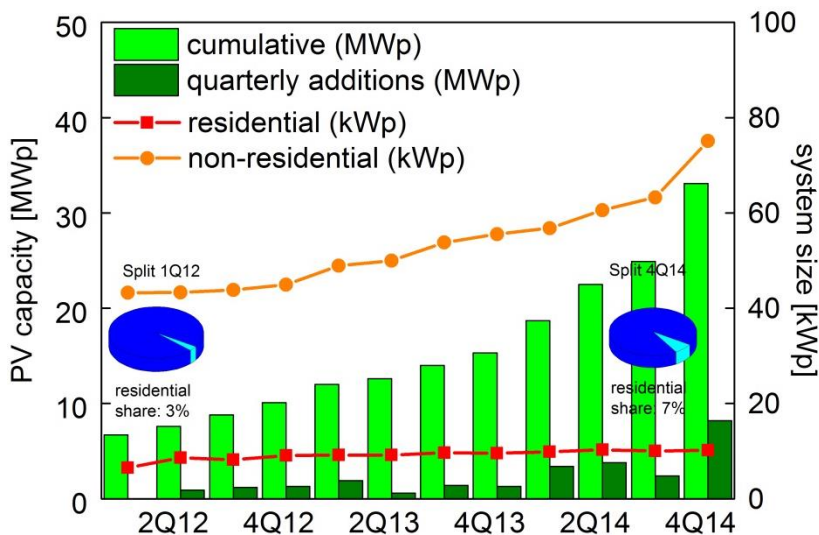


Figure 5: Quarterly and cumulatively installed PV capacity in Singapore for the 2012-2014 time period (NSR, 2015c).

In recent times, the Singapore government announced the “SolarNova Program”, where several agencies will use their building feedstock to host circa 350 MW_p of PV systems by 2020 (MTI, 2014). A tender call for the program was launched in June 2015, aiming at having 40 MW_p of PV capacity deployed by end of 2017 (CNA, 2015).

On top of the SolarNova initiative, the Public Utilities Board (PUB) – the agency responsible for the water treatment and distribution in Singapore – is conducting a 3 MW_p floating PV test-bed in an inland fresh water reservoir in the country (TODAY, 2014). The potential for deployment of hundreds of megawatts of floating systems onto local reservoirs has been touted. All in all, Singapore could have ~1-2 GW_p of cumulative solar PV systems deployed within the 2020-2030 year time span (LUTHER and REINDL, 2013).

In its year 2000 census (SDS, 2013), Singapore's population was reported at 4.03 million. Ten years later, in its most recent official survey, the population had grown to 5.08 million (+26% nominal increase, +2.3% CAGR), mostly due to the inflow of foreigners as part of the government strategy of economic growth (PMO, 2013). As a consequence of both population and economic spurts, energy utilization followed and can be visualized in Figure 6, also for a decade, but for a more recent time range, in the energy consumption patterns for the country as seen in (for the 2005-2014 timeframe, recorded CAGR of +2.9%).

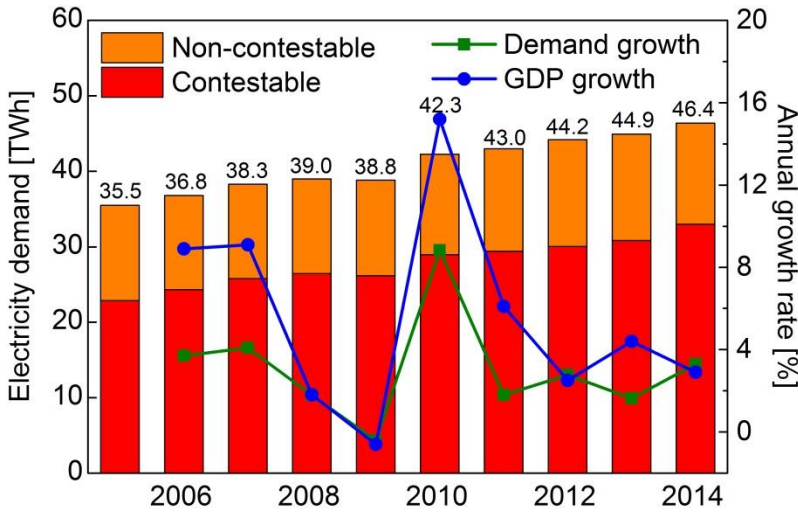


Figure 6: Annual electricity demand and gross domestic product growth in Singapore for the 2005-2014 period, adapted from (EMA, 2013).

It can be seen that in 2014, the total consumed electricity in Singapore was close to 47 TWh. Assuming an installed capacity of solar PV in the country of 33 MW_p and a PV system annual energy generation potential of 1.08 MWh/(kW_p per year), as analyzed by the National Solar Repository of Singapore (NSR, later discussed in sub-section 2.5.5 (NSR, 2015d)), electricity production arising from solar PV for the year could be estimated at ~35 GWh, or only 0.08% of the total amount of electricity consumed in the country in 2014. There is still considerable room for growth of the local PV market, which could make a promising case as a source of renewable energy for the future (LUTHER and REINDL, 2013).

Figure 7 shows that the majority of the electrical energy generation capacity in Singapore runs on fossil-fuels (oil for steam units and natural gas powering combined-cycle gas turbines, CCGT). Only a small portion can be linked to other sources of generation, in which solar would have a small percentage thereof. Due to idled capacities, oil-fired generators have been turned off starting in 2012. This has caused the electricity matrix of Singapore to become somewhat cleaner, since the CCGT plants are less polluting.

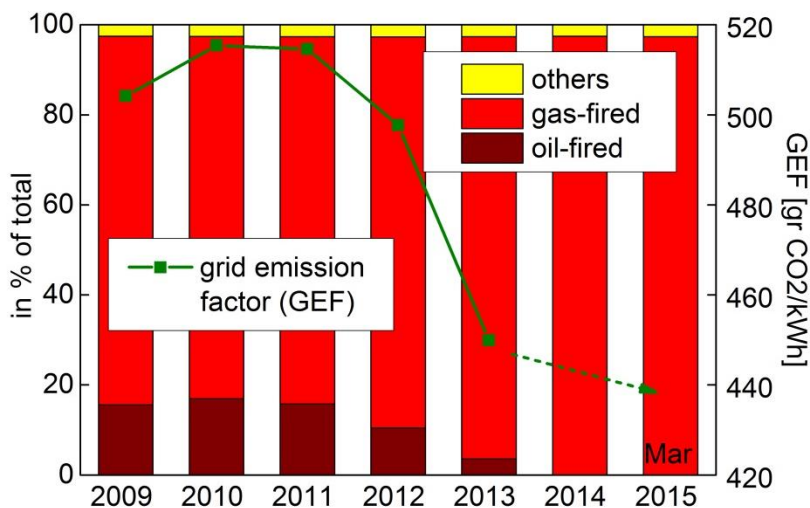


Figure 7: Electricity generation fuel type in Singapore for the 2009-2015 period, adapted from (EMA, 2013).

Another aspect pertaining to the Singapore economy is that the majority of fossil-fuels powering energy generation come from imports due to the absence of local natural resources. Singapore was the 8th highest world importer of oil products in 2012, as per the International Energy Agency (IEA) (IEA, 2014a). This is yet another reason why the local government has shown the commitment to invest in renewables, namely photovoltaics, due to the abundant solar resource in the tropical nation (long-term average annual irradiation = 1,631 kWh/m²), in order to reduce its dependency on foreign sources of energy (MEWR, 2009).

In general, the electricity load of the country peaks at close to 6.5 GW in the months of May and June, when ambient temperatures reach the highest values of the year. Figure 8 (left) (EMA, 2015)) shows the demand pattern for a May week in the country, when there is a

pronounced increase in the usage of air-conditioners (as an example). With the entire generation capacity of Singapore resting at ~ 12.8 GW (EMC, 2015), the peak represents only $\sim 55\%$ of the total authorized generation capacity, highlighting a robust reserve for the system, mainly driven by security issues. Also seen from Figure 8 (right) is the progressive increase in the energy demand curve for Singapore through the years, a phenomenon which can be partially explained by an increase in population as previously mentioned.

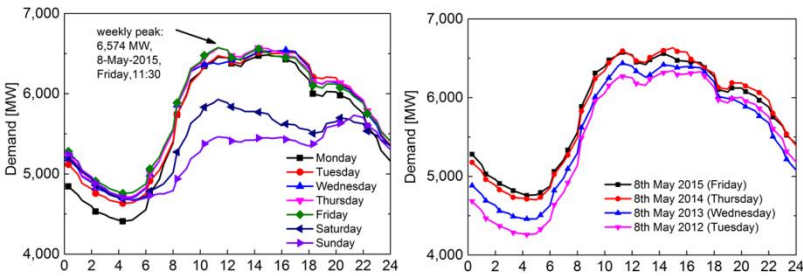


Figure 8: Daily energy consumption pattern for Singapore during a week in May 2015 (left), as well as progression of peak demand for the period of 2012-2015 (right), adapted from (EMA, 2013).

The speed of installation of photovoltaic systems for the years ahead could represent a rapid change of the energy landscape in Singapore, potentially making the island one of the places with the highest concentration of PV capacity in a city setting in the world (excluding open field solar farms). Figure 9 shows some examples of the urbanization of photovoltaics – a skyscraper at the Central Business District of Singapore (CBD) with a 75 kW_p PV system on its rooftop and a building integrated photovoltaic (BIPV) system on a residence at a residential condominium in Singapore. BIPV deployment worldwide is also targeted to experience strong growth rates ahead (PIKE, 2012), which would continue to promote the “urban solar” wave.



Figure 9: PV systems in Singapore exemplifying the urbanization of solar photovoltaics (NSR, 2015b).

Table 2 aims at presenting a vision of the future (+15 years) where the growth of the population and of PV system deployment for Germany and Singapore are contrasted. With an equivalent 2.8 MW_p of PV per km^2 of country area, Singapore is poised to have one of the densest fleets of PV systems in the world.

Table 2: Potential growth for photovoltaics and associated country metrics in Singapore and Germany, adapted from (EMA, 2014; IEA, 2014b).

Country	Population in 2014 [million inhabitants]	Population in 2030 ² [million inhabitants]	PV volume in 2014 [in GW_p]	PV volume in 2030 ³ [in GW_p]
Singapore (718 km^2)	5.47	7.51	0.33	2.00
Germany (357x10 ³ km^2)	80.72	87.43	38.2	56.7
Country	Watts per capita in 2014	Watts per capita in 2030	kW per km^2 in 2014	kW per km^2 in 2030
Singapore (718 km^2)	~5	~270	~45	~2,800
Germany (357x10 ³ km^2)	~475	~650	~110	~160

² For Germany, population growth is assumed 0.5% p.a., whereas for Singapore, a country experiencing much higher economic growth rates, the population growth assumed is 2.0% p.a., in line with (SDS, 2014).

³ For Germany, PV growth is assumed to be 2.5% p.a., in line with an already mature and saturated solar market. For Singapore, it follows strong expansion rate premises set in (LUTHER and REINDL, 2013).

As observed thus far in this overview, the deployment rate of solar PV systems worldwide has been considerable, with locations in the tropics now gaining momentum. With deeper levels of penetration of solar PV into grids, its professional and smooth integration becomes the next challenge. Some high penetration level examples are Italy (~8% of the total electricity generation), Germany (~6%) and Greece (~6%) (IEA, 2014c). For those countries, solar can already account for a considerable amount of the peak demand. When higher shares of peak PV are concerned, the island of Kauai, in Hawaii already has ~80% contribution coming from solar PV (FAIRLEY, 2015).

Apart from the massive growth rates reported, the up-and-coming challenge of solar PV lies on its integration impact onto the grid due to high solar power penetration levels, as previously mentioned, and its variability, a characteristic of the technology. Varying power output originates questions and concerns from the utility standpoint, especially in a tropical environment, with high cloudiness indices and erratic cloud motion (discussed in detail in section 2.3). Other questions arising on top of the variability of the power flow of PV systems itself are associated with voltage and frequency fluctuations, reverse and additional power flows and anti-islanding (if solar inverters will disconnect from the grid in case the latter is unavailable) (BRAUN *et al.*, 2012; STETZ *et al.*, 2015). For that reason, a new International Energy Agency Task Force was created within the Photovoltaic Power Systems Program, Task 14, named “High Penetration of PV Systems in Electricity Grids” (IEA, 2011). Among the goals of Task 14 are to work closely with utilities, industry players and stakeholders in developing technologies and methods to enable the widespread deployment of distributed, grid-connected PV systems.

Large-scale, non-rapid dispatch forms of electrical energy generation, namely nuclear, hydro or thermoelectric power plants have a longer start-up time. As an example, a 285 MW hydropower Francis turbine running with no load (at its “speed no load” setting) would take 3-min to start producing electricity, upon a decision to generate is made. If the turbine is completely stopped, the time between decision and generation would be around 10-min. As another example, a thermoelectric power plant on total stoppage would take many hours until reaching an operational condition where electricity can be generated. Even for a situation when there is ready steam for the turbines, a stopped unit could take up to 30-min upon generation and synchronism with the grid.

Gas turbines in Singapore and elsewhere can be part of spinning reserve systems, or energy generation potential that could be turned on at a relatively shorter period of time. The integration of all these sources of energy generation together with solar PV will be one of the technical challenges of this century.

Due to such increasing shares of PV in the generation mix and the variability associated with the solar technology, solar irradiance forecasting has gained momentum to assist grid operators meeting load demand and performing a smooth balancing between conventional electricity generation and solar PV and/or other variable renewable sources (e.g. wind). Forecasting irradiance for regulation (short-term interval horizons, which can act as complement to the grid), as well as for grid scheduling and unit commitment (for one-day ahead forecasts or times beyond that horizon), are paramount.

Knowledge of the future output of the sun's irradiance and consequently the energy generation on a PV system under a particular irradiance level becomes crucial in bridging a future where renewable and non-renewable power sources work concurrently to meet the world's electricity needs. This thesis addresses some of these challenges.

1.2 MOTIVATION

As seen in Table 1, the majority of the installed solar PV capacity of the world is located in Europe, United States and Japan, with China more recently climbing the ranks all the way to number two. Derived from that table, it can be observed from Figure 10 that the top-ten PV markets are located outside of the sun-belt region of the world, with the exception of a portion of Northern Australia and a small part of China. It can be inferred that more than 90% of all PV systems on the planet are not located in the tropics, which encompass the most solar-abundant regions of the world.

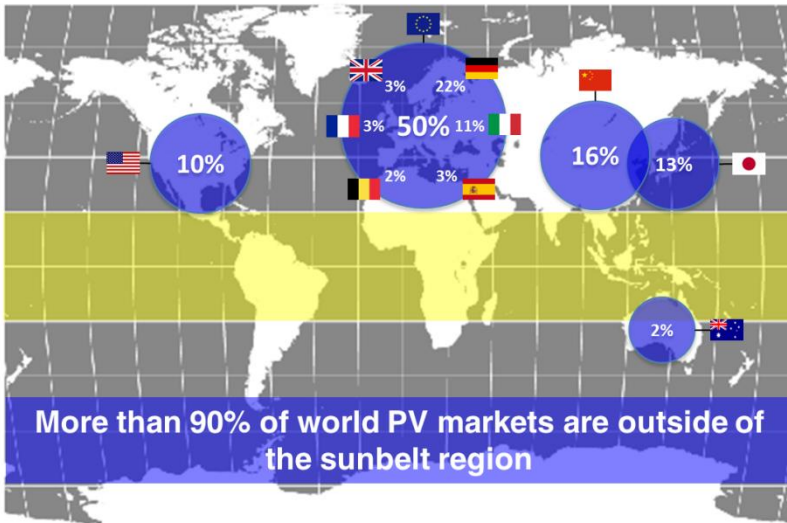


Figure 10: Location of the top-ten solar PV markets of the world as of end of 2014, adapted from (IEA, 2014c).

Consequently, it is not unusual that solar PV research efforts have been conducted by research centers located in temperate locations of the world, with some examples being the National Renewable Energy Laboratory (NREL) in the United States, the Fraunhofer Institute for Solar Energy Systems (ISE) in Germany, and the National Institute of Advanced Industrial Science and Technology (AIST) in Japan, among other renowned centers in countries like France and The Netherlands. Additionally, the majority of the R&D efforts on the topic of PV system

field performance are, in its large capacity, focused on installations at countries at the top-ten list of markets in the world.

It was also reported in section 1.1 the growth of PV systems and their role as major contributors to the electricity mix in countries. As ratios of solar PV in energy mixes climb from negligible towards considerable levels (10% and beyond), work in the area of solar irradiance forecasting starts to become increasingly relevant for the management of electricity grids. Consequently, solar resource estimation ahead of time is vital if desired to be an integral part of the entire energy generation operations from a utility stand-point, when regulating energy production dispatch of fossil-fuel based power generation.

Classical weather forecast (in terms of temperatures and precipitation) has reached nearly 100% accuracy for one day ahead and 70% of accuracy for five days anticipation in many parts of the world. For PV applications, where the sunlight intensity, or solar irradiance, is the object of interest, accuracies depend on time horizons of choice (from minutes up to a couple of days ahead) and region of the world (a temperate weather region is likely to have less cloud coverage in comparison to a tropical region). The forecast time horizons will dictate forecasting products, tailored for stakeholders (such as utilities) for their dispatch and commitment cycles of fossil-fuel and other sources of energy generation. This thesis focuses on solar irradiance forecasting for a tropical climate in Singapore and a critical time frame from the local utility's perspective – short-term intervals (from a few minutes up to 1-hr ahead of time), especially since electricity is traded in Singapore at 30-min intervals (EMA, 2013).

An added motivation for the case study in Singapore is the relatively small size of the island-state, with its $\sim 720 \text{ km}^2$ of area and only a small interconnection to the Malaysian power grid. The variability which can arise from PV systems due to the weather poses a much larger risk since the geographical smoothing effect is reduced. Drastic weather variations in Singapore (e.g. due to fast approaching storms common in the tropics, see example in Figure 11) make short-term solar irradiance forecasting a crucial part of PV grid integration and to properly manage and balance the grid.

Research on solar irradiance forecasting for PV applications is considerably new (less than 10 years of publications as described later in section 2.4), and when tropical regions are the object of study, the work is altogether novel.

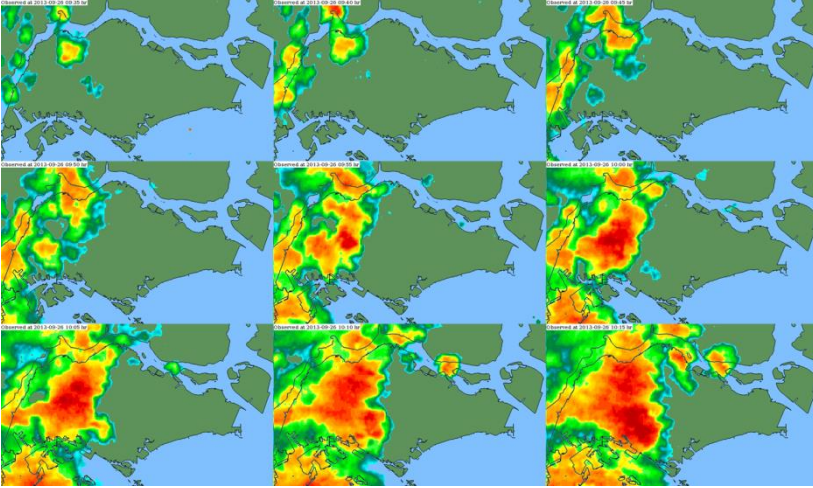


Figure 11: A so-called “Sumatra squall” with an approaching storm originating from Indonesia as captured by Doppler radar images in 10-min intervals, adapted from (NEA, 2012).

Solar irradiance forecasting is just the first mechanism in improving grid operations with a large share of renewables. The process of creating a resilient grid relies on further understanding of the conversion steps from irradiance all the way into final electricity for end users. To make matters more difficult, the area of PV systems performance modeling and assessment is still in its infancy for tropical regions, as it would be expected from the absence of relevant volumes of installations in these locations.

As an example, and mentioned in section 1.1, having solar PV systems in a densely-built environment, be it Singapore or other metropolises in the future, will create integration hurdles for the technology into existing building feedstock. The influence of shading from nearby buildings and structures exemplifies such integration challenges, but which can be mitigated (ZOMER *et al.*, 2014).

In this thesis, methods for short-term irradiance forecasting are executed for ground-measured solar irradiance data in Singapore and benchmarked. Also as part of the work, an attempt to develop a novel method to reduce prediction errors is developed. The discovery of areas of improvement helps delineate a path for similar work which could be experienced by other researchers in areas with similar weather patterns around the globe. Studying these extreme weather conditions as the one shown in Figure 11 and their effect on a growing number of solar

photovoltaic systems are topics of great interest to local power system operators.

The work of this doctoral thesis will therefore focus on pressing topics such as assessment of the solar energy resource ahead of time, but at the same time taking into account the amount of solar electricity generated at the end producer, after a PV system goes through its known loss mechanisms process. Therefore, the motivation and relevance behind this thesis stem from two fronts and can be summarized as follows:

- The increasing share of photovoltaics in electricity grids around the world has been overwhelming. PV will play a major role in future energy mixes. Forecasting of the solar resource will be key in coordinating dispatch and management of the existing power generation resources based primarily on fossil-fuels;
- The massive amounts of PV systems being deployed around the world and the need to understand their day-to-day and long-term behavior and optimization aspects. The output of systems, with the understanding of the entire flow mechanism from point A (“irradiance availability”) all the way to point B (“kWh delivered”), is and will be crucial.

Work on irradiance forecasting is pioneer in the climatic region of the world proposed here. Additionally, PV systems modeling, simulation and validation has also not been investigated extensively in sun-belt countries.

Finally, as the world moves increasingly towards the so-called “smart grids”, mechanisms such as trading of energy, variable tariffs and real-time controlled production & demand of electricity become “hot topics”. Thus, subjects such as the predictability of renewable energy solar assets are more and more relevant moving forward with the aim of forecasting, for example, PV system output ahead of time.

1.3 OBJECTIVES

1.3.1 Main Objectives

The main objectives of this thesis are to:

- a) Evaluate and compare short-term forecast methods for solar irradiance in Singapore, taking into consideration the challenging meteorological conditions found in tropical regions, minimizing loss of precision from the forecasts; and
- b) As a final use of the forecast products originated in a), simulate, determine and validate generated solar PV systems' energy output ahead of time.

1.3.2 Specific Objectives

The specific objectives of this thesis are to:

- Simulate and validate irradiances at given points of the Singapore island;
- Compare and contrast available irradiance forecast methods, be it via stochastic, artificial intelligence (e.g. artificial neural networks), or other novel methods;
- Simulate PV system performance based on given solar irradiance forecasts and loss mechanism parameters of PV systems modeling;
- Validate results using an existing network of PV systems under monitoring in Singapore;
- Investigate other aspects influencing PV system performance, such as transboundary haze episodes;
- Make proposals & assumptions of forecasting & PV system behavior for utility stakeholders in Singapore.

1.4 STRUCTURE OF THE THESIS

The thesis is structured such that chapter 1 presented an overview of the *status quo* of solar photovoltaics around the world and most notably in the tropics. Also within the chapter, the motivation behind this work was given, followed by the main and specific objectives of the thesis.

Chapter 2 provides a detailed literature review surrounding topics such as the modern state of PV systems technology, solar irradiance resource basics, the typical climate found in the tropics (and specifically for the case study of Singapore), the state-of-the-art of solar irradiance forecasting and finally PV system simulation & performance assessment considerations.

Chapter 3 touches on the methods proposed for the works contained in this thesis. It introduces how data was collected and how it was used in order to obtain the results presented in chapter 4, as well as discussions arising from the findings.

Chapter 5 summarizes the outcome of this work together with likely limitations encountered which in turn fuel suggestions for future works in the field.

Chapter 6 presents the publications derived from this thesis and other works by the author.

2. LITERATURE REVIEW

2.1 SOLAR PHOTOVOLTAICS

2.1.1 Solar PV systems technology

Photovoltaics (or commonly known as PV) is the static and direct conversion of sunlight into electricity (DGS, 2008). A classic PV system is made primarily of a combination of photovoltaic modules (Figure 12 left, mounted onto a residence's rooftop as an example (NSR, 2013c)) connected in series forming strings. These strings are then hooked up in parallel to solar inverters (Figure 12 right), which convert the produced DC (direct current) power from the modules into AC (alternate current) power, then fed into the grid of the building.



Figure 12: A residential 8.6 kW_p PV system in Singapore with thin-film modules and two inverters (NSR, 2013c).

Smaller PV installations such as the 8.6 kW_p thin-film system shown in Figure 12 are usually connected to low-voltage, single-phase grids (230 V_{AC}, 50 Hz for the case of Singapore). Bigger systems, such as the 300.4 kW_p polycrystalline setup at the Renewable Energy Corporation (REC) solar wafer, cell and module plant in Singapore (Figure 13, (NSR, 2013c)), might be connected to the medium-voltage grid of the facilities in which they are hosted.

Similar systems are flourishing in other tropical locations of the world, such as Brazil, as it could be seen in Figure 3 for the case of a medium-voltage connected system and Figure 14 for the first residential PV system connected to the electricity grid in the state of Minas Gerais, located in the city of Belo Horizonte, a 3.6 kW_p monocrystalline setup (SPB, 2012).



Figure 13: An industrial 300.4 kW_p PV system at the REC facility in Tuas, Singapore with polycrystalline modules (NSR, 2013c).



Figure 14: A 3.6 kW_p monocrystalline PV system in a residence in Belo Horizonte, Brazil (SPB, 2012).

Crystalline silicon wafer-based technologies have lead most of the development of solar photovoltaics. Its presence can be linked to 80-90% of the PV systems found in the world (SOLARBUZZ, 2013b). Thin-film amorphous silicon and other variants like microcrystalline, had a spurt of growth around the year 2005, increasing their market share from 10% to close to 20%. That was especially the case since a raw material bottleneck

occurred (2006-2008), favoring the rise of thin-film systems, which utilize less silicon for their production. However, due to ongoing consolidation in the PV manufacturing sector and continuous preference towards crystalline-based technology systems, thin-film products have been further diluted back to ~10% and below of the total market volume.

Monocrystalline silicon cell efficiency record is achieved with the deposition of a heterojunction intrinsic layer (“HIT cells” as trademarked by Sanyo, later acquired by Panasonic). The most recent record as of 2015 stands at 25.6%. For multicrystalline silicon, the record efficiency is 20.8% (GREEN *et al.*, 2015). In terms of other PV technologies, cadmium telluride (CdTe) modules and systems have been heavily deployed by American company First Solar. During tough economic market conditions (2011-2013), the company performed well and deployed MW-size solar parks primarily in the United States (see the 550 MW_{ac} solar farm in Figure 15 (FIRST_SOLAR, 2013)). First Solar announced in 2015 a breakthrough record efficiency of 21.5% for its CdTe cells (PV_MAGAZINE, 2015).



Figure 15: Desert Sunlight Solar Farm (550 MW_{ac} PV plant), built in California (FIRST_SOLAR, 2013).

Apart from efficiency improvements in solar cell technologies, a current trend in crystalline wafer-based modules is the launch of bifacial products, glass-glass laminates which allow light to go through the panel, which then bounces off the ground/roof underneath, returning partially to the panel, boosting its power output.

Another recent frontier in photovoltaic system deployment has been the launch of “floating PV systems”. These systems have been aimed

at minimizing land resource utilization, especially for area-stricken countries such as Japan or Singapore (NCCS, 2011). Other mentioned benefits of floating PV are the extra cooling provided by the water to the panels, thus allowing for a higher energy harvesting, as well as ability of the system to prevent algae growth (TRAPANI and REDÓN SANTAFÉ, 2015). Figure 16 shows two MW-level floating PV systems deployed in Japan in fresh water canals and reservoirs (NIKKEI, 2013; TECHXPLORE, 2015).



Figure 16: 1.2 MW_p floating PV system at the Okegawa (left) and 1.7 MW_p Hyogo (right) prefectures in Japan (NIKKEI, 2013; TECHXPLORE, 2015).

In terms of how different PV technologies react to the sun's electromagnetic irradiation, Figure 17 shows the relative spectral responses of different PV modules (multicrystalline Si (silicon), amorphous Si, CdTe and CIGS). The single-junction a-Si module has a peak response at around 600 nm and is able to convert light into electricity from ~320-800 nm. For the CdTe module technology, the corresponding range is 300-900 nm. The spectral response range for the CIGS module is around 350-1150 nm, similar to that of a crystalline silicon wafer-based module (LIU *et al.*, 2014b).

Modules are the driving force of the system, with the remaining “balance of systems” (commonly abbreviated as BOS) composed by inverters, mounting systems (for the interface between modules and ground/rooftop/floats), DC and AC cabling & switches/isolators, surge protections, etc. Modules have historically represented the majority of the cost of a PV system (in the order of 70% of the total cost), but this ratio has drastically changed, falling to around 50% in 2015 (see section 2.1.2).

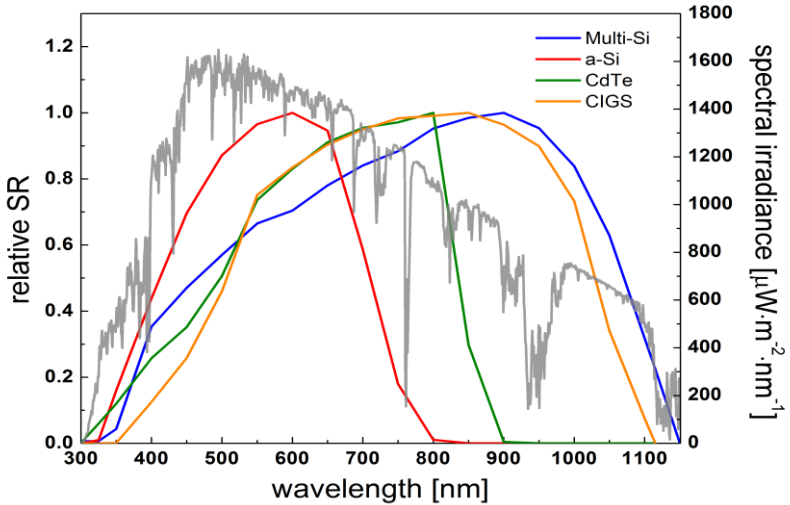


Figure 17: Relative spectral response of various PV technologies (multicrystalline Si, amorphous Si, CdTe and CIGS), measured under STC temperature (25°C), with the AM1.5G spectrum (grey) also shown as reference (LIU *et al.*, 2014b).

As much as solar PV can and have caused enthusiasm in governments and population for a faster rollout, a few aspects historically prevent even faster growth rates. They can be named as follows:

- Cost-competitiveness of photovoltaics (discussed in 2.1.2);
- Grid integration challenges (discussed in 2.1.3);
- Variability aspect of the energy generation profile from PV (discussed in 2.1.4);

Apart from the various challenges discussed next, solar PV has a bright future, as covered in subsection 2.1.5 with a market outlook.

2.1.2 Cost-competitiveness of photovoltaics

PV module prices, which have historically dictated the overall cost of a system, have reduced drastically (~60%) during the 2009-2013 period (SOLARBUZZ, 2013a), and were responsible for about only half of a PV system cost in 2014 (BSW, 2014). Consolidation happened in the module manufacturing industry, with several companies closing doors or acquired by other players. Big name companies such as Bosch exited the solar market altogether after major losses reported (PV-TECH, 2013). Traditionally, even well-established companies experienced turbulence in the PV business, with recent episodes such as former world number one Suntech (China) being acquired, and also other Chinese players in Hanergy and Yingli going through unstable periods (BLOOMBERG, 2015; WALL_STREET_JOURNAL, 2015). The price learning curve of photovoltaics (Figure 18) shows that with each doubling of the installed PV capacity worldwide, prices have come down by ~20% for the 34-year period (ISE, 2014).

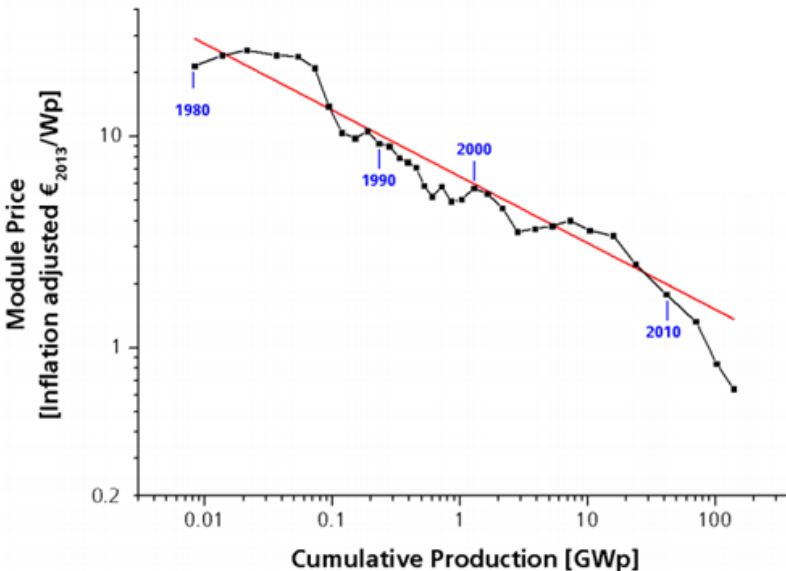


Figure 18: Price learning curve of photovoltaics (ISE, 2014).

As previously mentioned, the price of a PV system relied heavily on the solar module as the main component (circa 60-70% of the total investment). With the price erosion of the past years, the scenario has

reversed and BOS components now account to ~50% of the cost of a rooftop PV system in Germany (see Figure 19) (BSW, 2014), thus shifting some of the pressure to inverter makers and system integrators in general to become more competitive. For a solar farm in the MW range, the ratio could be even lower due to the likely economies of scale achieved when procuring solar panels in bulk volumes, and also to the fact that rooftop PV systems do not account for area-related costs, which is not the case for utility-scale, ground-mounted PV generators.

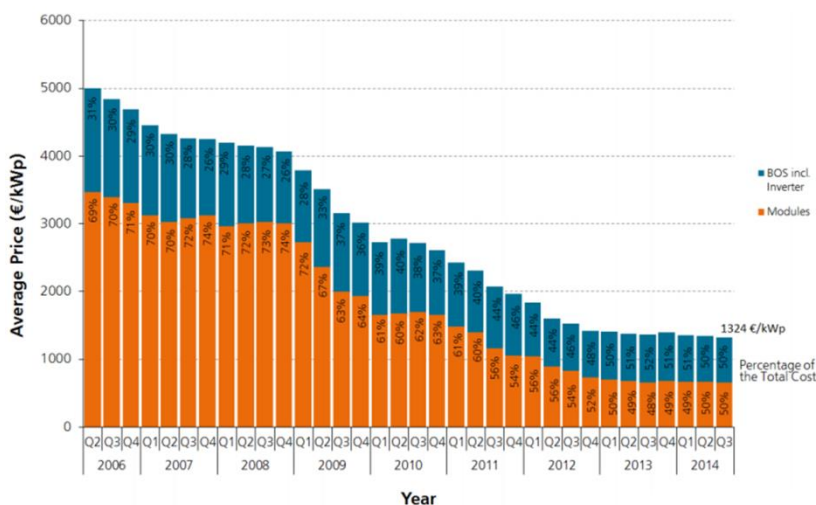


Figure 19: Evolution of average price for PV rooftop systems in Germany, including percentage of module cost in final system price (BSW, 2014).

Grid parity has been reached in many locations throughout the world, such as sunnier parts of the United States (California, Arizona, etc.), Italy and Australia, but also locations with high grid retail prices, such as Germany, Japan, Brazil, among others. A schematic of this phenomenon can be seen in Figure 20, where a combination of rising grid electricity prices (orange band, mostly pegged to oil prices) and declining costs of PV (green band, achieved for example with mass scale production and innovation), eventually leverages PV to a competitive state against other forms of electricity generation (LUTHER, 2009).

In late 2012, it was announced that Singapore had reached grid-parity (STRAITS_TIMES, 2012) for bigger-size PV systems (> 500 kW_p) versus grid retail electricity prices (of ~0.22 USD/kWh then). In 2015, even with declining worldwide oil prices causing grid tariffs to come

down to nearly 0.15 USD/kWh, grid parity is still present across all PV project sizes (BIERI *et al.*, 2015).

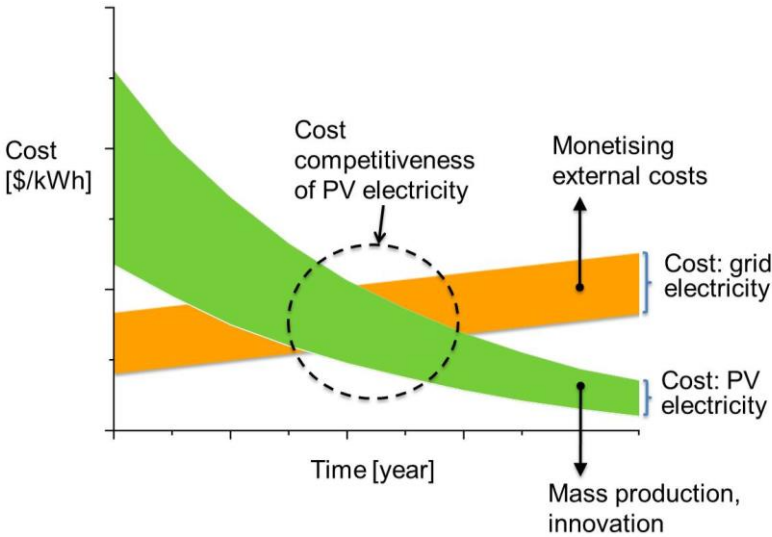


Figure 20: Grid parity drivers (LUTHER, 2009).

In Brazil, depending on the local tariff and solar resource irradiation resource availability, grid parity has also been present since 2012 (MONTENEGRO, 2013).

In order to understand corresponding costs of the PV technology in a net present value setting, equivalent to what a user would pay for electricity tariff today and thus allowing for a more straight-forward comparison with grid electricity prices, the levelized cost of electricity (LCOE) is introduced (Equation 1):

$$\text{LCOE} = \frac{\text{Total life cycle cost}}{\text{Total lifetime energy production}} \quad (1)$$

The formula can be further expanded (Equation 2) where the total life cost of the system is further developed into initial investment added to annual costs incurred (e.g. cleaning costs, if chosen), minus a depreciation value and a final residual value at the end of the lifetime of the system. This value is divided by the estimated yield of the system, deducted from an annual system degradation rate.

$$= \frac{\text{Initial investment} - \sum_{n=1}^N \frac{\text{Depreciation}_n}{(1+\text{discount rate})^n} + \sum_{n=1}^N \frac{(\text{Annual cost})_n}{(1+\text{discount rate})^n} - \frac{\text{Residual value}}{(1+\text{discount rate})^N}}{\sum_{n=1}^N \frac{\text{Initial yield} \times (1 - \text{System degradation rate})^n}{(1+\text{discount rate})^n}} \quad (2)$$

A list of countries experiencing grid parity and the gap between solar PV LCOE and electricity prices can be seen in Figure 21 (REUTER0053, 2015). As an example of this grid parity gauging as of 2015, a LCOE for a solar PV system in Brazil would be estimated at ~18 USD cents per kWh, whereas the grid electricity would be practically double of that, at ~36 USD cents per kWh.

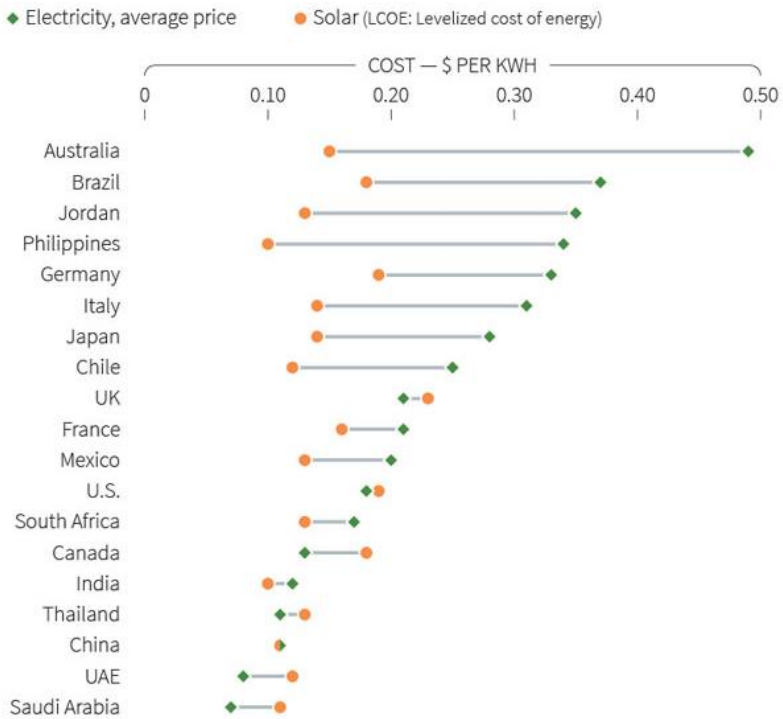


Figure 21: Key countries around the world experiencing grid parity (REUTERS, 2015).

2.1.3 Grid integration challenges

As PV markets mature, such as the case of countries like Germany or Italy, deployment rates tend to stabilize (Germany ~8% CAGR between 2012 and 2014, Italy ~6%, values that are much lower than worldwide growth rates, ~33% for the same period). Nonetheless, the steady deployment of systems, coupled with the adoption of energy efficiency practices, means more demand is met by photovoltaics, which become embedded and permanently relevant in a country's energy generation mix (at ~7% demand contribution levels for Germany, Italy and Greece (SPE, 2015)).

As an example of photovoltaics as a massive contributor to a country's grid on a day-to-day basis, inverter manufacturer SMA uses data output from PV systems in Germany under their portfolio to extrapolate power AC output data for the remainder capacity of the country in order to plot energy production graphs such as the ones shown in Figure 22 (SMA, 2015a). The total peak output power for a very sunny day in 2012 (25th May, shown on the top left of the figure), assuming a PV installed capacity in the country at that date of circa 27 GW_p, was 21.1 GW. With Germany having peak power usage at circa 80 GW, that was translated into solar PV covering more than 1/4 of the needs of the entire country at that particular instant in time. In a check on the same website at near summer times of the years 2013, 2014 and 2015, the following peaks were obtained: 24.2, 25.9 and 27.6 GW, respectively. Between the first year shown in the figure (2012) and the fourth (2015), the peak has jumped 6.5 GW, or a CAGR of 7%, in line with verified photovoltaic market growth rates.

As much as Figure 22 showed peak days throughout Germany, which help with peak shaving but which, at certain occasions, forces power to be exported to nearby countries, Figure 23 highlights another concern of utilities everywhere – days with varying power output among regions (left of the figure, with the example showing higher irradiance values in the South part of the country and cloudy conditions in the North); and days with very low production due to bad weather throughout (right of figure). In the example shown, the peak for the entire country on Christmas 2014 was registered to be only 4.2 GW, circa 15% of the high irradiance levels shown in Figure 22.

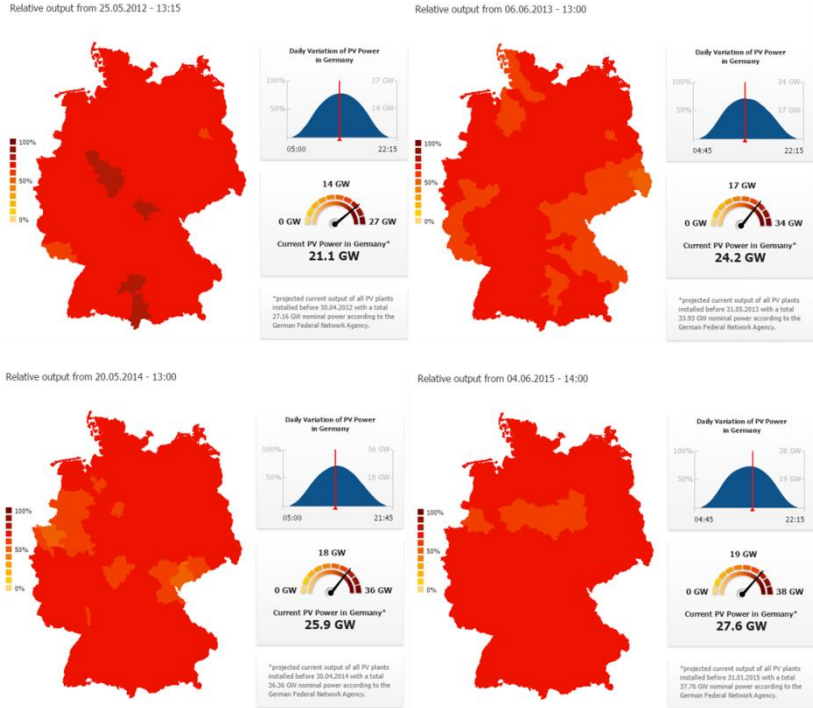


Figure 22: Progressive solar PV production peaks in Germany from sunny day examples from 2012 to 2015, adapted from (SMA, 2015a).

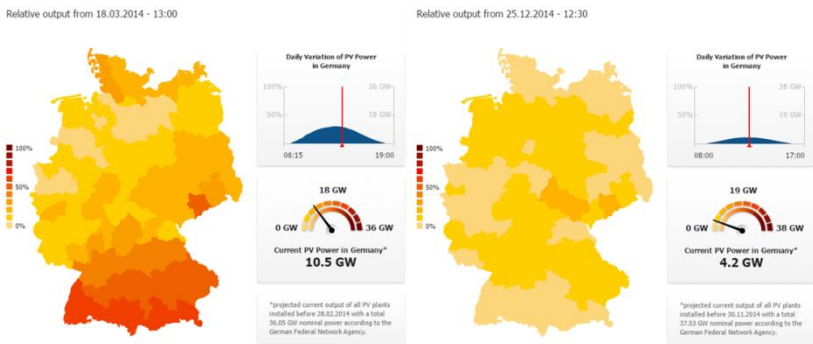


Figure 23: Variable and low irradiation day examples in Germany in 2015, adapted from (SMA, 2015a).

Installation rates in Europe are stabilizing at ~5% growth levels per annum. The moment in time when PV contributes considerably, even for a short-period of time to the entire electrical system, is already upon utility grids. To somewhat add to the concern level normally associated with PV, most of the National Renewable Action Plans (NREAPs) ended up far exceeding the expected targets for PV deployment set for the year 2020, which have already been met in the majority of European countries (IEA, 2011).

Other technical concerns arise from the presence of PV. A classic example is anti-islanding, which is the ability of a PV inverter to disconnect from the grid in case the latter is absent. Inverters will usually disconnect from the grid if voltage is not detected after 0.2 milliseconds (SMA, 2013b). From Figure 24, other key inverter post-manufacturing quality checks, tailored to provide resilience to these devices and the grid, can be seen.

AC communication	OK
<ul style="list-style-type: none"> Quality test - checking the communication with the inverter in night operation 	
Endurance test	OK
<ul style="list-style-type: none"> Quality test / burn-in test - operation of the inverter under full load 	
Leakage current monitoring	OK
<ul style="list-style-type: none"> Normative routine test of the RCMU - residual-current monitoring unit - according to VDE0126-1-1 	
Checking firmware versions	OK
<ul style="list-style-type: none"> Quality test - checking for approved firmware versions 	
HV test	OK
<ul style="list-style-type: none"> Normative routine test of electric strength by means of high-voltage test, e.g., according to EN 50178, EN 62109-1 or UL 1741 	
RISO check	OK
<ul style="list-style-type: none"> Normative routine test in accordance with VDE0126-1-1 - checking the insulation fault detection (on the DC side) 	
Vac adjust	OK
<ul style="list-style-type: none"> Normative routine test in accordance with VDE0126-1-1 - calibration of the grid voltage measurement 	
Checking of the measuring accuracy	OK
<ul style="list-style-type: none"> Quality test - checking the measuring accuracy of non-safety-relevant parameters 	
Energy test	OK
<ul style="list-style-type: none"> Quality test - checking the grid feed-in power over time 	

Figure 24: Inverter quality assurance report, highlighting some of the tests which individual units go through (SMA, 2013b).

As the topic of grid integration for huge levels of PV was identified, the IEA Photovoltaic Power System Program (PVPS) then created Task 14 with the goal of studying high penetration of PV systems in electricity grids. The Austrian Institute of Technology (AIT) is the operating agent of the task and identified challenges in the power system

and regional distribution levels for PV integration, as shown in Table 3 (AIT, 2012).

Table 3: Challenges and solutions to large-scale PV systems integration (AIT, 2012)

Power System Level	Regional Distribution Level
Managing variability of supply with PV	Managing voltage profiles
Ensuring security of supply	Avoiding overloading components
Matching supply and demand	Transforming passive distribution into active grids
Ensuring frequency stability	Integrating PV into smart grids

Germany's grid has progressively experienced higher levels of solar PV deployment as the years progressed. Figure 25 further depicts this phenomenon with the reverse power flow observed at a 110/22 kV substation in the service area of Bayernwerk AG, in Southern Germany. It can be detected that with the passing of time, the levels of AC power being fed into the grid increased summer by summer (STETZ *et al.*, 2014).

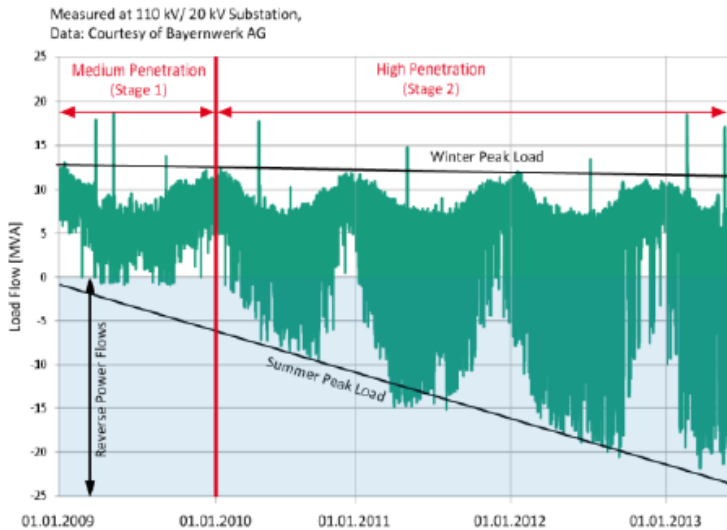


Figure 25: Power flow measured at 110/22 kV substation in Bavaria, South Germany, between 2009 and 2013 (STETZ *et al.*, 2014).

As ratios of solar PV increase in electricity mixes, new standards arise, as well as a deeper understanding of the challenges (BRAUN *et al.*, 2012). As an example of a future dominated by renewable energy generation, on a sunny, windy and cool spring weekend day in Germany, solar PV and wind power together are able to meet more than 50% of the noon peak loads. In those situations, base-load power plants need to be ramped down in order to guarantee power system stability (STETZ *et al.*, 2015).

Although perceived as a negative contributor to the grid in terms of keeping its stability, ongoing research efforts highlight that photovoltaics actually have shown to have a positive contribution to grid feeders (RÜTHER *et al.*, 2008).

2.1.4 Variability aspect of the PV technology

A further, and perhaps more intuitive challenge to photovoltaics integration, is the inconstant characteristic of the solar PV output. Short-term variability (caused by cloud motion) is the most notable contributor (see Figure 26 as an example of intra-day irradiance variability in Singapore).

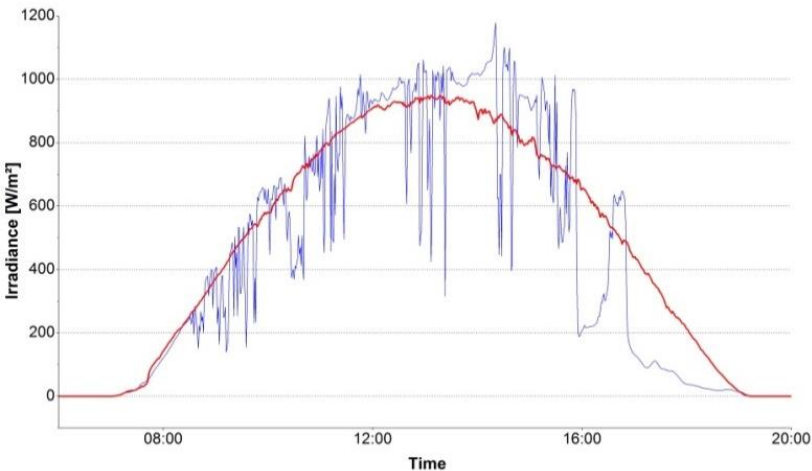


Figure 26: Measured clear sky irradiance day in Singapore (in red) and a day with broken cloud conditions (in blue) (SERIS, 2011).

Seasonal variability can be relatively well predicted, especially with the usage of typical meteorological year (TMY) irradiation sources,

which usually carry a $\pm 10\%$ maximum year-on-year variability, based on a minimum number of years of records of ten, but preferably thirty years (WILCOX and MARION, 2008). TMYs, however, do not address short-term variability (intra-day or a few days ahead).

In a relatively large area country like Germany, the variability of the solar irradiation distribution is smoothened with distance via the so called geographical smoothing. Additionally, even in case of peak variations such as the condition illustrated in Figure 23, export of peak electricity to nearby countries, e.g. Czech Republic for the case of the state of Bavaria in Southern Germany, guarantee system stability.

Hoff and Perez introduced the topic of the smoothing effect PV power output has over geographical distance (HOFF and PEREZ, 2010). Lave et al. fine-tuned such methods by using spatial-temporal correlations and tested their method at both a distributed fleet of residential PV systems in Japan as well as at a utility-scale PV plant in Nevada, USA (LAVE *et al.*, 2013).

Taking the case of Singapore as an opposite example, one would face a much more challenging environment for operations. Firstly, geographical smoothing is limited due to the small country area (roughly 40x20 km of dimensions). Occurrences of low or nearly zero irradiance levels in one area of the island, with high levels in the other, are possible (see Figure 27).

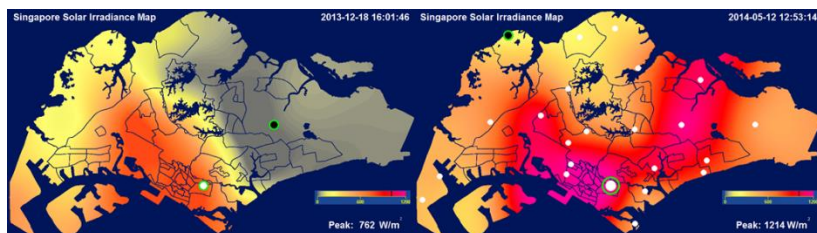


Figure 27: Irradiance variability in Singapore with examples of a) an instant with half of the island covered by rain (left) and b) high peaks of irradiance and cloudy conditions (source: SERIS).

2.1.5 PV market development and future outlook

As it was discussed in section 1.1, the development of solar PV during the past one and a half decades has been tremendous, with ~178 GW_p (SPE, 2015) of systems deployed to-date from almost negligible levels at the turn of the century.

Although markets in Europe will not be as robust as they used to be in recent years, the vigorous demand in new solar frontiers around the world is likely enough to sustain the overall global growth figures. Moving forward, major regions for PV development will be located primarily in Asia, with a key role expected to be played by China, Japan (see Japanese town with high penetration of PV in Figure 28) and India, all targeted to be top-five leaders in annual deployments. The United States and Brazil, two continental-area countries, are also poised to advance MW scale solar PV deployments in the near to medium future.



Figure 28: Japanese town with high penetration of residential solar PV systems (UEDA, 2010).

SolarPower Europe predicts that by 2019, the annual size of the world solar PV market could be anywhere between nearly 400 and 540 GW_p, see Figure 29 (SPE, 2015).

All in all, the steady growth of mature markets and the explosive doubling and tripling of capacities at new developing ones put solar photovoltaics in a position to become the renewable energy source of choice for the future of humanity. The IEA reports that PV could contribute 16% of the entire global electricity needs by 2050 (IEA, 2014b).

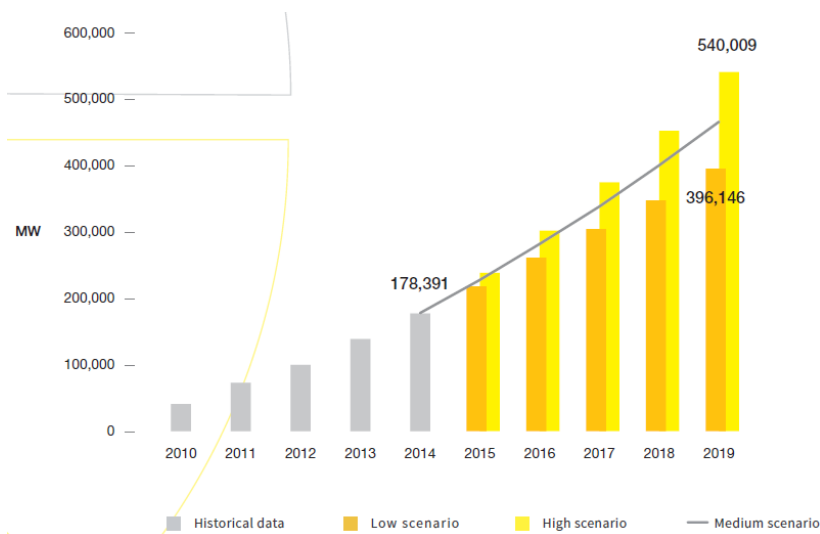


Figure 29: Future scenarios for the total volume of PV systems deployed worldwide up to 2019 (SPE, 2015).

Looking beyond, in its report on world future energy scenarios, Shell proposed two distinct visions leading to the year 2100 – one focused on the maintenance of the *status quo*, with increased expenditure on technology for exploration of existing and new sources of fossil-fuels; the other, a future where a greater focus on renewable energy deployment is at play. In the second vision, it is expected that solar PV will power more than one third of the entire humanity’s energy needs by 2100 (SHELL, 2013).

2.2 SOLAR IRRADIANCE AT THE EARTH'S SURFACE

2.2.1 Overview on solar irradiance

The solar energy resource availability at the Earth's surface has a wide range of applications ranging from meteorology, as the most classic example, to engineering, agriculture, medical fields and other areas of sciences (BADESCU, 2008). For the purpose of photovoltaic applications, it has had a major role in a region's solar potential assessment in order to estimate yield reports on the generation capabilities of a PV system, likewise for other solar-based technologies (such as concentrated solar photovoltaics, concentrated solar power and solar thermal). However, moving forward, a secondary aspect of solar irradiance starts to take the forefront of investigations – the forecasting of the solar resource ahead of time for a given location where renewable energy technologies, which are dependent on solar power, are located.

Acquiring solar irradiance data has been challenging for research groups around the world. In the United States, the ratio of stations collecting temperature data to those collecting irradiance measurements is 100:1. That number becomes even more staggering if the entire world is taken into account – 500:1 (BADESCU, 2008). For Singapore, as another example, two known irradiance stations are part of the long-term data acquisition network – Changi Airport and Paya Lebar Airbase (see both circled in red in Figure 30). In contrast, the National Environment Agency of Singapore (NEA) has officially 63 meteorological stations in its network (with ambient temperature collection stations, seen as a background map in Figure 30, (NEA, 2013a)), thus the discussed ratio of ambient temperature stations to irradiance stations would be ~30:1 for the country.

The solar irradiation reaching the top of the atmosphere, referred to as “solar constant”, has an approximate value of $1,366.1 \text{ W/m}^2$ (GUEYMARD, 2004). However, this is an old and outdated figure and has been since then corrected to $1,361 \text{ W/m}^2$ based on the Solar Radiation and Climate Experiment (SORCE) satellite (ROTTMAN, 2005). This total accounts for the integration on all possible wavelengths of the spectrum and is also associated with an air mass value of zero (“AM0”).

Air mass 1 (“AM1”) takes place at zenith, when the sun is at the highest position in the sky for a given location, thus the shortest atmosphere length between the Earth's surface and space. At that position, and taking atmosphere losses into account, such as absorption and refraction by molecules in the air, Rayleigh scattering, aerosol

presence, bring the irradiance value on the surface of the planet to about $1,000 \text{ W/m}^2$.

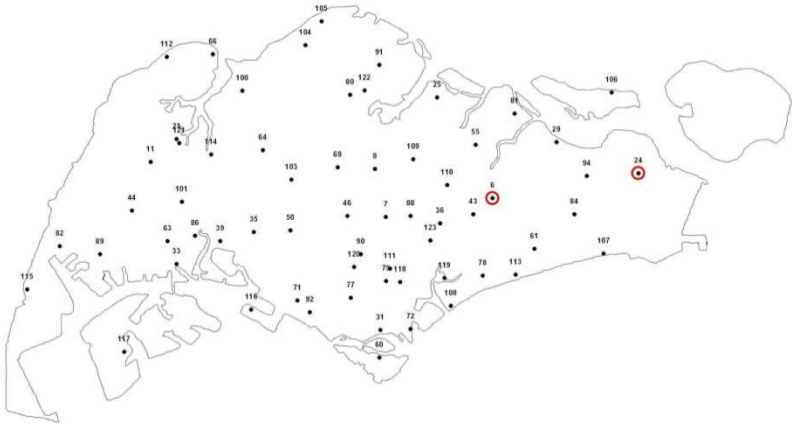


Figure 30: 63 weather stations in Singapore, with the two only government irradiance measuring stations marked in red, adapted from (NEA, 2013a).

The main components of the solar irradiation can be divided into global horizontal irradiation (GHI), diffuse horizontal irradiation (DHI) and direct normal irradiation (DNI) as the principal parameters. Figure 31 illustrates the components and decompositions of the irradiation (BADESCU, 2008).

The direct component of the irradiance (DNI, also known as the solar beam), forms an angle between a flat surface and the solar zenith angle (z), complementing this angle would be the solar elevation (h). The relationship between the components of the solar irradiance on the surface of the Earth can be described as per Equation 3.

$$\text{GHI} = \text{DNI} \cdot \cos(z) + \text{DHI} = \text{DNI} \cdot \sin(h) + \text{DHI} \quad (3)$$

For the situation of a tilted surface, typical for PV systems, Equation 3 can be further rewritten into:

$$\text{GHI} = \text{DNI} \cdot \cos(\theta) + R_d \cdot \text{DHI} + R \quad (4)$$

where θ is the incidence angle to the normal of a tilted surface, R_d is a reduction of the sky view factor and anisotropic scattering, and R is the radiation reflected from the ground into the tilted surface, also visualized

in Figure 31 (BADESCU, 2008). This factor would be dependent on the albedo of the surface.

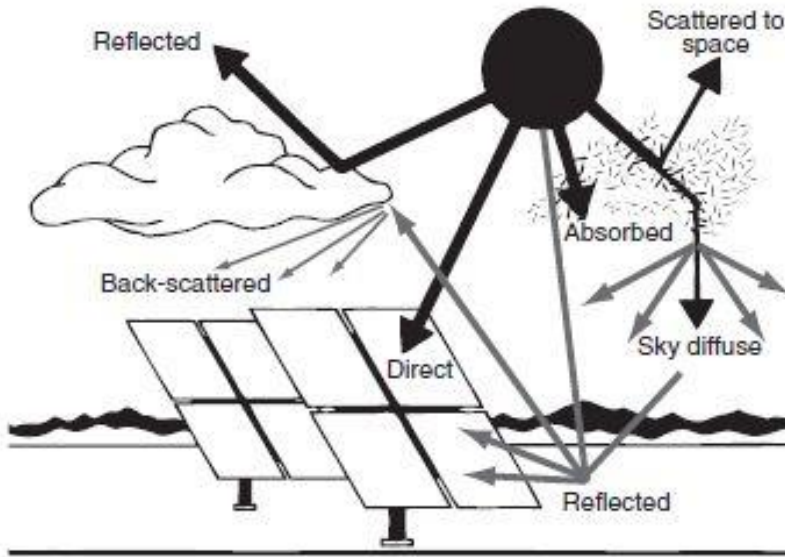


Figure 31: Solar irradiation components (BADESCU, 2008).

For solar irradiance modeling in PV applications, only the three components GHI, DNI and DHI are normally used. Section 2.2.3 addresses these parameters.

Figure 32 is a representation of the sun path diagrams for three locations of the world – Singapore ($\sim 1^\circ\text{N}$, left), Florianópolis, Brazil ($\sim 27^\circ\text{S}$, middle) and Freiburg, Germany ($\sim 48^\circ\text{N}$, right), which describe the sun's path on the sky for a given year (GAISMA, 2013). These locations were chosen here to illustrate such polar charts for a combination of case studies, namely an Equatorial location, one in the Southern hemisphere, and one in the Northern hemisphere, respectively. At the same time, the varying absolute value for the latitude (from latitudes nearly zero, to 48, through 27 degrees), allows for visualization of the variation path of the sun in the sky at three considerably different locations of the world.

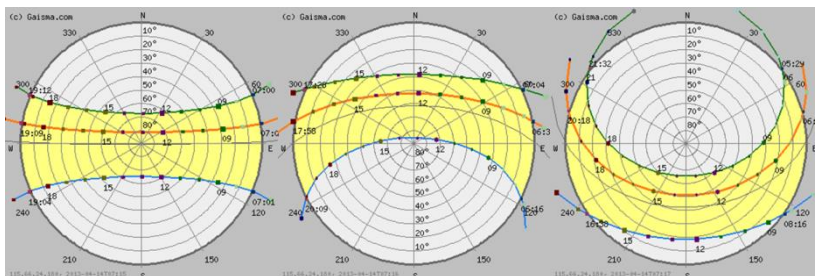


Figure 32: Sun path diagrams for the cities of Singapore, Florianópolis and Freiburg (from left to right), adapted from (GAISMA, 2013).

The green path in Figure 32 is equivalent to the position of the sun in the sky on June 20/21 (summer solstice for a location in the Northern hemisphere such as Germany and Singapore, winter solstice for a location in the Southern hemisphere, such as shown for Florianópolis). Conversely, the blue path represents the solstice for the opposite yearly situation (i.e. on December 21/22). The gray paths are the equinoxes in March and September, where the sun-hours within a day have the same duration. Finally, the orange line represents the sun path on the day of the access to the website, in this case 14th April (GAISMA, 2013).

The sun path for a location closer to the Equator is relatively equal in terms of the sun's "traveling path" in the Northern or Southern portions of the sky, thus the duration of daylight is similar in length and longer than at locations away from the Equator. This guarantees, in general, higher irradiation records for locations in the tropics.

Having the sun directly overhead cannot be achieved on a location outside of the region between the two tropics ($\sim 23^\circ\text{N/S}$), also possible to be visualized in Figure 32 for both Florianópolis ($\sim 27^\circ\text{S}$, middle) and Freiburg ($\sim 48^\circ\text{N}$, right), as seen by the yellow sun path range not overlaying the central circle representing a standing person/PV system on the polar chart.

For solar resource maximization, it is common to tilt a PV system to the latitude of a location and towards the opposite hemisphere where the system is installed (DGS, 2008). This is the primary reason for modules being tilted (discussed in section 2.2.3). Secondly, it is also important to tilt modules to guarantee the so called "self-cleaning effect" from the rain onto the front glass surface of the modules to prevent soiling accumulation (covered in section 2.5.2).

2.2.2 Measuring solar irradiance

For measurements of the sun's irradiance, three types of detectors are used: (1) thermopile, (2) black-body cavity and (3) solid-state (semiconductor) sensors (BADESCU, 2008). These devices work via different physical principles from one another and thus register different values at different accuracies.

Thermopiles are devices that convert thermal energy to electrical energy, with the generation of a voltage output based on the heat flux from the solar irradiance (for the case of pyranometers). Thermopile-based detectors cover the whole shortwave spectrum, however limited to 290-2,800 nm (used in most pyranometers) (BADESCU, 2008).

Solid-state (semiconductor) sensors react to a certain irradiance value by generating a current, which is proportional to the radiation flux. As they are typically made of silicon, which has a narrower spectral response (300-1,200 nm) (KING *et al.*, 2004), these devices do not pick up the broad range of the sun's irradiance as a thermopile does, making them less accurate measuring devices.

Figure 33 shows three types of irradiance devices installed at the SERIS meteorological station, all measuring the global horizontal irradiance – a class II research-grade pyranometer (thermopile, CMP11 from company Kipp & Zonen, far left), a second type of pyranometer (also a thermopile, SPN1 from Delta-T, next to it, which also measures diffuse horizontal irradiance within the same device via a shading mask) and a silicon sensor (semiconductor, here from maker Mencke & Tegtmeier). The comparison output for GHI readings highlights the spectral response effects, especially when benchmarking the silicon sensor, which has a narrower spectral response against the other sensors.



Figure 33: Three irradiance devices measuring global horizontal irradiance located at the SERIS meteorological station in Singapore (source: SERIS).

Figure 34 shows the GHI readings for all the previously mentioned sensors under a clear sky condition in Singapore in 1-min time steps. The silicon sensor, which is further calibrated at the Fraunhofer Institute for Solar Energy Systems (ISE), measured 3.9% less irradiation than the CMP11 pyranometer for that day. The SPN1 readings highlight variations in accuracy even between such devices working under the same physical principle.

These readings highlight the different spectral response of these devices, also a further conclusion from Figure 17 whereby various PV technologies would behave differently accordingly to the spectrum signature of the solar irradiation at a particular location.

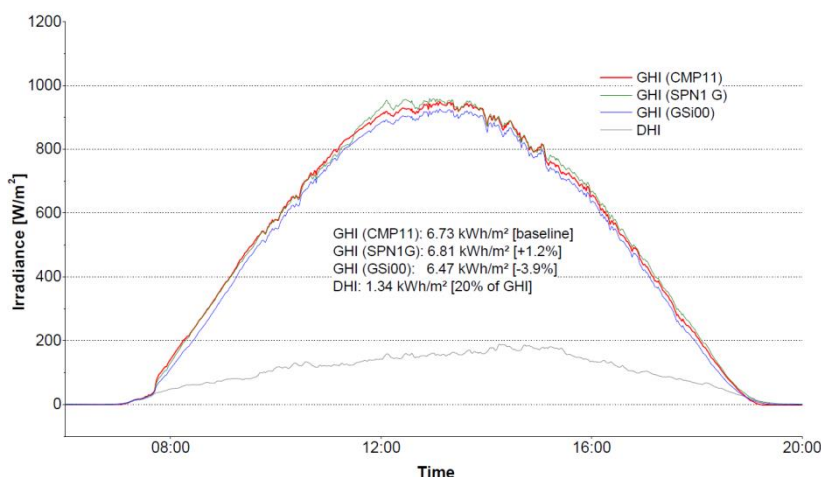


Figure 34: GHI and DHI readings on a clear sky day in Singapore measured by several irradiance devices (source: SERIS).

Additionally, it can be seen that the DHI component for the given date accounts for 20% of the GHI total, a situation which is rare for a tropical location such as Singapore, later discussed in more detail under section 2.3.2.

2.2.3 Irradiance models for PV applications

Models to predict the irradiance on a tilted plane are important in helping with the assessment of the performance of PV systems (see 2.5.1). Some of these models perform more accurately than others. Perez, Liu & Jordan and Klucher are a few of the leading models in this field.

In the past, many authors presented their models to predict solar radiation on inclined surfaces from the measured global horizontal irradiance (GHI) and diffuse horizontal irradiance (DHI) (GUEYMARD, 1987; HAY and DAVIES, 1980; KLUCHER, 1979; LIU and JORDAN, 1961; PEREZ *et al.*, 1990; PEREZ *et al.*, 1987; PEREZ *et al.*, 1986; TEMPS and COULSON, 1977). The models usually differ in the way the diffuse radiation is calculated. The first generation model proposed the conversion of the global horizontal to the tilted irradiation by assuming that the total sky diffuse irradiation content is isotropically distributed (LIU and JORDAN, 1961). However, this assumption is not strictly true. Newer models treat the diffuse radiation component as anisotropically distributed, where the irradiance is treated as the sum of circumsolar and background sky diffuse components (GUEYMARD, 1987; HAY and DAVIES, 1980; KLUCHER, 1979; PEREZ *et al.*, 1990; PEREZ *et al.*, 1987; PEREZ *et al.*, 1986; TEMPS and COULSON, 1977).

Figure 35 shows one of the findings of Khoo, Nobre *et al.* where the application of these irradiance models in Singapore was conducted. It illustrates a polar contour plot of annual tilted irradiance for various orientations and tilt angles in the country. It can be seen that a surface oriented towards East with tilt angle of $\sim 10^\circ$ will yield maximum annual irradiation (equal to $1,535 \text{ kWh/m}^2$) (KHOO, NOBRE, *et al.*, 2014). This could be explained from the fact that Singapore is usually sunnier in the morning part than in the afternoon as indicated and also due to late afternoon rain showers, typical of a tropical location.

Secondly, a publication by Yang, Dong *et al.* addressed transposition and decomposition models via a reverse process of modeling irradiance at tilted surfaces by utilizing data from tilted silicon sensors themselves deployed in the field at PV system sites, with the aim of finding GHI and then validate the conversion from GHI readings recorded by another irradiance instrument on site (YANG, DONG, *et al.*, 2013). The work demonstrated low errors in the conversion between tilted global irradiation in the plane of the array of a PV system back into GHI values. Such finding allows that irradiance devices deployed at PV systems at a certain location be converted into GHI values and contribute to solar resource mapping for a region and even forecasting efforts.

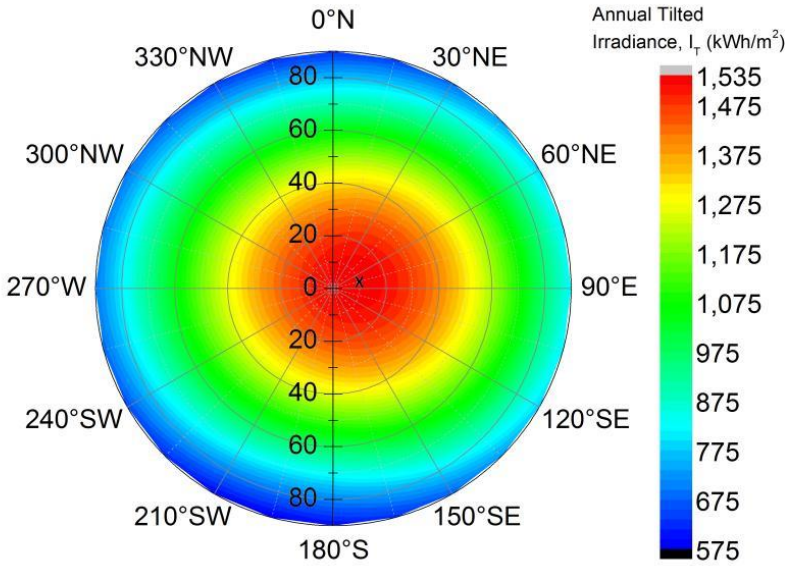


Figure 35: Extrapolation of empirical data for the SERIS meteorological station showing highest point of irradiation capture for ~10° of tilt, East oriented (KHOO, NOBRE, *et al.*, 2014).

A further contribution addressed improvements of the Perez model for the target location of Singapore by making adjustments to the model via readings from available flat and tilted irradiance devices (YANG, D., YE, Z., *et al.*, 2014). Notwithstanding the mentioned publications, the Perez model still provides sufficiently low errors, also for a tropical location in Singapore, thus being commonly used for simulations for projects in the Southeast Asia region and for modeling within this thesis.

2.2.4 Irradiation data sources and considerations

In order to work with irradiance models for a certain region of the world for any particular goal – but especially for renewable energy (e.g. resource assessment for photovoltaics applications) – one usually sets out to find existing historical data for the site of interest. That is often not easy as the availability of ground irradiance data is poorly linked with the availability of meteorological stations (as presented in 2.2.1).

A solution around that would be satellite data. However, data from such imagery inherently carry complications, such as accuracy compromises between temporal and spatial synchronization to Earth's ground measurements for later validation. Moreover, some sources have been known to overestimate values due to difficulty in accounting for terrain and other geological formations. NASA satellite-derived data (NASA, 2013) is a good example of such over- and sometimes underestimation. As a further example, the Brazilian Institute for Space Research (Instituto Nacional de Pesquisas Espaciais – INPE) in its atlas for solar irradiance resource in Brazil (PEREIRA, E.B. *et al.*, 2006) has reported overestimation of global horizontal irradiance (GHI) values from satellite models versus ground measurements.

A typical meteorological year (TMY) is an average of at least 10 years of meteorological data from a certain location of the world. The difference between TMYs and the actual present year under evaluation could fluctuate, according to normal year-on-year variations, $\pm 10\%$ (WILCOX and MARION, 2008). Ranges venturing outside of this threshold are considered rare and are normally associated with extreme weather phenomena (e.g. during an El Niño year).

When using TMY data from a country or region, a user has to take into consideration one important aspect: the data might have been recorded from a period of time long ago, from e.g. 1960-1980. In their work, Robert et al. (ROBERT and KUMMERT, 2012) studied the effect of using older TMY data for designing net-zero energy buildings of today. It was investigated in the publication that global warming considerations and weather change should be taken into account when performing simulations with older irradiation data, so that results do not deviate from what the weather will be like 20-30 years from now.

Another irradiation database source commonly used in PV applications is from the software Meteonorm, from company Meteotest, with over 8,000 weather stations worldwide. The database is made available in the commonly-used, commercial-based PV system simulation software PVSYS (METEOTEST, 2015).

2.3 CHARACTERIZING TROPICAL CLIMATE

2.3.1 Preliminary remarks

When dealing with solar irradiance forecasting and, at the same time, with the performance of photovoltaic systems based on a given solar energy resource, one must understand the weather characteristics of the location under investigation.

For Singapore, the country covered in this thesis, high average daily ambient temperatures and relative humidity are found year round. Located at 1 degree North of the Equator, and having a climate classified exclusively as tropical (FONG, 2012), Singapore has little or unnoticeable seasons, except for a clear differentiation between rainy and dry seasons, characterized by the presence of monsoons.

For a PV system, the local weather conditions can be translated into what circumstances an installation experiences on a daily basis. As an example, Figure 36 shows module temperatures in Germany and in Singapore, highlighting the warmer condition the tropical location system experiences in relation to the temperate location. At $1,000 \text{ W/m}^2$, a PV panel in Singapore is $\sim 10^\circ \text{C}$ hotter than in Germany.

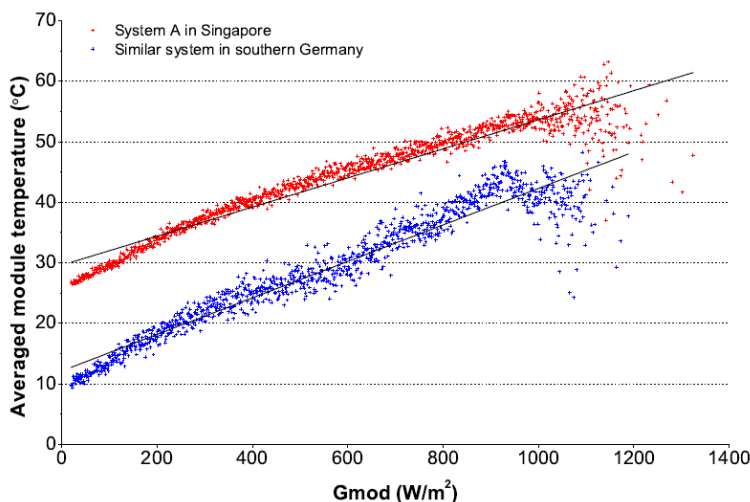


Figure 36: Module temperature increase versus irradiance on module plane as registered in Singapore and Germany (NOBRE et al., 2015 (under preparation)).

2.3.2 Singapore climate

Storms are common in tropical regions. For the case of Singapore, fast approaching rain clouds from Malaysia (from the North) and from Indonesia (from the East, West and South) can change weather conditions and irradiance levels quite rapidly. As an example, and as previously shown in Figure 11, a “Sumatra squall”, a commonly known weather phenomenon in the region, is characterized by a fast-moving and sudden rain-storm front originating from Indonesia, however, predominantly from the West (FONG, 2012).

There are two monsoon seasons in Singapore – a Northeastern, taking place between November and March, and a Southwestern, between April and June. The rainiest months of the year are usually November and December (FONG, 2012).

The local solar resource is abundant. A recorded TMY for annual global horizontal irradiance (GHI) and diffuse horizontal irradiance (DHI) is 1,631 and 926 kWh/m² respectively for a ground meteorological station at Changi Airport (METEONORM, 2013). These annual averages represent a diffuse share of ~57% from the total global irradiance, characterizing common cloudy conditions for Singapore.

SERIS has commissioned in May 2010 a comprehensive meteorological station, with some of its sensors seen in Figure 37. The station was deployed primarily due to the lack of PV-focused irradiance measurements available in the country. The setup possesses 9 silicon sensors installed at several tilt angles (0, 10, 20, 30 and 40 degrees facing an arbitrary orientation, followed by 4 façade silicon sensors tilted at 90 degrees, facing North, South, East and West). Additionally, the station has two pyranometers for global (GHI) and one for diffuse irradiance (DHI) as previously shown in Figure 33, among other classical meteorological sensors such as air temperature & relative humidity, wind speed & direction, and atmospheric pressure.



Figure 37: SERIS meteorological station rack, with tilted silicon sensors ranging from 0 to 40 degrees (source: SERIS).

From Figure 38, which stems from data records of the SERIS meteorological station for year 2011, it can be seen that the little seasonality in Singapore is demonstrated by a small variation of the ambient temperature profile in the country, with a daily annual average around 27-29°C. Dips can be seen between the months of November and February, which are associated with the Northeastern monsoon period.

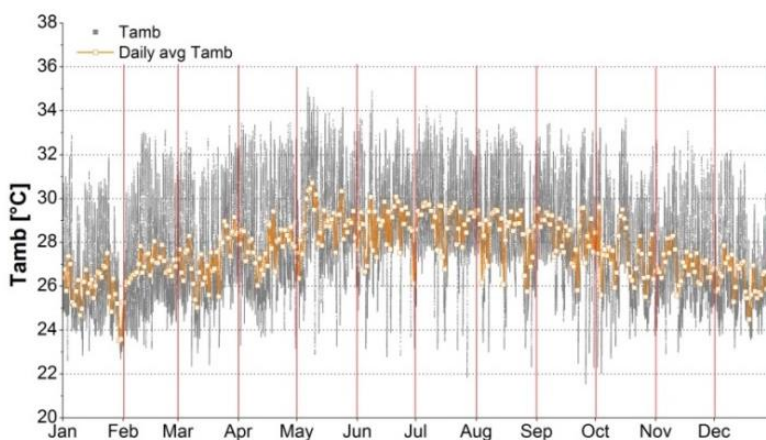


Figure 38: Ambient temperatures in Singapore for the year 2011. The daily averages are plotted in orange (SERIS, 2011).

The irradiance profile for the country also shows little seasonal variations. The SERIS meteorological station has recorded for 2011 the following results for global and diffuse irradiance components as shown in Figure 39. Important to note is the high diffuse content, registered at 55% for the year depicted (METEONORM, 2013).

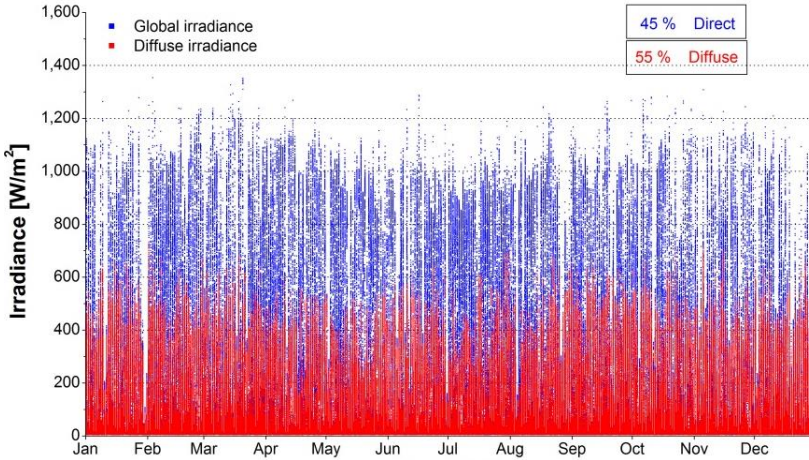


Figure 39: Global (GHI) and diffuse horizontal irradiance (DHI) in Singapore for the year 2011 (SERIS, 2011).

The numbers shown in Table 4 highlight the high diffuse irradiation component in a tropical location, with shares of diffuse over global irradiation (diffuse fraction, k_d) of above 50%. The typical meteorological year (TMY) averages for Singapore are also shown. It is extremely rare to have a total clear sky day condition in Singapore. One of such occurrences was the 5th of August 2011 and the plot of global horizontal irradiance (GHI) recorded by the SERIS meteorological station was seen in Figure 26. The cloudless day shown as a red line is an extremely rare condition, taking place once or twice throughout a year. The time series in blue, also plotted in the same figure, is more representative of a typical day in the island, with ups and downs in irradiance due to high cloud content and motion.

The clear sky example presented in Figure 26 also brings another piece of important information about irradiance conditions in the Singapore environment – the peak irradiance achieved at an approximate zenith time of 13:15 pm from that August day shows irradiances around 920-950 W/m², not reaching the theoretical value of 1,000 W/m²,

discussed in section 2.2.1. That can be explained by the fact that Singapore has high values of relative humidity (see Figure 40), thus the water vapor content in the air presents extra blockage for the light to reach the Earth's surface. Moreover, it could be inferred that the presence of aerosols in Singapore's air has levels above thresholds which would normally be found in non-heavily urbanized locations of the world.

Table 4: Typical meteorological year averages for Singapore and results for 2011 through 2014 for the SERIS meteorological station. TMY source: (METEOTEST, 2015). Other data source: SERIS.

	TMY	2011	Δ TMY	2012	Δ TMY	2013	Δ TMY	2014	Δ TMY
GHI [kWh/m ²]	1,631	1,552	-4.8%	1,595	-1.9%	1,578	-3.2%	1,658	+1.7%
DHI [kWh/m ²]	926	854	-7.8%	872	-5.8%	858	-7.3%	898	-3.0%
k_a [%]	56.8%	55.0%	-1.8%	54.7%	-2.1%	54.4%	-2.4%	54.2%	-2.6%
Tamb [°C]	27.7	27.6	-0.4%	27.8	+0.4%	27.9	+0.7%	28.0	+1.1%

In terms of relative humidity records in this tropical location, the daily average values are quite high in the 80s (see in purple in Figure 40), with daily readings ranging from 50-100% (SERIS, 2011).

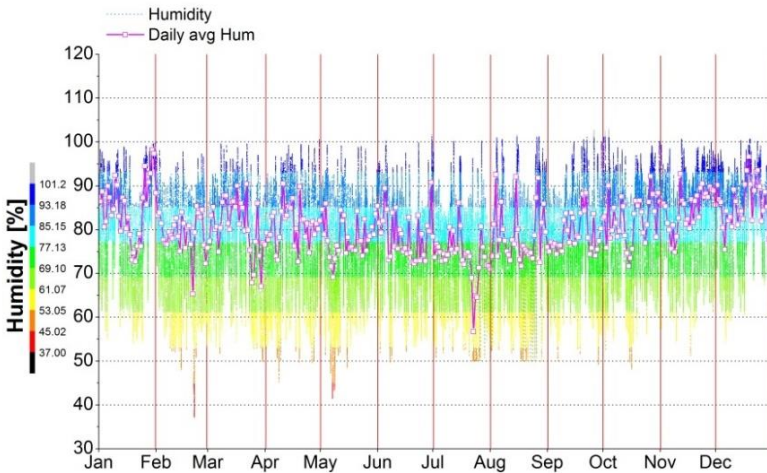


Figure 40: Relative humidity in Singapore for the year 2011 (SERIS, 2011).

In cloudy days, the so called “cloud-edge effect”, or potentially a “cloud-enhancement effect” (see Figure 41, left and right respectively), might take place whereby reflection at the cloud borders increases solar irradiation at the surface depending on the geometry sun-cloud-ground (cloud-edge effect), or light that is enhanced by a cloud working as a lens (cloud-enhancement effect), increasing irradiance measured values above the theoretical clear sky solar irradiance. Either one of these two phenomena could be seen in Figure 26 (as the blue time series), with readings going above the theoretical ground maximum baseline. Burger and R  ther (BURGER and R  THER, 2006) reported such occurrences versus PV system inverter behavior and how it can affect overall system performance. Almeida et al. reported an irradiance peak of 1,590 W/m² in S  o Paulo (ALMEIDA *et al.*, 2014).

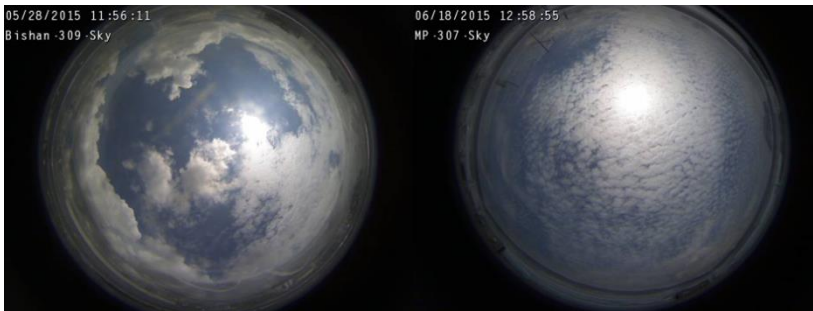


Figure 41: Examples of cloud-edge and cloud-enhancement effects, as captured by SERIS’ sky cameras and validated by ground-measurement irradiance spikes ($\text{GHI} > 1,000 \text{ W/m}^2$) on sensors (source: SERIS).

The statistics of solar irradiance in Singapore for one year (2011) are plotted in Figure 42. On the left, irradiance occurrences above 950 W/m² are equal to 4% of the cases. On the other hand, the right graph shows the irradiance energy distribution (hence irradiation itself), with circa 12% of the energy resource above the 950 W/m² threshold.

With Singapore being a small country (~720 km²) and with a relatively flat terrain, weather conditions do not vary considerably through its land area. Although some districts like Clementi (at slightly higher ground, 50-100 m AMSL) and the Bukit Timah Reserve are rainier than others, the solar irradiance resource is relatively constant, at a typical meteorological year average of 1,631 kWh/(m².yr) (METEONORM, 2013). Thus far, via SERIS’ recordings in several areas of the island

through the past five years (2010-2015), the annual irradiation records have not crossed the $\pm 10\%$ variation thresholds of the TMY.

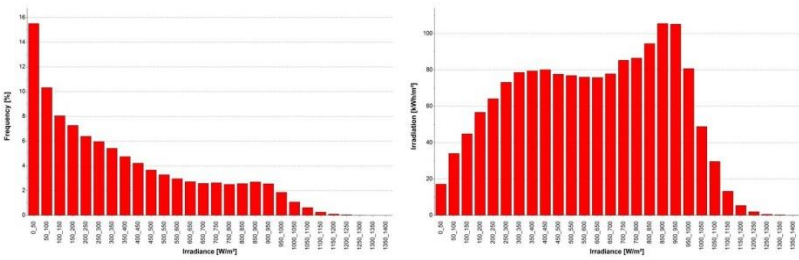


Figure 42: Irradiance frequency (left) and energy distribution (right) in Singapore for 2011 (SERIS, 2011).

Singapore’s National Environment Agency (NEA) has a weather radar (Selex Model Meteor 1600S-89 Dual Polarization S-Band radar) located at Changi Airport in the Eastern part of the island. This Doppler radar captures images as the one seen in Figure 43, but also earlier in Figure 11. The range of the radar is 70 km.

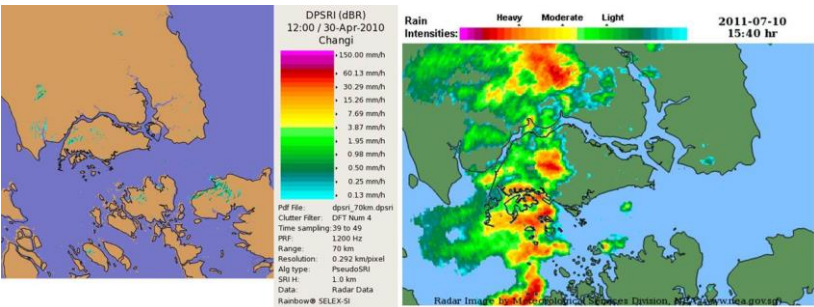


Figure 43: Singapore weather radar located at Changi Airport (FONG, 2012).

The solar energy resource in Asia is abundant. Figure 44 shows a satellite-derived irradiance map from company GeoModel Solar presenting excellent resource for upcoming PV growth markets such as China, India, Thailand, Malaysia and Philippines (SOLARGIS, 2012).

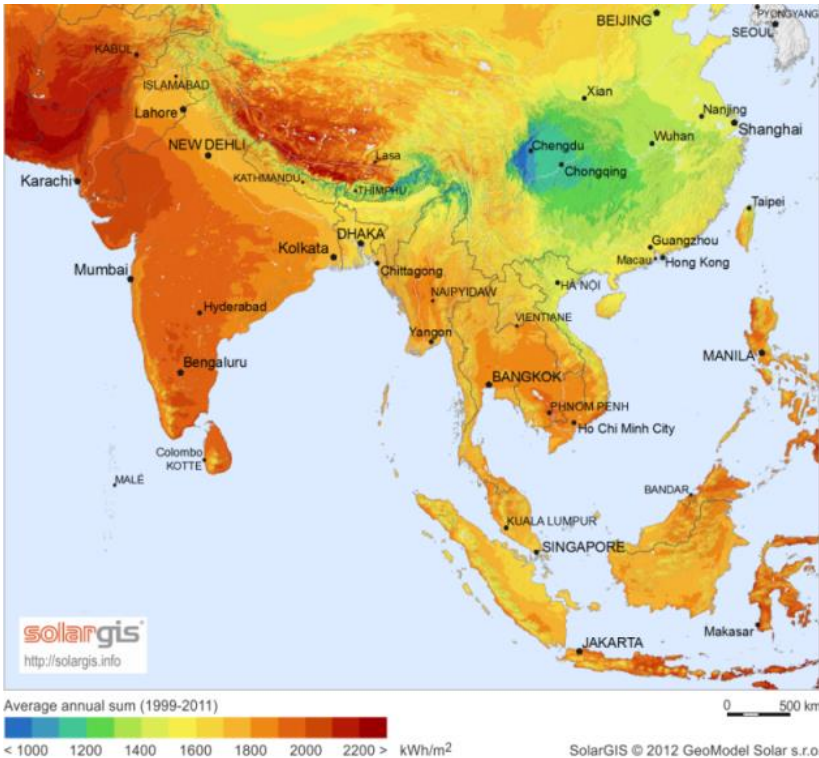


Figure 44: Average annual global horizontal irradiation profile for South and Southeast Asia (SOLARGIS, 2012).

Apart from the presence of rain showers, constant cloud motion and their lower cloud base height in the tropics make it generally difficult to predict irradiance conditions for short-term PV applications. An extreme condition observed frequently during the rainy season is a prolonged precipitation episode across the island due to its small size. Under such condition, PV power output drops virtually everywhere in Singapore, which would need to be compensated by conventional power generators in a future with a considerable share of solar PV.

Beyond fast-changing irradiance levels due to clouds, specific weather conditions occur in Singapore, especially entire days of island-wide rain showers (“washouts”) or instances when air pollution from nearby forest fires (“haze”) cover parts or the total area of the city-state (see 2.3.3). For washouts, the challenge to grid operators lies on the diminishing solar PV power output almost entirely in Singapore in a short

period of time, whereas hazy skies reduce the power output of PV systems by noticeable levels, as it is addressed in the literature review (in 2.3.3), later in a section of the method of this thesis (see 3.4.3), with results on the topic shown in 4.2.2.

Table 5 presents weather statistics for 2013 and 2014 as recorded by SERIS' meteorological station and by the National Environment Agency (NEA, for the case of the air pollution readings) (NEA, 2014b). The number of days with the occurrence of sudden storms, washouts and haze episodes are listed. It can be seen that nearly one third (32%) of the days in 2013 had drastic variations of irradiance values from the presence of sudden storms, with a smaller number taking place in 2014 (27%).

All in all, more than 40% of the days in 2013 posed some level of severe weather event, be it a storm, a washout or a hazy day (with strong air pollution concentrations). In comparison, the sunnier year of 2014 had severe episodes in about one third of the total number of days of that time span. Total annual irradiation for 2013 for an average of nine ground measurement sites spread across the island via calibrated silicon sensors was 1,491 kWh/m², whereas for 2014 for the same stations the value was 1,580 kWh/m², i.e. ~6% higher than the previous year.

Table 5: Weather statistics for 2013 and 2014 in Singapore including days with sudden storms, total “washout” conditions and with strong air pollution (“haze”) (NOBRE et al., 2015 (submitted)).

Month	Sudden storm days		Washout days		Haze days		Average daily irradiation	
	2013	2014	2013	2014	2013	2014	2013	2014
Jan	8	5	3	2	0	0	3.84	3.94
Feb	8	2	4	0	0	0	3.42	5.25
Mar	13	8	0	1	0	0	4.93	5.04
Apr	8	13	2	1	0	0	4.25	4.51
May	9	9	1	2	0	0	3.92	4.21
Jun	8	8	0	0	18	0	4.42	4.23
Jul	9	8	3	2	0	0	3.96	4.04
Aug	10	7	1	3	0	0	4.32	3.89
Sep	6	4	5	0	0	4	3.95	4.92
Oct	13	10	0	1	0	6	4.67	4.55
Nov	14	15	2	1	0	1	3.85	3.96
Dec	9	9	3	3	0	0	3.44	3.45
Total	115	98	24	16	18	11	1,491	1,580
%Year	32%	27%	7%	4%	5%	3%	n/a	n/a

Figure 45 shows a sequence of sky images encompassing the period when a sudden storm approached a ground measurement station. Every image interval is spaced 5-min apart. It can be observed in the sequence that in a matter of circa 30 minutes, the sky conditions went from relatively clear (irradiance $\sim 800 \text{ W/m}^2$) to a total “washout” condition, with irradiance nearly zero. The irradiance profile for the day is shown on the top left of the image, with a red square delineating the period which the images belong to.

In Figure 46, a typical irradiance day in Singapore is illustrated, where variable cloud cover conditions are present. The interval between sky images is also 5-min as per Figure 45. It can be observed that virtually half of the images have the sun covered by a broken cloud, which equate to an irradiance level – as per top left of the image and at that time of the day – of $\sim 400 \text{ W/m}^2$, whereas the other half of the images show nearly the entire circumference of the sun clear from clouds, with equivalent irradiances of $\sim 1,000 \text{ W/m}^2$.

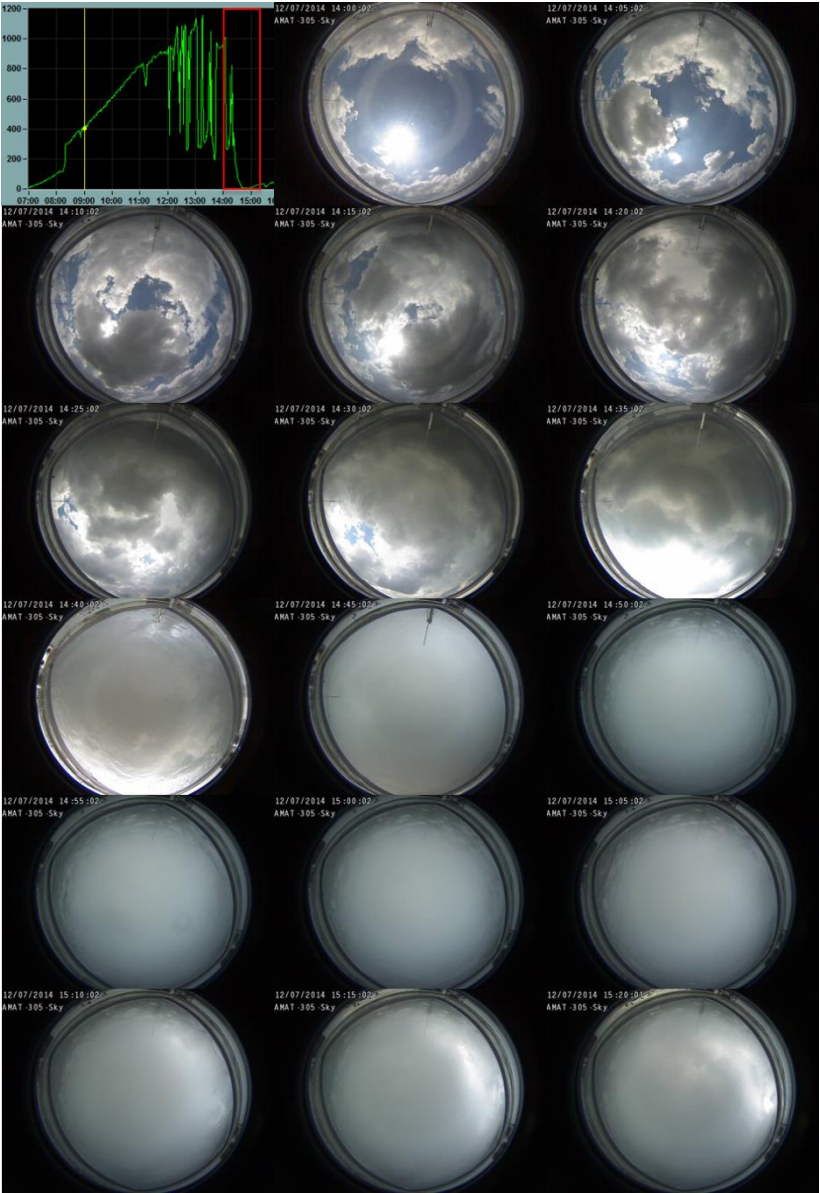


Figure 45: Sequence of sky images during a sudden approaching storm in Singapore, 14:00-15:20, in 5-min intervals (source: SERIS).

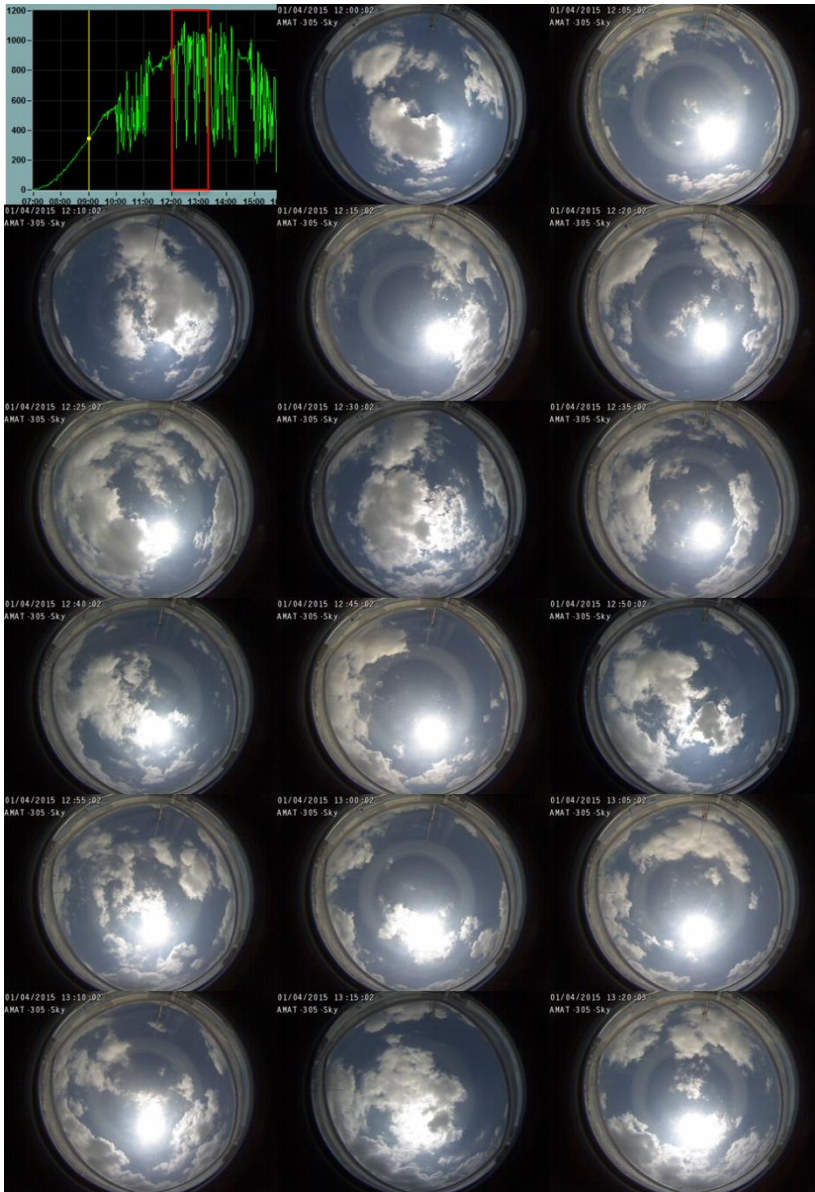


Figure 46: Sequence of sky images during a typical irradiance day in Singapore, 12:00-13:20, in 5-min intervals (source: SERIS).

When severe weather events happen as previously discussed for Singapore, they present challenges in predicting solar irradiance but also opportunities for innovative ways of improving these forecasts. Figure 47 (top) shows the observed global horizontal irradiance (green continuous line) in 15-min intervals at a central meteorological station in Singapore on a day when a sudden storm hit the island (21st Apr 2013). Such a day is similar in weather as shown in Figure 45. The 15-min ahead Auto-Regressive Integrated Moving Average (ARIMA) and Persistence irradiance forecasts are shown (red-dashed and blue-dotted lines respectively). The resulting error spikes between the forecasts and the measured values of irradiance can be seen and are also quantified in Figure 47 (bottom). Such higher uncertainties occurred due to sudden drop in irradiance caused by the arrival of dark rainy clouds. Since both ARIMA and Persistence forecasts are dependent on past information for the calculation of the step-ahead irradiance, the error in the prediction is unavoidable. Such peaks in the forecast error time series present opportunities for enhancement of short-term irradiance forecasts.

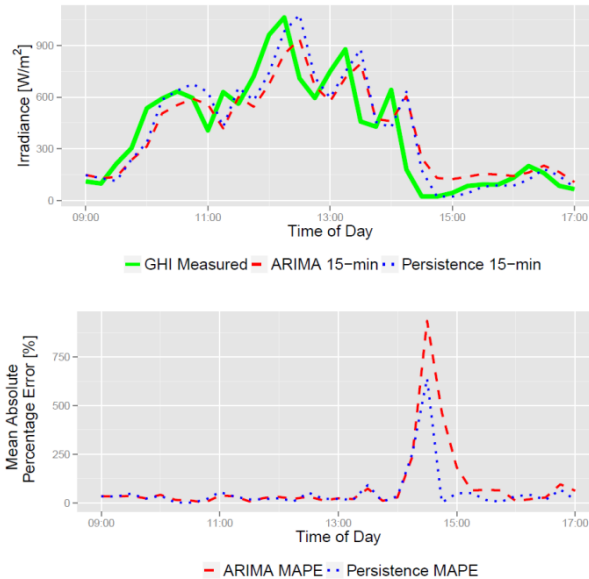


Figure 47: Top – Measured and forecast values for global horizontal irradiance (GHI) at a central meteorological site in Singapore in a day with a sudden storm, and associated errors (NOBRE et al., 2015 (submitted)).

2.3.3 Air quality issues in Southeast Asia

Air pollution caused mainly by forest fires for agricultural purposes (anthropogenic-induced haze) in Southeast Asia has become a problem in recent decades (BRAUER and HISHAM-HASHIM, 1998; FIELD et al., 2009; NICHOL, 1998; QUAH, 2002). The clearing of forest vegetation and land for farming purposes has sparked continuous political debate among nations as the resulting smog covers skies above vast land areas (HUSSAIN, 2013; ZENGKUN, 2013a). Fires often originate from within Indonesian borders, with the wind transporting smoke clouds to neighboring countries such as Singapore and Malaysia (MIETTINEN and LIEW, 2009; VELASCO and ROTH, 2012). In Singapore, located 150-300 km East of most forest/land fire “hot spots” in Sumatra, Indonesia, a so-called “haze season” is an annual event, causing reduced air quality which, in turn, trigger population and government outcry (TEO, 2013; ZENGKUN, 2013b). Depending on the prevailing wind direction, some of the fires might also originate from Borneo, ~600 km East of Singapore (VELASCO and ROTH, 2012).

Most haze periods take place between the months of August and October, which coincides with the dry monsoon season (Southwest monsoon) for the region (NEA, 2014a). Haze events are further accentuated through the absence of rain showers, as air pollution fumes take longer to dissipate. Figure 48 shows two images of the Marina Bay area in downtown Singapore under moderate and unhealthy air pollution levels during the haze crisis of June 2013.

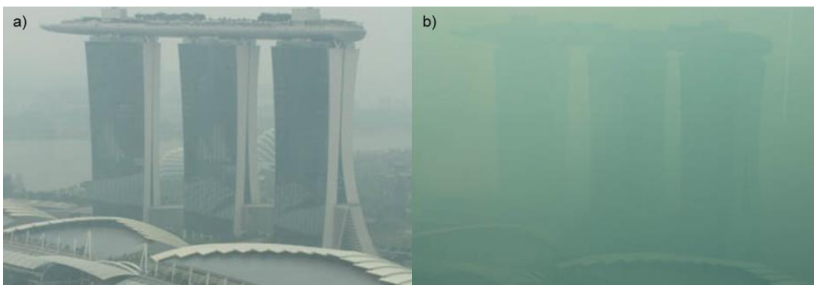


Figure 48: Images of the Marina Bay area in downtown Singapore on (a) a day with air quality in the moderate range and (b) on a day with values in the very unhealthy range. Photo courtesy of Monika Bieri-Gmuier.

The National Environment Agency of Singapore (NEA) created the Pollutant Standards Index (PSI) in 1997, which aims at informing stakeholders and the general public on daily air quality levels in the country (VELASCO and ROTH, 2012). The PSI measures concentrations of particulate matter of 2.5 microns in size (PM_{2.5}), among other pollutants (NEA, 2014b). NEA used concentration of particulate matter of 10 microns in size (PM₁₀) up to March 2014 as a primary indicator of the air pollution levels, with the PM_{2.5} readings being incorporated into the scale from April 2014 onwards. A PSI under 50 receives a qualitative rating of “good”, with other PSI ranges categorized as “moderate” (51-100), “unhealthy” (101-200), “very unhealthy” (201-300) and “hazardous” (> 300). NEA monitors PSI at 5 major areas of the island (North, South, East, West, and central) at 1-hour intervals, generating 3-hour and 24-hour pollutant concentration reports. Before the haze crisis of June 2013, PSI readings were taken in 3-hour intervals. As of early 2015, the most recent major haze event took place in June 2013, with the 24-hour average PSI reaching a peak of 246, and the 1-hour reading reaching an all-time high of 401 a few days later (NEA, 2013b). Prior to June 2013, readings were only taken every 3 hours. Figure 49 shows the historical frequencies for 24-hour PSI concentrations for the time period of 2009 to 2013, as recorded by the local environment agency. An average of 7% of all days in the 5-year span fell outside of the “good” range of the scale. The 24-hour average of PSI values for May through July 2013 (bottom) shows an 18-day strong haze period in which the pollutant index crossed into the “very unhealthy” range.

It is only natural that the first major concern when haze occurs is linked to medical implications in terms of the detrimental influence air pollution has on the health of children, elderly and individuals with heart or respiratory illnesses (FRANKENBERG et al., 2005; JAMROZIK and MUSK, 2011; SASTRY, 2002). Haze could also affect other aspects of life, such as the ecosystem and climate change, but those effects are still being investigated (VELASCO and ROTH, 2012).

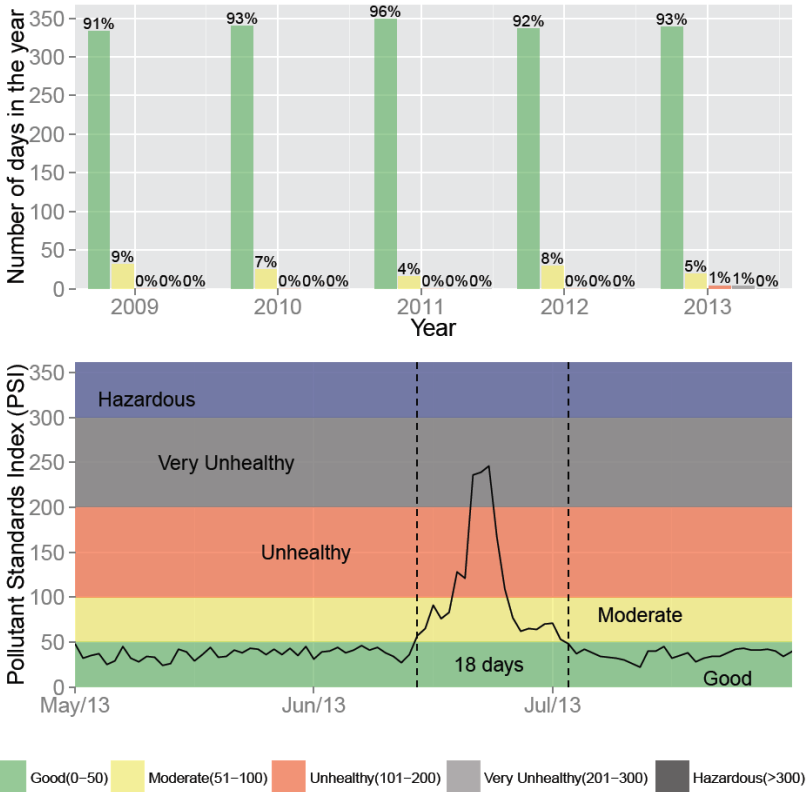


Figure 49: Five categories of the Pollution Standards Index (PSI) plotted for their annual frequencies and for a period of three months (NOBRE et al., 2015 (accepted)).

Singapore's air quality levels also get affected by its industrial sector, which includes refineries, chemical and electronic industries, and power plants for electricity generation (which however burn natural gas and hence are less polluting than e.g. coal- or oil-fired power plants) (VELASCO and ROTH, 2012). Furthermore, the country has one of the busiest ports and airports in the world, a population of 5.4 million in a small area and nearly one million vehicles on the streets (LTA, 2014). All these components present additional sources of pollutant gases and aerosols that contribute to day to day poor air quality levels in the country. A baseline PSI of 30 to 50 points is therefore seen on a regular basis (see Figure 49 bottom for PSI records prior to the haze crisis of June 2013).

In a trivial sense, the haze blocks the irradiation from reaching the Earth's surface. Although investigations on the haze influence on irradiation date back decades, they were either linked to examples in military applications (CHEN, 1975), or to medical studies (health-related hazards), such as UV exposure (ESTUPIÑÁN *et al.*, 1996). In Brazil, the presence of aerosols from forest fires was assessed to explain deviations in satellite data which are concurrently used for the assessment of irradiances levels in parts of the country (PEREIRA *et al.*, 2000). In regards to the topic of air pollution with a direct link to renewable energy usage, available works are limited, without straight results to haze and real-world PV system performance in the field. Calinoiu *et al.* reported a loss of irradiation of 20% at the surface during periods of strong air pollution in Romania with the goal of assessing the impact of such occurrences on future solar PV deployment (CALINOIU *et al.*, 2013). Faine *et al.* investigated spectral, air mass and also aerosol optical depth (turbidity) changes in their pioneer work in the 90s. Simulations were used to obtain results of the effects of the parameters to various high and low band gap PV devices (FAINE *et al.*, 1991). More recently, Fernández *et al.* evaluated change in spectra at five different locations in the world (measured by local meteorological stations). The authors evaluated the consequences of the changed spectra to their four different simulated high concentrator photovoltaic modules (FERNÁNDEZ *et al.*, 2014).

The spectrum shift caused by the haze can be observed to affect PV system performance. Liu *et al.* presented measured daily performance ratios of 10 PV systems in Singapore for the period of May 2013 to July 2013 (see Figure 50). Five amorphous silicon thin-film systems (top five curves) and five multicrystalline silicon wafer-based systems (bottom five curves) are shown. The lines represent the 3-day moving averages as a guide to the eyes, with the haze period marked by vertical dashed lines (LIU *et al.*, 2014b).

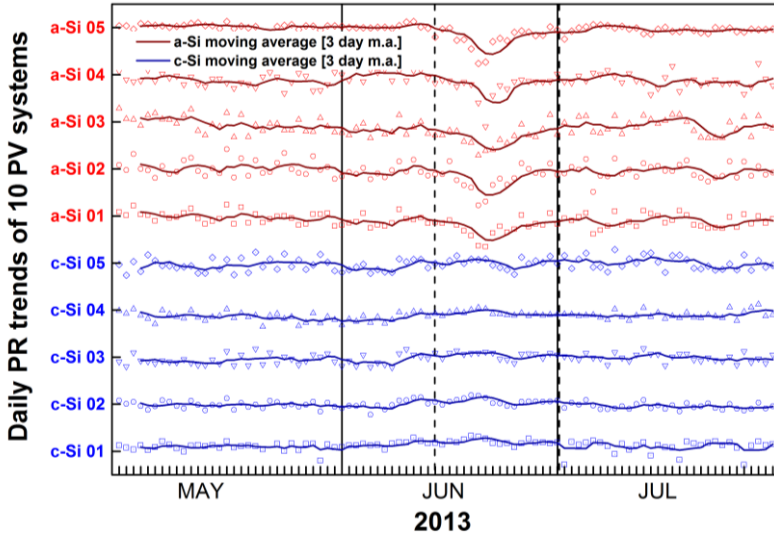


Figure 50: Measured daily performance ratios of 10 PV systems of two main technologies in Singapore for the period of May to July 2013 (LIU *et al.*, 2014b).

The influence of haze, which has been occurring on an annual basis lately in Singapore, is therefore a phenomenon that needs to be understood and quantified for a realistic assessment of the performance and yield of future PV installations. Especially during the recent haze event of June 2013, PV system owners and investors have sought for answers on the amount of energy loss which would eventually have affected their assets' returns on investment.

2.3.4 Other tropical climates around the globe

A list of countries across the world which have tropical weather within their territories, as classified by the Köppen-Geiger climate classification (PEEL *et al.*, 2007), can be seen in Table 6.

Table 6: List of countries with tropical climate conditions, adapted from (PEEL *et al.*, 2007).

Country	Continent	Population [million inhabitants]	Latitude Range	Time Zone [UTC]
India	Asia	~1,210	8-35°N	+5.5
Indonesia	Asia	~256	5°N-10°S	+7/9
Brazil	South America	~200	4°N to 33°S	-2/5
Nigeria	Africa	~175	4-14°N	+1
Philippines	Asia	~101	6-19°N	+8
Vietnam	Asia	~91	8-23°N	+7
Thailand	Asia	~67	6-20°N	+7
Malaysia	Asia	~31	1-7°N	+8
Peru	South America	~31	1-18°S	-5
Chile	South America	~18	17-55°S	-3/5
<i>Singapore</i>	<i>Asia</i>	~6	~1°N	+8
TOTAL		~2,187		

The selection of the ten countries as per Table 6 (plus Singapore the location of study within this thesis) is aimed at highlighting countries with substantial presence of tropical climate. They account to a considerable amount of inhabitants of the planet.

As these countries are mostly developing nations, it is expected that they are bound to have strong and growing energy needs for years and decades to come.

Somewhat exploring on the weather patterns in one of these example nations, Brazil and its enormous land area (8.5 million km², being the fifth biggest country in the world), possesses a variety of climate conditions throughout its territory, but in its great majority tropical and subtropical weather. For Brazil, and as previously mentioned in 2.2.4, INPE has produced a solar resource atlas based on satellite measurements and solar radiative models (PEREIRA, E.B. *et al.*, 2006). Figure 51 shows two of such images produced by the publication.

The North part of the country at the Amazon basin area is the rainiest region of Brazil, also the cloudiest (PEREIRA, E. B. *et al.*, 2006).

That makes the Northern territory of the country and these locations near the Equator cloud-rich, which can be seen from Figure 51, right. The city of Belém (~1°S) has a similar climate to the one found in Singapore.

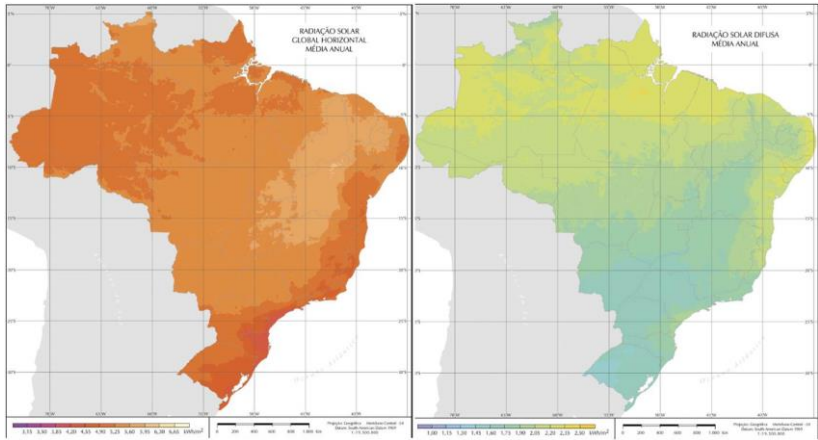


Figure 51: Annual global horizontal irradiance (GHI) and diffuse horizontal irradiance (DHI) in the Brazilian territory (PEREIRA, E. B. *et al.*, 2006).

The irradiation in Brazil is strongest in the region covering the Northeastern territory all the way to the Southeastern region. The highest irradiance months are during spring (Sep-Oct) with the lowest in winter (Jun-Jul). The annual average for GHI (Figure 51, left) highlights these regions in the lightest shade of orange. Total annual irradiance levels range from a lowest of 1,550 kWh/m², in the Southern part of Brazil at the North portion of the state of Santa Catarina, to 2,350 kWh/m², in the best solar-resource area, in the Northern areas of the state of Bahia (PEREIRA, E. B. *et al.*, 2006). To exemplify the solar potential of the country, the least sunny capital in Brazil receives ~40% more solar irradiation than the sunniest region in Germany (RÜTHER, 2004).

Table 7 shows key meteorological information for photovoltaic purposes for nine capitals in Brazil, organized from latitudes closest to the Equator to furthest from it (NASA, 2013). From a pool of the mentioned cities, annual average of global horizontal irradiation (GHI) is 1,790 kWh/m², once again emphasizing the excellent solar resource found in the South American country.

Table 7: Key meteorological parameters for PV applications for some capitals in Brazil (NASA, 2013).

City State	Belém PA	São Luís MA	Salvador BA
Latitude [°]	1°S	3°S	13°S
GHI [kWh/m²]	1,956	2,180	1,977
Avg. k_a [%]	53.9%	60.3%	55.5%
Avg. T_{amb} [°C]	26.5	26.5	25.7
City State	Brasília DF	Belo Horizonte MG	Rio de Janeiro RJ
Latitude [°]	16°S	20°S	23°S
GHI [kWh/m²]	1,902	1,838	1,599
Avg. k_a [%]	55.4%	54.6%	47.8%
Avg. T_{amb} [°C]	23.8	21.3	22.9
City State	São Paulo SP	Florianópolis SC	Porto Alegre RS
Latitude [°]	24°S	28°S	30°S
GHI [kWh/m²]	1,660	1,470	1,528
Avg. k_a [%]	50.3%	45.3%	47.4%
Avg. T_{amb} [°C]	21.5	20.7	19.6

As a comparison, Table 8 shows the same characteristics found in Table 7 but for capitals in the top-6 countries in installed PV capacity in the world (adapted from Table 1). The average annual global irradiation for these locations is 1,290 kWh/m², 28% below the ones in Table 7.

Table 8: Key meteorological parameters for PV applications for the capitals of the top-6 countries in installed PV capacity in the world (NASA, 2013).

Capital Country	Berlin Germany	Beijing China	Tokyo Japan
Latitude [°]	53°N	40°N	36°N
GHI [kWh/m²]	968	1,533	1,344
Avg. k_a [%]	38.5%	54.9%	46.3%
Avg. T_{amb} [°C]	9.4	8.1	13.9
Capital Country	Rome Italy	Washington D.C USA	Paris France
Latitude [°]	42°N	39°N	49°S
GHI [kWh/m²]	1,443	1,383	1,067
Avg. k_a [%]	49.7%	47.0%	39.9%
Avg. T_{amb} [°C]	14.6	12.5	11.2

2.4 SOLAR IRRADIANCE FORECASTING

2.4.1 Preliminary notes

Global efforts on solar irradiance forecasting have intensified in the past half-decade (2010-2015) with the strong growth on levels of penetration of PV and other renewables into grids. Inman *et al.* summarized several methods and examples for solar irradiance forecasting (INMAN *et al.*, 2013). In the comprehensive review, cited publications were shown which tackled different forecast horizons and investigation locations around the world. Among ~100 cited works of forecasting techniques applied for solar PV, the great majority of publications were for studies in the United States, Europe and Japan, which highlights that research efforts on this topic were, and still are, primarily focused where solar PV markets are prolific. As previously addressed, those locations also happen to be primarily dominated by more temperate climates.

Research on solar irradiance forecasting has focused mostly on 1-hour to 3-hour intervals (intra-day forecasts) and day-ahead intervals (MARQUEZ and COIMBRA, 2011; MARQUEZ *et al.*, 2013; PEDRO and COIMBRA, 2012).

Various forecasting techniques were developed and demonstrated at many locations in the world, as mentioned, predominantly where PV deployment has flourished, using several methods such as numerical weather prediction models (DIAGNE *et al.*, 2014; LARA-FANEGO *et al.*, 2012; LORENZ *et al.*, 2012; MATHIESEN and KLEISSL, 2011; PEREZ *et al.*, 2013), stochastic methods, e.g. auto-regressive integrative moving average (ARIMA) (MASA-BOTE and CAAMAÑO-MARTÍN, 2010; YANG, SHARMA, *et al.*, 2015), artificial intelligence, e.g. artificial neural networks (ANN) (CAO, J. C. and CAO, S. H., 2006; FONSECA JUNIOR *et al.*, 2014; MARQUEZ and COIMBRA, 2011; MELLIT and KALOGIROU, 2008; MELLIT and PAVAN, 2010), sky/satellite imagery analysis (MARQUEZ and COIMBRA, 2013; YANG, H. *et al.*, 2014) and even a combination of techniques (DA SILVA FONSECA *et al.*, 2012; DONG *et al.*, 2014; MARQUEZ *et al.*, 2013; NONNENMACHER and COIMBRA, 2014). Previous works on solar forecasting in Singapore have used some of these approaches (DONG *et al.*, 2014; 2013; YANG, D., DONG, Z., *et al.*, 2014; YANG *et al.*, 2012; YANG, WALSH, *et al.*, 2013).

Figure 52 shows range of appropriate techniques utilized in solar irradiance forecasting.

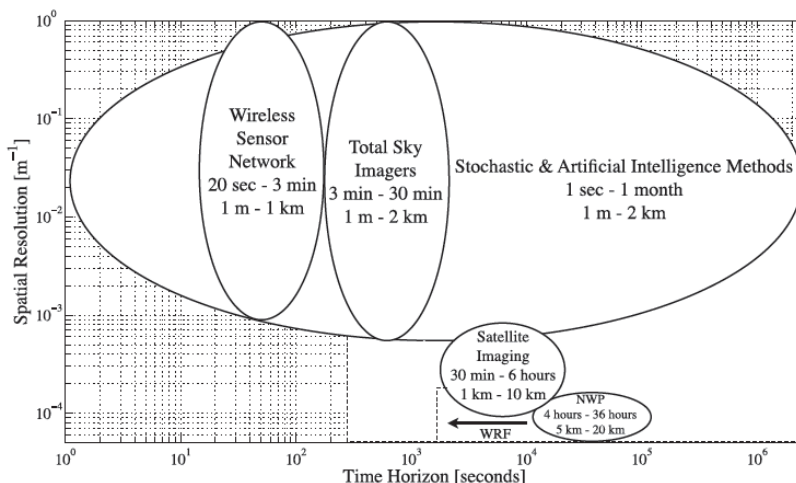


Figure 52: Time horizon versus spatial resolution for solar irradiance forecasting and suitable techniques for application. Source: (INMAN *et al.*, 2013)

The leading groups in the world for solar irradiance forecasting are relatively new, with most of the research having taken place in the 2010 to 2015 span, as some of the literature presented attest. Some of these names and associated publications can be mentioned below:

- Energy Meteorology Unit of the University of Oldenburg, Germany: (LORENZ *et al.*, 2012; LORENZ *et al.*, 2011);
- University at Albany, United States and National Renewable Energy Laboratory (NREL), Golden, Colorado: (PEREZ *et al.*, 2010; PEREZ *et al.*, 2007);
- University of California San Diego (UCSD), United States of America, with the Coimbra Forecasting Group: (CHU *et al.*, 2013; INMAN *et al.*, 2013; MARQUEZ and COIMBRA, 2011; 2013; 2012; MARQUEZ *et al.*, 2013; NONNENMACHER and COIMBRA, 2014; PEDRO and COIMBRA, 2012; ZAGOURAS *et al.*, 2015);
- University of California San Diego (UCSD), United States of America, with the Kleissl Group: (CHOW *et al.*, 2015; CHOW *et al.*, 2011; GOHARI *et al.*, 2014; KLEISSL, 2013);

LIPPERHEIDE *et al.*, 2015; MATHIESEN *et al.*, 2013; MATHIESEN and KLEISL, 2011; URQUHART *et al.*, 2015);

- Brazilian Institute for Space Research (INPE): (LIMA *et al.*, 2014; MARTINS *et al.*, 2012).

Some isolated work has taken place in China (CAO, J.C. and CAO, S.H., 2006; CHEN *et al.*, 2011), Japan (DA SILVA FONSECA *et al.*, 2012; FONSECA JUNIOR *et al.*, 2014; FONSECA_JR. *et al.*, 2013), Italy (MELLIT and PAVAN, 2010), Saudi Arabia (EISSA *et al.*, 2013), and a few other locations.

Other factors could play a role in irradiance forecasting beyond cloud coverage, such as aerosol concentration (GUEYMARD, 2012). Comments on aerosol influence were made in subsection 2.3.3 and are later addressed in other areas of this thesis.

Section 2.4 serves as identification of relevant literature in the solar irradiance forecasting area of photovoltaics. It helps set the tone for the state-of-the-art in this specific field.

2.4.2 Stochastic methods

Pedro and Coimbra investigated a mix of results for the Persistence method (assuming the next time horizon to be the same condition as the previous one), nearest neighbor (estimation of a station reading based on the closest site from it) and ARIMA (autoregressive integrating moving average) for a site in California (PEDRO and COIMBRA, 2012).

Yang *et al.* (YANG *et al.*, 2012) have tested an ARIMA method using cloud cover index with some success for Singapore.

Other research covering stochastic methods include (MARQUEZ and COIMBRA, 2011; MASA-BOTE and CAAMAÑO-MARTÍN, 2010; YANG, SHARMA, *et al.*, 2015). It is common that a combination of techniques is involved, in order to also explore lower errors. In most of the cases, a stochastic element is present, as part of the works of (ARYAPUTERA *et al.*, 2015; CHU, LI, *et al.*, 2015; CHU *et al.*, 2013; CHU, URQUHART, *et al.*, 2015; DONG *et al.*, 2014; LIPPERHEIDE *et al.*, 2015; MARQUEZ *et al.*, 2013; NONNENMACHER and COIMBRA, 2014).

2.4.3 Satellite and numeric weather prediction

When using satellite data, one of the challenges is in the temporal and spatial synchronization between the satellite image itself and ground measurement recorded (JOURNÉE *et al.*, 2011). A satellite image taken on top of Southeast Asia is seen on Figure 53, with Singapore highlighted.

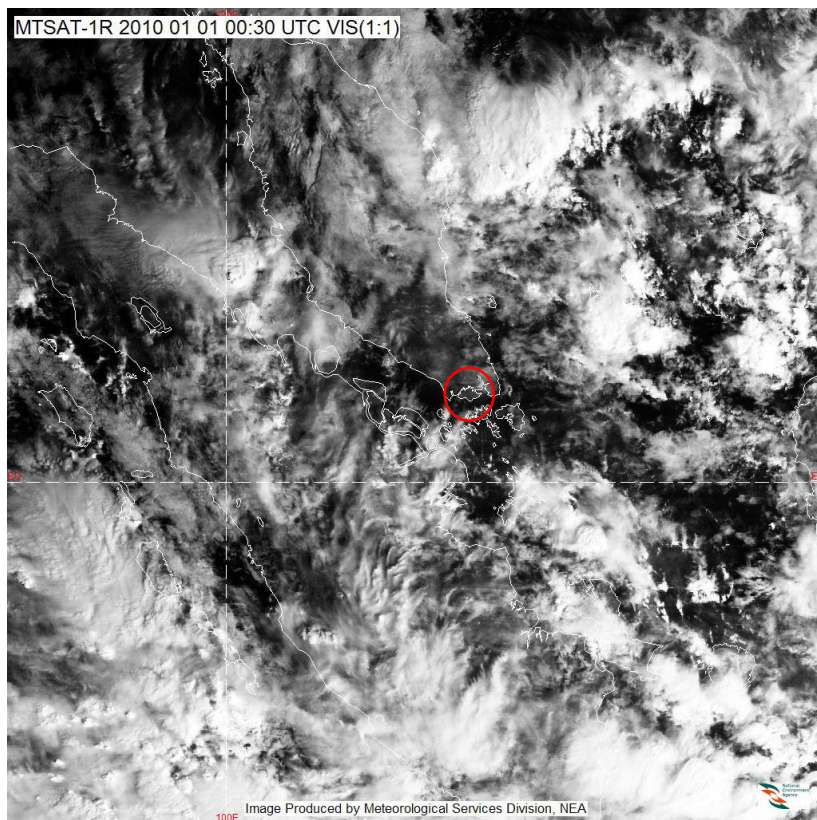


Figure 53: Southeast Asia satellite image with Singapore highlighted inside the circle (NEA, 2010).

Work has advanced in the analysis of pre-processed regional NWP forecasts, such as presented by Lorenz (LORENZ *et al.*, 2012; LORENZ *et al.*, 2011). Mathiesen and Kleissl also worked with a NWP for the forecasting trials in the United States (MATHIESEN and KLEISSEL, 2011).

The WRF numerical model (Weather Research and Forecasting Model) has been developed as a co-operation among several research institutes in the world. It has first been used for classical numerical weather predictions, later being adapted for wind applications in renewable energy. Recently, WRF has gained momentum for day-ahead solar irradiance forecasting efforts.

Lima et al. used the WRF model together with other statistical methods for forecasts for the Northeastern region of Brazil. Since the climate varies considerably in the region, a cluster analysis was used. The forecast horizon was set for one day-ahead (LIMA *et al.*, 2014).

As the thesis focuses on short-term solar irradiance forecasting, the utilization of numerical methods such as WRF, or of satellite images, are not explored. Figure 53 showing a satellite image from Southeast Asia, with Singapore marked within the red circle, with the totality of the island being only made of a couple of pixels in the image, highlight the vast extension involved in modeling the weather, thus making it difficult to utilize short-term resources with these products.

2.4.4 Artificial intelligence methods

An artificial neural network (ANN), with an schematic shown in Figure 54, is a massive parallel processor, made up of simple processing units (neurons), which have the ability of storing knowledge (synaptic weights) and making it available for posterior use (HAYKIN, 1999). The resemblance of ANN with the brain lies on the fact that it has the ability to learn from experience from the environment through a learning process and store knowledge.

Major benefits of neural networks can be linked to their ability to operate nonlinearly, which makes them suitable for handling phenomena with complex physical models, which, in most cases, are difficult or impractical to solve via linear functions. The adaptive nature of ANNs is an added advantage as their synaptic weights can vary with time.

The connections between neurons are given in the form of weights (the influence of one neuron versus the next), through synapses or connecting links. A linear combiner (summing junction in Figure 54) merges the respective synapses between neurons.

The bias acts in the process by creating an effect of increasing or lowering the net input into an activation function, depending on whether it is a positive or negative bias, respectively.

UCSD has published works with several configurations of neural networks for applications based on data from California (MARQUEZ and

COIMBRA, 2011), (PEDRO and COIMBRA, 2012) and (MARQUEZ *et al.*, 2013). Mellit has investigated a neural network in Italy focused on daily irradiance and ambient temperature from the previous day as input parameters (MELLIT and PAVAN, 2010). The goal was to test ANNs for one-day-ahead forecasts. The method involved testing different configurations of hidden neurons and layers almost at random. After a few trials, the authors opted for the most successful method (i.e. the one with the smallest RMSE) and proceeded from there into the results validation for a PV system in Italy using a simplistic PV performance model.

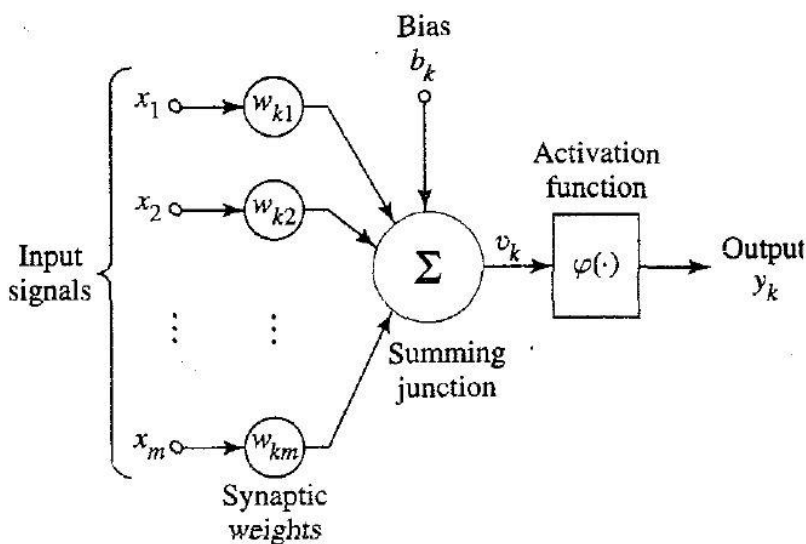


Figure 54: Artificial neural network schematic based on a nonlinear model of a neuron (HAYKIN, 1999).

In Brazil, Martins *et al.* (MARTINS *et al.*, 2012) have combined input parameters from a mesoscale model (Eta model, running at INPE) for training of an ANN, with training and validation taking place based on two ground-measurement solar radiation stations. RMSE improvement in the forecasts was in the order of 30%.

2.4.5 Sky imagery utilization

Sky imagers (more recently being replaced by cheaper CCD cameras with fish-eye lenses pointing at the sky) can capture stills such as the ones shown in Figure 55.

Cloud vectors and classification can be assessed with post-processing software. In Brazil, Mantelli Neto has written a thesis on evaluation of sky images for cloud assessment in the Brazilian territory (NETO, 2010).



Figure 55: Sky images from cameras with fish-eye lenses (source: UCSD).

Comprehensive overviews on sky camera utilization for short-term forecasting purposes are given by groups in the United States and Australia (URQUHART *et al.*, 2015; WEST *et al.*, 2014).

Significantly fewer publications can be found in the literature on short-term forecasting applications (sub-hour level). Marquez and Coimbra (MARQUEZ and COIMBRA, 2013) used sky images in Merced, California to create short-term forecasts of direct normal irradiance of a few minutes up to 15-min. The authors concluded that a 5-min forecast horizon presented the most significant accuracy for their dataset. Yang et al. (YANG, H. *et al.*, 2014) also utilized sky images in California to perform short-term forecasts. In winter, with more cloud cover in the region, the method proved more effective than in summer conditions, where persistence forecasts prevail due to the near clear-sky conditions. Normalized root mean square errors (nRMSE) ranged from 20-27% for 5- and 10-min prediction horizons.

Nguyen and Kleissl explored 2D and 3D methods to determine cloud base heights (NGUYEN and KLEISSL, 2014), which are features of interest in assisting short-term solar irradiance forecasting efforts.

A network of sky cameras has been deployed in Singapore by SERIS to assist on such forecasting efforts. Figure 56 shows the marked locations of these devices in the Singapore map. At the time of the submission of this thesis, thirteen cameras had been deployed. The institute makes live images available via its National Solar Repository of Singapore (NSR) website (NSR, 2015e).

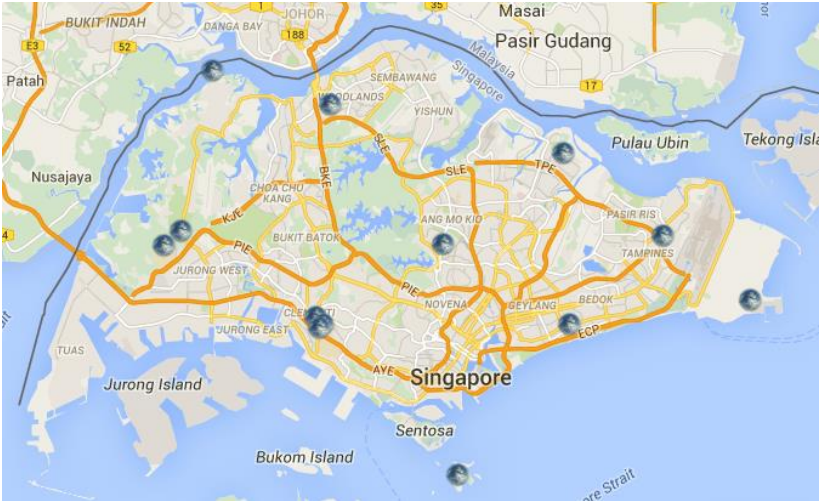


Figure 56: Deployed network of thirteen sky cameras in Singapore (NSR, 2015e).

2.4.6 Research on short-term solar irradiance forecasting

Research on solar irradiance forecasting has focused mostly on 1-hr, intra-day (a few hours) as well as day-ahead intervals, and predominantly in countries where PV has reached considerable penetration levels. The great majority of the forecast horizons have been focused at 1-hour to 3-hour intervals (thus in the intra-day range) (MARQUEZ and COIMBRA, 2011; MARQUEZ *et al.*, 2013; PEDRO and COIMBRA, 2012).

For short-term applications (minutes to sub-hourly), much less publications can be found, such as Marquez and Coimbra who used a total sky imager in California (MARQUEZ and COIMBRA, 2013), Yang *et al.* also utilizing a sky imager in the US state to perform short-term forecasts (YANG, H. *et al.*, 2014).

Yang *et al.* used a dense monitoring network of irradiance detectors in Hawaii to correlate lagged time series in the small sample area for very short-term irradiance forecasting. Lasso regression is implemented as a parameter selection method. Results achieved showed a further improvement over Persistence and other time series methods (YANG, YE, *et al.*, 2015).

2.4.7 Solar irradiance forecasting in the tropics

Previous work on forecasting in Singapore has used primarily statistical approaches (DONG *et al.*, 2014; 2013; YANG, D., DONG, Z., *et al.*, 2014; YANG *et al.*, 2012; YANG, WALSH, *et al.*, 2013). Yang *et al.* (YANG *et al.*, 2012) used the cloud cover index as a model input parameter, achieving normalized root mean square errors of circa 20% for 1-hour prediction intervals. The same authors published a novel method on spatial temporal kriging for interpolating forecast purposes. With this, they argue that the area of Singapore and the specific solar PV systems within it, based on their location, could have dedicated forecasting products (YANG, D., DONG, Z., *et al.*, 2014).

Dong *et al.* (DONG *et al.*, 2013) used an exponential smoothing state space model (commonly abbreviated as ETS) apart from ARIMA. A forecast interval of 5-min was implemented, achieving normalized root mean square errors of 17-33%. When comparing the new proposed model to ARIMA, the authors obtained a few percentage points of improvement, with some months with virtual similar forecast accuracies. In a hybrid approach, using satellite imagery and the ETS model, Dong *et al.* (DONG *et al.*, 2014) investigated hourly solar irradiance forecasting, with

normalized root mean square errors (nRMSE) ranging from 20% to 45%, with larger errors occurring during the monsoon season.

Sharma et al. (SHARMA *et al.*, 2015 (in press)) executed a wavelet neural network (WNN) taking averaged irradiance values of 13 stations distributed across Singapore for hourly intervals of prediction. Results for four different seasons of the year showed slight forecast skill improvement over ARIMA, and also over a simpler artificial neural networks (ANN) method.

Aryaputera et al. (ARYAPUTERA *et al.*, 2015) ran the WRF numerical model for Singapore, aiming at obtaining day-ahead forecasts for the island. RMSEs of ~45% were obtained, with a slight improvement over the Persistence method for such 24-hour-ahead products.

In other tropical and subtropical studies, Khatib et al. (KHATIB *et al.*, 2012) generated a four feedback forward propagation neural network using relative humidity, ambient temperature, global horizontal irradiation and wind speed with data from Kuala Lumpur, Malaysia.

In a subtropical study, Martins et al. (MARTINS *et al.*, 2012) applied ANNs for two sites in Southern Brazil using the new model to refine inherent known biases associated with an existing numerical weather model. Confidence and reliability were improved by more than 30% for both sites under study.

2.5 PV SYSTEMS SIMULATION AND PERFORMANCE

2.5.1 Yield and performance ratio of PV systems

Solar photovoltaic panels are rated at the end of a manufacturer's production line according to the Standard Test Conditions (STC) for PV modules, which are characterized as the laboratory indoor setting for flash testing set at 1,000 W/m² irradiance, 25°C PV cell temperature and spectral distribution of light equivalent to 1.5 AM (air mass) spectrum (IEC, 2011).

Upon commissioning of a PV system, its quality assessment and continuous performance are important gauges to owners and financiers on the return on investment for the particular asset. It is important to observe and compare performance ratio (PR), which is based on in-plane irradiance and total annual yield measured in kWh/kW_p per year, versus benchmark values for a given place where the asset is located.

Performance ratio is an internationally-recognized assessment parameter for the verification of system design and operational quality. As per IEC 61724 standards (IEC, 1998), performance ratio is defined as the ratio of the final PV system yield (Y_f) over the reference yield (Y_r):

$$PR = \frac{Y_f}{Y_r} \quad (5)$$

The final PV system yield (Y_f) is the net AC energy output (E_{AC}) divided by the nameplate DC power (P_0) of the installed PV array, i.e.:

$$Y_f = \frac{E_{AC}}{P_0} \quad (6)$$

with the units of hours or kWh/kW_p representing the number of hours that the PV array would need to operate at its rated power to provide the same amount of energy on an annual basis.

The reference yield (Y_r) is the total in-plane irradiance G_{mod} , divided by the photovoltaic reference irradiance, $G_0 = 1,000 \text{ W/m}^2$, i.e.:

$$Y_r = \frac{\sum^t G_{mod}}{G_0} \quad (7)$$

which represents an equivalent number of hours at the reference irradiance set-point. Thus, PR can be expanded by substituting Y_f and Y_r into PR as:

$$PR = \frac{E_{AC}/P_0}{\Sigma^t G_{mod}/G_0} = \frac{G_0}{P_0} \times \frac{\Sigma^t P_{AC}}{\Sigma^t G_{mod}} \quad (8)$$

where P_{AC} is the AC power output of a PV system. It should be noted that G_{mod} here should be measured by an irradiance measurement device with the same orientation and tilt as the PV array such as the one shown in Figure 57.



Figure 57: Silicon sensor installed in the plane of the photovoltaic array, here 10 degrees (source: SERIS).

With these boundary conditions for performance ratio assessment, it could be inferred that PV systems installed at façades could, for example, still have a high PR, although their annual yield would be considerably lower than a rooftop system due to less irradiance reaching the module plane on the vertical surface. From a system design perspective, however, it is sufficient to analyze performance ratio alone as a parameter to maximize performance at any given site.

The performance ratio is in general independent of the irradiance conditions at a given site and is therefore a good indicator of the comparison of the performance of PV systems in different locations. PR can also be used to measure the behavior of a system over time (JORDAN and KURTZ, 2013; RUTHER *et al.*, 2010a), also being regarded as a PV system design quality metric.

The irradiance sensor for the measurement of performance ratio is usually a calibrated pyranometer. However, due to high costs of these

devices, it has become increasingly common to measure performance of PV systems with off-the-shelf, yet properly calibrated silicon sensors.

Figure 58 summarizes the deviation in monthly totals from three irradiance sensors under monitoring at the SERIS meteorological station. The baseline, represented by the black line, is associated with the readings of a calibrated pyranometer (manufacturer: Kipp & Zonen, type: CMP11).

Secondly, the orange circles are the deviation of a second pyranometer (manufacturer: Delta-T, type: SPN1), showing higher readings (average +1.4%) versus the baseline. This difference could be explained by the different sensor construction, with a dome type which includes a shading mask and internal unit algorithm running relationships between seven sets of thermopiles for the acquisition of the DHI reading.

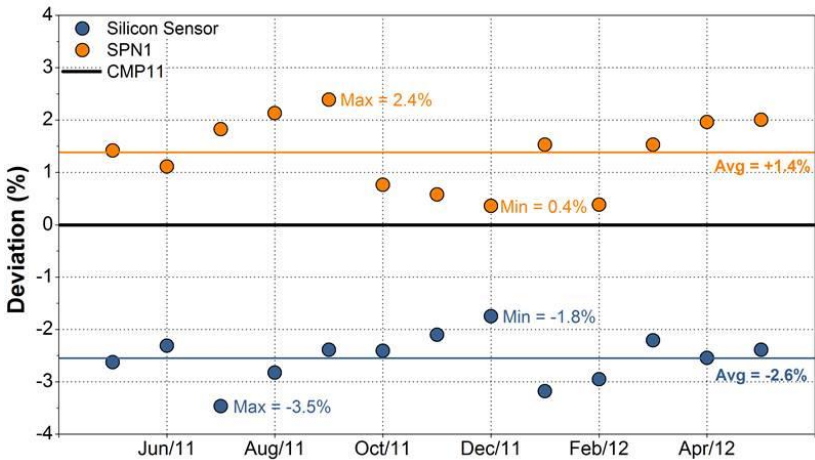


Figure 58: Three sensors measuring global horizontal irradiance under comparison. The CMP11 pyranometer acts as a baseline (source: SERIS).

Thirdly, a silicon sensor (manufacturer: Mencke & Tegtmeier, type: Si-02-PT100-K, calibrated at Fraunhofer ISE's CalLab), shown as blue circles in the figure under discussion, has clear readings below a pyranometer (average -2.6% as recorded at the station for the period displayed). This is the case as the spectral response of silicon is narrower when compared with a pyranometer, as previously mentioned in subsection 2.2.2. Nevertheless, a silicon sensor can be calibrated to account for this issue.

As seen in Figure 58 with the lower readings versus a pyranometer,

the fact that a silicon sensor behaves like a solar module (flat plate semiconductor), reflecting part of the light on its front glass (versus a pyranometer which absorbs most of the spectrum of the light from all angles through its glass dome, see Figure 33), it can be concluded that the performance ratio, when calculated based on readings from a pyranometer, will show lower values than for sites where irradiance recordings come from silicon sensors.

Reich et al. (REICH *et al.*, 2012) pointed out that there is a strong temperature dependence of the performance ratio since the energy produced by a PV system will be affected by module temperature. Therefore, PV systems in temperate zones will have a higher PR than comparable systems (with respect to module technology, inverters and level of ventilation) in tropical regions of the world. Nobre et al. (NOBRE, YE, *et al.*, 2012) verified performance ratios in tropical Singapore with best PRs around 83% which are below those reported by Reich et al. as state-of-the-art systems in Germany (close to and approaching consistently the 90% mark, see Figure 59). This apparent ~6-7% gap in performance between tropical- and temperate-zone located PV systems has been the topic of study of the author with published and under preparation works.

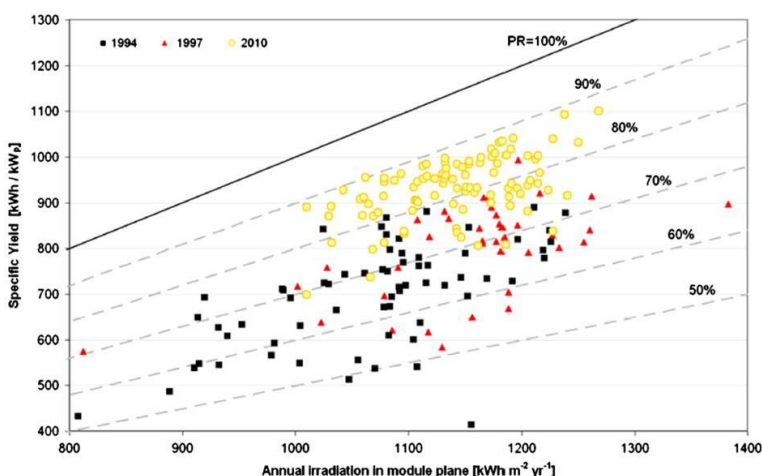


Figure 59: Evolution of performance ratio in Germany through the past 2 decades (REICH *et al.*, 2012).

Another factor which can be observed in Figure 59 is that PV systems' yields and performance ratios have evolved through the past two decades. One can clearly see the migration of performance ratios towards the upper 70s (of percentage points) and later towards the 80-90% band as time progressed. These improvements can be traced back to four major reasons namely: (1) advances in inverter efficiency and reliability, with units both reaching specification maximum efficiencies close to and slightly above 98%, versus low 90s circa 20 years ago. Additionally, inverters trip less in relation to its electric grid interactions today than earlier models, increasing overall system uptime; (2) solar module tolerances, with PV modules being segregated at the factory now with "plus-tolerances", meaning if one acquires a 250 W_p module, the actual output of the module is 250 W plus a certain value (for example 5 W), versus 10-20 years ago when product tolerance would have been 250 W plus, but also minus 5 W; (3) overall improvement of balance of systems components (BOS) aligned with system integrators' increased learning curves while making use of best practices of PV systems; and (4) advanced monitoring systems, many operating in real-time nowadays, which are now able to communicate system issues to owners upon occurrences, thus minimizing total system downtime.

Apart from the IEC standards, the International Energy Agency published the Analytical Monitoring of Grid-connected Photovoltaic Systems: Good Practices for Monitoring and Performance Analysis which discuss state-of-the-art of monitoring, PV loss mechanisms which are only detected by research-grade systems, promote the understanding of long-term system behavior and finally to divulge lessons from bad performing systems (WOYTE *et al.*, 2014).

2.5.2 Loss mechanisms of PV systems

A performance ratio of 0.80 (or 80%) has historically been considered a good benchmark for a PV system in any location of the world. However, as reported by Reich et al., more recently installed solar systems in Germany have been performing at near 90% levels (REICH *et al.*, 2012).

The 10-20% losses which would be associated with a 90-80% PR PV system arise from a series of mechanisms which are described as follows:

a) Solar irradiation in the module plane

According to the location of a solar system in the world, together with its chosen tilt (inclination) and azimuth (orientation) angles, gains or losses in irradiance capture occur.

Common system design practices suggest a tilt angle that matches the latitude of the site or is close to it (DGS, 2008). However, other considerations should be taken into account before a decision on installation angles are taken (see soiling losses).

In terms of azimuth, Northern locations will profit most from systems facing South. Conversely, systems in the Southern hemisphere should face the North for energy capture maximization.

For locations close to the Equator, which is the case of Singapore, it is possible that orientation towards North or South does not play such a major role, rather optimum performance is dictated by weather trends, for example concentration of rain showers in the afternoon would mean systems facing East will capture more sunlight and thus produce more electricity (KHOO, NOBRE, *et al.*, 2014).

Nonetheless, irradiation capture gains in the order of 10-15% could be achieved in a city like Freiburg, Germany (latitude = 48°N) by tilting a PV system to ~40° towards South. In low latitude locations, irradiation gains are little upon slight tilts.

As solar is still a young contributor to energy mixes in the world, together with the fact that feed-in tariffs and other compensation schemes to solar PV are usually linked to fixed payment amounts, we have not reached a turning point when it might be interesting to maximize even the orientation of systems, thus generating more energy in the early morning or late afternoon portion of the day according to tariff variations. Orientation of systems could play a major role in a solar-dominated future where shift in demand might be desired (HUMMON *et al.*, 2012).

b) External shading

External shading can be caused by horizon obstructions, e.g. mountains and buildings, but also closer structures such as chimneys and trees.

Although older methods exist, where one can draw obstructions with the use of a transparent paper, new and more modern options to evaluate losses for external shading are presently available such as 3D modeling (e.g. software Autodesk Ecotect, Google SketchUp) or with new tools normally with a fish-eye camera device at hand (e.g. SunEye tool, from company Solmetric (SOLMETRIC, 2013).

Tropical locations have fewer problems with external shading due to high altitude angles of the sun in the sky. In Singapore, for example, the lowest sun angle throughout the year is $\sim 65^\circ$. Systems have shown to operate at high PR levels even when faced with challenging built-environment surroundings (ZOMER *et al.*, 2014).

c) Internal shading

Internal shading takes place when portions of the solar system itself cast a shade onto other system sections. Row-induced shading is an area of concern for MW-size power plants but also inherent to smaller systems which might be commissioned in several smaller sections due to space constraints that can end up shading one another.

d) Soiling losses

When PV modules get dirty from dust or biological sources (e.g. bird droppings), the amount of light reaching the photovoltaic elements will be reduced. Soiling losses are normally estimated at 1% (REICH *et al.*, 2012) but are extremely location-dependent, e.g. would be higher in arid countries (H. QASEM, 2011).

As discussed in loss mechanism a), if modules are installed at shallow angles ($<10^\circ$) for maximization of solar resource for locations close to the Equator, that could be detrimental in terms of soiling accumulation as rain cannot exert a proper self-cleaning effect onto the modules' glass front surface. Figure 60 shows progressive images taken of a PV system in Singapore installed at zero degree tilt angle (i.e. flat), thus completely foregoing the self-cleaning effect, which can be demonstrated by the considerable amount of dirt accumulation at the side of the modules, covering active PV cell areas.



Figure 60: Progression of soiling accumulation in an unmaintained PV system due to a flat tilt angle (source: SERIS).

e) Reflections

A PV module has a front-glass cover (in the majority of technologies). Although special glass types with increased light-trapping properties are present for most manufacturers, even such a special treatment surface will reflect part of the incident light.

For this loss contributor, long-term experience from scientists have indicated deductions to be around 3% (HEYDENREICH, MÜLLER, *et al.*, 2008). For a location near the Equator like Singapore, with higher solar elevation angles (as per Figure 32), the reflection losses tend to be lesser than compared to winter periods in a country like Germany, when the sun is low in the sky, thus causing greater loss of irradiation due to reflections.

Khoo et al. also studied angular reflectance losses among the classical type of flat glass (planar) and a textured version special glass. The textured glass was measured to show 1.4% better light trapping capacity than the planar one after a 6-month testing period. Simulations year-round also showed better performance by the special glass type (KHOO, SINGH, *et al.*, 2014).

f) *Irradiation mismatch*

For the irradiation deviations from the standard test conditions (STC) value of $1,000 \text{ W/m}^2$, Figure 42 shows for example how irradiance values throughout a year will vary at the $0\text{--}1,200 \text{ W/m}^2$ range. Therefore, irradiance losses (or in this case under-, or for less instances over-production, i.e. $> 1,000 \text{ W/m}^2$ conditions) will occur for every instance the conditions are not at the STC set-point. Software computes these deductions based on the input meteorological file for a location, which would inherently carry such irradiance statistics, thus allowing for loss estimations in the order of 3%.

g) *Spectrum mismatch*

For the spectral mismatch from the standard test conditions (STC) value of 1.5 AM, PV systems will be exposed to a different variation of air masses during the day due to sun path geometry but weather conditions. A common estimation for these losses is around 1%, also seen in Heydenreich et al. (HEYDENREICH, MÜLLER, *et al.*, 2008) and Reich et al. (REICH *et al.*, 2012).

Ye et al. justified a red-shift spectrum in the tropical climate of Singapore as a reason for better performance of thin-film systems over silicon wafer-based ones (YE *et al.*, 2014a). Liu et al. demonstrated that the red-shift is strongly reduced under hazy skies originated by forest fires in nearby Indonesia. Such contrary spectrum shift direction to the publication by Ye was shown to diminish performance ratios of thin-film systems under polluted skies (LIU *et al.*, 2014b).

h) *Temperature dependency*

The single heaviest contributor to losses in the performance of PV systems is the module temperature. STC conditions are set at 25°C , which is far from the real-world operating environment systems face. Modules are usually $25\text{--}30^\circ\text{C}$ hotter than the ambient temperature (ROSS, 1976).

Module temperature losses are even more important in the tropics as reported by Ye et al., (YE *et al.*, 2013) and Nobre et al. (NOBRE, YE, *et al.*, 2012), see subsection 2.6.2. For silicon wafer-based technology, a typical value for the temperature coefficient loss for maximum power is $0.4\%/K$.

i) Module and string mismatch

Module mismatch in recent times is not such a considerable system loss contributor as it once was (REICH *et al.*, 2012). With tighter tolerances from manufacturers, module sorting became non-advantageous versus the time consumption needed due to bigger system sizes. Losses are constrained to values well below 1%.

System strings going into the same inverter MPPT also require careful designing. With two strings, even with the same number of modules, but different tilt or orientation angles can cause string mismatch on the inverter MPPT, thus constraining the optimum operation conditions of that system section to the weakest link (with the worst I-V curve maximum power point tracking relationship), thus causing underperformance for the system as a whole (DGS, 2008).

j) Ohmic losses

DC-wiring losses are often restricted to assumptions in the order of 1.5% but can be calculated based on cable lengths and cross sections (DGS, 2008).

For AC cabling losses, it is relative to the point of measurement of the AC energy being produced by the system. If the energy produced by the inverter is recorded by the inverter meter itself, AC ohmic losses could be assumed to be negligible. However, most utility energy meters are found at a certain distance from the inverter, mostly in separate distribution boards, thus creating a second section of ohmic losses, although small, until the final energy recording which later is used for performance ratio calculation.

k) Inverter losses

Inverters have become more efficient with the growth of the photovoltaic market and subsequent technology advances. Some units (e.g. SMA 60 kVA transformerless series) can achieve up to 98.8% maximum efficiency (SMA, 2015b).

The selection of inverter to PV ratio has been discussed for many years now with a loading ratio of 1.25 commonly used as a threshold (DGS, 2008). Burger and Rüther investigated such ratios in relation to local solar resource (BURGER and RÜTHER, 2006). Cloud-edge/enhancement effects, as discussed in subsection 2.3.2, could account for inverter cut-offs and loss of revenue in a PV system.

The “Brazilian efficiency” concept for inverters was first proposed and investigated in a master’s dissertation at Universidade de São Paulo, USP (PINTO, 2012). It bases the loading profile of the inverter similarly to what the European (EU) and California (CEC, California Energy Commission) efficiencies do for their respective regions. However, it takes into account the irradiance distribution profile for Brazil as a whole. Zomer et al started the first implementation of the Brazilian efficiency into software analysis of PV module performance assessment (ZOMER *et al.*, 2013).

l) Inverter transformer losses

Since the inverters of all systems under study in this thesis are transformerless and not connected to any medium voltage level, transformer losses are considered to be zero. However, big size PV systems could receive energy meters at both the pre- and post-transformer positions, with revenue meters mostly located at the closest point to grid interfacing.

2.5.3 Other factors influencing performance

The following mechanisms are usually not part of PV systems simulation software. However, these contributors do affect performance and are most of the times rejected. They are discussed next:

m) Wind speed

Increased ventilation in the surroundings of a system brings module temperatures down, consequently increasing system power output (ROSS, 1976).

Readings from the SERIS meteorological station (year 2011, see Figure 61) have shown lower average wind speeds of 1.4 m/s in Singapore, which motivated the foregoing of these sensors at PV system sites in local investigations.

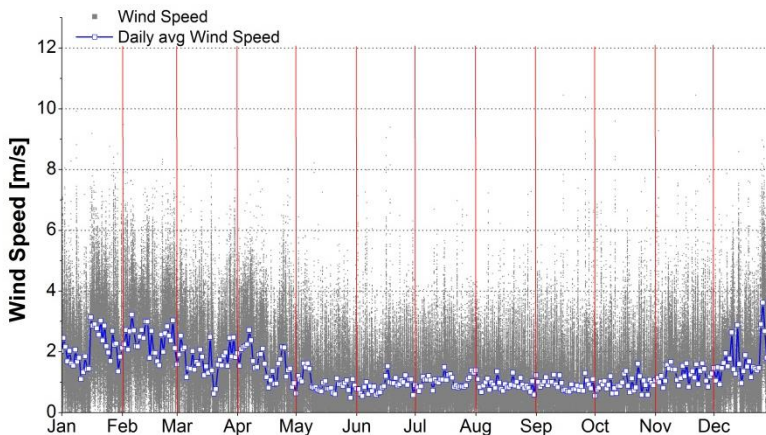


Figure 61: Wind speed as recorded by the SERIS meteorological station for the year 2011 (SERIS, 2011).

Veldhuis et al. validated PV power modeling in Singapore and Indonesia, with and without wind taken into account. Root mean square errors (RMSEs) between simplistic models adopted by Ye et al. (YE *et al.*, 2013), not considering wind, versus more complex ones with wind influence, have shown small error variations and to work effectively in Singapore (VELDHUIS *et al.*, 2013; VELDHUIS *et al.*, 2015).

n) System downtime

According to IEC standards on the performance assessment of PV systems (IEC, 1998), downtimes caused by various failures should be considered when assessing system quality. In its total life-cycle analysis, downtime affects LCOEs (BIERI *et al.*, 2015). One of the most classical forms of downtime is an inverter trip, which again could happen for a variety of reasons, such as grid imbalances. Once inverters are down, the PV system goes into open-circuit voltage (V_{oc}) and is not generating electrical energy any longer. Other examples of system breakdowns are burnt surge arrestors (due to lightning) or burnt fuses. Some examples of scheduled downtime are PV system maintenance or in some cases, monitoring system maintenance, which could affect recordings on site for irradiance and energy values being produced.

Investors usually take in their business plans an arbitrary value of 1% deduction in overall system performance (i.e. usage of a 99% uptime) (BIERI *et al.*, 2015).

o) Optical depth of local atmosphere

Aerosols present in the air block sunlight from reaching the Earth's surface. Optical depth (transmission of light from the top of the atmosphere down to the ground) is affected by, for example, air pollution.

For Singapore, it is somewhat common that forest fires in nearby Indonesia set smoke clouds in the region, especially during the months of August and September (driest periods of the year when fires are used for agriculture clearing), see 2.3.3. The example of haze influence on an irradiance sensor and on a PV system is shown in Figure 62, with the clear sky irradiance and theoretical maximum power indicated.

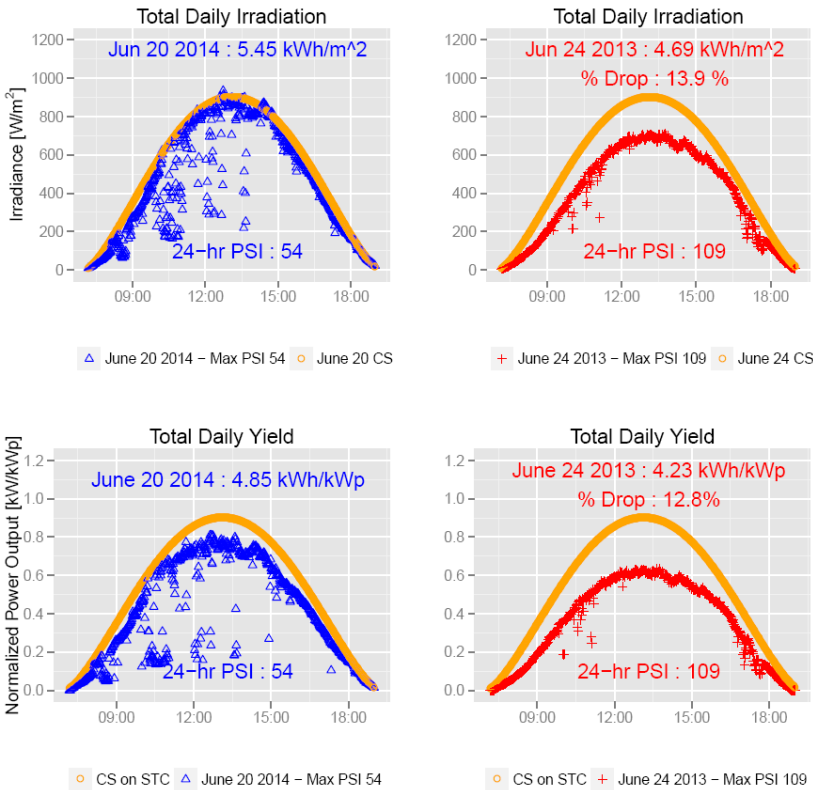


Figure 62: Irradiation on ground level and yield of a PV system on both a clear sky day (PSI = 54) and on a hazy day (PSI = 109) (NOBRE et al., 2015 (accepted)).

Figure 62 (top row) shows the in-plane global irradiance of a PV system on a relatively clear sky day in June 2014 (with a 24-hour Pollution Standards Index, PSI average of 54) compared against the time series on a hazy, yet cloudless day in June 2013 (24-hour PSI = 109). A reduction of approximately 14% in irradiation is shown for the comparison of those two days. When performing the same check on the normalized AC power output of a PV system for the same two days, the reduction in electricity production follows a similar pattern (~13% reduction, Figure 62, bottom row). While there is a clear visual effect on the dimming of the irradiation at ground level on this exceptional day (hazy but cloudless), the quantification of the haze effect is a challenging exercise for typical day to day conditions, when clouds are likely to be present in the tropical climate of Singapore. Determining the weather conditions with and without the presence of the haze and how that affects existing PV systems in Singapore is a complex exercise.

Burning of biomass is also present in Brazil and could affect aerosol particle concentration (MARTINS *et al.*, 2008). Although great forest reserves are farther apart from big centers, it is highly possible that with the deployment of larger volumes of PV systems, some of these installations in the future end by suffering loss of power due to nearby fire particulate emissions, or even in some cases, industrial pollution emissions. Major city-centers like São Paulo pose similar challenges in terms of hazy skies as shown in Figure 62. However, the smog in this case is caused mostly by automobile exhaust as well as potentially, to some level, by industrial emissions.

p) PV system degradation

PV systems do degrade with time. A combination of soiling accumulation which might not be entirely removable, increase in series resistance in aging solar cells, module delamination, front glass “yellowing” caused by extended UV-exposure, among other factors could trigger an ageing mechanism to PV modules and consequently to systems. NREL has studied more than 4,000 research results throughout the world (JORDAN and KURTZ, 2013) and has summarized their finds to degradation rates of an average of -0.5% per annum, which is also a widely utilized figure both from module manufacturers perspective (when planning their warranties) but also from investors (when conducting their business plans). A recent study, however, showed an average degradation of -0.8% per annum of a 20-year-old PV system in Colorado, United States (JORDAN *et al.*, 2015). Another study in a subtropical island in

the south of Brazil showed an average output reduction of -0.55% per year for a thin-film amorphous silicon PV installation over a 15-year period (DO NASCIMENTO and RUTHER, 2014).

In a constantly hot and humid climate, these numbers have been demonstrated to be higher. Degradation on single piece PV modules was assessed by Ye et al. in Singapore with annual rates ranging from -0.8% to -6.0% depending on the module technology (YE *et al.*, 2014b). On a system level, Nobre et al. reported median annual degradation rates of -1.2% for crystalline-based systems in Singapore (NOBRE *et al.*, 2013).

One way to monitor system degradation is via long-term PR assessment as shown by Rüther et al. (RUTHER *et al.*, 2010a) and Kiefer et al. (K. KIEFER, 2010). A novel method was proposed by the author of this thesis where both DC and AC sides of PV systems were investigated, with continuous daily performance ratio readings, which later receive a statistical treatment, whereby a 2-sigma filter is applied to remove values of performance which are not associated with the customary behavior of the PV system. Figure 63 displays one of the example analysis conducted, with degradation assessment both on the DC- and AC-sides of a PV system. In this example, the system's DC-side, e.g. solar modules and cabling all the way to the inverter's input, has shown degradation through ~1,100 days of approximately -0.6% per annum (dark blue circles, daily PR values). The light blue circles represent daily PR values on the AC-side of the system, taking the entire ensemble into account, all the way to the final energy meter. For the PV system shown, an AC-side degradation of -0.8% was found.

In the investigation as a whole, results have shown median degradation rates above current literature values (-0.5% p.a. for AC-side degradation) for both silicon crystalline wafer-based and silicon thin-film technologies (-0.7% p.a. for DC- and -1.5% p.a. for AC-sides of silicon wafer-based systems and -1.2% p.a. (DC) and -1.6% p.a. (AC) for silicon thin-film based systems). While these conclusions are limited by the number of years for which data are available, for the first 1.5 to 3 years of operation, there is no trend that the degradation would slow down with time thus far. More investigations were performed and addressed in publications and results and discussions section of this thesis.

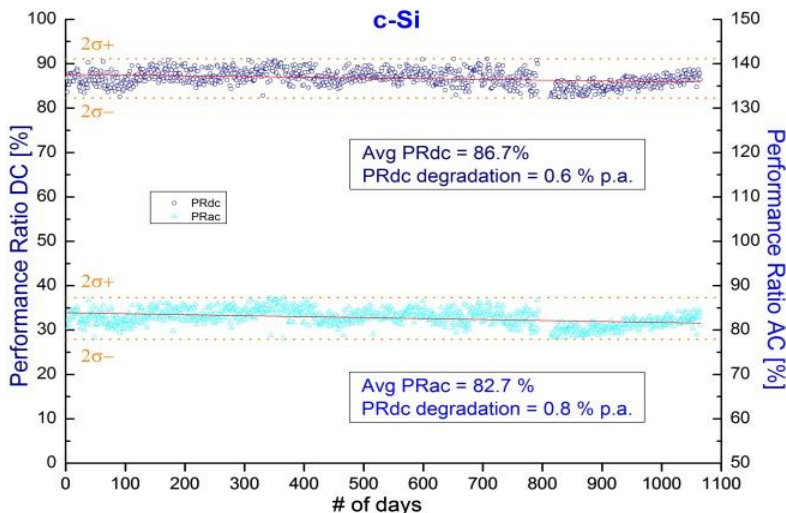


Figure 63: Degradation of a PV system in Singapore after ~1,100 days of operation (NOBRE *et al.*, 2013).

2.5.4 PV system performance in warm climates

With more and more large photovoltaic (PV) markets emerging in hot and humid tropical areas, PV systems are to be specifically designed in line with the local conditions to ensure optimized performance. Newly-installed systems in Germany, the country currently with the largest installed capacity worldwide, have improved their performance ratios (PR) from the 50-75% range in the late 80s to close to 90% for state-of-the-art systems in recent times (REICH *et al.*, 2012) and shown in 2.5.1.

It is only natural that most of the research on PV topics has been focused where booming markets are. In the area of PV systems, isolated efforts have taken place for PV systems in the tropics (FAN, 2007; RUTHER *et al.*, 2010a; b; WITTKOPF *et al.*, 2012).

A more comprehensive investigation has shown a performance ratio median close to 80% for crystalline wafer-based PV systems in tropical Singapore (NOBRE, YE, *et al.*, 2012). In the work, the performance ratios of 11 silicon wafer-based systems for the one-year measurement period were shown (Figure 64). The best-in-class system (A) operated with a PR of 82.6% and the worst-performing system (K) delivered only a PR of 58.1%. Typical system flaws leading to lower performance include for example: unreliable components (modules,

inverters failures), wrong selection of cable sizes, a faulty AC switch frequently causing electrical trips, or burnt fuses.

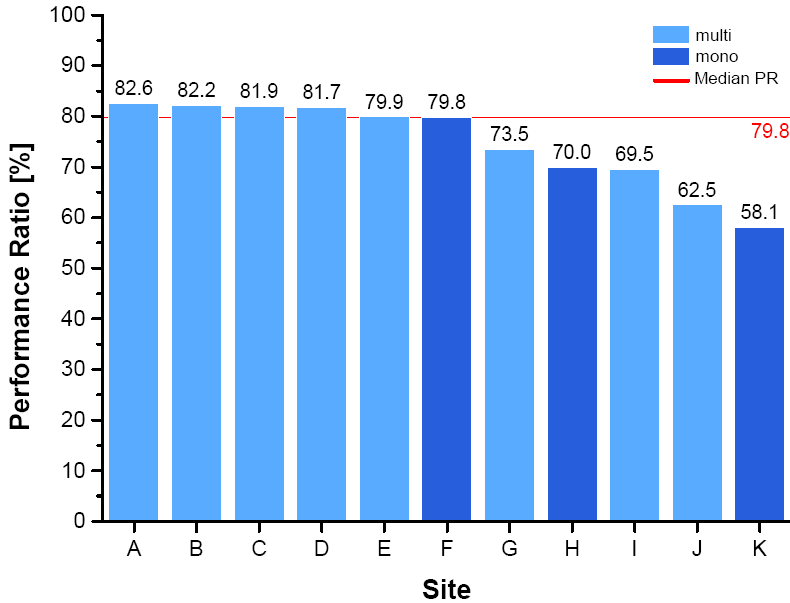


Figure 64: Performance ratio of 11 crystalline wafer-based systems in Singapore (NOBRE, YE, *et al.*, 2012).

At the time of the investigation on the previously mentioned work, those systems represented approximately 20% of the entire PV installed capacity in Singapore (~4 MW_p). This shows that it is not uncommon to observe PR values of 80-82%, despite the harsh tropical climate conditions found – annual ambient temperatures between 23-35°C and relative humidity levels between 60-85% (NEA, 2009), with low seasonality effects for the country.

With the Fraunhofer Institute for Solar Energy Systems (ISE) demonstrating that state-of-the-art photovoltaic systems in Germany have reached the 90% performance ratio mark (REICH *et al.*, 2012), the investigation for similar results for a tropical location were set for the understanding of PR behavior in such harsh environments. Module temperature was found to contribute between 45-60% of all losses from PV systems in Singapore. As module temperature is the most influential parameter, a subsequent publication under preparation aims to tackle the

reasons for the delta in PRs between temperate and tropical locations. Figure 65 gives an indication of the reasons behind the effects, with module temperature in Singapore in general much hotter than in Germany. State-of-the-art PV systems in Singapore can operate today at ~85% PRs whereas European systems can reach up to 90%, as previously presented.

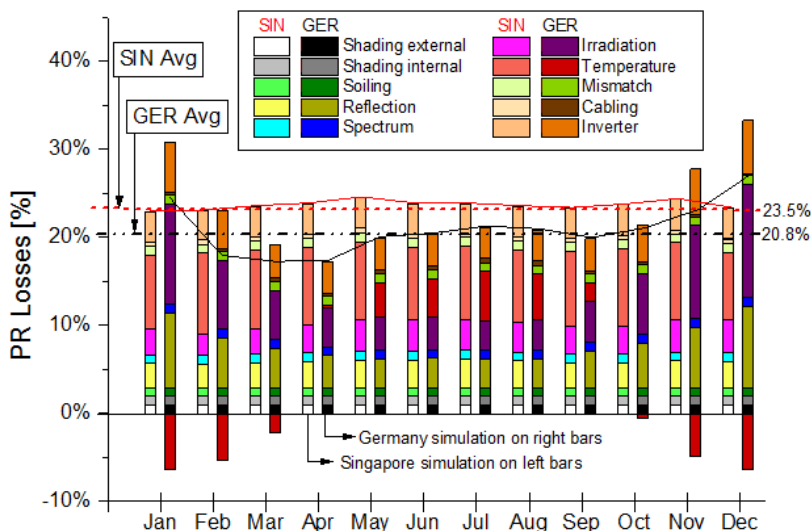


Figure 65: The monthly spectrum of variation in the PR losses between a PV system in Singapore and one in Germany (NOBRE et al., 2015 (in preparation)).

2.5.5 National Solar Repository of Singapore

The National Solar Repository of Singapore (NSR) was officially launched in November 2010, part of the local government initiative through its Economic Development Board (EDB) to promote solar photovoltaics in the country. The repository works as a database and information portal for relevant stakeholders in solar photovoltaics in Singapore (NSR, 2013a).

The repository has a three-fold goal:

- Create awareness about existing photovoltaic installations in Singapore, generating enthusiasm with the population about this form of clean energy technology;
- Help optimize performance of solar PV installations in Singapore by comparing and analyzing system behavior on a monthly and annual basis, setting country-wide benchmarks for system technology;
- Act as the information platform in the country for solar PV basics or whom to contact for installation financing of a solar system.

The NSR contains information on several types of PV systems such as the ones shown in Figure 66. PV installations in commercial buildings (left) are monitored for their output on a monthly basis, together with industrial sites (top right), residential systems (middle right) and educational or research systems (bottom right). Some of the systems provide daily output records, which allow for more detailed investigations by the initiative.

As of late 2014, the NSR platform tracked one fourth of the PV systems available in Singapore (in terms of volume, circa 9 MW_p out of a total of 33 MW_p deployed in the country). Photos of the systems and their locations are shown in a map, as well as the system characteristics in a database.

Perhaps most importantly is the information the initiative provides on system performance. Figure 67 is a summary of systems' annual yields (MWh/kW_p per year) for the year 2013. The results account for systems' failures in the field, e.g. inverter downtime and are thus not adjusted for only optimum performance values. The average of 1.08 MWh/kW_p for 56 systems in the country (approximately one third of the entire installed capacity of solar PV in Singapore at the time of the analysis) highlights

the current state-of-the-art for the country in PV system technology (NSR, 2013b). The average irradiation as measured by several SERIS meteorological stations indicated an annual value for GHI of 1,578 kWh/m², which allows the inference that the average system performance ratio in Singapore is just under 70%, a value which is far from what state-of-the-art PV systems can ultimately deliver today, thus, an indication that system design and implementation is not optimum in the country.

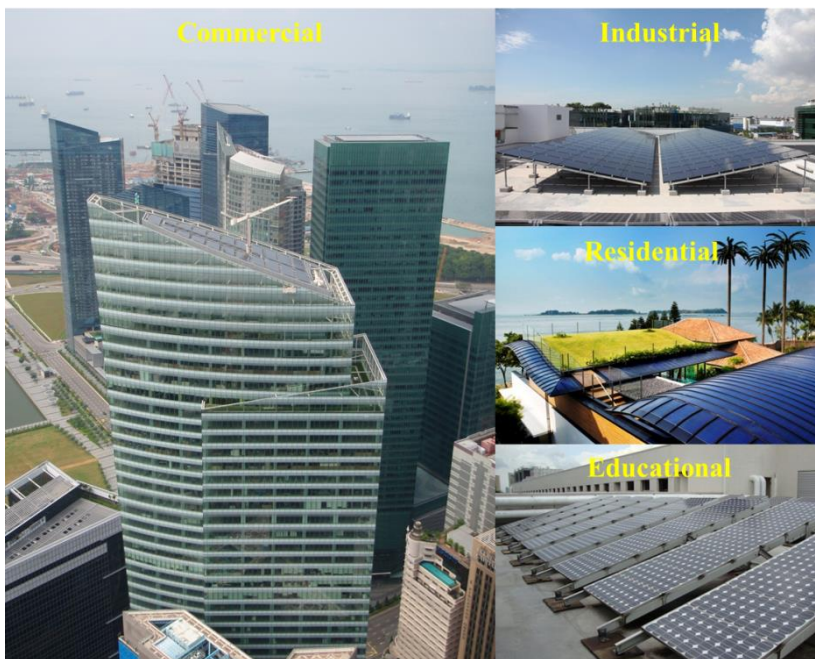


Figure 66: NSR PV system category examples – commercial, industrial, residential and educational systems are categorized in the database (NSR, 2013c).

The solar resource as assessed by the SERIS meteorological station is perhaps the most reliable reading of solar irradiance in the country for PV applications, with highest data availability (above 99.5% of data collected) and optimum data reliability (weekly cleaning of sensors and tight maintenance practices). The average daily global horizontal irradiance recorded over the same 2.5 years was 4.32 kWh/m² per day, which would represent a meteorological year average of 1,577 kWh/m², -3.3% versus long-term TMY for Singapore as portrayed in subsection 2.3.2. All in all, with shallow installation tilt angles, it could be assumed

that this average output for 43 installations has a performance ratio of approximately 72%. As demonstrated in the previous subsection, a research median of ~80% had been validated, an 8% gap versus the country's benchmark. This highlights that there is considerable room for improvement for PV systems performance throughout the island as new installations come online.

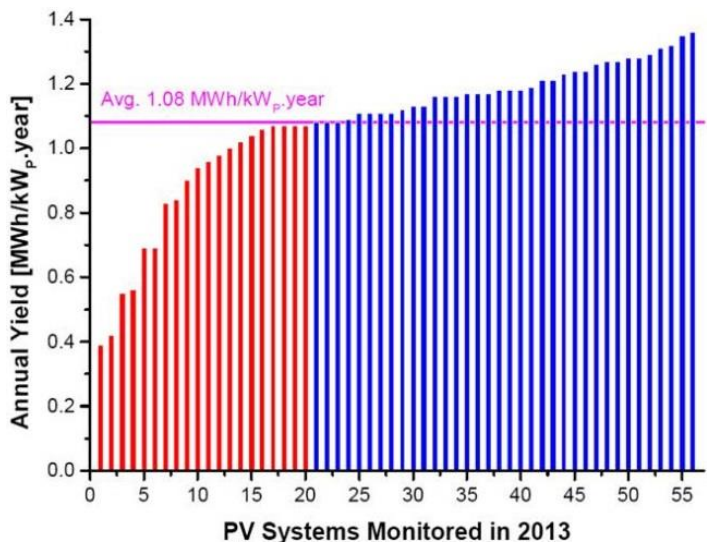


Figure 67: NSR 2013 benchmarking results for PV systems in Singapore (NSR, 2015d).

2.6 PV SYSTEMS MODELING

2.6.1 Available tools

One of the most used commercially available software for PV system modeling is PVSYST (PVSYST, 2013). Most system integrators use this tool for system design, performance assessment and DC electrical range checks such as for operational voltages and currents of module strings.

Another software commonly used is PV*SOL, from the Solar Design Company (PV*SOL, 2013).

As an example of other software, for its CERP-02 research project on PV systems performance in the tropics, SERIS used the PV systems modeling software “Zenit”, from the Fraunhofer Institute for Solar Energy Systems (ISE). The in-house built software is a compendium of two decades of experience of the German institute in PV systems yield and performance assessment.

2.6.2 Existing research in PV systems modeling

Heydenreich et al. (HEYDENREICH, MUELLER, *et al.*, 2008) tested a PV power model using three parameters (a, b, c) to characterize the efficiency curves of PV devices. The authors applied flash testing to several crystalline silicon modules in order to empirically test the appropriate three parameters intended. The formula for the model follows:

$$\eta_{mpp,25}(G_{mod}) = aG_{mod} + b \ln(G_{mod} + 1) + c \left[\ln^2 \left(\frac{G_{mod}+e}{G_{mod}+1} \right) - 1 \right] \quad (9)$$

where $\eta_{mpp,25}$ is the efficiency of the PV module at 25°C at its maximum power point (MPP) efficiency, G_{mod} is the irradiance on the plane of the array, and a, b, c the model values derived empirically in the study. Continuing, Equation 9 yields the module MPP efficiency only at the condition of device temperature at 25°C. For the efficiency adjustment at other temperature ranges, Equation 10 should be applied:

$$\eta_{mpp,25}(G_{mod}, T_{mod}) = \eta_{mpp,25}(G_{mod}) [1 + \alpha(T_{mod} - 25^\circ)] \quad (10)$$

where η_{mpp} is the efficiency of the photovoltaic device at a given temperature, T_{mod} is the module temperature and α is the temperature coefficient of the MPP power. A common value for α in crystalline silicon

modules is $-0.0045^{\circ}\text{C}^{-1}$, as found in the specifications of the majority of PV panels. In order to estimate module temperatures, the following Equation is valid, for the condition of no wind, which is often the case in Singapore:

$$T_{mod} = T_{amb} + \gamma G_{mod} \quad (11)$$

where T_{amb} is the ambient temperature, with γ commonly referred to as the Ross coefficient, dependent on installation mounting type (ROSS, 1976). A typical value used for γ is $0.020^{\circ}\text{Cm}^2\text{W}^{-1}$ for ground-mounted installations with good ventilation.

State-of-the-art PV systems in Germany started to achieve close to 90% performance ratios, with temperature-related losses accounting for ~20% and ~45% of the total system losses for winter and summer months, respectively (REICH *et al.*, 2012). A recent study on PV simulation using 29 PV systems in Spain and predominantly in Germany showed differences in yield estimations and actual field output due primarily to solar brightening (the irradiation databases, based on past decades records, present lower annual irradiation levels than recent records). The combined uncertainty of yield predictions today lies at 8%, as shown in Müller *et al.* (MÜLLER *et al.*, 2015).

After using numerical weather prediction forecasts for the entire Europe zone, Lorenz *et al.* (LORENZ *et al.*, 2011) have performed an up-scaling routine for PV systems in Germany using a baseline of representative installations in order to predict future system output for the many thousands of other systems in the country. Input parameters were forecasted irradiance up to two days ahead in hourly resolutions, achieved by the numerical model prediction, with ambient temperature playing a role in determining module temperature (as per Equation 11) taking into account a number of assumptions.

As an example in Asia, researchers conducted a comprehensive investigation on power forecast for day-ahead applications in more than 700 PV systems in Japan (FONSECA_JR. *et al.*, 2013). The study found that for systems tilted above 40 degrees, higher forecast errors were identified in the modeling.

2.6.3 Challenges of modeling in tropical conditions

With a research-grade software which had been previously and extensively validated in a temperate location of the world (HEYDENREICH, MÜLLER, *et al.*, 2008; REICH *et al.*, 2012), the

software from Fraunhofer ISE was further put to test at a different climatic condition in the world in tropical Singapore.

Detailed loss mechanisms are shown as two-bar clusters (see Figure 68, with measured (left bars) and simulated (right bars) values of 11 silicon wafer-based PV systems under monitoring in Singapore. Simulation of systems A through F were within $\pm 2\%$ of the actual measured results, while PV systems G through K experienced technical faults during operation, causing larger deviations of the measured values from the "ideal behavior", which is the outcome of the simulation software.

Simulations were performed with the software "Zenit", developed by Fraunhofer ISE and adjusted by SERIS for the local irradiance and temperature conditions in the tropics. The irradiance data inserted into the simulation is the same as read by the silicon sensors on site, hence soiling and reflection losses are not computed, assuming that the same conditions experienced by the silicon sensors will prevail also at the PV systems (since both are of similar materials and installed at the same inclination angles) and, for Singapore, kept uncleaned.

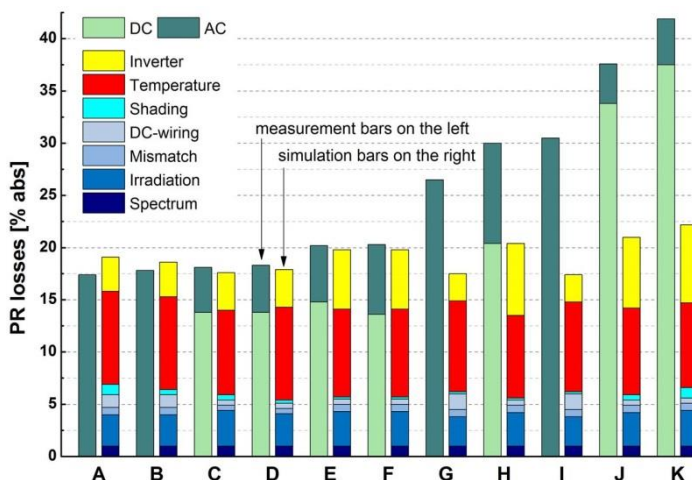


Figure 68: Simulated versus measured loss mechanisms of 11 PV systems in Singapore (NOBRE, YE, *et al.*, 2012).

Analyzing systems A through F, it can be seen that the largest difference between measured and simulated results was 1.7% for system A, which is in line with previous publications that reported uncertainties in the $\pm 2.0\%$ range (REICH *et al.*, 2012). For the subsequent systems G

through K, individual explanations were given to their sub-optimum operational (measured) behavior (NOBRE, YE, *et al.*, 2012).

Zomer *et al.* used Zenit for simulations of PV systems in Brazilian airports (ZOMER *et al.*, 2013), as well as taking the “Brazilian Efficiency” for inverters (PINTO, 2012) into account.

Ye *et al.* showed that module temperatures in the field in Singapore can reach almost a 3-fold variation from coolest to hottest systems (see Figure 69). The scatter of the temperature differences were explained qualitatively in the publication as being caused by four major factors: (1) roof top material, usually made of concrete or metal; (2) module-to-ground separation, from a few centimeters all the way to more than 1 m gap; (3) whether modules are framed or frameless, with the framed ones presenting an extra barrier for natural ventilation flow; and (4) other environmental aspects, such as being close to a nature reserve, as opposed to being located in a highly-dense environment and subjected to “urban heat islands” (YE *et al.*, 2013).

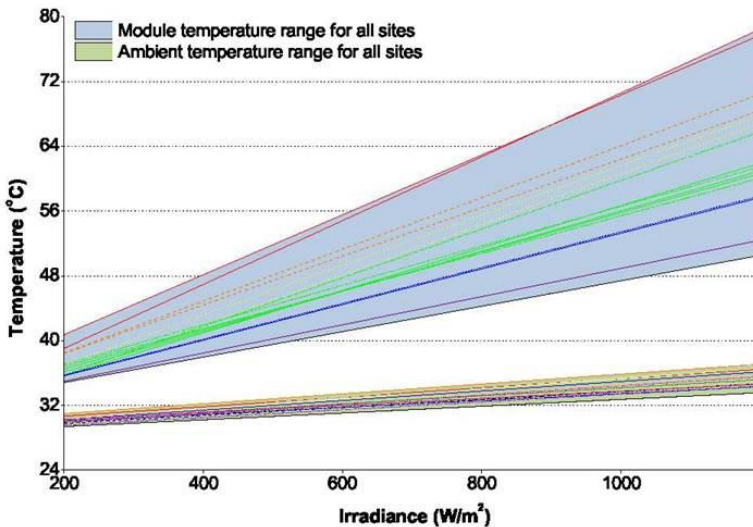


Figure 69: Module and ambient temperature variations with irradiance for 17 PV systems in Singapore (YE *et al.*, 2013).

Nobre *et al.* have demonstrated that this model is valid for a different tropical location around the world. Three PV systems in Brazil were used within the calculation methodology which had been previously proposed for Singapore (NOBRE, MONTENEGRO, *et al.*, 2012).

3. METHOD

3.1 PRELIMINARY REMARKS

3.1.1 R&D supporting infrastructure and overview

This thesis had the goal of advancing knowledge on short-term solar irradiance forecasting in tropical regions of the world, together with adding further value by including actual power output know-how gained from already deployed PV systems in preparation for a future with a considerable share of renewables in electricity matrices.

Research data collection within past R&D projects in Singapore started in 2009 for PV systems and weather parameters alike. With the accumulation of historical data from these projects, plus the addition of new meteorological stations and PV installations to the country's network, past and present datasets allowed and continue to allow new findings in solar resource forecasting and systems behavior for the tropics.

As stated in the objectives, enhancements to solar irradiance forecasting on short time scales (such as 15-min, 30-min and 1-hr forecast horizons) were covered first. After obtaining irradiance values ahead of time, PV systems performance was taken into account, both by understanding loss mechanisms in PV systems as well as their long-term operational behavior, trying to minimize errors throughout the processes.

Sources of data enabling the investigation towards its main and specific goals stem from research projects from the Solar Energy Research Institute of Singapore (SERIS), namely:

- ➔ Irradiance and general meteorological data arising from the Clean Energy Research Program (CERP-04 project call) – “Novel monitoring and control unit for enhanced availability and reliability of solar PV systems – optimization of photovoltaic electricity generation in tropical power grids through radiation forecasting and system monitoring”, a 3-year long research project managed by SERIS, which took place between 2011 and 2014;
- ➔ PV systems operational data from the CERP-02 project call – “High performance PV systems for tropical regions – optimization of system performance”, a 3-year long research project, also managed by SERIS, between 2009 and 2012;

- ➔ PV systems monthly energy output data (for some sites, daily) from the National Solar Repository of Singapore (NSR) initiative, an ongoing research activity led by SERIS, which allows for country-wide up-scaling exercises.

Although the CERP-02 and -04 projects were officially completed, the data acquisition is still ongoing, which allows for further weather knowledge gains and long-term PV system behavior studies.

This thesis focuses on irradiance forecasting at short-term intervals together with a full PV power conversion routine validation of the predicted results towards PV system performance assessment ahead of time. In a sense, an “irradiance-to-kWh” chain of events but taking place before the electricity is actually produced. Figure 70 illustrates and summarizes the work intended, with inputs for proposed forecasts powered by algorithms using from meteorological parameters, as well as data from PV systems readily available for method validation.

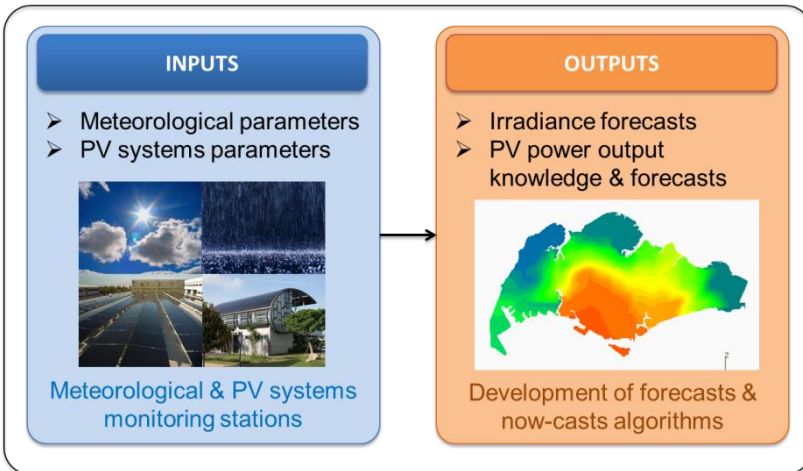


Figure 70: Illustration of proposed method: “Irradiance-to-kWh” simulation and validation (adapted for this thesis).

The network of ground-irradiance sensors deployed in Singapore is one of the densest in the world. It is also easy to maintain due primarily to the proximity of stations to the SERIS building (longest distance which the team needs to commute for access is ~35 km).

Existing stochastic and artificial intelligence methods are explored for short-term irradiance forecasting. The performances of the methods

are compared to determine which are more suitable for this region of the world. Additionally, a novel Hybrid model is introduced in an attempt to curtail prediction errors.

Empirical data of the thesis comes from a fine-grid area of ground-based stations measuring global horizontal irradiance as well as other meteorological parameters. The network of 25 ground-measurement stations was completed in November 2013. The PV sites used for power conversion modeling were first deployed in January 2010, with fifteen sites at the completion of this thesis accounting for ~ 1 MW_p of PV systems of various sizes, technologies and tilt & azimuth angles.

3.1.2 Boundary conditions of the investigations

Forecasting irradiance for photovoltaic applications means essentially predicting the global horizontal irradiation (GHI) at future time steps. The thesis is centered on a short-term application setting.

Challenges do exist in modeling irradiance on the plane of the array of a PV system, and later photovoltaic energy generation (kWh), at lower irradiance values ($< 100 \text{ W/m}^2$) due mainly to:

- i. Complex shading onto irradiance devices due to external nearby structures (buildings, trees), as well as horizon shading from a heavily-urbanized environment as the one found in Singapore;
- ii. Precision of irradiance measurement devices (especially silicon sensors) at very steep solar elevations angles, which take place in early mornings and late afternoons;

Moreover, electricity demand peaks usually occur between 10 am and 5 pm for Singapore (see Figure 8) as well as the majority of the electricity production from solar PV systems (see Figure 42, with most of the irradiance values falling within the $300\text{-}900 \text{ W/m}^2$ range). Therefore, the algorithms and tests within this thesis focus on an 8-hour window of interest – ranging from 9 am to 5 pm – on a daily basis.

Validation of the proposed and under scrutiny methods is achieved through data from $\sim 1 \text{ MW}_p$ worth of PV systems from an existing portfolio ($\sim 3\%$ of the installed capacity of the country as of December 2014). Up-scaling is later investigated thanks to data from the National Solar Repository of Singapore (NSR), with $\sim 9 \text{ MW}_p$ of systems ($\sim 1/4$ of the installations in the country in volume terms). Up-scaling is later described in subsection 3.4.4.

For the forecasting windows, the shortest interval is set for 15-min, with a second interval selected for 30-min, matching dispatch cycle of electricity trading in Singapore (EMA, 2013). A further horizon window of 1-hr is also put to test.

3.2 SOURCES OF DATA

3.2.1 Ground-measured irradiance data

This thesis focuses on solar irradiance forecasting for the location Singapore together with power conversion for PV applications. Figure 71 shows the ground-based meteorological station network deployed by SERIS throughout the island as part of the research project “CERP-04”.

In order to obtain the ground measurement readings at a good spatial resolution, 25 stations of the project were distributed across Singapore using a 5x5 km grid as reference, trying to achieve the best distribution possible. Some locations are off-bound military zones or protected tropical rain forests or reservoirs, which prevented a more uniform distribution of the meteorological stations.

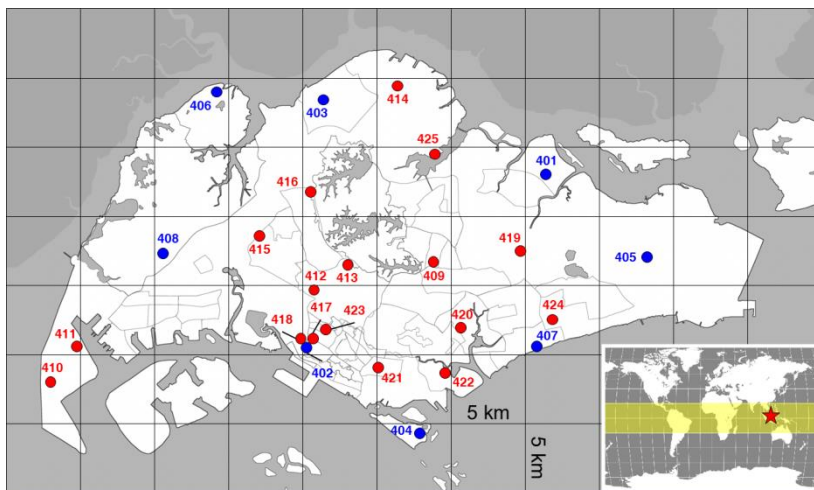


Figure 71: Singapore’s 25 ground-based stations of the CERP-04 research (adapted for this thesis).

The original CERP-04 network of stations is composed of eight stations which are called “superstations”, with the remaining seventeen named “basic stations”. The difference between these stations lies on the variety of meteorological sensors installed in each of them. A superstation has two readings of global horizontal irradiance (GHI), one with a calibrated silicon sensor (manufacturer: Mencke & Tegtmeier, Germany) and one with an SPN1 pyranometer (manufacturer: Delta-T, United Kingdom). The SPN1 pyranometer also measures the diffuse irradiance via an internal algorithm and readings from seven small thermopiles, with

a shadow mask mounted inside its glass dome. Other sensors available at a superstation are ambient temperature, relative humidity, wind speed, wind direction and finally an air pressure sensor. A basic station, on the other hand, is a small setup and has only the calibrated silicon sensor, ambient temperature and relative humidity sensors. Such selection of sensors guaranteed that all 25 stations of the network had a “common denominator”, that is, three key readings which are crucial for irradiance mapping and forecasting, as well as necessary inputs for PV systems simulation, when needed. A basic and a superstation can be seen in Figure 72.



Figure 72: Basic meteorological station #425 (left) and superstation #408 (right, wind sensors not pictured) (source: SERIS).

The sensors deployed at super and basic stations of the island-wide network are described in Table 9. The three sensors present in all stations (common denominators) for the entire island are marked in red. The superstation sensors are further described in the table (marked in blue), together with all associated uncertainties of these devices.

Due to the high costs of a superstation, only a certain number of them were deployed arising from project budget constraints. The goal therefore was to disperse them in a way that they cover strategic points of the island, with special attention in putting several of these stations on the

outskirts of Singapore, with such a strategy later leveraged and discussed in subsection 3.3.2.

Table 9: Measurement uncertainties of super and basic stations of the network (source: adapted from sensor manufacturers).

Parameter	Description/ Device	Manufacturer/ Model	Uncertainty	Super/ Basic
GHI_{Si}	Global horizontal irradiance/ silicon sensor	Mencke & Tegtmeier/ Si-02-PT100-K	±2.0% lab ⁴ , ±5.0% field	Basic
T_{amb}	Ambient temperature/ PT100 probe	Thies Clima/ PT100, Class B	±0.2 K	Basic
H_{amb}	Relative humidity/ capacitive element	Thies Clima/ 1.1005.54.000	±2.0%	Basic
GHI_{SPNI}	Global horizontal irradiance/ pyranometer	Delta-T/ Sunshine pyranometer	±5.0%	Super
DHI_{SPNI}	Diffuse horizontal irradiance/ pyranometer	Delta-T/ Sunshine pyranometer	±5.0%	Super
W_s	Wind speed/ cup anemometer	Thies Clima/ 4.3519.00.141	±0.5%	Super
W_D	Wind direction/ wind vane	Thies Clima/ 4.3129.60.141	±2°	Super
Air_p	Air pressure/ barometer	Thies Clima/ B-278-1T	±0.3 hPa at 20°C	Super

Table 10 describes each station in terms of district location in Singapore, its global positioning system (GPS) coordinates and altitude. All GPS coordinates were acquired with a Garmin Forerunner 310XT GPS watch, with a stated precision according to satellite signal strength at the moment of recording of ±10 m.

⁴ All silicon sensors of the SERIS research projects are calibrated either at the Fraunhofer Institute for Solar Energy Systems' (ISE) CalLab or at the National Metrology Centre in Singapore (NMC) at highest accuracy levels available for research applications. Based on previous experience of ISE, silicon sensors are exchanged in the field after a period of two years of exposure, which is performed even after the R&D project completion. All other sensors have calibrated certificates from their respective manufacturers and are safe to use upon failure.

Table 10: Basic characteristics of 25 ground-measuring meteorological stations in Singapore (adapted for this thesis).

ID #	Station Name	District in Singapore	Latitude [N]	Longitude [E]	Altitude [m]	Date Deployed
S1	401	Punggol	1°23'58"	103°54'33"	54	Oct/12
S2	402	Clementi	1°18'02"	103°46'16"	63	Jul/11
S3	403	Woodlands	1°26'38"	103°47'03"	45	Apr/12
S4	404	Sentosa	1°14'57"	103°50'29"	36	May/12
S5	405	Changi	1°21'10"	103°57'55"	45	May/12
S6	406	Lim Chu Kang	1°26'45"	103°42'39"	57	Jan/13
S7	407	Marine Parade	1°18'09"	103°54'44"	26	Nov/12
S8	408	Boon Lay	1°21'18"	103°41'33"	57	May/12
B9	409	Bishan	1°20'52"	103°50'29"	52	Feb/13
B10	410	Tuas	1°16'26"	103°37'21"	60	Jun/13
B11	411	Tuas	1°17'55"	103°38'25"	26	Dec/11
B12	412	Bukit Timah	1°20'00"	103°46'22"	50	May/12
B13	413	Bukit Timah	1°20'43"	103°47'30"	55	Oct/12
B14	414	Sembawang	1°27'11"	103°49'15"	60	Jan/12
B15	415	Bukit Batok	1°21'43"	103°44'40"	53	Nov/12
B16	416	Bukit Panjang	1°23'23"	103°46'23"	60	Jul/13
B17	417	Clementi	1°18'09"	103°46'22"	26	Apr/13
B18	418	Clementi	1°18'24"	103°46'23"	44	May/13
B19	419	Hougang	1°21'08"	103°55'22"	51	Nov/12
B20	420	Lavender	1°18'34"	103°51'42"	50	Sep/13
B21	421	Redhill	1°17'21"	103°49'01"	55	Jul/13
B22	422	CBD	1°16'59"	103°51'07"	99	Nov/13
B23	423	Dover	1°18'40"	103°46'32"	57	Jul/13
B24	424	Frankel	1°18'54"	103°54'55"	20	Apr/13
B25	425	Lower Seletar	1°24'35"	103°56'51"	10	Aug/13

3.2.2 Operational data of PV systems

Via its CERP-02 research project “High Performance PV Systems for Tropical Regions – Optimization of System Performance”, SERIS deployed close to 1 MWp worth of PV systems monitoring setups (spread over fifteen sites, see Figure 73, and accounting for a total of 33 sub-systems, see Table 11. Site selection, which took place in 2009, was based on the maximum possible diversity of PV systems in Singapore available at that instant in time, in terms of geographic spread around the island, variety of PV technologies (monocrystalline, multicrystalline and thin-film based), system sizes (ranging from a couple of kWp all the way to the biggest site of ~230 kWp), and commissioned by different system integrators.

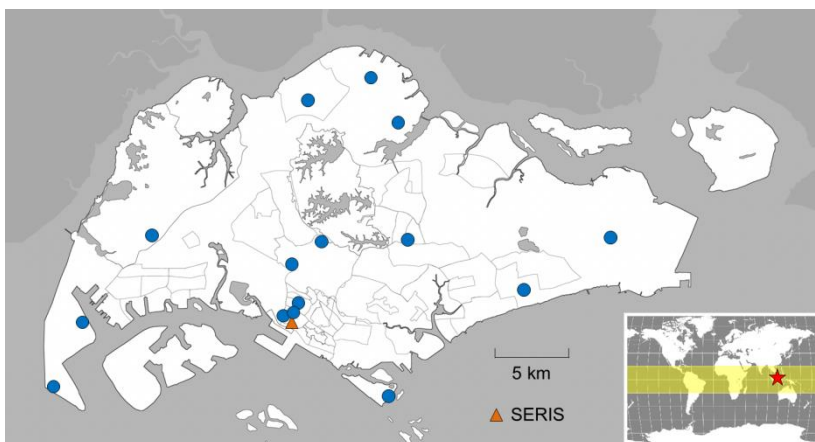


Figure 73: Location of 15 PV sites from the SERIS CERP-02 research in Singapore (adapted for this thesis).

From Table 11, showing the basic sub-systems’ characteristics, it can be attested that even though Singapore is located at 1°N of the Equator, theoretically calling for a flat installation for maximum irradiance harvesting, the preferred installation tilt angle is approximately 10°, which facilitates the “self-cleaning effect” of the modules through rain. The proximity to the Equator allows for no predominant azimuth, with most PV systems following the building geometry. However, as shown in Figure 35, it has been previously investigated that the best tilt and orientation angles for PV systems in Singapore are ~10° and ~90° East-facing, respectively (KHOO, NOBRE, et al., 2014).

Table 11: Basic information for 33 PV sub-systems under monitoring at 15 sites via the SERIS' CERP-02 research project (adapted for this thesis).

PV #	Technology	Size [kW _p]	Tilt [°]	Azimuth [0-360°]	District in Singapore
101a	a-Si	4.9	12	50 NE	Sentosa
102a	p-Si	5.2	11	10 N	Clementi
103a	m-Si	4.8	15	200 SW	Dover
104a	p-Si	15.0	6	220 SW	Woodlands
105a	m-Si	10.4	7	205 SW	Sembawang
106a	p-Si	13.5	6	130 SE	Tuas
106b	p-Si	167.4	10~16	130 SE	Tuas
107a	p-Si	60.8	10	10 N	Tuas
107b	p-Si	91.1	10	190 S	Tuas
108a	p-Si	3.8	flat	-	Bukit Timah
109a	a-Si	5.1	10	220 SW	Bishan
110a	a-Si	162.7	5	340 N	Changi
111a	a-Si	4.8	19	70 NE	Frankel
111b	μc-Si	3.8	6	250 SW	Frankel
112a	m-Si	2.1	10	0 N	Clementi
112b	p-Si	2.0	10	0 N	Clementi
112c	a-Si	2.1	10	0 N	Clementi
113a	HIT	6.3	10	200 SW	Clementi
113b	a-Si	4.0	10	200 SW	Clementi
113c	p-Si	5.6	10	200 SW	Clementi
113d	p-Si	4.6	10	200 SW	Clementi
113e	p-Si	4.6	10	200 SW	Clementi
114a	p-Si	19.7	10	0 N	Boon Lay
114b	p-Si	19.7	10	180 S	Boon Lay
114c	p-Si	19.7	10	90 E	Boon Lay
114d	p-Si	19.7	10	270 W	Boon Lay
114e	p-Si	42.1	10	0 N/180 S	Boon Lay
114f	p-Si	95.9	10	0 N	Boon Lay
114g	p-Si	14.1	10	0 N/180 S	Boon Lay
115a	m-Si	43.2	8	110 SE	Yishun
115b	p-Si	37.4	8	110 SE	Yishun
115c	a-Si	42.0	8	110 SE	Yishun
115d	m-Si	14.5	3	20 N	Yishun
TOTAL		952.8			

All SERIS monitoring systems record the investigated parameters as one minute averages, with a sampling rate of 1 Hz. All measurements are performed with identical sensors, under same calibration routines, thus guaranteeing a reliable comparison between sites.

For the PV systems monitoring setups, the sensors deployed in the field and their uncertainties are summarized in Table 12. Silicon sensors

carry a laboratory accuracy of $\pm 2\%$, as previously reported. Other uncertainties of the monitoring system are based on sensor manufacturer's specifications.

Table 12: Measurement uncertainties of the PV system monitoring setup of CERP-02 sites (source: adapted from sensor manufacturers).

Parameter	Description/Device	Manufacturer/Model	Uncertainty
G_{mod}	In-plane irradiance/ silicon sensor	Mencke & Tegtmeyer/ Si-02-PT100-K	$\pm 2.0\%$ lab, $\pm 5.0\%$ field
T_{amb}	Ambient temperature/ PT100 probe	Thies Clima/ PT100, Class B	± 0.2 K
T_{mod}	Module temperature/ PT100 probe behind panel	Thies Clima/ PT100, Class B	± 0.2 K
P_{AC}	AC power/ analogue, with current transducers	Ziegler & Müller/ EDM-400	$\pm 0.5\%$
E_{AC}	AC energy/ integrator meters, with pulses	Ziegler & Müller/ EDM-400	$\pm 1.0\%$
I_{DC}	DC current/ shunts	Ziegler & Müller/ 10-20 A shunts	$\pm 0.2\%$
V_{DC}	DC voltage/ voltage transducers	Ziegler & Müller/ 300-600 V transducers	$\pm 0.5\%$

All PV systems investigated have DC strings under monitoring, as well as the site's AC inverter outputs. In some of the subsystems, the full DC side of the PV array is included as part of the monitoring setup, while for other larger and more complex systems, only one or some reference DC strings were chosen for the monitoring.

No wind sensors (for speed and direction measurements) were originally installed at sites, since wind speed in Singapore is relatively low, with daily mean values not higher than 2.8 m/s (NEA, 2009). The SERIS meteorological station installed at its headquarters rooftop reported a daily average of 1.4 m/s for 2011, as shown in Figure 61.

It is expected that loggers utilized in the research add errors in the order of $\pm 0.2\%$. Some further errors may be introduced in the form of transducers, e.g. those needed to read the shunt voltage measurements. Eventually, it can be expected that the overall uncertainty of the performance ratio measurements under these conditions is within $\pm 3.0\%$, in line with previous similar scientific investigations conducted in Europe (MÜLLER *et al.*, 2015; REICH *et al.*, 2012).

3.2.3 Robustness of the data collection infrastructure

A challenge on the data collection front for such locations in the tropics concerns the logging hardware infrastructure. The rough environment conditions posed to monitoring system housings under the sun present challenges for the logger and other components such as sensor transducers. As seen in the thermal image of Figure 74, the temperature inside a monitoring cabinet in Singapore can easily reach values above 50°C and due to the annual weather similarity, with the absence of seasons, these conditions happen almost on a daily basis. Therefore, industrial-grade setups were used for the logging hardware (here from company National Instruments). Such practice of using higher-end monitoring systems hardware guaranteed overall system data availability rates greater than 99.5% throughout the course of the investigations.



Figure 74: Thermography of a monitoring cabinet at around noon (source: SERIS).

In order to properly perform correlation exercises between stations, time synchronization is critical. All 25 meteorological stations of the network, as well as the 15 PV system sites, run according to the same time server at the SERIS' PV Systems Monitoring Laboratory. Once the clock at a remote station deviates by 150 ms against the master clock of the server, a correction routine is applied. This method guarantees that remote stations are at a maximum 0.3 seconds adrift from one another.

3.3 METHODS FOR IRRADIANCE FORECASTING

3.3.1 Utilization of existing forecasting techniques

The thesis investigations saw tests with several forecasting techniques as follows:

[1] Persistence

Persistence is the most common method utilized in general forecasting practices, also serving as a benchmark tool against other proposed methods. It assumes the next step of the time series has equal conditions to the present. In the case of solar irradiance forecasting, it is assumed that the cloud cover remains the same for the next time step. The formulation for Persistence used in the investigations is represented as:

$$k_{t+1} = k_t = \frac{G_t}{G_t^{clear}} \quad (12)$$

where k_{t+1} is the forecasted clear sky index in the next time step, k_t is the value of clear sky index at the present time step, G_t is the value of global horizontal irradiance and G_t^{clear} is the value of the clear sky irradiance, both at present. The Persistence forecast value for the global horizontal irradiance, G_{t+1} , is then completed as:

$$G_{t+1} = k_t G_{t+1}^{clear} \quad (13)$$

with the clear sky index k_t in the present multiplied by the clear sky irradiance value at the next time step (G_{t+1}^{clear}). As per objectives of the thesis, the investigatory focus lies on short-term applications. Thus, the forecast horizons used equal to 15-min, 30-min (matching the trading interval for electricity in Singapore) and 1-hr.

[2] Auto-regressive integrated moving average (ARIMA)

This forecast is performed on the univariate time series of clear sky indices. Each forecast step fits a new ARIMA or ETS model (see method [3]), and then makes a one-step ahead forecast $t + 1$ based on the fitted model.

The univariate ARIMA uses the Hyndman-Khandakar algorithm for automatic modeling (HYNDMAN and KHANDAKAR, 2008), where

the best ARIMA model is selected for each forecast step according to AICc (corrected Akaike information criteria).

The outline of the algorithm is further described as follows:

- The number of differences d is found by using repeated KPSS (Kwiatkowski–Phillips–Schmidt–Shin) tests;
- The values of p and q (the autoregressive and moving average components of the chosen ARIMA function) are selected by minimizing the AICc after differencing the data d times. The algorithm applies a stepwise search to traverse the model space instead of exploring all the possible combinations of p and q ;
 - Finding the smallest AICc (namely, the best model) is achieved by selecting from the following four configurations: ARIMA (2, d ,2), ARIMA (0, d ,0), ARIMA (1, d ,0), ARIMA (0, d ,1). If $d = 0$, the constant c is included; if $d \geq 1$, the constant c is set to zero (namely, the current model);
 - Variations on the current model are considered such as varying p and/or q by ± 1 ; and include or exclude c from the current model. The best model considered so far (either the current model, or one of these variations) becomes the new current model;
 - The previous step is repeated until no lower AICc can be found.

Pedro and Coimbra in the United States (PEDRO and COIMBRA, 2012), Masa-Bote and Caamaño-Martín in Spain (MASA-BOTE and CAAMAÑO-MARTÍN, 2010), and Dong et al. and Ye et al. in Singapore (DONG *et al.*, 2013; YANG, D., DONG, Z., *et al.*, 2014), are some of the works in the past years applying variations of ARIMA for solar forecasting purposes.

[3] ETS (exponential smoothing state space) model

Exponential smoothing state space (commonly abbreviated as ETS) considers time series as a combination of three components, namely, the trend (T), the seasonal (S) and the error (E) components. The trend component consists of the combination of a level term (I), and a

growth term (b). When describing the forecast trend T_h over the next h time periods, l and b can be combined in the following five ways:

- None: $T_h = l$
- Additive: $T_h = l + bh$
- Additive damped: $T_h = l + (\phi + \phi^2 + \dots + \phi^h)b$
- Multiplicative: $T_h = lb^h$
- Multiplicative damped: $T_h = lb(\phi + \phi^2 + \dots + \phi^h)$

where $0 < \phi < 1$ is a damping parameter. Besides the trend component, the seasonal components can be additive ($T + S$), multiplicative ($T \times S$) or none. This gives rise to the 15 combination of time series components shown in Table 13 (YANG, SHARMA, *et al.*, 2015).

Table 13: Possible combination of time series components in an exponential smoothing model (YANG, SHARMA, *et al.*, 2015).

Trend	Seasonal		
	N (None)	A (Additive)	M (Multiplicative)
N (None)	N,N	N,A	N,M
A (Additive)	A,N	A,A	A,M
A _d (Additive damped)	A _d ,N	A _d ,A	A _d ,M
M (Multiplicative)	M,N	M,A	M,M
M _d (Multiplicative damped)	M _d ,N	M _d ,A	M _d ,M

Suppose the errors in an exponential smoothing state space model (which refers to error, trend and seasonal components) can be either additive or multiplicative, then there are in total 30 ETS models. Following the framework terminology given in (HYNDMAN *et al.*, 2008), each state space model according to its Error, Trend, Seasonal configurations, respectively, is labeled. For example, ETS (M, N, and N) corresponds to simple exponential smoothing with multiplicative errors.

For the usage of ETS within this thesis, the models are run without seasonal component, since the forecast is performed on time series of clear sky indices. Yang *et al.* (YANG, SHARMA, *et al.*, 2015) and Dong *et al.* (DONG *et al.*, 2013) have published articles on solar irradiance forecasting using ETS.

The Persistence forecasting methods, as well as the ARIMA and ETS ones were run in the statistical software “R Studios”.

[4] Artificial neural networks (ANN)

Artificial neural networks (ANN) were created from the observation of neurons as a special type of cell. In most cases, signals are propagated from neuron to neuron until they reach the desired target (HAYKIN, 1999). This signal propagation is the basis of an ANN architecture, where artificial neurons are arranged in layers along which the original input is processed in order to formulate a desirable output.

A classic example of ANN architecture was shown in Figure 54. An input layer takes the original data, which is processed along internal neuron layers, called hidden layers until a corresponding value is obtained in an output layer. ANNs are commonly used in classification and forecasting problems (HAYKIN, 1999). Works by Marquez et al. (MARQUEZ *et al.*, 2013), Pedro and Coimbra (PEDRO and COIMBRA, 2012), Marquez and Coimbra (MARQUEZ and COIMBRA, 2011), Mellit and Pavan (MELLIT and PAVAN, 2010) and Cao and Cao (CAO, J. C. and CAO, S. H., 2006) are examples of ANN applied to solar irradiation modeling.

Mathematically, an ANN can be represented as an equation, which is composed by functions $f(x)$, called activation functions. Those functions compose a weighted sum as shown in Equation 14:

$$y = \left(\sum_j w_j f_j \left(\sum_{i,j} W_{ij} x_i \right) \right) \quad (14)$$

where x is the input vector $[x_1, x_2, \dots, x_n]$; f is the activation function, used for each neuron in the hidden layer; W_{ij} are elements of the weight matrix, which connects input layer to the hidden layer, from i th neuron in the input layer to j th neuron in the hidden layer; and w_j is the element of the weight vector connecting the hidden layer to the output layer. This model represents an ANN with one hidden layer and a single neuron in the output layer. An ANN output is provided by the combination of weights and activation functions.

For the experiments with ANN proposed in this thesis, the following settings are applied:

- For 1-hr forecasting horizon, an input layer with 24 neurons: one neuron for hour in t and twenty-three others with irradiance values observed in steps $t - 23$ to t (i.e. information from the last 24-hrs);

- For 30-min forecasting horizon, an input layer with 13 neurons: one neuron for hour in t and twelve others with irradiance values observed in steps $t - 11$ to t (i.e. information from the last 6-hrs);
- For 15-min forecasting horizon, twenty-four steps were considered (i.e. also with information from the last 6-hrs);
- A hidden layer with two neurons was utilized;
- An output layer with one neuron represents the target irradiance value in $t + 1$;
- The activation function for the hidden layer is the hyperbolic tangent sigmoid, and for the output layer, the linear transfer function is applied;
- The ANN is trained with adaptive gradient descent with momentum training method.

All ANN architecture, tests and validations were conducted in the software “Matlab”.

As a tropical location, Singapore lacks the typical seasons of the year, rather having dry and wet seasons (FONG, 2012). The training performed for the ANNs uses past comparable months for the analysis. For example, March 2014 data is used for training and March 2015 for validation, thus maximizing on weather similarities among the involved datasets.

3.3.2 A Hybrid short-term irradiance forecasting method

For the works surrounding this thesis, the author studied the weather in Singapore and how existing forecasting methods behaved at various conditions and their apparent shortfalls. A concept was created for a new Hybrid method (method [5] to be tested), which takes into account meteorological input data acquired through a network of ground-measuring weather stations deployed by SERIS in Singapore. In the method, the concept of “sentries” is adopted, whereby all perimeter stations of the island work as a “watchdog” or “sentinel”, detecting variations of entrance/exit of clouds, rain clouds and any other detectable meteorological phenomena of interest (see Figure 75). As inputs, values such as relative humidity, global horizontal irradiance and air pressure were fully utilized. Thus, the locations of the superstations, when envisioned, followed this method concept.

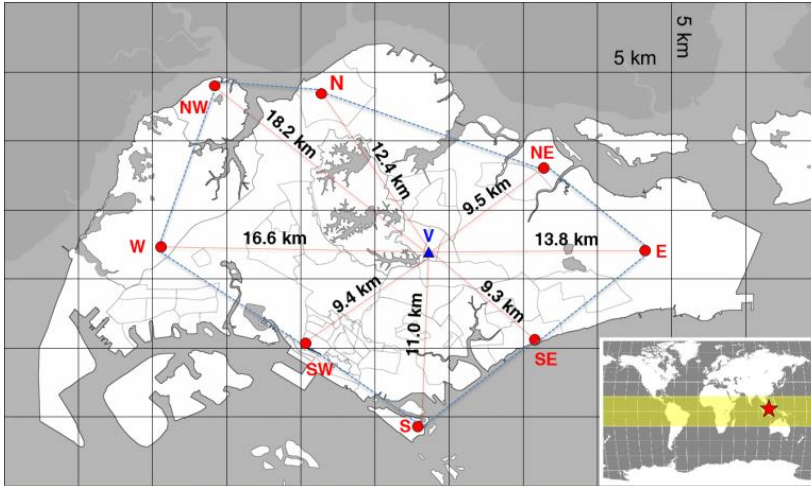


Figure 75: Map of Singapore presenting the location of the nine meteorological stations used in the proposed Hybrid method (NOBRE et al., 2015 (submitted)).

In the novel concept, the Persistence and ARIMA forecasting methods were combined to obtain irradiance forecasts, together with the following parameters used to feed the Hybrid algorithm decision tree (as “triggers”): global horizontal irradiance (GHI), air pressure, relative humidity and clear sky index. Additionally, air pollution readings based on the Pollutant Standard Index (PSI) provided by the National Environment Agency of Singapore (NEA) were also used for the analysis.

Trigger #1: Air pressure

Based on air pressure readings from stations positioned at the boundaries of Singapore, it is aimed that early detection of approaching storms originating from Malaysia (to the North) and Indonesia (Sumatra to the West and Borneo to the East), as well as from Southern islands of Singapore and Indonesia, will lead to enhanced short-term irradiance forecasts. Although broken clouds do form within the island, the approximation of storm phenomena, originating outside of Singapore and traveling towards it, proves to be an invaluable opportunity for enhanced solar irradiance forecasts.

Figure 76 shows the air pressure time series variation between minute (t) and the previous minute ($t - 1$). The pressure variation observed at typical clear sky conditions is shown as red circles (on the top of the

graph). As a comparison, the blue triangles show the air pressure variation at a station to the West of Singapore for the same day as earlier depicted in Figure 11 (i.e. during the arrival of a Sumatra squall). Circa 20-min before the actual arrival of the darker and heavier rain clouds (the time interval was also validated by ground measurements of irradiance), air pressure varied due to the thicker cloud front pushing the air ahead.

For the proposed Hybrid method, any triggering of air pressure variation at the eight outskirt stations is perceived as the arrival of rain clouds and is thus associated with a soon-to-happen, sudden reduction of solar irradiance. The path of the storm is assumed to be linear, although such extrapolation (as exemplified in Figure 11) is not always the case.

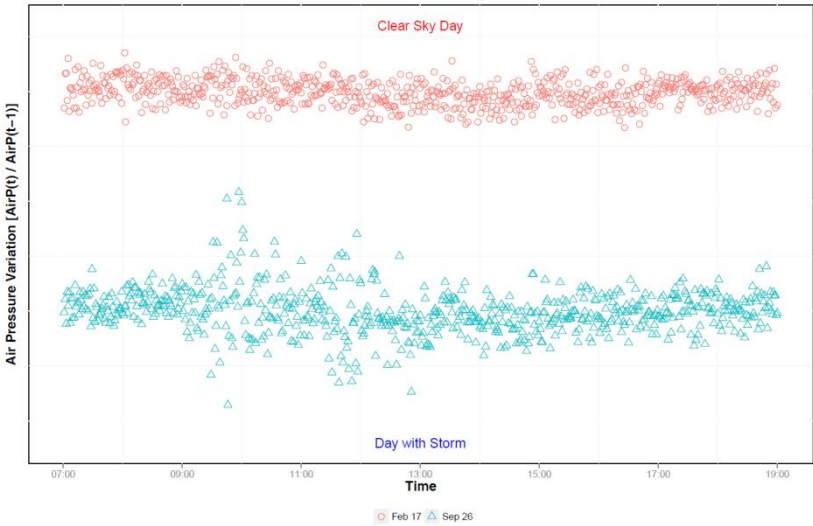


Figure 76: Typical air pressure variation on a 1-min basis for a clear sky day conditions and during an approaching storm (NOBRE et al., 2015 (submitted)).

Trigger #2: Global horizontal irradiance and clear sky index

The clear sky index (k_t , defined as the ratio between the measured global horizontal irradiance and the clear sky irradiance computed for the location) can also be used as an additional input parameter to the Hybrid forecasting model as it is closely related to the cloudiness status of the atmosphere.

In order to better understand certain weather phenomena in Singapore, Figure 77 (top) shows the clear sky indices (based on values of irradiance on ground level measured against an established clear sky model for the island). This graph is assembled using data for two years (2013 and 2014) and binned in 1-hour intervals throughout the day (from 9 am to 5 pm, in eight bin classes). This portion of the graph indicates cloudier afternoons in Singapore, what would be expected for a tropical location.

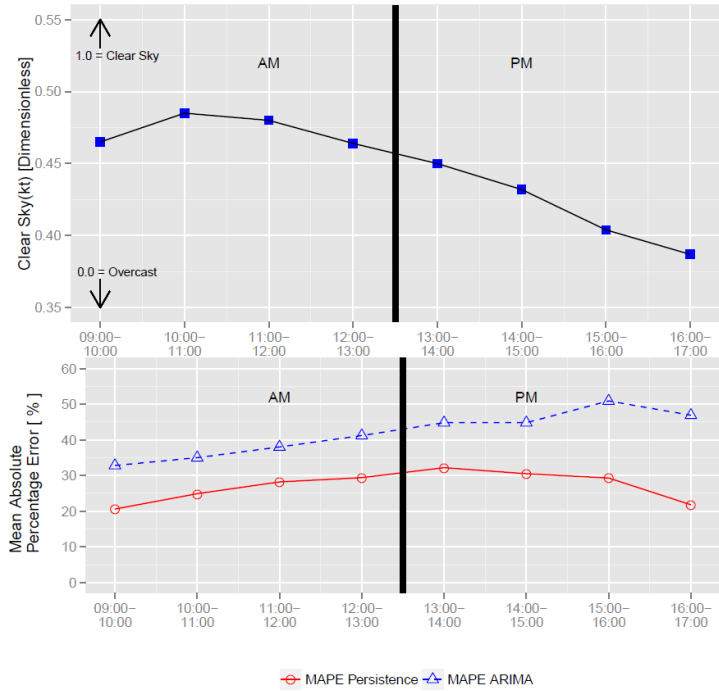


Figure 77: Clear sky indices binned in eight time hourly intervals in the day, indicating cloudier afternoons versus mornings (top). ARIMA versus Persistence forecast mean absolute percent errors (MAPEs) plotted against hourly binning through the day (bottom) (NOBRE et al., 2015 (submitted)).

Additionally, Figure 77 (bottom) shows the ARIMA and Persistence mean absolute percentage errors (MAPEs), also organized per the eight bin classes discussed. This graph already indicates a greater underperformance of the ARIMA forecast in the afternoon portion of the day.

Clear sky conditions are found when the clear sky index is > 0.70 , although such days are rare in Singapore. The criterion for overcast conditions was set for > 0.40 in the investigations, which mostly occurs in the afternoon. For the Hybrid method here proposed, ARIMA is selected when the diffuse ratio falls between the 0.40 and 0.70 interval. Both upper and lower values of the threshold were arbitrarily selected based on observations of the local weather. The interval chosen delivered satisfactory performance for the trigger points. Once again, it can be observed in Figure 77 (top) that periods in the morning are less cloudy than in the afternoon, which is typical for tropical locations where rain showers often happen in the middle to late afternoon.

Trigger #3: Relative humidity

The relative humidity data (H_{amb}) are used as a trigger parameter to identify the start of the rain storm. The large positive growth rate of H_{amb} indicates when and where rain showers occur. Additionally, the H_{amb} decreases upon the end of a rainstorm, which assists in the identification of improving weather conditions ahead. The great majority of storm events registered within the two years of data covered in analysis conducted occurred from the middle to late afternoon, often dissipating after sunset.

Trigger #4: Pollution Standards Index (PSI)

The PSI values, covered in subsection 2.3.3, are also used as one of the triggers in the Hybrid method. PSI data acquired from NEA is made available in 1-hr intervals. For the first step of the algorithm, the PSI levels are checked island-wide. For a condition of levels above 100, the Persistence forecast method is triggered.

Proposed Hybrid short-term forecasting

The proposed Hybrid forecast algorithm, combining the Persistence and ARIMA methods, uses storm approximation triggers from boundary stations to help forecast irradiance conditions expected at the reference station after a certain time lag (validation station “V” in Figure 75). The series of triggers were set according to pre-determined meteorological conditions, dictating the swapping between the two utilized forecasting methods – the air pressure sensors are used for storm approximation detection (e.g. the storm shown in Figure 11), and relative

humidity sensors (for rainfall start, progression and dissipation). In terms of the air quality monitoring, the hourly PSI readings from the NEA measurement network across Singapore were also directly taken as input parameters.

In a nutshell, the forecasting algorithm targets three severe weather conditions, when it is expected to outperform solo ARIMA or Persistence forecasts: (1) sudden storms, (2) washouts, and (3) haze episodes. The proposed Hybrid method is shown in the form of a flow diagram in Figure 78. ARIMA and Persistence codes were run with the software R Studios. The Hybrid code was organized and developed under a “LabVIEW” interface routine (from National Instruments), for both historical checks, but also for a live code which runs at SERIS’ PV System Technology Laboratory. Only forecasts within the 8-hr window between 9 am and 5 pm are taken into account, as previously discussed under 3.1.2.

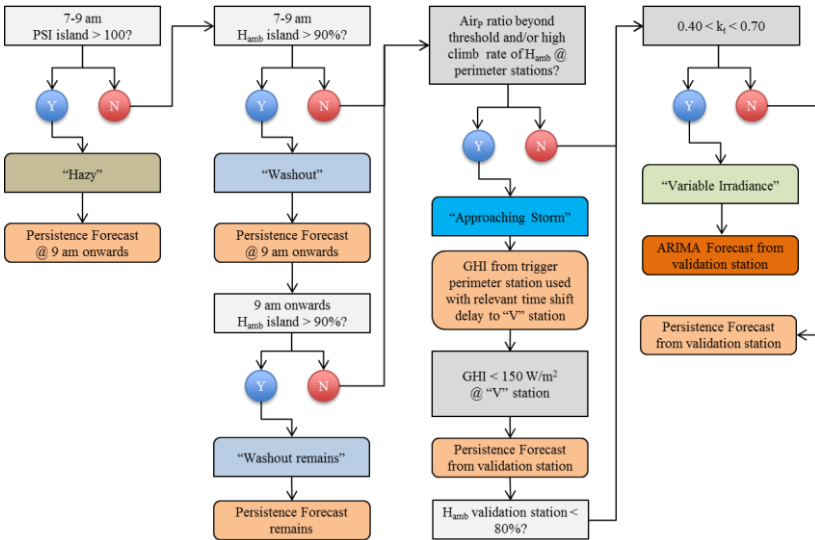


Figure 78: Schematic diagram of the proposed Hybrid algorithm for short-term irradiance forecasting during severe weather events in Singapore (NOBRE et al., 2015 (submitted)).

Case study #1: Sudden storms

Storms were defined as instances when air pressure sensors indicated a certain 1-min variation from an arbitrary threshold. The trigger fine-tuning was facilitated by the use of Doppler radar images as shown in Figure 11. Radar images contribute not only to the learning curve in adjusting the air pressure trigger threshold, but also for understanding common storm velocities and paths.

As Singapore possesses tropical climate, the majority of its rain showers take place in the afternoon after sufficient thermal exchange has occurred between the Earth's surface and the atmosphere. From data analysis of a two-year database, the most common timeframe for sudden storms was registered within the 2 pm to 4 pm period. Figure 79 shows one of such storms. In this particular example, global horizontal irradiance (red squares) almost reached 0 W/m², while relative humidity presents a fast increase with the arrival of the storm.

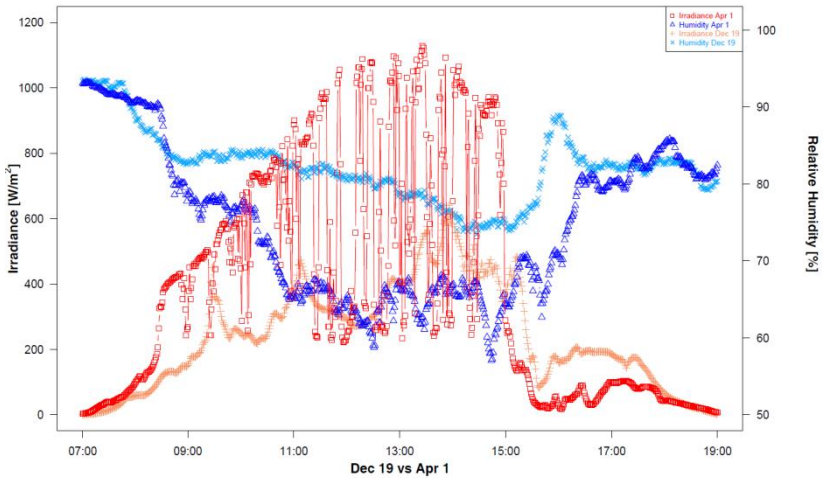


Figure 79: Global horizontal irradiance during a variable and a cloudy day. The variable day experienced a sudden storm after 15:00, which can be visualized by the sharp increase in relative humidity associated with the presence of rain (NOBRE et al., 2015 (submitted)).

As highlighted earlier in Figure 47, the main contribution of the storm detection system proposed lies on the fact that the Hybrid model allows avoidance of peak errors inherently present in current time series-based forecasting methods such as ARIMA and Persistence, which rely

on previous irradiance steps data. Using the information of peripheral ground measurements before the arrival of storms at a given point of the island allows reduction of prediction errors.

Case study #2: Washouts

A washout event occurs when rain showers prevail during the entire time period of interest, leading to extremely low total irradiation levels. For the Hybrid algorithm, a daily irradiation of 1.50 kWh/m^2 was arbitrarily set as a threshold below which all days are classified as washout days. The average long-term daily irradiation value for Singapore is 4.47 kWh/m^2 (as per subsection 2.3.2), which accounts to an annual typical meteorological year of $1,631 \text{ kWh/m}^2$. A washout day is also shown in Figure 80 for comparison purposes against a variable day. Although the figure was assembled to show normalized output of PV systems, the maximum GHI throughout Singapore never reached 200 W/m^2 for the entire day, with the relative humidity also never going below 90%.

PV systems in Singapore should perform at an average of 80% performance ratio for well-designed systems and 85% for leading-edge installations (KHOO, NOBRE, *et al.*, 2014; NOBRE, YE, *et al.*, 2012). During peak-hours of solar irradiance, even with cloud-edge and cloud-enhancement effects, PV systems in Singapore tend to have maximum AC power outputs of approximately 85-90% of their nameplate capacities. Figure 80 shows the normalized AC power output of ten existing PV systems of different sizes and technologies located across Singapore during a so called “washout” day. The highest value recorded for any of the systems was ~10% of the rated nameplate capacity, with the average value of the ten systems, shown as a thick black line in Figure 80, reaching only ~6% of an equivalent maximum nameplate installation. As a comparison, the normalized AC power output on a typical irradiance day is shown in the same figure, with an average peak of ~78% just before noon.

The use of the Persistence forecasting method when washout conditions are identified in Singapore does not necessarily entail the improvement of a short-term irradiance forecast. It rather serves as an indication to stakeholders and other scientists in the field that the use of a simple Persistence allows for minimum forecasting errors against other more complex methods (such as ARIMA or ANN).

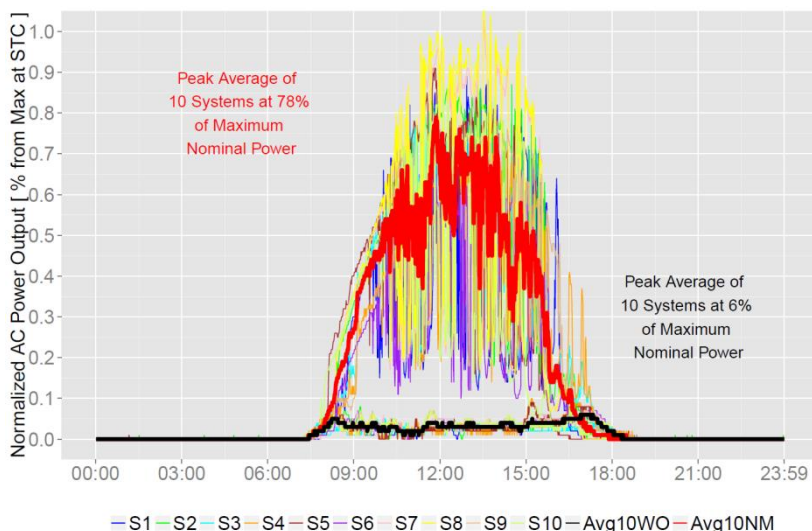


Figure 80: Normalized 1-min AC power output from ten existing PV systems located across Singapore representing different sizes and technologies on a “washout” day and also on a typical day (NOBRE *et al.*, 2015 (submitted)).

Case study #3: Haze periods

The topic of haze was covered in detail in subsection 2.3.3., which can be summarized by the period when forest fires for agriculture land clearing, mainly in Indonesia, trigger air pollution events in Singapore. Generally, haze episodes occur during the dry season and tend to last for 7-10 days on average, depending on prevailing wind speeds and directions. Apart from its influence on the performance of PV systems (LIU *et al.*, 2014b), the haze situation has a somewhat similar effect on PV yields as washout days do, whereby short-term irradiance forecasting provided by the Persistence method achieves lower or on-par accuracy against more complex methods, such as the ARIMA model.

As a method step for the Hybrid algorithm, only haze events presenting PSI larger than 100 were considered. This set point was based on previous studies (LIU *et al.*, 2014b; NOBRE *et al.*, 2015 (submitted)). For such conditions, it is common that the diffuse fraction of solar irradiance reaches high values, comparable to those in washout events. As mentioned before, the reduction in the forecast uncertainty is likely better accomplished by the use of the Persistence method.

Readings for PSI levels were obtained via the NEA website (NEA, 2013b). The PSI data reflects a total of six pollutants including total particulate matter (PM10) and fine particulate matter (PM2.5). PSI data provides accurate information on air quality, taking measurements from a network of air monitoring stations located in different areas of Singapore.

Validation

A ground measurement site located at the center of Singapore (station “V” in Figure 75) is used as reference to validate the forecast outputs provided by the Hybrid model proposed. For the tests of the method, ten days with approaching storms (five from 2013 and five from 2014) were randomly selected among the pool of available stormy days, ten days with washout conditions, and ten days from a strong haze episode in 2013 and a lighter one in 2014 were also arbitrarily chosen for testing and validation purposes. The pool of potential case studies was earlier presented in Table 5.

As gauge of the benchmarking among various methods, the normalized root mean square errors (nRMSE) is calculated for the Hybrid method, as well as for Persistence-only and ARIMA-only using the validation site.

For usage of the method at other locations in Singapore other than the selected station “V”, it is necessary to gauge whether the chosen site falls in central parts of the island – in which situation the methodology could be implemented on a similar basis, with minor adjustments to the travel distance for storms. For near coastal areas, the necessary adaptation of the method lies on the fact that the time gained in detecting an approaching storm is reduced, thus potentially compromising the results for cases of very fast storms. For this reason, the method goes through a variation proposed by the author as presented later in section 3.3.4.

3.3.3 Benchmarking of methods

The efforts from other early works in irradiance forecasting in Singapore included stochastic models such as ARIMA, Persistence, exponential smoothing state space (ETS) and numerical weather prediction (NWP, via the WRF model) (ARYAPUTERA *et al.*, 2015; DONG *et al.*, 2014; 2013; YANG, D., DONG, Z., *et al.*, 2014; YANG *et al.*, 2012; YANG, SHARMA, *et al.*, 2015).

Within this thesis, specific case studies are addressed (sudden storms, washouts and hazy conditions) in the testing and validation of the novel Hybrid method. Apart from those exercises, all five methods discussed in 3.3.1, i.e. [1] Persistence, [2] ARIMA, [3] ETS, [4] ANN, and the [5] proposed Hybrid (covered in 3.3.2), are tested for a one-year period of data (from April 2014 to March 2015) using the central ground-measuring station “V” (in Figure 75) as validation site.

For the short-term solar irradiance forecasting investigations, the normalized root mean square error (nRMSE) is further used as a figure of merit to determine forecast efficacy on a month-by-month basis, see Equation 15.

$$nRMSE = 100\% \sqrt{\frac{1}{N} \sum_{t=1}^N (G_{fc} - G_m)^2} \quad (15)$$

where G_{fc} is the forecasted irradiance in $t + 1$ time step and G_m is the measured irradiance also in the future step.

The forecasting skill “s” is defined to measure the improvement of the proposed Hybrid model against the simplistic Persistence method, as a baseline. The value of “s” is calculated by Equation 16.

$$s = 1 - \frac{nRMSE}{nRMSE_{persistence}} \quad (16)$$

3.3.4 Expanding the Singapore sensing network

Although a proposed novel method is tested for a central location of the island (validation station “V” in Figure 75), it is desired that other sites within Singapore do not suffer from large forecasting errors when, for example, a sudden storm crosses the perimeter of the country. Therefore, it is proposed that the existing remote sensing network is expanded to include an additional number of six remote stations – four of them in islands surrounding Singapore (Pulau Ubin in the Northeast, Jurong Island in the Southwest, and St. John’s Island & Pulau Semakau to the South). A fifth and sixth stations at the East and West borders of Singapore complete the expansion works, at Changi Bay and Tuas Checkpoint, respectively. See Figure 81 for the six expansion sites (“E”) and further station details in Table 14. Stations which are still to be deployed (“TBD”) by the submission date of this thesis are marked in *italics*.

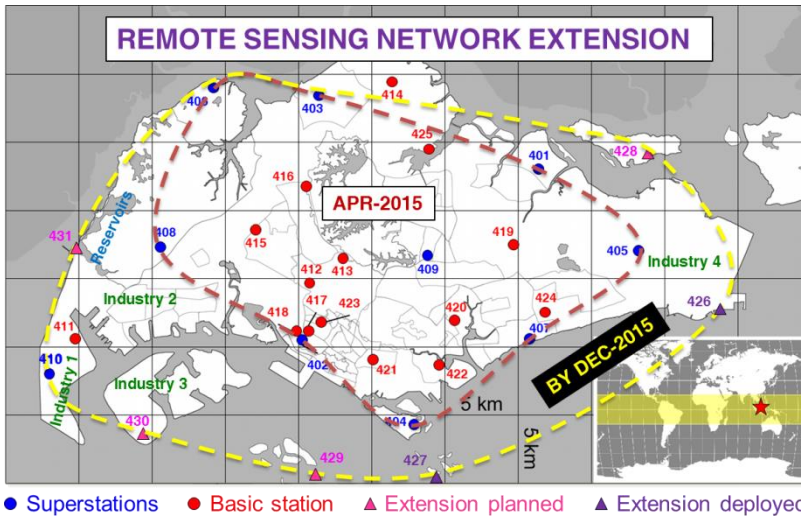


Figure 81: Existing (as of November 2013) and proposed stations (by end 2015), as well as perimeter belts of superstations (NOBRE et al., 2015 (in preparation)).

On top of the new perimeter station additions, the expansion plan includes the revamp of basic station #410 into a superstation, thus allowing for an early warning detection system for the Tuas South industrial area (“Industry 1”). Other major industrial areas are marked in

Figure 81, where large manufacturing plants and warehouses provide premium space for the deployment of PV systems. Furthermore, station #431 is to be located just outside Tuas Checkpoint (the second link bridge connecting Singapore and Malaysia). The presence of this station allows for a warning system station for several water catchment reservoirs to the West of the island, earmarked for floating systems deployment, having already been assessed to potentially host hundreds of MW of PV systems.

Table 14: Basic characteristics of six ground-measuring meteorological stations for a remote sensing network expansion in Singapore (NOBRE et al., 2015 (in preparation)).

ID #	Station Name	District in Singapore	Latitude [N]	Longitude [E]	Altitude [m]	Date Deployed
E1	426	Changi Bay	1°18'57"	104°00'55"	12	May/15
E2	427	St. John's Isl.	1°13'04"	103°50'58"	27	Jun/15
E3	428	Pulau Ubin	1°24'12"	103°58'09"	9	TBD
E4	429	Pulau Semakau	1°12'03"	103°46'50"	5	TBD
E5	430	Jurong Island	1°13'51"	103°40'45"	15	TBD
E6	431	Tuas Checkpoint	1°20'55"	103°38'16"	8	TBD

The smaller perimeter belt shown in Figure 81 (in brown), takes into account the most outward stations of the network possessing superstations (as of the completion of the original network in November 2013). It encompasses an area of roughly 500 km², covering most of the country's highly populated areas (made up by Housing & Development Board buildings, also known as "HDBs", which host ~40% of all PV systems in Singapore to date, with further plans for expansion).

Although the majority of the areas outside of this perimeter are military training zones or heavy industry-specific areas (such as oil refineries in Jurong Island, "Industry 3"), the available number of industrial rooftops to the Southwest- ("Industry 2") and East-ends ("Industry 4") of Singapore, added with the fresh water reservoirs on the edges of the West part of the island, make the extension of the network a desired research sub-product. The proposed expanded perimeter belt (in yellow) encompasses an area of ~800 km², 60% more than the original network, and likely to contain the great majority of bigger volume PV systems in the country in a foreseeable future.

This portion of the method promoted the expansion of the network and allowed for the demonstration that outward stations indeed can help with short-term forecasting enhancements for PV systems located outside of the original belt of meteorological stations.

3.3.5 Sky imagery as short-term forecasting support tool

As presented in 2.4.5, sky imagery utilization has been previously used as means of forecasting solar irradiance. Due to cloud motion physics, the technique is highly suitable for short-term applications, as clouds within the field of vision of the camera take a few minutes to enter, cross and exit the image. For this reason, the deployment of fish-eye lens sky cameras in Singapore was promoted, with the network shown in Figure 56 containing thirteen cameras as an outcome of the efforts promoted within this thesis.

In the publications cited, usually cloud height or speed are studied, so that it can be estimated where clouds are headed and their dynamics. Via a paper by Yang et al. (YANG, WALSH, *et al.*, 2013), block matching algorithms (BMAs) were explored in creating motion vectors describing changes in the irradiance conditions on a 2D map of Singapore. The work further introduced the use of BMAs for cloud-contour tracking, by comparing two images in $t - 1$ and t . To avoid problems of mapping of the many resulting vectors of the image, a grouping of five points was proposed, which are then seen as red small motion vectors in Figure 82. The orientation of the vector shows the resulting direction, with the length of the vector proportional to the speed of motion of the cloud segment.

Figure 82 shows three sky images taken in 1-min intervals, with the vector fields created between images one and two, and then between images two and three, shown at the bottom of the figure. A further enhancement promoted by the author of this thesis to the concept first proposed by Yang et al. was the creation of a resultant vector (shown in blue in the figure) which is a representation of the predominant cloud group direction of motion for the entire image, with the length of the vector also representing the traveling progression of the cloud grouping. Precise determination of cloud speeds and their height go beyond the scope of works included in this thesis.

In typical days, irradiance levels in Singapore can vary dramatically as earlier shown in Figure 26 and Figure 46. For such days, it is expected that cloud vectoring, based primarily on broken clouds, likely yields irregular cloud speeds and directions throughout the island, thus making it difficult for their use in the forecasting products. However, it is proposed that minutely vector creation for the deployed cameras will assist wind direction gauging, which in turn have two uses: a) determination of predominant wind directions across Singapore, with similar vectors throughout the island likely indicating major cloud events (e.g. storms) approaching or progressing through the island, and b) assist

haze episode arrival, development and dissipation, as air pollution is highly correlated to prevailing wind conditions.

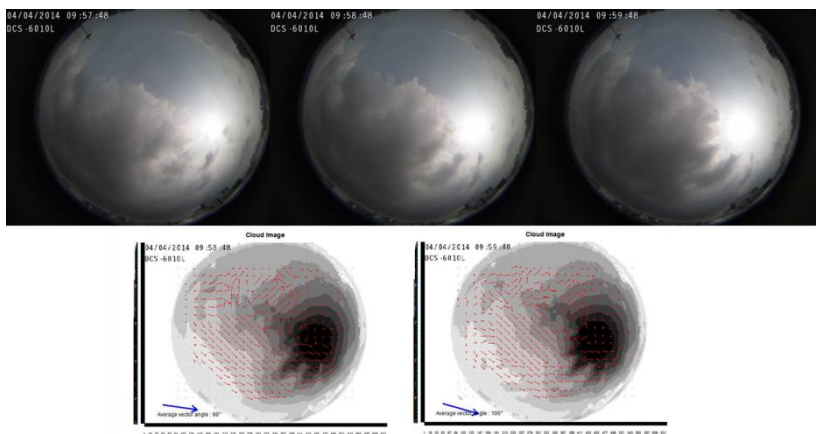


Figure 82: Example sequence of three sky images and associated output cloud motion vectors (NOBRE *et al.*, 2015 (in preparation)).

Finally, with a hybrid investigation containing irradiance drop at stations in a sequence, together with cloud vectoring, and Doppler radar assistance, approaching and developing storm directions are investigated to act as a support tool to other forecasting methods.

3.4 METHODS FOR PV SYSTEM POWER CONVERSION

3.4.1 Single system modeling opening remarks

When developing and performing new solar irradiance forecasting methods, it is aimed that deviations between measured and predicted values progressively decrease towards an “unattainable no-error” condition. When launching a novel algorithm such as the one discussed in 3.3.2, the main intent is to prove its higher accuracy versus previously deployed methods. It is often the case in the relatively new field of solar irradiance forecasting that constant, but gradual improvements are made. As a consequence of the efforts invested in reducing forecasting errors, it is hoped that such improvements are not achieved in vain, when performing power generation estimations for PV systems, in a future dominated by a vast amount of these renewable energy sources. A coarse implementation of PV simulation or up-scaling routines might wipe out any improvements achieved from forecast algorithms.

In subsection 2.6.2, formulation for PV system modeling was introduced. When using the equations presented, Figure 83 summarizes the efficacy of the model, here for a PV system in Singapore and at a condition of low wind speeds.

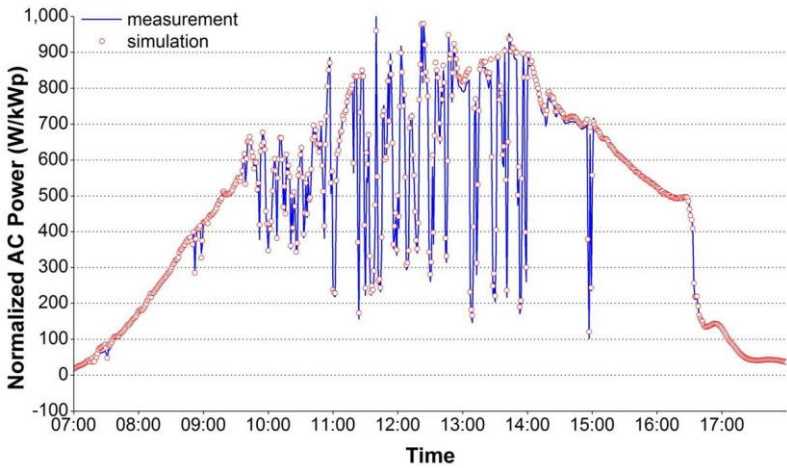


Figure 83: Simulated versus measured AC power output of a PV system in Singapore under low wind speeds (source: SERIS).

Figure 83 plots the minutely AC energy output values simulated for a single day, with the model using measured in-plane irradiance from a calibrated silicon sensor on site. It is contrasted by the actual measured AC power output read from an AC meter at the output of a PV inverter. For this particular example, the fit of the two curves is within 0.5% of error, which highlights the good fit of the formulation, but also the quality of this particular system presented (as it is later presented in 3.4.2). This was addressed in section 2.5, whereby an accurate PV system power output modeling depends on several factors, like the age of the system as an example (e.g. smaller simulation errors for systems which have yet to suffer major degradation effects), among other influences, which are discussed within section 3.4.

As PV systems performance in warm climates are concerned (covered in 2.5.4), understanding how systems behave in such locations plays a crucial role in power conversion forecasting and error curtailment. For that reason, and as yet another example, special attention should be given to the estimation of module temperature based on system mounting conditions, which could account for an almost 3-fold temperature variation between sites in a tropical climate, see Figure 84 (YE *et al.*, 2013). Subsection 3.4.2 covers how error minimization is intended within the investigations of this thesis.

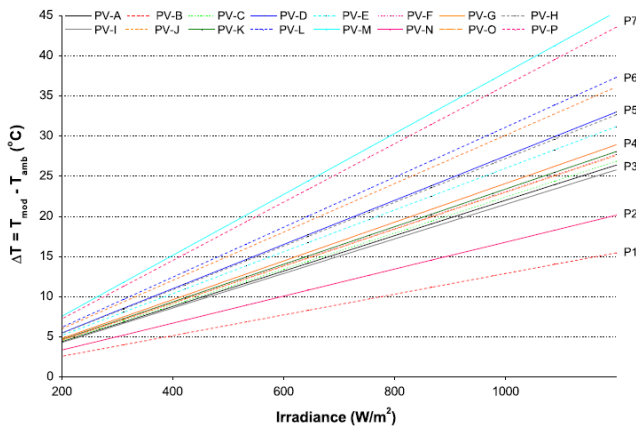


Figure 84: Seven categories presented for module temperature variation in Singapore (YE *et al.*, 2013). Utilization for the method was further validated for PV systems in Brazil (NOBRE, MONTENEGRO, *et al.*, 2012).

3.4.2 Factors heavily influencing PV system modeling

From the list of factors influencing PV modeling described in section 2.5.2 and 2.5.3, this thesis addressed the following five strong contributors: a) PV system modeling, b) temperature losses, c) shading influences, d) long-term degradation and e) irradiance availability due to air pollution levels. Various case studies presented allowed the gauging of simulation efficacy for the power conversion in the tropical environment of Singapore.

[A] System modeling

Well-known formulae as per Equations 9-11 are implemented as a validation tool for systems in a tropical environment. First, it is assumed only global horizontal irradiances and ambient temperatures are known. For Equation 11, a typical concrete rooftop value of $\gamma = 0.023 \text{ }^{\circ}\text{Cm}^2\text{W}^{-1}$ is used, as per (YE *et al.*, 2013). Secondly, for a better validation against real-field operations, the model with known in-plane irradiance and module temperature parameters is tested, thanks to the network of PV systems deployed in the country as previously described in 3.2.2. Finally, a simplistic method using a fixed value of performance ratio (0.80 as commonly used by system integrators in Southeast Asia) is tested using data for a then new PV system;

[B] Temperature losses

Simulation of power output for a PV system (“system 1”) is made taking into consideration a common mounting system loss factor for Singapore ($\gamma = 0.023 \text{ }^{\circ}\text{Cm}^2\text{W}^{-1}$), as shown in a) above and binned as the slope P3 in Figure 84. The system simulation is then tested taking into account that the validation system (“system 2”) is in fact mounted on a metal rooftop, thus experiencing hotter module temperatures (binned as the slope P6 in Figure 84). Such systems are commonly found in Singapore (e.g. on factory/warehouse rooftops, see Figure 13, as well as private houses, see Figure 12, as examples). System 2 of the analysis has similar age and is located ~2 km from system 1, thus experiencing nearly identical weather conditions;

[C] Shading influences

Two PV system sections on the same building complex (a hospital in Singapore, see Figure 85) are used for demonstration on how shading could negatively affect power forecasting. Shaded and unshaded systems are contrasted in the analysis. This system was the last installation added to the network of sites under research-grade monitoring (system #115 in Table 11).

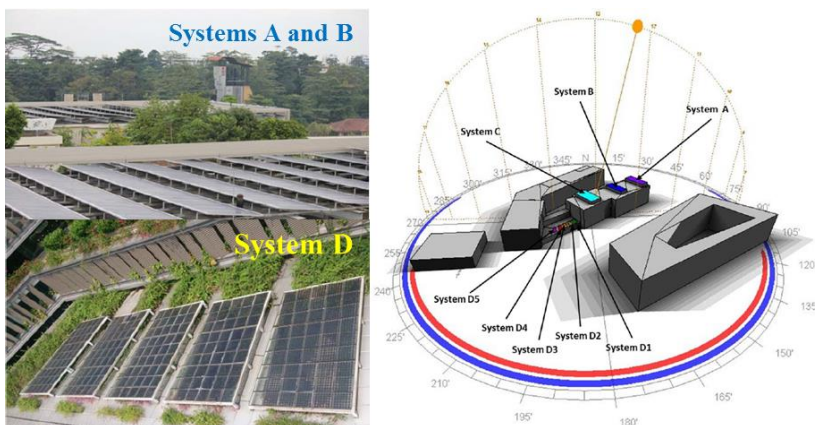


Figure 85: Hospital complex in Singapore, home of four PV system sections (A, B, C and D), three of which are unshaded (A, B and C). The glass-glass canopy PV system in section D is heavily shaded by the surrounding hospital wings (source: SERIS, adapted for this thesis).

[D] Long-term degradation

PV system power outputs at a given site, but with readings that are five years apart, were shown to highlight the critical influence that aging has on simulation and power forecasting. In Figure 86, aging is showcased by contrasting a high performing system (with a performance ratio decay of -0.5% per annum) versus a system which operated well for its first two years of life but later suffered from severe soiling accumulation due to a construction site nearby, without going through a complete cleaning routine since then (here PR decay of -3.3% p.a.).

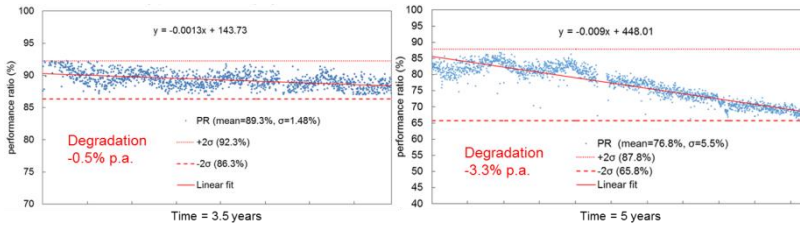


Figure 86: Daily performance ratios of a high performing PV system (left) and of a poorly maintained one (right), with estimated degradation rates after several years of operations of -0.5% and -3.3% per annum (NOBRE *et al.*, 2015 (in preparation)).

[E] Irradiance availability due to air pollution

Comparisons on PV system power output were made between a clear sky day with low air pollution levels against hazy skies which took place in June 2013 (similar period as shown in (LIU *et al.*, 2014b) and addressed throughout this thesis in other works by the author).

Data used for the exercises [A] through [E] stem from a variety of systems within the portfolio described in Table 11. The data periods used in the investigations depend on the challenge at hand. For example, to demonstrate degradation influences, analyses from datasets five years apart are used, thus highlighting system output baseline differences between a newly system deployed (in this case back in 2010) versus half-decade later (i.e. in 2015).

It is proposed that a generic formulation for PV power conversion is achieved within the thesis, which is then applied for alternative validations, such as up-scaling routines discussed in 3.4.4.

3.4.3 Modeling influences due to haze

In Figure 62, when discussing other factors that influence PV systems performance, it was seen how hazy conditions in Singapore clearly affected the yield of PV systems in June 2013. Quantifying such impact, and even estimating economic implications from it, are areas of interest for governments and policy makers, as argumentation builds up when air pollution occurs whether it was caused by neighboring countries. Within this thesis, the impact of haze on the power output of solar photovoltaic (PV) systems in Singapore was also investigated, with the goal of understanding implications to PV power conversion routines, to gauge implications to forecasting activities and to address considerations for a future where solar could contribute ~20% of the total electricity demand for the country.

It is trivial to realize that the presence of haze will generate loss of solar irradiance reaching the Earth's surface. However, gauging the effects is a more difficult task. Although diminishing levels of illumination on the ground are obvious when air pollution is high (as shown in Figure 62), one must be able to differentiate between the reductions in irradiance caused by haze or caused by clouds, or by a combination of both. Furthermore, haze not only has an impact on the light intensity (which affects the electric current), but also on the PV module temperature (which affects the voltage). In this thesis, a novel filtering technique was proposed to eliminate cloud effects, thus allowing the gauging of the full impact of the haze alone. As discussed in section 2.3.3, although other air pollution sources do exist in Singapore, such as caused by refineries and the country's car fleet, the investigations conducted in this thesis are exclusively associated with a haze episode triggered by forest fires well documented in the Southeast Asia region during June 2013.

A clear sky day was also determined as a baseline for Singapore, and compared against increasing air pollution conditions. Finally, an analysis of ten existing PV systems' operational behavior in Singapore (five of crystalline wafer-based and five of thin-film technologies) was conducted.

In order to observe the reduction of irradiation at ground level for polluted days as a function of PSI levels (PSI values above 50, with the descriptor "good"), a first necessary step is to determine a baseline situation, which are the irradiance conditions on a clear sky day without haze (PSI < 50). Due to rapidly changing weather conditions and various layers of clouds, clear sky days in tropical locations are rare. Therefore,

it is not really feasible to obtain the baseline days by measurement records alone. Instead, such days are best derived from measured data on non-clear sky days using statistical methods.

The main task of the presented method is to separately quantify and eliminate variability caused by haze, clouds or high moisture levels in the air. In this portion of the thesis, it is proposed the use of three filters for the elimination of cloudy or near-cloudy conditions during specific PSI conditions. That is achieved by performing a sampling analysis on irradiances recorded at the SERIS meteorological station using a calibrated pyranometer. These filters are described and demonstrated in the following paragraphs.

In Figure 87, Filter #1 (“Humidity Filter”, top row graphs) is used to eliminate events when the relative humidity is above 80%. This way, rainy conditions or pre/post rain periods, where clouds are present, are discarded. The selection of the value threshold was obtained from experience and long-term weather observations. Red triangles throughout Figure 87 represent eliminated points at the given filter step, while blue circles have passed the respective criterion. Three days with sunny, rainy and intermediate characteristics are shown to illustrate the performance of the filters.

Next, Filter #2 (“Diffuse Irradiance Fraction Filter”, shown in Figure 87, middle row graphs) is implemented on all points that have passed the previous step. The diffuse irradiance fraction is defined as the ratio between measured diffuse horizontal irradiance and the global horizontal irradiance. The filter works as a mechanism to remove situations with high cloud cover, however no rain. The threshold set was 0.50, with data points being eliminated when ratios are above the selected value. Surviving points are shown in blue circles, while red triangles represent the eliminated points at the current filter. Black crosses are those points eliminated in the previous Filter #1 step.

Filter #3 (“Clear Sky Irradiance Band Filter”, seen in Figure 87, bottom row graphs) is the last step of the irradiance loss analysis, which ensures that the targeted data for the clear sky conditions are within ± 100 W/m² irradiance of the modeled clear sky values. The clear sky irradiance model utilized in this study was adopted from reference (YANG, D., WALSH, W. M., *et al.*, 2014). Filter #3 works to remove situations of either cloud-edge/cloud-enhancement effects when irradiance tends to be higher due to either reflected light between the ground and the base of clouds, followed by reflections back at irradiance measurement devices, or enhanced by a thin layer of clouds (see Figure 41). Also, it assists in

the elimination of points which were not removed within the robustness of Filter #2 (e.g. a point where the diffuse irradiance fraction might have been 0.48, yet clearly outside of the range expected for a clear sky condition, with values for irradiance lower than expected). The selection of the arbitrary value of 100 W/m^2 was based on finding a set point which would not cause the elimination of an excessive number of points from the analysis, yet strict enough to remove values obviously outside of the expected clear sky range. Points outside of the $\pm 100 \text{ W/m}^2$ clear sky irradiance band are shown as red triangles in the final filter step graphs, with removed points from Filter #2 marked as orange asterisks. Black crosses are those points eliminated in the previous Filter #1 step.

In order to avoid variations of the daily irradiance profiles throughout the year due to the position of the sun in the sky (with varying zenith and altitude angles), only data points from the June months from 2010 to 2013 were used in the analysis (N.B. June 2013 was the month of the major haze event reported). Data are taken from the SERIS meteorological station, which started operations in May 2010, thus a total of 120 June calendar days were available and used for the analysis, also to reduce the impact of the year-on-year variability of the irradiance due to the position of the sun in the sky. One-minute global horizontal irradiance averages were used for the assessment based on readings of a pyranometer. The data points are combined forming a so-called “average solar irradiance day” for the month of June for the given air pollution conditions. The analysis is further expanded to include readings originating also from a calibrated crystalline silicon sensor (which has a narrower spectral response range than a pyranometer).

24-hour PSI averages were used for the selection and categorization of the available June days. Days were separated into four arbitrary categories: a) $\text{PSI} \leq 50$, b) $50 < \text{PSI} \leq 75$, c) $75 < \text{PSI} \leq 100$, and d) $\text{PSI} > 100$ in an attempt to gauge the loss of irradiation with increasing levels of air pollution. Days within the same PSI binning were processed through the filters and averaged together for every one-minute step of irradiance values. PSI data from a NEA station nearby to the SERIS meteorological station was used as provider of the air pollution readings.

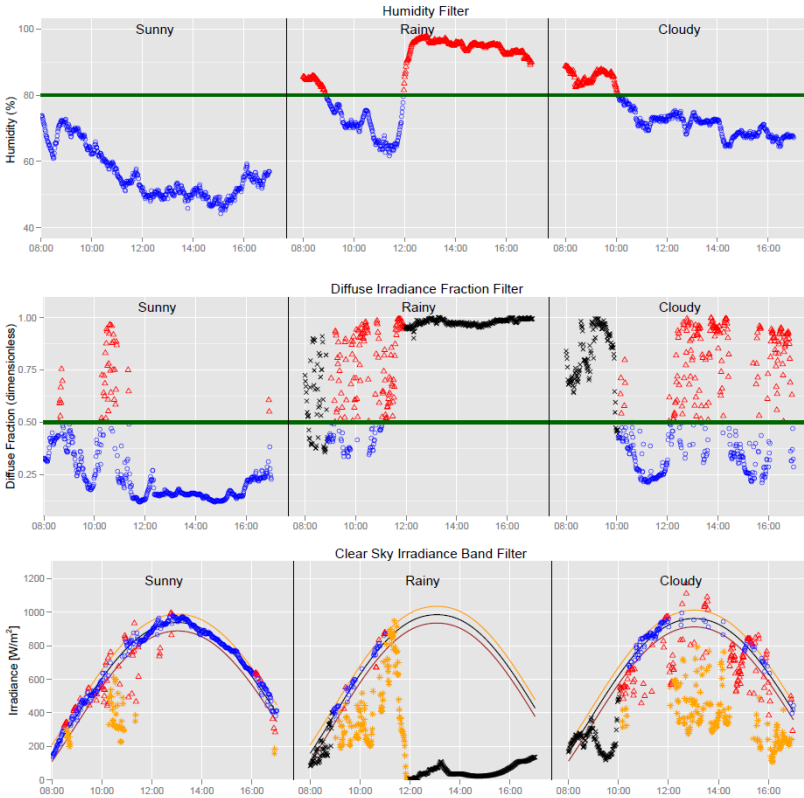


Figure 87: Demonstration of the performance of three filters in three types of days (sunny, rainy and cloudy conditions) to derive the progressive sky conditions for the haze evaluation (NOBRE et al., 2015 (accepted)).

After assessing reduction of irradiation on ground level at a single point at the SERIS meteorological station, an assessment and benchmarking is proposed for the power output of ten PV systems in operation in Singapore through the same time period of the analysis for their clear sky day behavior, using in-plane irradiance sensors. Additionally, an assessment of haze influence to these systems' performance metrics was conducted, taking yield (in kWh per kW_p per day) and performance ratio (PR) as key indices for the comparison. The extraordinary day when a hazy but cloudless day occurred (24th June 2013, previously graphed in Figure 62) was used for benchmarking. For a more diverse comparison, both crystalline silicon wafer-based and thin-film technology based PV systems were evaluated.

3.4.4 Country-wide up-scaling routines

Byproducts of irradiance forecasts in a future of massive PV development will be estimations of the amount of photovoltaic power delivered to the grid in a large area of interest, e.g. a city, where thousands of solar installations are present. When PV systems are improperly modeled, either as a single unit or as a fleet, irradiance forecasting errors are further compounded, making PV power predictions less robust.

Thanks to daily available power output records of PV systems from the National Solar Repository (discussed in 2.5.5), day-by-day simulation exercises are made possible for the suggested method here presented for an up-scaling routine for Singapore.

In this regard, ten PV systems (accounting for ~10% of the volume of installations in Singapore as of end of 2014) were selected for validation of the proposed up-scaling method. These systems are shown in Table 15 with their basic characteristics needed for the exercises. The selection of these systems was based on amassing a variety of system sizes, with different roof types, ages and scattered across Singapore.

Table 15: PV systems basic characteristics used in the detailed up-scaling exercises. Systems' age are based as of the date of the tests, March 2015 (adapted for this thesis).

System #	Installed Capacity [kW _p]	Nearest Superstation [km]	System Age [years]	Type of Roof	Tilt [deg]	Azimuth [0-360]
901	1,006.8	2.1	1.5	Clay tiles	23	0/180
902	999.9	4.0	2.1	Metal	5	90/270
903	707.5	5.2	1.0	Concrete	10	160/340
904	133.6	5.6	0.5	Metal	10	160/340
905	122.6	6.6	5.1	Concrete	10	140
906	44.8	1.3	4.2	BIPV Metal	flat-10	90/270
907	14.4	6.6	5.1	BIPV Airgap	4	90/270
908	12.2	1.5	0.5	Metal	10	150/330
909	5.2	3.5	7.2	Metal	8	10
910	3.8	5.6	8.9	Metal	flat	flat
Total	3,050.8	4.2	3.6			

~10% of total volume in SIN

Avg. distance

Avg. system age

The derived power conversion generic formula (outcome of 3.4.2) is used for the up-scaling exercises. A typical month was chosen (March 2015), found to have daily irradiation records as close to the Singapore long-term average as possible. Stations used as source of meteorological parameters are chosen based on the “nearest neighbor” concept,

discussed in one of the publications of the author of the thesis (NOBRE, YANG, *et al.*, 2014).

In the up-scaling refined portion of the method, these ten systems went through the following simulation sequence:

- 1) Determination of nearest neighbor superstation within the SERIS network (as per Figure 71);
- 2) Conversion of global horizontal irradiation (GHI) and diffuse horizontal irradiation data (DHI) on hourly time steps into irradiance on module plane (G_{mod}), using the Perez model;
- 3) Utilization of hourly values of G_{mod} , together with readings for ambient temperature (T_{amb}) in Equations 9-11. Module temperatures (T_{mod}) to be estimated via previous publications (NOBRE, MONTENEGRO, *et al.*, 2012; YE *et al.*, 2013) in accordance with roof types and discussed in 3.4.1. This step guarantees hourly intervals of power output estimations for the PV systems. Calculating daily electricity generation for the systems was up-scaling test result #1. This value is further converted and normalized as per a system's installed capacity, thus becoming the yield of the system (" Y_{AC-1} ", in kWh/kW_p per day). This facilitates inter-comparison between systems;
- 4) As mentioned, the generic formulation in 3.4.2 was taken into consideration when fine-tuning and executing the up-scaling routine;
- 5) In up-scaling test #2, the commonly used practice of arbitrarily selecting a value of performance ratio is used (PR = 0.80 method). This accounted for up-scaling test result #2 (" Y_{AC-2} ");
- 6) Comparison of both estimated values for daily system's yield in kWh/kW_p (Y_{AC-1} and Y_{AC-2}) with measured ones (" Y_{AC-0} ") and calculate the mean average percentage errors (MAPEs), thus promoting a benchmarking of the more refined versus crude methods.

4. RESULTS AND DISCUSSIONS

4.1 SHORT-TERM FORECASTING RESULTS

4.1.1 Novel short-term forecasting method findings

The investigation on short-term forecasting using the described Hybrid method in 3.3.2 was first presented as a concept of using boundary meteorological stations in Singapore in an “alarm detection system” for approaching storms, which in turn helped reduce forecasting errors in a tropical location like Singapore (NOBRE, SEVERIANO_JR., *et al.*, 2014). In more recent investigations on the topic, two other extreme weather phenomena were added to the analysis – “washout days” (days with extreme rain events) and also “hazy days” (where air pollution was considerably high). The work was also further expanded with the addition of data from 2014, together with the previously presented 2013 case studies in order to further strengthen the applicability and robustness of the envisioned method.

As described in 3.3.2, ten random days, among the portfolio of stormy days, were selected for the evaluation of the algorithm. The findings for the first case study analysis are summarized in Table 16. It shows results for the ten selected “sudden storm” days. The proposed Hybrid method achieved performance improvements of ~10% in absolute terms if compared with the Persistence method as a forecasting baseline. Also noticeable is the fact that ARIMA underperformed against the Persistence model for days with extreme weather conditions. This can be explained by the classical storm duration in Singapore starting in mid- or late afternoon, with dissipation near sunset or shortly after it. This allows the Persistence forecast to thrive, which is one of the reasons for this method being chosen as an algorithm of choice for the Hybrid model after a storm has reached the validation station.

An example of the better performance of the Hybrid method is shown in Figure 88 (top), with the forecasted irradiance (black dash line) following the measured irradiance (green continuous line) thanks to an earlier-detected approaching storm. The minimization of the forecast error can also be visualized in Figure 88 (bottom), where ARIMA and Persistence forecasts demonstrated their known under-performances due to their reliance on past irradiance step information.

Table 16: Sudden storm forecasting error improvement when using the novel Hybrid method (NOBRE et al., 2015 (submitted)).

Day	Persistence [nRMSE]	ARIMA [nRMSE]	Hybrid [nRMSE]	Uncertainty reduction [% abs, with Persistence as baseline]
21-04-13	57.4%	62.2%	44.5%	12.9%
19-09-13	23.3%	23.5%	16.6%	6.8%
26-09-13	46.8%	59.6%	36.7%	10.1%
04-11-13	25.2%	24.7%	17.1%	8.1%
18-12-13	48.1%	42.7%	38.7%	9.4%
20-03-14	41.6%	40.2%	32.6%	9.0%
06-06-14	51.3%	54.0%	44.0%	7.3%
03-09-14	33.7%	39.8%	19.3%	14.4%
11-11-14	50.0%	48.5%	30.0%	20.0%
07-12-14	31.7%	30.8%	29.7%	2.0%
Average	40.9%	42.6%	30.9%	10.0%

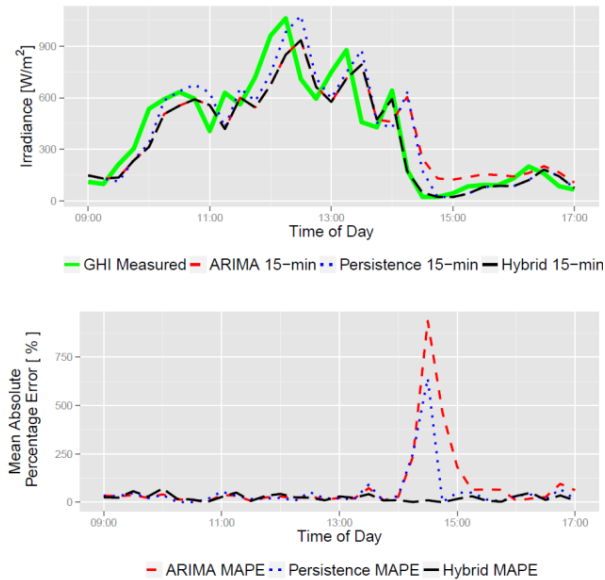


Figure 88: Measured GHI at a central site in Singapore, with the forward ARIMA, Persistence and proposed Hybrid 15-min forecasts (top). The MAPE is given, showing considerable error spikes upon the arrival of the storm for both Persistence and ARIMA methods, but not for the proposed Hybrid model (bottom) (NOBRE et al., 2015 (submitted)).

Results for the second case study addressing ten random washout events are presented in Table 17, including the total daily irradiation, as well as the nRMSEs obtained by using the Persistence-only and ARIMA-only forecast methods. In such example data, the Persistence forecast vastly outperformed ARIMA, which would be expected for a situation of total cloud cover condition (very low k_t values), which suits Persistence. The error avoidance column aims at highlighting detrimental errors for non-adaptive short-term forecasting models, which rely on running a single algorithm throughout all daily and yearly conditions.

Table 17: Case study on washout conditions in Singapore and error avoidance by selection of the Persistence method over ARIMA (NOBRE et al., 2015 (submitted)).

Day	Daily irradiation [kWh/m ²]	Persistence [nRMSE]	ARIMA [nRMSE]	Error avoidance [% abs]
28-04-13	1.32	21.1%	37.2%	16.1%
29-05-13	1.37	22.9%	27.2%	4.3%
05-09-13	1.50	40.9%	54.1%	13.2%
15-09-13	1.38	26.4%	37.9%	11.5%
02-12-13	0.98	34.8%	60.1%	25.4%
06-01-14	1.44	42.3%	39.6%	-2.7%
16-03-14	1.36	36.4%	74.6%	38.2%
18-11-14	1.12	14.7%	29.3%	14.6%
04-12-14	1.27	27.8%	35.1%	7.3%
19-12-14	0.56	39.5%	81.6%	42.1%
Average	1.23	30.7%	47.7%	17.0%

Finally, the third set of case studies is aimed at simplifying short-term irradiance forecasting during strong haze episodes, acting similarly to the washout events. The PSI threshold criterion of 100 was easily crossed in 2013, when Singapore experienced a notorious haze season, reaching unhealthy air quality levels for several days. In 2014, the number of occurrences of haze days was lower.

Table 18 shows the results of Persistence-only versus ARIMA-only forecasts. The error avoidance metric did not indicate much lower values for the hazy, as they were for the washout days (with the use of Persistence), but indicated nevertheless that future short-term forecasting methods may as well use the more simplistic Persistence forecast during such air pollution events. In any case, it is important to remember that haze comes associated with loss of irradiation at ground level. Thus, a limitation in the maximum output of PV systems must be accounted for,

also when modeling its grid integration impact due to the energy generation shortfall expected.

Table 18: Case study on hazy days in Singapore and error avoidance by selection of the Persistence method over ARIMA (NOBRE et al., 2015 (submitted)).

Day	PSI [highest daily value]	Persistence [nRMSE]	ARIMA [nRMSE]	Error avoidance [% abs]
18-06-13	128	4.5%	6.3%	1.8%
19-06-13	121	5.4%	5.7%	0.3%
20-06-13	236	6.6%	6.4%	-0.2%
21-06-13	239	17.3%	16.3%	-1.0%
22-06-13	246	11.7%	11.7%	-
23-06-13	167	13.4%	13.0%	-0.4%
24-06-13	243	10.4%	9.7%	-0.7%
07-10-14	125	17.7%	16.6%	-1.0%
12-10-14	105	22.3%	21.8%	-0.5%
20-10-14	106	17.8%	18.9%	1.1%
Average	172	12.7%	12.6%	-0.1%

The novelty of the proposed method lies on the prediction of massive drops in irradiance (i.e. consequently power output of PV installations) caused by approaching storms approximately 15-30 minutes in advance – which is typically sufficient to ramp-up conventional generation capacities (in Singapore, gas-fired turbines). Furthermore, the sensor network allows the identification of washout conditions before sunrise, allowing the grid operator to also react in advance and compensate for the missing solar power in such days.

Most cloud motion tends to come from the West parts of Singapore (thus coming from Sumatra in Indonesia, as per example animation of the Sumatra squall in Figure 11). The caveat: it is expected that there is a tendency for better forecasts for the Eastern parts of the island as most cloud activity for Singapore initiates from the West.

4.1.2 Benchmarking of various forecasting methods

The novel Hybrid forecasting method fared better than the use of existing techniques for a 15-min forecasting interval window. The following tables highlight the month-by-month results for the five tested methods proposed in 3.3.1 and 3.3.2, using three prediction horizons (15-min, 30-min and 1-hr), as discussed throughout this thesis.

Table 19 presents the short-term irradiance forecast results for an ensemble of five types of forecast methods for 15-min prediction intervals. The average monthly normalized root mean square errors (nRMSEs) are based on a central meteorological station in Singapore (station “V” in Figure 75) as validation site. In bold are lowest average errors among the tested forecasts within a particular month. In italics, the average one-year errors per forecast type are also shown. The month-by-month average total daily irradiation is also presented for the same validation station, with the highest irradiation month shown in red and the lowest in blue.

Table 19: Average monthly 15-min normalized root mean square errors (nRMSEs) for five short-term solar irradiance forecasting methods for a centrally located weather station in Singapore (NOBRE et al., 2015 (submitted)).

Month	Avg. total daily irradiation [kWh/m ²]	(1) Persistence [%]	(2) ARIMA [%]	(3) ETS [%]	(4) ANN [%]	(5) Hybrid [%]
04-14	4.33	30.2	30.4	30.3	30.9	29.7
05-14	4.05	32.4	32.2	32.7	32.3	31.2
06-14	4.19	29.4	28.7	29.1	29.2	27.3
07-14	3.99	30.4	29.6	30.5	30.6	28.3
08-14	3.77	34.5	33.1	35.2	34.0	32.5
09-14	4.90	24.8	24.3	24.6	25.9	23.0
10-14	4.36	26.6	26.2	26.6	27.3	25.6
11-14	3.87	34.5	33.5	34.6	32.7	32.0
12-14	3.45	34.5	34.7	34.7	34.1	32.7
01-15	4.47	31.3	28.9	29.3	32.1	28.6
02-15	4.84	27.9	26.3	27.1	28.1	26.2
03-15	4.61	32.7	31.8	31.6	31.6	30.4
Avg.	4.18	30.8	30.0	30.5	30.7	29.0

The proposed Hybrid method achieved the lowest annual average nRMSE (29.0%), followed by ARIMA (30.0%). It can also be seen that the month with the highest levels of irradiation (September 2014, with an equivalent average total daily irradiation of 4.90 kWh/m²) produced the lowest errors, whereas December 2014 had the highest errors in the study (December is one of the wettest monsoon months, with 2014 having had an equivalent average total daily irradiation of only 3.45 kWh/m²). Even though conditions of total cloud coverage (“washout” days) could bring

down absolute daily forecasting errors, these months are still characterized by many sudden storm conditions, thus leading to higher error values for the entire month.

Taking a 30-min forecasting horizon into account (see Table 20), the Hybrid model also displayed the lowest nRMSEs at 30.7% for the entire period of study among the five studied methods. For the 30-min tests, the Persistence forecast was the model with the second lowest errors at 32.3%. In February 2015, Persistence even slightly outperformed the Hybrid forecast.

Table 20: Average monthly 30-min normalized root mean square errors (nRMSEs) for five short-term solar irradiance forecasting methods for a centrally located weather station in Singapore (NOBRE et al., 2015 (submitted)).

Month	Avg. total daily irradiation [kWh/m ²]	(1) Persistence [%]	(2) ARIMA [%]	(3) ETS [%]	(4) ANN [%]	(5) Hybrid [%]
04-14	4.33	34.0	34.4	34.7	33.5	33.3
05-14	4.05	35.5	35.3	36.2	34.9	34.1
06-14	4.19	29.7	30.3	30.8	30.2	26.9
07-14	3.99	32.0	33.3	33.4	31.9	30.1
08-14	3.77	39.0	37.3	39.8	37.2	37.0
09-14	4.90	25.9	26.4	25.4	27.6	23.6
10-14	4.36	29.8	32.0	31.3	30.6	29.2
11-14	3.87	38.0	38.2	39.3	36.3	35.3
12-14	3.45	36.3	39.9	38.1	33.9	34.6
01-15	4.47	29.0	28.9	28.7	30.9	27.9
02-15	4.84	25.7	28.6	26.9	27.4	25.8
03-15	4.61	32.4	35.2	33.5	32.3	30.7
Avg.	4.18	32.3	33.3	33.2	32.2	30.7

Table 21 presents the month-by-month improvement of the Hybrid model over the Persistence in absolute percentage points on the RMSE and also as per metric “s” shown in Equation 16 for the months under evaluation. A “s” value of zero equals a certain forecast method is as effective as the Persistence method.

Taking sunny and cloudy conditions into account, for the months of September and December 2014, respectively, Figure 89 highlights the mean average percentage errors (MAPEs) of the ARIMA forecasts for a 15-min horizon window for the studied months. As expected, for the sunny month, with clearer skies and less storms present, the majority of the forecasting errors occurred at low values, which conversely peaks for the cloudy month, where 20% occurrences of the MAPE values took place above 50% of error (versus 6-7% occurrences for the sunny month). Approaching storms tend to generate large deviations in the forecasts, with prediction errors greater than 100% in certain cases, which naturally

is an area of concern to grid operators. As shown earlier in Figure 88, one of the goals of the Hybrid model had been to curtail large errors at instances of approaching storms, something that the ARIMA and Persistence models fail to do.

Table 21: Improvement of the proposed Hybrid method versus the Persistence method (as baseline) on a month-by-month basis, using both absolute errors percentage improvement but also the performance metric “s” (NOBRE et al., 2015 (submitted)).

Month	Avg. total daily irradiation [kWh/m ²]	Hybrid 15-min [% improv. abs]	Hybrid 15-min [value of s]	Hybrid 30-min [% improv. abs]	Hybrid 30-min [value of s]
04-14	4.33	0.5	1.1	0.7	1.4
05-14	4.05	1.2	3.9	1.4	1.5
06-14	4.19	2.1	4.7	2.8	1.7
07-14	3.99	2.1	4.5	1.9	1.9
08-14	3.77	2.0	3.8	2.0	3.3
09-14	4.90	1.8	6.6	2.3	5.6
10-14	4.36	1.0	4.1	0.6	1.7
11-14	3.87	2.5	4.3	2.7	2.2
12-14	3.45	1.8	4.0	1.7	2.5
01-15	4.47	2.7	4.1	1.1	2.7
02-15	4.84	1.7	4.4	-0.1	0.3
03-15	4.61	2.3	4.0	1.7	2.1
Avg.	4.18	1.8	4.1	1.6	2.2

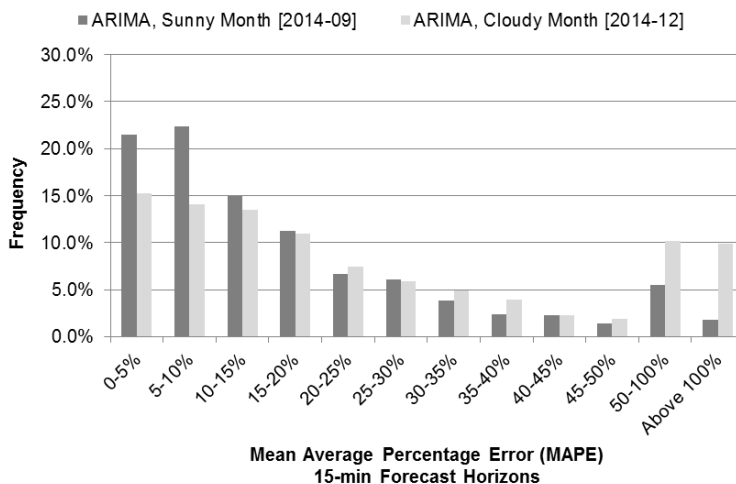


Figure 89: Mean average percentage errors (MAPE) for ARIMA 15-min forecasts for a sunny and a cloudy month (NOBRE et al., 2015 (submitted)).

Finally, the average monthly, 1-hr forecast horizon, normalized root mean square errors are shown in Table 22.

Table 22: Average monthly 1-hr normalized root mean square errors (nRMSEs) for five solar irradiance forecasting methods for a central weather station in Singapore (NOBRE et al., 2015 (submitted)).

Month	Avg. total daily irradiation [kWh/m ²]	(1) Persistence [%]	(2) ARIMA [%]	(3) ETS [%]	(4) ANN [%]	(5) Hybrid [%]
04-14	4.33	41.7	42.2	45.3	36.6	40.9
05-14	4.05	41.1	43.8	41.7	38.0	38.7
06-14	4.19	34.4	36.7	37.8	31.0	32.1
07-14	3.99	43.7	53.8	45.8	34.7	43.3
08-14	3.77	46.9	46.4	47.5	39.9	43.9
09-14	4.90	29.5	31.9	31.6	27.6	28.1
10-14	4.36	38.7	40.5	43.8	34.3	37.0
11-14	3.87	45.2	45.1	48.3	38.7	41.9
12-14	3.45	44.6	50.6	47.0	36.9	43.6
01-15	4.47	32.6	37.5	35.8	29.4	35.2
02-15	4.84	36.0	47.2	44.7	27.8	38.3
03-15	4.61	39.6	45.0	49.2	32.0	37.7
Avg.	4.18	39.5	43.4	43.2	33.9	38.4

Here, the proposed Hybrid still outperformed the Persistence method (by ~1% in absolute nRMSE terms), however, an ANN considerably reduced errors in a longer horizon setting. This could be explained by the fact that once storms arrive in Singapore, they tend to move very fast through the island. This means the irradiance smoothing effect in 1-hr average terms reduces the storm's "irradiance drop" impact. Explaining differently: the Hybrid method promotes reduction of errors in one/two forecast windows after storm arrival. When 1-hr averages are used, the Hybrid code does not contribute much to error reduction since the peaks of irradiation variation are smoothened out throughout the two/four forecast windows, for 15-/30-min, respectively, within a 1-hr time step.

Notwithstanding the better performance of ANNs in a 1-hr setting, the Hybrid algorithm still proved to be efficient in a short-term setting, especially for the same energy trading interval in Singapore (i.e. 30-min).

As presented in previous sections, rain cloud motion in Singapore could present challenging conditions for irradiance modeling and forecasting in the relatively small area of interest. In order to achieve a good accuracy for short-term forecast horizons, time horizon investigations as well as station-pairing relationships are crucial.

4.1.3 Case study when extending the sensing network

In subsection 3.3.4, it was proposed that six new ground-measuring meteorological stations are deployed at strategic positions, even farther than existing sites and towards the outside contours of Singapore. Two of such stations were deployed as the start point of the expansion works. They allow in a first stage the demonstration of the intent of the extension initiative and justifications to such an investment.

Figure 90 is a Doppler image registered on the 30th May 2015 when a storm approached Singapore from its East-Southeast border. Under the former network perimeter of meteorological stations, delineated by the brown belt superimposed onto Figure 90, station #405 is the first “line of defense” in detecting changing weather conditions. GHI declined on that day to 100 W/m² at 14:50. The new station in #426, on the other hand, already had diminishing GHI values at 14:30, 20-min before lowering levels at station #405. Additionally, at 14:20, the air pressure trigger in #426 had already detected the approaching storm, which straight-forward helps forecasting efforts ahead at the particular station.

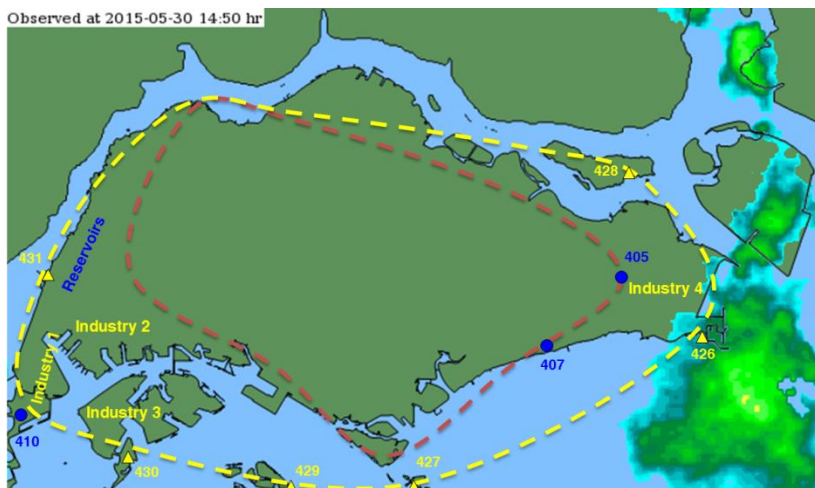


Figure 90: Approaching storm originating from E-SE on 30th May 2015, first captured by new expansion station #426 at Changi Bay (NOBRE et al., 2015 (in preparation)).

As a reference, station #426 is ~7 km apart from its nearest station at #405. The next station, #407, is further away (~12 km), but also experienced improvements in short-term forecasting thanks to the new

presence of the superstation at the ocean line in Changi Bay. In fact, several HDB residential blocks have PV systems at or near the location in #407, which would, under the normal network architecture, suffer from forecasting error peaks with the storm arrival.

Table 23 shows the 15-min and 30-min Persistence forecasting for stations #405 and #407 without any assistance from the new station. The table then highlights the new and lower errors when using knowledge ahead of time provided by station #426.

Table 23: Daily nRMSE results for selected case studies with a storm approaching from E-SE, with and without the use of a new deployed superstation (NOBRE et al., 2015 (in preparation)).

Station/Forecast Horizon	Persistence [nRMSE]	Hybrid [nRMSE]	Uncertainty Reduction [% abs]
#405/15-min	22.2%	20.2%	-2.0%
#405/30-min	24.2%	21.0%	-3.2%
#407/15-min	21.6%	19.0%	-2.6%
#407/30-min	25.2%	21.1%	-4.1%

Also as previously discussed, the importance of the expansion of the network of stations in Singapore is further justified by the fact that massive volumes of PV systems might be embedded in regions currently outside of the maximum reach of the existing weather stations. For the example shown here, an industrial area (“Industry 4”) benefited from the existence of station #426. Results have shown give enough evidence to stakeholders (e.g. grid operators) that the investment on extra stations is needed for further error curtailment in an area of interest.

4.1.4 Cloud vectoring demonstration and functionality

It was intuitive to derive that by extending the network of remote sensing stations, that a) a longer reach on weather knowledge would be achieved and b) that areas of Singapore not covered by the maximum range of superstations could be addressed. The expansion project for the stations is a “low hanging fruit”, which can be easily realized with further hardware investments and use of the existing system software backbone infrastructure.

However, extending a network addresses primarily areas of the island not previously covered. With the sky camera network deployment, it was intended that new insights into the Singapore climatic conditions are brought to light.

Here, two case studies are presented. The first one sees a moving Sumatra squall on the 1st July 2015 entering Singapore from the W-NW border. The sequence of Doppler images covering a period of 1.5 hours is shown in Figure 91. Via the sky camera network, selecting eight cameras at specific locations of the island, the vector directions were obtained for 1-min resolution and averaged to match the same interval as the Doppler images.

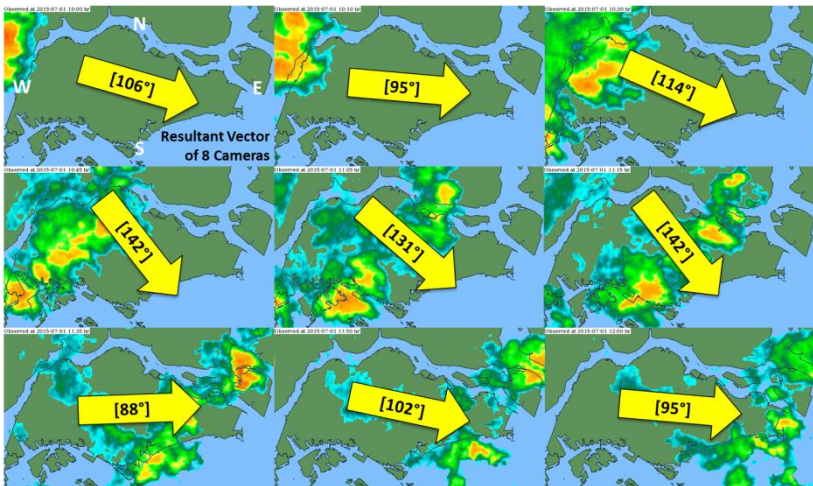


Figure 91: Storm progression through Singapore, with resultant vector taking eight sky cameras into account for predominant cloud direction path (NOBRE et al., 2015 (in preparation)).

The resultant vector direction for every interval between Doppler images yielded the yellow arrows shown in Figure 91. These directions showed a good agreement with the storm progression. Such findings assist knowledge gaining of cloud physics for the country.

The second case study also tackles the progression of a Sumatra squall occurring on the 4th July 2015. Figure 92 shows the squall Doppler radar sequence at the bottom of the image. The eight sky cameras vector directions are plotted at an approximate location where the devices are installed in the country.

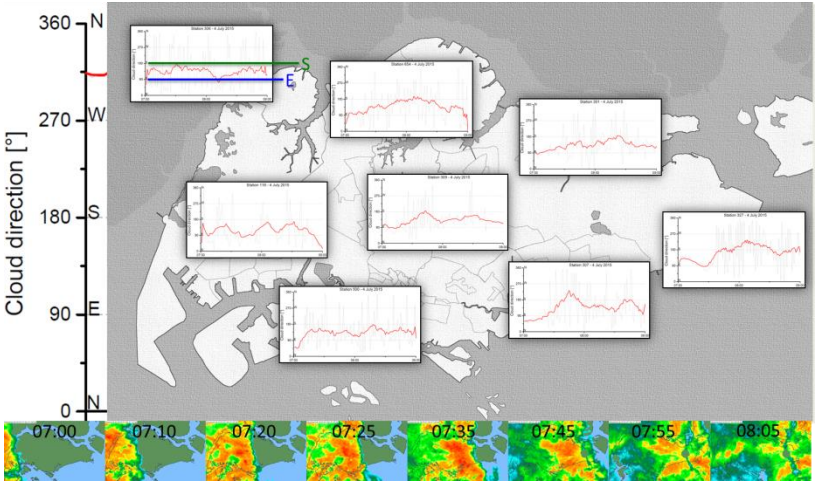


Figure 92: Storm progression through Singapore, with resultant vectors from eight sky cameras (NOBRE et al., 2015 (in preparation)).

In Figure 92, a good agreement is seen between actual storm traveling path (as per Doppler radar images, indicating a West-East direction), with actual cloud vectoring information (also primarily showing an Eastwards and South-eastwards path. This particular finding is an indication that information from one location of the island can serve to the benefit of other locations, even several kilometers away. Cloud vectoring can also potentially assist in future investigations on haze arrival and dissipation.

4.2 POWER CONVERSION SIMULATION RESULTS

4.2.1 Results on factors affecting PV power output

The following are results achieved while investigating five heavy influencers to PV system power output.

[A] Test #1: System modeling

A previous work by Mellit and Pavan (MELLIT and PAVAN, 2010) suggested that an arbitrary value of performance ratio could be used in order to promote modeling of the PV power after obtaining the forecast values for irradiance. As seen from results next, testing the parameters over five challenges described in subsection 3.4.2, this proves to be an over-simplification for a diverse fleet of PV systems and environment.

In Test #1, which deals with the PV modeling selection, Equations 9-11 were used, modeling the PV system power output first when G_{HI} and T_{amb} are the only known parameters. A nRMSE of 3.8% was achieved for data from March 2010 for a then new crystalline wafer-based system in Singapore (see Table 24, also displaying all other tests executed). When testing the second model, with G_{mod} and T_{mod} known, a more refined fit was achieved, with the lowest nRMSE of the three tested models, at 1.9%. The estimation via an arbitrary performance ratio (here 0.80) generates the highest errors, with nRMSE of 5.4%. The use of such a generic value of PR has not only a higher error but would also influence other tests discussed next.

Table 24: AC power output conversion model normalized root mean square errors according to the five test sequences proposed in the investigations (NOBRE et al., 2015 (submitted)).

	Test 1 (PV simulation models)			Test 2 (Temperature)		Test 3 (Shading)		Test 4 (Degradation)		Test 5 (Air pollution)	
Testing sequence	GHI, T _{amb} known	G _{mod} , T _{mod} known	PR estimated (0.80)	0.023°Cm²W⁻¹ (concrete roof)	0.032°Cm²W⁻¹ (metal roof)	Unshaded system	Shaded system	Year-1 system	Year-5 system	Clear sky days	Hazy days
AC power output conversion [nRMSE, %]	3.8	1.9	5.4	4.6	9.3	8.7	32.1	3.4	9.0	2.5	2.4

[B] Test #2: Temperature losses

Continuing the tests, a typical rooftop mounting Ross coefficient of $\gamma = 0.023^{\circ}\text{Cm}^2\text{W}^{-1}$ was chosen (Test #2), based on (YE *et al.*, 2013) as the simulation baseline. For a concrete rooftop, the PV power output modeling error showed a nRMSE of 4.6%. When assuming the same value of γ but using a metal rooftop-installed PV system, the nRMSE further increases to 9.4%, highlighting the importance of knowing system details to be considered during power output modeling. The heating profile for the two PV systems is shown in Figure 93 (left), where visually one can attest from the time series that the metal rooftop causes a higher module temperature when compared to the concrete one, which is estimated, for the given day in the example, as being ~15% higher for the metal rooftop on average.

The variation of module against ambient temperature with regards to irradiance on module plane at the sites allows the plotting of the graph on Figure 93 (right). The slope of the linear fit indicates the value for the Ross coefficient, here for March 2010, $0.032^{\circ}\text{Cm}^2\text{W}^{-1}$ and $0.025^{\circ}\text{Cm}^2\text{W}^{-1}$, for metal and concrete roofs, respectively. Roof color was not one of the aspects addressed in the investigations. The two test sites used for the analysis are ~2 km apart with nearly identical irradiation patterns for the period of study. Models used were for G_{mod} and T_{mod} known.

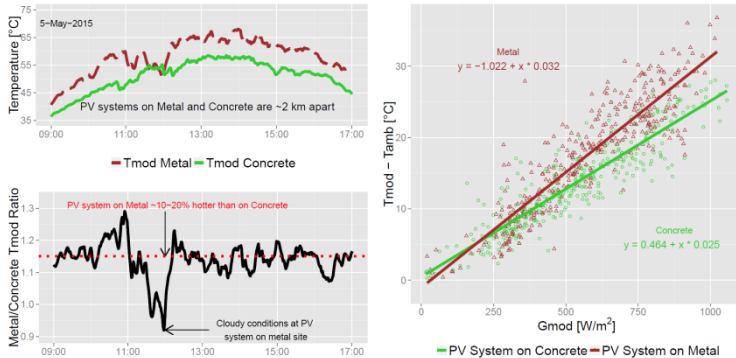


Figure 93: Module temperatures time series at two PV systems ~2 km apart (top left). The modules on a metal rooftop are in average ~15% hotter than the concrete one (bottom left). The temperature difference between module and ambient temperatures on the metal rooftop are compared against a system on a concrete rooftop (right) (NOBRE *et al.*, 2015 (submitted)).

[C] Test #3: Shading influences

Test #3 discusses shading in a densely-built environment as commonly found in Singapore, which can also lead to considerable deviations in the PV power conversion. In Figure 94 (left), the normalized power AC output of two PV systems on the same building are plotted, with one section of the system clearly shaded in the mid-afternoon. Figure 94 (right) portrays the readings of two irradiance sensors at the shaded and unshaded locations averaged for an entire year. The afternoon shading is clearly seen, but also in other parts of the day a lower level of irradiance is detected at the canopy location. All in all, irradiation at the shaded canopy is 27% lower than on the top of the building. The irradiance reduction experienced in this case study was observed to curtail power output of up to 90%. This type of shading is usually classified as “hard shading”. For “soft shading”, generally cast by trees, chimneys, elevator shafts or other smaller objects, which leave parts of the system still exposed to the full sun, losses can amount to anywhere between 30% and 60%, based on own measurement data in Singapore. Data simulated is from March 2015, for an already 5-year old system at the hospital complex discussed (system #115). The nRMSE for the unshaded system was higher when compared to a newer system. Taking the shaded section into account, the error climbs to 32.1%. The model used for Test #3 assumed G_{mod} and T_{mod} known.

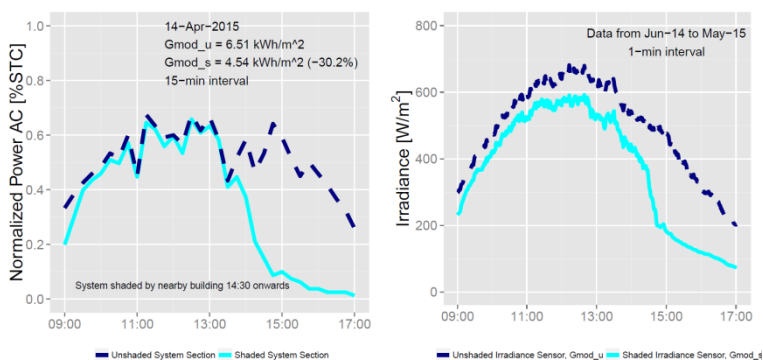


Figure 94: Normalized power AC output sections of a shaded and unshaded PV systems (left). One year data for two irradiance sensors are shown for both conditions investigated (NOBRE et al., 2015 (submitted)).

[D] Test #4: Long-term degradation

In Test #4, data from a PV system in its early months after deployment was used (March 2010, year one of operations) to evaluate the power output simulation from that period in time. The nRMSE was found to be 3.4%, with G_{mod} and T_{mod} known, with a PR for the month of 81.2%. When simulating the same system five years later, nRMSE was calculated at 9.0%, with PR for the month at 78.1%. The degradation trend for the system is shown in Figure 95 (left). It is important to note that the PV system used for this example obviously has experienced a long-term performance decay of approximately -1.0% per annum, i.e. above levels typically reported in literature (-0.5%, as per (JORDAN and KURTZ, 2013)). Figure 95 (right) shows the normalized power AC output of the system on a sunny day in 2010 and a similar day in 2015. The reduction in power generation potential of the system can be clearly seen.

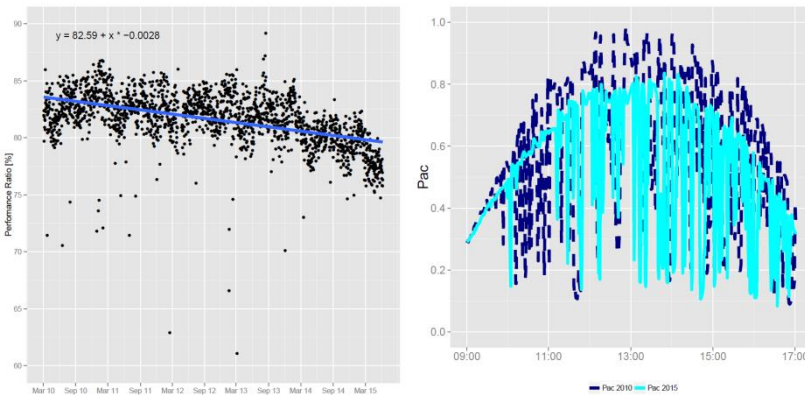


Figure 95: 5-year period of a PV system's daily performance ratios (left). The power output of a single typical day five years apart also shows the noticeable system degradation (NOBRE et al., 2015 (submitted)).

On the topic of system degradation, the author has worked on the benchmarking of several PV systems in Singapore, which includes the reporting of advanced decay of systems' performance ratios, such as the one shown in Figure 96, which belongs to the heavily soiled flat installation in Figure 60.

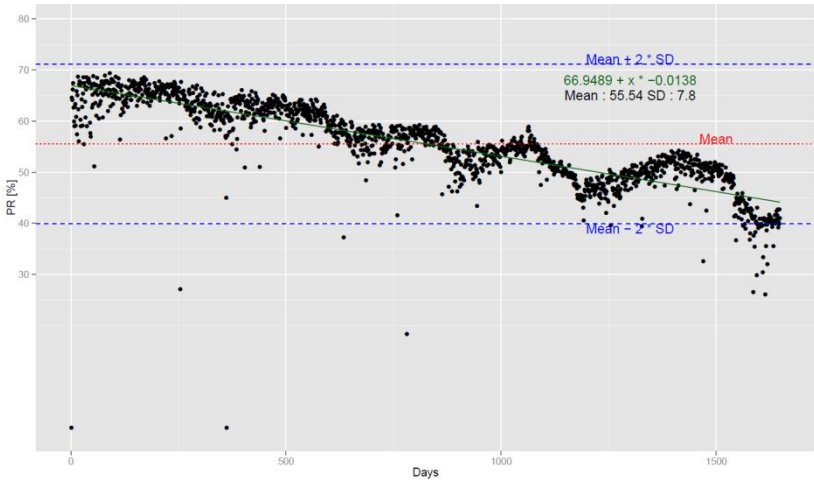


Figure 96: Recorded 5-year degradation records for the PV system shown in Figure 60, where advanced soiling has been detected (NOBRE *et al.*, 2015 (in preparation)).

[E] Test #5: Irradiance availability due to air pollution

The final test describes the influence of air pollution levels as object of study, with G_{mod} and T_{mod} known (Test #5). Figure 97 (left) plots the normalized power AC output of a crystalline wafer-based PV system on an extremely hazy day (pollutant standards index, PSI > 200) in June 2013. The PV power conversion works well nonetheless (nRMSE = 2.4%, nRMSE for clear skies = 2.5%), as from the perspective of the simulation model, the haze acts simply as a cloudy day. This would not be the case if the simulated PV system were a thin-film technology one, as demonstrated in (LIU *et al.*, 2014b), since the haze affects the spectrum of the irradiation in a detrimental way for those systems. Figure 97 (right) shows the ratio for power AC between an air-polluted versus a clear sky day. The days are 30 days apart so that the degradation of the system does not play an influencing role. For the two days compared, a reduction in power of circa 25% can be seen.

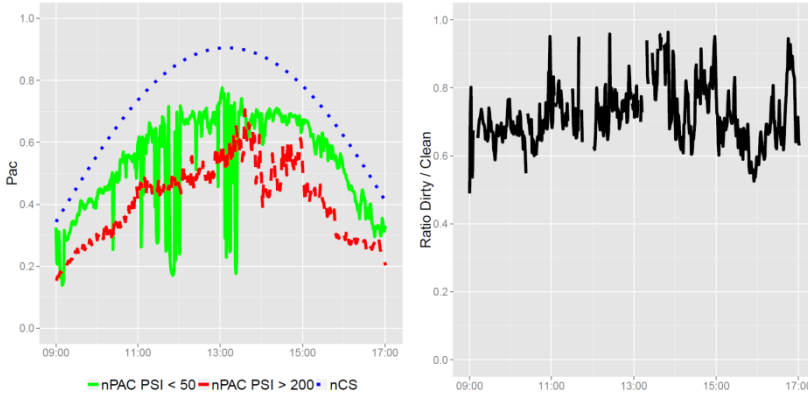


Figure 97: PV system normalized power AC output on a day with clean skies (PSI < 50) and with polluted skies (PSI > 200) (left). The hazy sky day incurs ~25% power output for the PV system (NOBRE *et al.*, 2015 (submitted)).

PV power conversion forecasting guidelines

Figure 98 shows the Persistence forecasting being utilized together with the PV power conversion modeling as discussed in section 5.1 of this work (here, G_{mod} and T_{mod} known are used). When not considering the system aging aspect into account, the power output modeling error is further transmitted to the power forecasting. The five tests discussed in sections 4.2 and 5.1 are repeated, taking a simplistic Persistence forecasting into account, with results shown in Table 6.

Notably, when Tests #1 through #4 are shown to induce power conversion errors, these are further transferred to the overall system level and possibly aggravate the effects from assessing what the level of PV power produced at the present moment in time will be, as well as for a country's fleet power output. In that sense, older PV systems or systems installed on metal rooftops seem to especially cause overestimations of the amount of power to be generated.

On the other hand, taking the fact that other larger degradation levels have been reported in Singapore likely due to soiling accumulation for installations at shallow tilt angles (NOBRE *et al.*, 2013), forecasting power output for solar systems in this tropical environment could further be over-estimated, if installations follow the common belief of matching their tilt angles to the local latitude, versus adopting a minimum 10-degree tilt angle to promote the so called self-cleaning effect from rain.

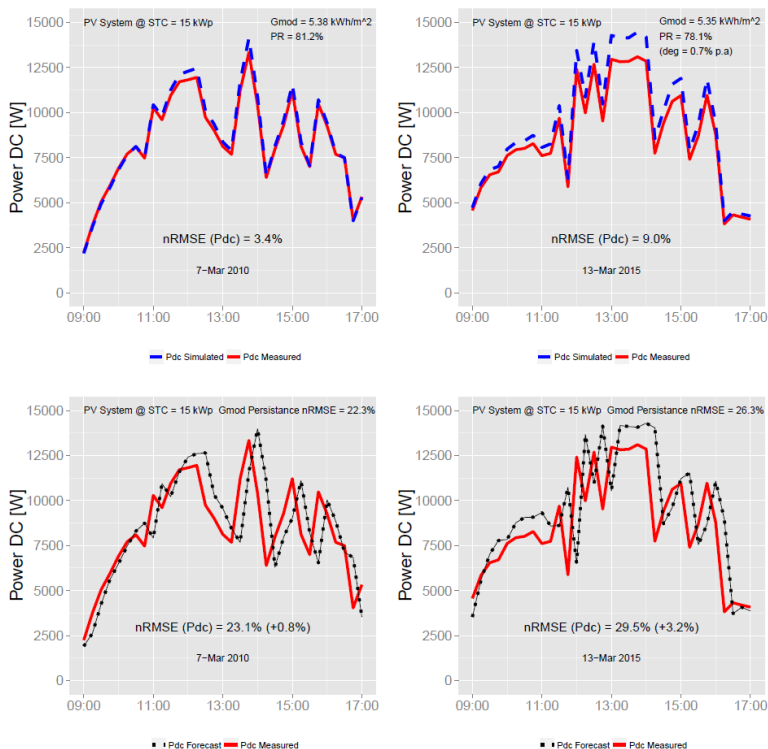


Figure 98: Simulated versus measured power DC for a 15 kWp PV system during its first year of operation (top left) and five years later (top right). A larger error was observed for the now older PV system when a simple Persistence forecast was performed (NOBRE et al., 2015 (submitted)).

Important to note when forecasting under hazy conditions is that PV power conversion and forecasting does not get considerably affected when systems are made of crystalline silicon technologies; however, grid operators ought to be aware that a general reduction of PV power generation in the absence of regular clouds in the sky, as shown in Figure 97 (right).

Summarizing, Table 25 aims to provide guidelines and execution steps for both power conversion and power forecasting for a PV system in a tropical setting, not considering the relatively low wind influence.

Table 25: Power conversion guidelines for a PV system in a tropical environment assuming low wind speeds (NOBRE et al., 2015 (submitted)).

Step	Formula	Recipe	Remark
1	Perez model	Generate G_{mod} values based on global horizontal irradiance readings	As demonstrated in (Yang, Dong et al. 2013, Khoo, Nobre et al. 2014) Skip step 1 if G_{mod} is known
2	$T_{mod} =$ $T_{amb} + \gamma G_{mod}$	Choose $\gamma = 0.032^{\circ}\text{Cm}^2\text{W}^{-1}$ for metal and $\gamma = 0.025^{\circ}\text{Cm}^2\text{W}^{-1}$ for concrete rooftops	Skip step 2 if T_{mod} is known
3	$\eta_{mpp}(G_{mod}, T_{mod}) =$ $\eta_{mpp,25}(G_{mod}) [1 + \alpha (T_{mod} - 25^{\circ}\text{C})]$	Choose $\alpha = -0.0045^{\circ}\text{C}^{-1}$ for crystalline wafer-based systems	Adjust α based on known specification sheet of solar modules
4	$\eta_{mpp}(G_{mod}, T_{mod}) =$ $\eta_{mpp}(G_{mod}, T_{mod}) * (sh)$	Choose value of “shading coefficient” (sh) according to shading severity Use $sh = 0.10$ for hard shade Use $sh = 0.45$ for soft shade	Assessment in shading condition at specific times of the day/year to be considered
5	$\eta_{mpp}(G_{mod}, T_{mod}) =$ $\eta_{mpp}(G_{mod}, T_{mod}) * (1 + deg)$	Choose value of “degradation rate” (deg) according to system age Use $deg = -1.2\%$ per annum for tilt angles $< 10^{\circ}$ Use $deg = -0.8\%$ per annum for tilt angles $> 10^{\circ}$	Special attention to be given in knowing the start performance baseline of a PV system
6	$\eta_{mpp}(G_{mod}, T_{mod}) =$ $\eta_{mpp}(G_{mod}, T_{mod}) * (air)$	Choose value of “air pollution” (air) according to condition at hand $air = 0.80$ for PSI > 200	PSI = Pollutant Standards Index, air pollution metric for Singapore, see (Velasco and Roth 2012; Liu, Nobre et al. 2014)

Although the essence of this investigation was carried out in tropical Singapore, the systematic can be adjusted to other weather conditions. For a temperate climate, the metal/concrete rooftop dynamic would play a different role due to different ambient temperature and wind conditions, also from the fact that other types of mounting system situations could be found, such as ground-mounted installations in non-area-constraint countries. Similarly, PV systems in open areas would not face the challenging shading conditions found in an urban context. Thirdly, degradation rates, an important topic of study for the long-term stability of PV installations, are likely to be less influential in temperate locations, with milder weather and steeper tilt angles of installation, which facilitate a better cleaning effect of the panels. Finally, the occasional situation of the haze pollution in Singapore could also be of relevance elsewhere, with varying polluting agents (e.g. smog, particles from construction/transportation, sandstorms), and possibly different duration, intensity, seasonality, and movement patterns.

4.2.2 Air pollution investigation findings

As the topic of air pollution was perceived to be of interest for the future planning of the grid in Singapore due to seasonal tendencies of haze episodes, this topic was further explored during the past years within the course of this thesis.

Figure 99 shows examples of global horizontal irradiance time series for three weather conditions – a sunny, a rainy and a cloudy day in Singapore, respectively, and the progression of the data points being eliminated through the three proposed filters in 3.4.3.

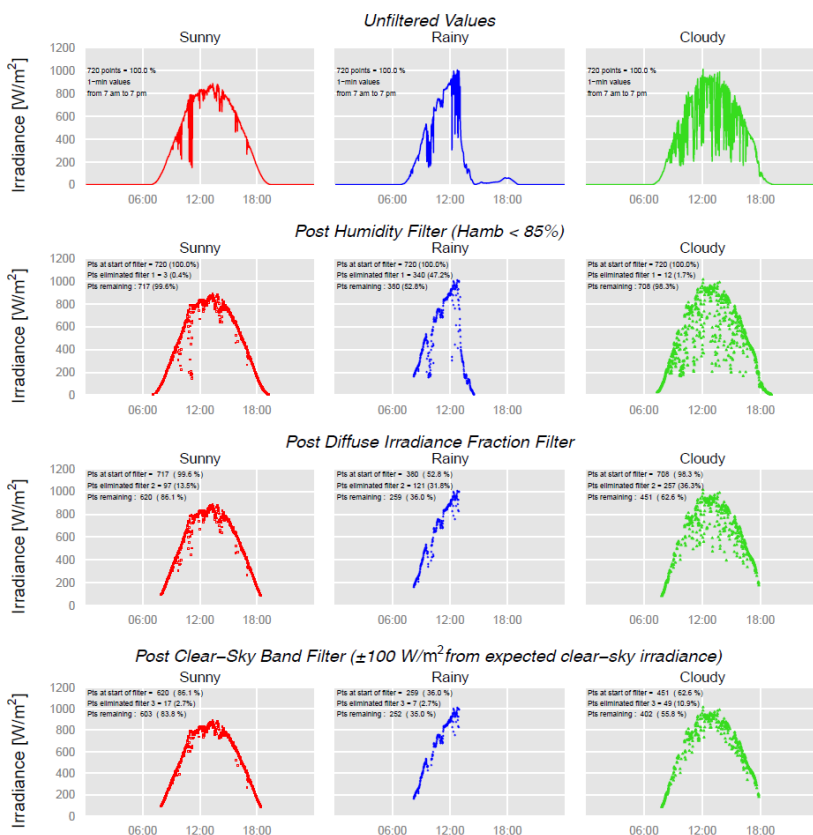


Figure 99: Filter performance progression for three different weather conditions (NOBRE et al., 2015 (accepted)).

Figure 100 shows one-minute averaged time steps for post-filtered irradiance values (as black dots) taking into account June data only, as well as the curve fits optimized for the available data points (orange lines). As an example, for all days categorized with PSI values below 50, the calculated average solar irradiance day indicated a total irradiation of 6.70 kWh/m². The modeled clear sky irradiance for all June days is plotted as a guide to the eyes (red dotted line). The areas under the curve fits represent the calculated irradiation found for the four selected air pollution levels. The readings used are for global horizontal irradiances recorded at the SERIS meteorological station using a calibrated pyranometer as a measurement device.

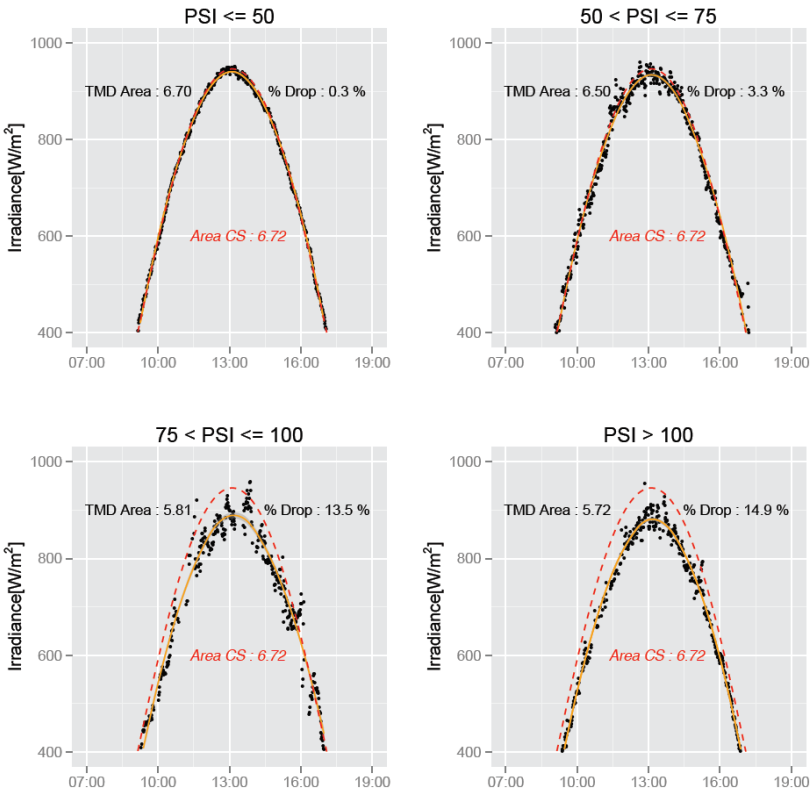


Figure 100: Post-filtered resulting daily irradiance averages for four varying levels of air pollution (NOBRE et al., 2015 (accepted)).

As values of air pollution increase, irradiation at ground level is reduced. Starting from the second PSI bin (50-75), irradiation levels dropped by 3.3% against the modeled clear sky days, followed by 13.5% for the third PSI bin (75-100) and finally by 14.9% for all days with PSI above 100. Figure 101 summarizes these findings not only for the case of the measurements by a pyranometer, but also with the use of a silicon sensor at the same meteorological station. As mentioned earlier in this thesis, a reduction of irradiation of ~5% due to the narrower spectral range of the silicon sensor was expected. Loss of irradiation with an increase of air pollution showed similar trends to the results assessed with the use of a pyranometer. A linear fit is included as a guide to the eye.

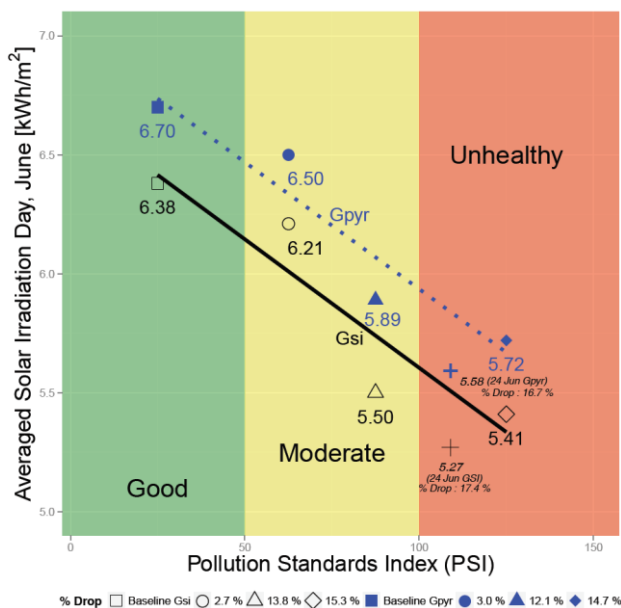


Figure 101: Calculated typical solar irradiation day (in kWh/m²) using June data for several ranges of the Pollutant Standards Index (PSI). Readings for a pyranometer and from a silicon sensor are shown (NOBRE et al., 2015 (accepted)).

The irradiation level for the exceptional day with hazy but cloudless conditions (PSI = 109, on 24 June 2013, shown in Figure 62) is also plotted in Figure 101. Irradiance measurements carry an uncertainty of anywhere between 2% and 5%, depending on the sensor type used in

the analysis, hence that day's readings are within the uncertainty of the analysis.

Table 26 shows the in-plane irradiation for ten PV systems during the June clear sky day conditions, following the same methodology carried out earlier for Figure 100. Irradiation losses between clear sky conditions and the hazy day of 24 June 2013 ranged between 13% and 22%. These variations likely depend on irradiation values, as well as haze levels throughout Singapore, which tend to vary up to 20 PSI points within the five locations monitored by NEA. Also, tilt angles and orientations of the in-plane irradiation sensors would yield slight differences for the given June day, even for a low latitude location such as Singapore (1°N of the Equator).

Table 26: Daily total irradiation on module plane, PV systems' yield and performance ratio (PR) for clear sky conditions ("clear") as per method described in this work (combination of days with $\text{PSI} < 50$) and during a strong hazy conditions day (24th June 2013, "hazy"). PV systems are located in several parts of Singapore and installed at different tilt angles and azimuths (NOBRE et al., 2015 (accepted)).

System name	$G_{\text{mod clear}}$ [kWh/m ²]	$G_{\text{mod hazy}}$ [kWh/m ²]	ΔG_{mod} [clear as baseline]	Yield clear [kWh/kWp]	Yield hazy [kWh/kWp]	Δ Yield [clear as baseline]	PR clear [%]	PR hazy [%]	Δ PRabs [clear as baseline]
c-Si 01	5.62	4.73	-15.8%	4.47	3.79	-15.2%	79.5%	80.1%	0.6%
c-Si 02	5.62	4.73	-15.8%	4.39	3.74	-14.8%	78.1%	79.1%	1.0%
c-Si 03	5.84	4.69	-19.7%	5.20	4.23	-18.7%	89.0%	90.2%	1.2%
c-Si 04	6.00	4.84	-19.3%	4.86	3.99	-17.9%	81.0%	82.4%	1.4%
c-Si 05	6.00	4.84	-19.3%	4.84	3.95	-18.4%	80.7%	81.6%	0.9%
Average	5.82	4.77	-18.0%	4.75	3.94	-17.0%	81.7%	82.7%	1.0%
Stdev	0.19	0.07		0.33	0.19				
a-Si 06	5.62	4.73	-15.8%	5.10	4.13	-19.0%	90.7%	87.3%	-3.4%
a-Si 07	5.84	4.69	-19.7%	5.46	4.29	-21.4%	93.5%	91.5%	-2.0%
a-Si 08	6.42	5.56	-13.4%	5.48	4.64	-15.3%	85.4%	83.5%	-1.9%
a-Si 09	5.90	4.90	-16.9%	4.50	3.36	-25.3%	76.3%	68.6%	-7.7%
a-Si 10	6.47	5.06	-21.8%	4.78	3.60	-24.7%	73.9%	71.1%	-2.7%
Average	6.05	5.09	-17.5%	4.92	3.89	-21.2%	81.1%	76.4%	-4.7%
Stdev	0.38	0.35		0.43	0.52				

The specific yields (in kWh/kW_p per day) for the ten PV systems under evaluation are also shown in Table 26. Derived energy yield losses of thin-film based PV systems due to haze were, on average, some 4% (absolute) lower than losses for crystalline silicon wafer-based PV systems. In contrast, the performance ratio for the systems shows a slight increase of PR for the crystalline silicon systems, while the thin-film systems suffer from an average drop of nearly 5%. Such a mechanism

was investigated by Liu et al. (LIU *et al.*, 2014a), demonstrating that a spectrum shift during the haze season is more detrimental to thin-film based PV systems in Singapore than for crystalline silicon based ones. Ye et al. (JIAYING *et al.*, 2014) reported similar effects but for single modules of four thin-film PV technologies under assessment in Singapore. Rüther and Livingstone (RÜTHER and LIVINGSTONE, 1995) and Rüther et al. (RÜTHER *et al.*, 2002) have also previously reported on spectral effects on the performance of thin-film silicon PV devices, showing the beneficial effects of blue-rich content of sunlight, emphasizing the fact that due to their narrower spectral range, thin-film PV devices are much more sensitive to spectral shifts in the content of sunlight than bulk crystalline silicon devices. Dirnberger et al. (DIRNBERGER *et al.*, 2015) elaborated on the spectral response of several PV technologies although the air pollution situation was not part of the study.

One other impact to analyze is the change in ambient and module temperatures, knowing that the reduction of PV power output through high module temperatures is the single-largest loss factor for PV systems in Singapore (YE *et al.*, 2013). Results are shown in Table 27. In spite of a slight increase in ambient temperature recorded during the hazy day, ambient temperatures in general throughout the various sites still fell within the 2-sigma standard deviation zone from the average temperature found on a clear sky day. It is noticed, however, that the module temperatures were lower on hazy days for both crystalline silicon wafer based and thin-film based systems when compared to temperatures on a clear sky day. A lower total irradiation on the modules results in cooler PV cells. This should particularly be the case for red-rich spectra as blue photons contribute stronger to thermalization losses in the PV cells, i.e. a smaller fraction of their energy is used for the photovoltaic effect, and hence they contribute more strongly to heating up the module. Such variations would affect voltage of PV devices, but the energy amounts involved in this situation are, however, quite small and of a second order of influence, with the effect of the higher direct irradiance of clear days expected to be the dominating effect. Therefore, impacts on the irradiance levels which directly affect current driven in the photovoltaic systems would have a predominant contribution level to the impact of haze on the yield of PV systems.

To conclude the haze investigations for PV applications in Singapore, the technical assessment of its impact was merged with financial implications for a future substantial fleet of systems in the country. Table 28 presents some of the assumptions and findings derived

from the techno-financial model investigated, with a 3 GW_p fleet of systems losing near 120 GWh and 26 million SGD in revenue during a 10-day haze episode which mimics the June 2013 haze crisis.

Table 27: Daily total ambient and module temperature averages for clear sky conditions (NOBRE et al., 2015 (accepted)).

System name	T _{amb} clear [C]	T _{amb} hazy [C]	Δ T _{amb} (clear as baseline)	T _{mod} clear [C]	T _{mod} hazy [C]	Δ T _{mod} (clear as baseline)
c-Si 01	33.1	34.1	3.0%	46.5	45.0	-3.2%
c-Si 02	33.1	34.1	3.0%	44.2	43.2	-2.3%
c-Si 03	31.6	32.7	3.5%	43.0	42.7	-0.7%
c-Si 04	31.8	33.2	4.4%	44.2	43.0	-2.7%
c-Si 05	31.8	33.2	4.4%	46.9	45.1	-3.8%
Average	32.3	33.5	3.7%	45.0	43.8	-2.5%
Stdev	0.8	0.6		1.7	1.2	
a-Si 06	33.1	34.1	3.0%	45.2	43.9	-2.9%
a-Si 07	31.6	32.7	3.5%	41.9	41.8	-0.2%
a-Si 08	31.7	32.5	2.5%	44.8	43.8	-2.2%
a-Si 09	32.4	33.1	2.2%	44.2	40.8	-7.7%
a-Si 10	32.5	33.7	3.7%	42.8	42.6	-0.5%
Average	32.3	33.2	3.0%	43.8	42.6	-2.7%
Stdev	0.6	0.7		1.4	1.3	

Table 28: Preliminary findings on loss of revenue to a future fleet of PV systems in Singapore during a 10-day haze episode which mimics the June 2013 crisis (NOBRE et al., 2015 (in preparation)).

Parameter	2014	2020	2030
PV systems deployed [MW _p]	33	650	3,000
Crystalline silicon share [%]	90%	95%	97%
System yield [kWh/kW _p]	1,100	1,112	1,132
Electricity tariff [SGD/kWh]	0.243	0.200	0.232
Energy loss in haze [GWh]	~1.5	~26.5	~119.3
Energy loss in haze [MSGD]	~1	~4.5	~25.8

The investigations on the effects of haze on PV systems in Singapore presented throughout this thesis have been published as a contribution in the IEEE’s “Journal of Photovoltaics” (LIU *et al.*, 2014b), see 6. Work on aspects of irradiation attenuation due to haze and loss of revenue in PV applications are part of the outcome of investigations within this thesis, with the paper on irradiation reduction due to air pollution accepted in the journal “Renewable Energy”.

4.2.3 Results on up-scaling exercises

As 90-95% of the installed capacity of PV systems in Singapore is of crystalline wafer-based technology, the up-scaling routine tested within the thesis focused on those systems. Via the National Solar Repository database, system size, age, tilt, orientation, roof material, system surroundings (shading potentials), etc. are obtained and used in the up-scaling routine, as presented in Table 15.

Individual results for the ten systems under investigation, accounting for ~10% of the volume of installations in Singapore, can be seen in Table 29.

Table 29: Up-scaling routine executed for March 2015 (NOBRE et al., 2015 (in preparation)).

System #	G_{mod} [kWh/m ²]	$Y_{\text{AC-0}}$ [kWh/kWp]	$Y_{\text{AC-1}}$ [kWh/kWp]	$Y_{\text{AC-2}}$ [kWh/kWp]	MAPE-1 [%]	MAPE-2 [%]
#901	138.5	3.14	3.27	3.57	13.8%	4.1%
#902	147.0	3.68	3.66	3.79	3.0%	0.6%
#903	151.3	3.70	3.72	3.90	5.5%	0.5%
#904	143.0	3.61	3.70	3.69	2.2%	2.4%
#905	147.7	3.56	3.56	3.81	6.9%	0.1%
#906	150.6	3.86	3.67	3.89	0.7%	4.9%
#907	147.7	2.43	2.66	3.81	56.7%	9.3%
#908	151.3	4.00	3.97	3.90	2.4%	0.7%
#909	136.2	2.97	3.12	3.51	18.5%	5.2%
#910	135.0	2.07	2.27	3.48	68.6%	9.8%
Avg.	144.8	3.30	3.36	3.74	17.8%	3.8%

The system yields via the method which utilizes Equations 9-11 ($Y_{\text{AC-1}}$) proved to be considerably more accurate than the coarse PR = 0.80 method ($Y_{\text{AC-2}}$), when compared to the actual registered yields at sites ($Y_{\text{AC-0}}$), with an average MAPE of 3.8% versus 17.8%.

An example of severe errors with the PR = 0.80 method are seen in systems #907 (severely shaded) and #910 (severely soiled). These two systems alone highlight areas of focus of this thesis of PV system modeling concerns.

New and professionally installed systems such as #904 and #908 also give an indication that such devices, when new, can indeed be estimated as having a performance ratio of 80%, however, with little time elapsed, start to deviate considerably from benchmark results.

Also worth noting is the average system yield for the month, 3.30 kWh/kW_p per day, with a March G_{mod} resource average of 144.8 kWh/m². This is translated to a PR of only ~71%, once again highlighting that there

is room for improvement in system performance in Singapore towards international benchmark levels above 80%.

Simulating a single PV system on a regular or detailed basis can ultimately create minimum errors in such exercises, as the user gets more and more familiar with the system's characteristics and behavior as the modeling repetitions continue. However, when modeling a fleet of systems, a few challenges that occur are volume of the fleet, correctness of the information gathered from a system and sensor accuracy & maintenance practices for the benchmarking of the validation.

The National Solar Repository of Singapore allows for the tapping of further PV data for future exercises. Although this data is not as precise as other research-grade datasets available, also not with the same time resolution of 1-min, monthly (and daily) energy readings allow for up-scaling exercises in terms of how the average output of a considerable amount of systems in the country's PV fleet would be.

Extrapolating to 100% of the PV facilities on a country-level could give utility operators in Singapore initial indication on PV system output on an island level for at least monthly intervals (at first). It is expected that such method is still more accurate than the one shown in Figure 22 for Germany (SMA, 2013a), as the ratio of empirical to up-scaled data for the pool of systems in Singapore is greater than for the European country. Such products can today be run on a monthly basis (for 25% of systems up-scaled to 100%, a ratio of 1:4), and on a daily basis only for a ratio of ~1:20. Dilution of the initiative database capabilities is continuous, with more systems deployed and NSR not able to add systems fast enough to match the solar market growth rates.

Finally, with a good up-scaling routine derived via the investigations of this thesis, the amount of total solar electricity produced in Singapore for a given month can be better estimated. For the case study addressed, it would have meant that monthly solar PV output would have been 3.38 GWh (based on the recorded monthly yield of 3.30 kWh/kW_p per day and a country installed capacity of 33 MW_p). Encouraging is that even without the readings from the ten PV systems presented, only with the available irradiance network in the country plus database information on system characteristics, one would have been able to calculate a monthly energy generation potential of 3.48 GWh, slightly overestimating it by a couple percentage points.

5. CONCLUSIONS

5.1 ON THE MAIN FINDINGS OF THIS THESIS

The following set of conclusions can be drawn from the investigations surrounding the works of this thesis.

5.1.1 On short-term forecasting for the tropics

In this thesis, methods for short-term irradiance forecasting were benchmarked. Also included was the development of a novel method to reduce prediction errors, based on weather observations and readings from a remote sensing network. Improvements in short-term irradiance forecasting were achieved for three severe weather conditions, namely: storms, washout days and haze days.

The storm detection triggers by far provided the best enhancement in the short-term forecasts (for 15-min and 30-min horizons), with nRMSE of the proposed Hybrid method reducing absolute errors by an average of 10.0% versus a baseline Persistence forecasting approach. Stormy days are good targets for prediction improvements due to the sudden nature of weather phenomena in the tropics and “over-reliance” of stochastic methods in past data.

The novel Hybrid algorithm also addressed complete “washout” days (i.e. with continuous rainfall) where it was proposed the use of the Persistence forecasting method throughout. The third severe meteorological condition was haze from transboundary forest fires. A further recommendation resulting from the findings is that the Persistence forecasting method be also used during periods of intense air pollution, simplifying forecasting methodologies.

The new developed algorithm now runs live at the SERIS’ PV System Monitoring Laboratory. It assists the team in understanding local weather as well as observing forecasting error behavior (see Figure 102 for a developed user interface).

The work presented here was designed for a location at the center of the sensor network (center of the island). The achieved uncertainty reduction likely would not be the same for peripheral areas, which would be at the mercy of the arrival of sudden storms with little or no warning. Therefore, areas of future improvement were addressed via a remote sensing network extension. It was demonstrated that such decision would help reduce forecasting errors at other parts of the island nearer to the sea. The network expansion was underway at the closure of this thesis.

Furthermore, the use of sky cameras for cloud motion tracking was shown to assist in detection and modeling of cloud patterns and thus help to further improve irradiance forecasting. Sky cameras would also allow for a better understanding of cloud physics, as well as assist future local scientists in the development of new forecasting algorithms for short-term purposes.

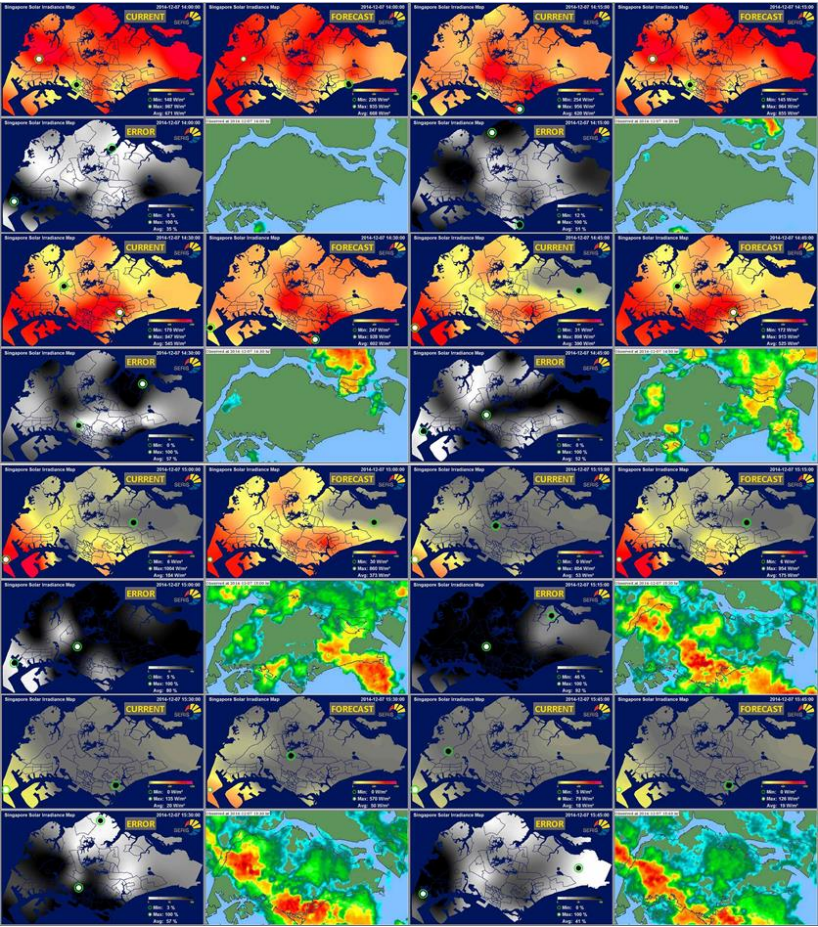


Figure 102: Live map (top left of each image sequence, here 15-min), including forecasting (top right), error (bottom left) and Doppler radar (bottom right) developed within the works of this thesis.

The increasing penetration levels with variable solar PV in electric power systems worldwide will require both short and long-term prediction forecasts of the irradiance in order to assist the balancing of energy generation from renewables and fossil-fuel-based sources, as well as the proper conversion of irradiance forecasts into actual PV power generation readily useable by grid-operators. In Singapore, as an example of a liberalized electricity market in a tropical location, energy trading is carried out at 30-min intervals, whose system would benefit most from forecasts similar to the ones presented in this work. It also assists a future energy market where solar photovoltaics play a larger role, with contribution levels that may account for as much as 20% of the energy needs of the city-state.

The discovery of areas of improvement helps delineate a path for similar work which could be experienced by other researchers in areas with similar weather patterns around the globe. Studying these extreme weather conditions as the one shown in Figure 11 and their effect on a growing number of solar photovoltaic systems are topics of great interest to various power system operators.

Although Singapore has a relative small area versus countries or even states within a certain country, the island does mimic the size of major city centers, thus allowing for the replication of similar remote sensing networks and meteorological boundary condition assessment as the ones discussed in this work, likely for locations with similar climate patterns.

5.1.2 On PV systems power conversion

Small gains in forecast accuracy, when obtained, can be quickly wiped out when using only a rough power conversion methodology, typical of present analyses in the field. Challenges in PV power generation and forecasting for a tropical, densely-built environment in Singapore were introduced, tested and verified, demonstrating the significant errors introduced when they are not considered.

Based on these findings, guidelines were given to facilitate better power simulation and forecasting in the future. Although this thesis conducted tests at a tropical location, the parameters considered can be adjusted according to other weather conditions at hand.

For air pollution aspects, i.e. anthropogenic-induced haze for the case of Singapore, global horizontal irradiation was assessed via a series of proposed filters in order to gauge the reduction of irradiation at ground level caused by haze, primarily originating from forest and agricultural

land clearing fires mostly in Sumatra (Indonesia). Blockage of sunlight due to haze was investigated in neighboring Singapore, 150-300 km away from the majority of the fire “hot spots”.

A novel filtering technique was proposed and implemented to differentiate between the impacts from clouds and air pollution caused by haze on the reduction on irradiance levels on the ground. Parameters used in the filtering included relative humidity and clear sky indices in order to sequentially remove the effects of rain and clouds on irradiation levels. A third filter was proposed in order to eliminate cloud-edge/enhancement effects (over-irradiances) or near cloudy conditions which could fall within sensor accuracy levels.

Global horizontal irradiance level reductions reached ~25% during a strong haze episode of June 2013, both when performing the analysis with the use of a pyranometer as well as with a crystalline silicon sensor that has a narrower spectral range.

The yield of ten PV systems across Singapore – both of crystalline wafer-based and thin-film silicon technologies – was investigated. PV systems suffered losses ranging from 15-25% when haze was strong at record air pollution indices in the unhealthy range registered for Singapore in June 2013. Thin-film technology-based PV installations experienced greater losses than crystalline wafer-based systems due to spectral effects. Ambient temperatures during haze periods were slightly higher than on clear sky days, whereas module temperatures were lower, likely due to loss of direct irradiation reaching solar module surfaces.

With more widespread use of PV generation expected in Singapore, a near-future scenario with 1 GW_p of deployed installations connected to the grid is likely to happen within the next 5-8 years. If major haze from Southeast Asia hits the country by then, associated losses, even though such episodes have a short duration of a few days or weeks, could be considerable. The effect for future scenarios (in 2020 and in 2030) was calculated, with losses due to a week’s worth of haze in the millions of dollars. Similar effects could take place elsewhere in the world with rising air pollution levels affecting the output (and eventually also the profitability) of solar PV renewable energy technology. Calculating the economic losses due to haze is a natural next step, adding to the ongoing argumentation between countries on issues related to reduction of air pollution levels, which so far have focused primarily, and naturally, on health issues.

Performance ratios of a-Si based and c-Si based PV systems operating in Singapore were found to behave differently during the haze

event in June 2013. It was showed that this effect can be attributed to a change in the generated short-circuit current resulting from a change in the spectral composition of the incident sunlight. During the haze period, a red-shift of the spectrum reaching the module planes was observed. This shift can be attributed to scattering of light at airborne haze particles. This change in the spectral composition negatively impacted a-Si systems, which mostly rely on short wavelengths (< 650 nm), but had a slight positive effect on c-Si systems which have the best spectral response at near-infrared wavelengths (800 to 900 nm). A clear correlation exists between the spectral changes and the performance ratios, as was validated by measurements as well as statistical analysis. As a rule of thumb, it can be concluded that the impact of haze on the PV power output is most severe for PV systems employing high-bandgap solar cells (such as a-Si solar cells), whereas crystalline silicon modules continue to perform well (efficiency-wise) under such conditions.

When dealing with irradiance forecasting, artificial intelligence techniques and time series analysis use past data in order to estimate the future irradiance value horizon. For a forecast algorithm, lower irradiance values during haze events will simply be perceived as cloudy conditions, not up to full expected irradiation levels according to the modeled clear sky irradiance bell-shape profile. However, attenuation of irradiation does play a role in diminishing maximum output of systems and consequently lowers returns on investments. While the latter directly affects system owners and investors, the former is a technical component which plays a role in future energy pricing and market forces, as limited availability of solar PV power output due to haze means more fossil-fuel generation of electricity is needed to supply the loads. This is the situation in Singapore, which is primarily generating electricity from natural gas power plants.

While this analysis was performed for Singaporean conditions, it is believed that it can also provide useful insight into PV systems deployed at other locations where the spectrum seen by the modules is affected by haze. For instance, industrial smog in China and forest fire smog in Brazil may affect PV system performance in a similar way. Quantification of the impact of haze on the solar irradiance could be the subject of future works.

5.2 LIMITATIONS OF THE WORK

The findings of this thesis are constrained to the location Singapore, a relatively small tropical island in Southeast Asia, with hot and humid weather throughout the year, yet a bustling city center with a rapidly growing population and expanding PV fleet. Although it is expected that several of the findings introduced could be applicable to other tropical locations of the world, particular weather phenomena must be taken into consideration for individual cases, such as the example of rain squalls in Singapore.

The thesis does not address the impact energy storage might have on the future of PV technology and its interface with local grids. Advancements of the knowledge ought to be considered for similar works in the future, e.g. the use of battery storage solutions likely will impact solar technology forecasting efforts and electricity pricing in a few years to come. Deployment of storage solutions, such as pumped hydro, likely will walk hand in hand with the topic of solar irradiance forecasting in future grids' operation protocols.

5.3 SUGGESTIONS FOR FUTURE WORKS

5.3.1 Hybridization and new forecasting methods

The use of sky cameras for cloud motion tracking could assist in detection and modeling of cloud patterns and thus help to further improve irradiance forecasting. Sky cameras would also allow for a better understanding of cloud heights, velocities and more refined trigger set-points as presented in this work. This thesis briefly introduced a local network of sky cameras and highlighted some of its potentials, which has since then allowed future generations of scientists to commence efforts on the enhancement of forecasting methods (see Karthik et al. in 6.1.).

Extended usage of the Doppler radar images (see Figure 103) is another possible area of expansion, since it has a 70 km radius range from its home base at Changi Airport, extending well into the ocean and nearby islands and peninsular Malaysia. Such range likely would play a role in enhancements in intra-day forecasting, e.g. 1-hr to 3-hr ahead of time.

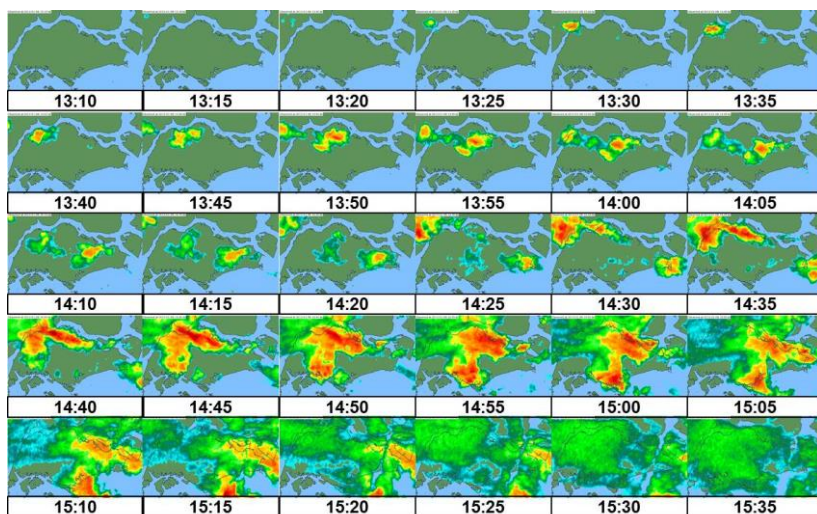


Figure 103: Doppler radar animation for 6/Jan/2013. Adapted from (NEA, 2013).

The Doppler radar could assist with weather phenomena motion such as Sumatra squalls, which come from the West part of Singapore traveling eastwards. From Figure 103, it is possible to identify patterns reaching the other end of the island in approximately 1 hour (covering a

40 km stretch in such a time). That could give a hint on cloud system traveling speed. Rain cloud systems seem to have speeds in the order of 30-60 km/h and heights of approximately 1-2 km. Such topics are worth exploring in order to enhance solar irradiance forecasting methods.

The artificial neural network implemented on this thesis was a classic architecture, without exogenous inputs. More complex ANN configurations for the location Singapore are being envisioned for future doctoral and post-doctoral studies.

Furthermore, machine vision software for vector assessment can be implemented, giving information on system travel orientation and velocity (between image frames). Such parameters could eventually a) be implemented as part of neural networks inputs or b) overrule other forecasting algorithms which have failed to detect the approximation of such dynamic weather systems.

SERIS completed its ground-based irradiance network in Singapore in late 2013 and is expanding it, as discussed, during 2015 and beyond. The acquisition of greater volumes of weather and PV system data start to leverage new solar irradiance forecast methods and PV modeling improvements.

5.3.2 Detailed up-scaling exercises and 3D modeling

Figure 104 shows a rough geographical concentration of PV installations as of the end of 2014 for Singapore.

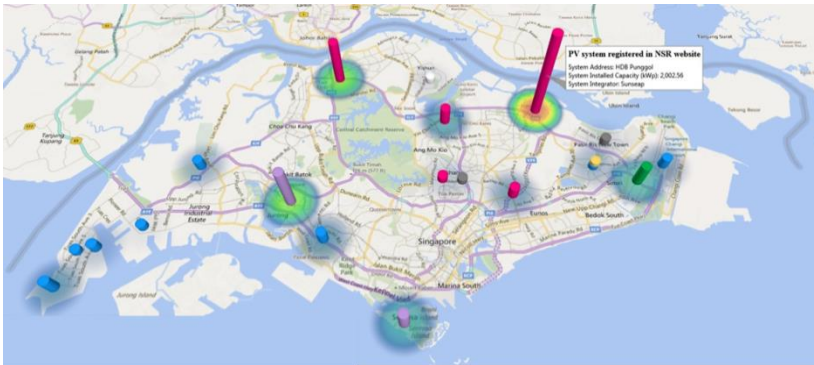


Figure 104: Geographical distribution of the highest concentrations of PV systems in Singapore in terms of installed capacity in 2014 (source of data: National Solar Repository of Singapore, adapted for this thesis).

SERIS has acquired laser data from the surface of Singapore, which will power 3D models of existing building feedstock and facilitate PV potential analysis, as well as solar resource availability onto rooftops. The combination of real-time forecasting, PV power conversion and building integrated photovoltaic potential for the country is definitely an area of interest for future R&D efforts.

5.3.3 Replication of remote sensing networks

Although Singapore has a relative small area versus other countries or even states within a certain country, the island mimics the size of major city centers, thus allowing for the replication of a similar meteorological remote sensing network. A city such as San Francisco in the United States (see Figure 105) has a small area of around 10x10 km, yet with ~30 MW_p of solar systems deployed by 2014, such a PV fleet would be able to benefit from enhanced PV power output forecasts.

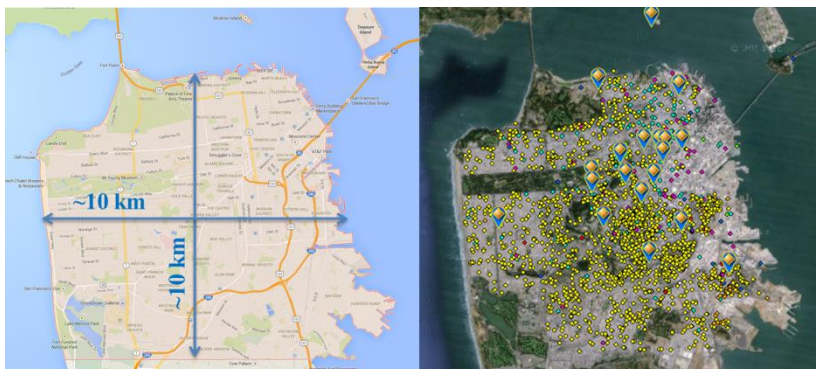


Figure 105: City of San Francisco, CA, USA (~10x10 km) and ~30 MW_p worth of solar PV systems (adapted for this thesis).

Another such example is the state-capital island of Florianópolis, in Brazil, with an area of roughly 2/3 of Singapore, and where PV systems are about to become widespread, as PV-generated electricity has recently reached grid parity. Such remote sensing networks will allow for a better and smoother integration of photovoltaics into an urban setting. Figure 106 shows the map of Florianópolis and additionally the one for the city of Belo Horizonte, another location in Brazil where PV is garnering considerable interest, with several systems already deployed.

Similarly to what was presented in this thesis, remote sensing networks could be expanded to cities in an attempt to learn the local

weather patterns and prepare these locations for higher levels of renewable energy penetration in the future. Table 30 presents some of these potential locations around the world.

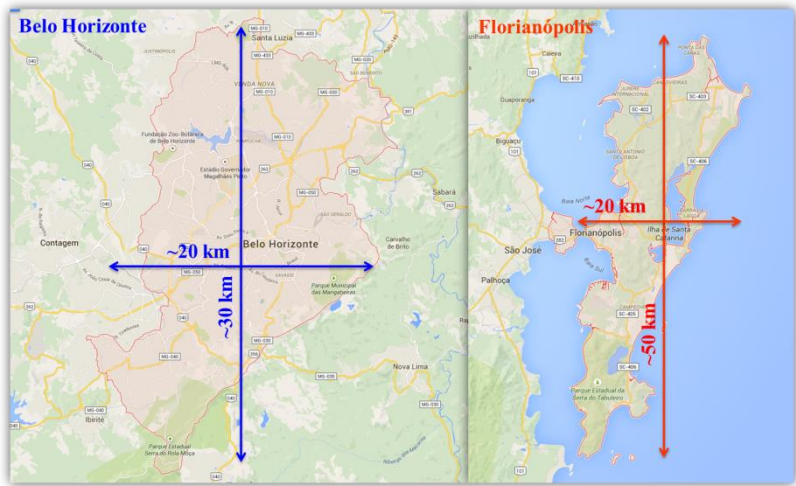


Figure 106: Cities of Belo Horizonte (~20x30 km, left) and Florianópolis (~20x50 km, right) (adapted for this thesis).

Table 30: Cities around the world where remote meteorological sensing networks could be deployed. Singapore is shown as a baseline (adapted for this thesis).

City	Country	Population [in million inhabitants]	Area [km ²]	Density [inhabitants/ km ²]	PV Volume [MW _p]
Florianópolis	Brazil	0.42	433	970	<5
San Francisco	USA	0.85	121	7,022	35
Munich	Germany	1.41	310	4,500	50
Oahu (island)	USA	1.42	1,545	632	220
Belo Horizonte	Brazil	2.49	331	7,528	<5
Santiago	Chile	5.15	641	8,470	<5
Singapore	Singapore	5.47	718	7,615	40

5.3.4 Other relevant works

Another area which remote sensing networks can assist is in solar resource mapping. Figure 107 shows the first irradiation map for Singapore which was derived from the existence of the network described in this thesis. The mapping exercise allowed the gauging of East and South parts of Singapore as being the most solar-resource-rich on the island. Although the selection of the location of PV systems stumbles on the fact that space is an issue in Singapore, for bigger area locations like Brazil, or other new tropical market frontiers, the siting of renewable energy projects is indeed dependent on local solar resource. The Brazilian Solar Atlas is an example of a tool which allows renewable energy project location selection, however, many areas of the world still lack either satellite models like the Atlas or ground-stations, as the ones shown in this thesis for Singapore.

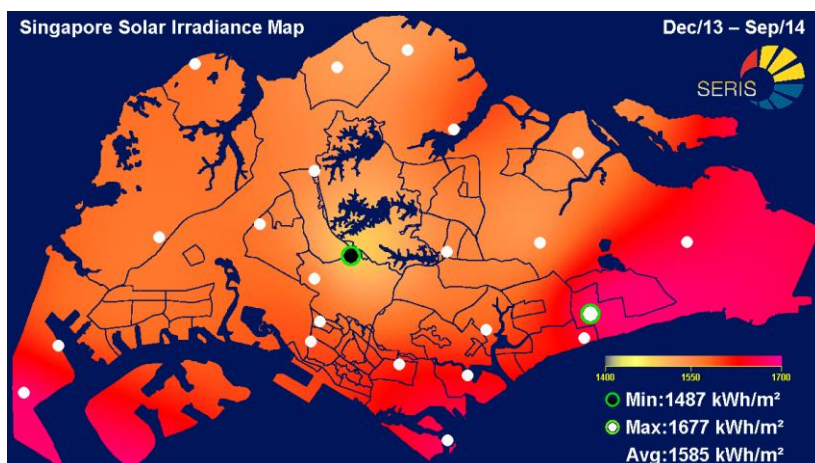


Figure 107: Example of irradiance map, which was developed for Singapore during the course of this thesis.

Still on the topic of solar resource mapping and worth noting is that not only photovoltaics projects depend on the gauging of irradiation, rather PV system performance assessment, asset operations & maintenance, and to support other renewable energy projects like solar thermal, or concentrating PV. Even other areas of science, such as agriculture or medical, have needs in knowing and tapping the local solar energy potentials, both on a historical basis, but live, moving forward.

6. PUBLICATIONS

At the time of the submission of this thesis (December 2015), the following works had been published, submitted for publication (under evaluation), or under revisions by co-authors prior to submission, either in peer-reviewed journals or conferences, where indicated.

Within a category, publications are listed chronologically, starting from most recent.

For the latest list of publications by the author on this thesis, the following link in the platform “Research Gate” is made available: https://www.researchgate.net/profile/Andre_Nobre3.

6.1 THESIS RELATED PUBLICATIONS

Published (in peer-reviewed journals)

LIU, H., NOBRE, A.M., YANG, D., YE, J., MARTINS, F.R., RÜTHER, R., REINDL, T., ABERLE, A.G., PETERS, I.M. **The impact of haze on performance ratio and short-circuit current of PV systems in Singapore.** IEEE Journal of Photovoltaics, <http://dx.doi.org/10.1109/JPHOTOV.2014.2346429>.
Impact factor: 3.00

NOBRE, A.M., KARTHIK, S., LIU, H., YANG, D., MARTINS, F.R., PEREIRA, E.B., RÜTHER, R., REINDL, T., PETERS, I.M. **On the impact of haze on the yield of photovoltaic systems in Singapore.** Accepted in “Renewable Energy”.
Impact factor: 3.47

Submitted (under evaluation by publishing house)

NOBRE, A.M., SEVERIANO JR. C.A., KARTHIK, S., KUBIS, M., ZHAO, L., PEREIRA, E.B., MARTINS, F.M., RÜTHER, R., REINDL, T. **PV power conversion and short-term forecasting in a tropical, densely-built environment.** Submitted to “Renewable Energy”.
Impact factor: 3.47

NOBRE, A.M., SEVERIANO JR. C.A., KARTHIK, S., KUBIS, M., ZHAO, L., MARTINS, F.M., RÜTHER, R., REINDL, T. **A meteorological sensing network for improved short-term solar irradiance forecasting for PV applications in Singapore.**

Submitted to “Renewable Energy”.

Impact factor: 3.47

Under revision by co-authors

NOBRE, A.M., SEVERIANO JR. C.A., KARTHIK, S., YANG, D.; KUBIS, M., PEREIRA, E.B., MARTINS, F.M., RÜTHER, R., REINDL, T. **Extending a ground-based meteorological sensing network for enhanced short-term solar irradiance forecasting for photovoltaic applications in a tropical environment.**

To be submitted to “Remote Sensing of Environment”.

Impact factor: 6.39

NOBRE, A.M., KARTHIK, S., MÜLLER, B, REISE, C., RÜTHER, R., REINDL, T. **Performance ratios and degradation rates of photovoltaic systems in a tropical environment.**

To be submitted to “IEEE Journal of Photovoltaics”.

Impact factor: 3.00

NOBRE, A.M., BIERI, M., KARTHIK, S., MARTINS, F.R., PEREIRA, E.B., RÜTHER, R, REINDL, T., PETERS, I.M. **Techno-economic analysis of the haze influence on photovoltaic systems in Singapore.**

To be submitted to “Energy Policy”.

Impact factor: 2.58

KARTHIK, S., ZHAO, L., RÜTHER, R., WALSH, W.M., NOBRE, A.M. **Short-term irradiance forecasting using ground-based sky cameras for photovoltaic applications in Singapore.**

To be submitted to “Solar Energy”.

Impact factor: 3.47

Published (in conference proceedings)

KARTHIK, S., ZHAO, L., NICHOLLS, A.D., PYAE, S., KUBIS, M., NOBRE, A.M. **Short-term irradiance forecasting using ground-based sky cameras.** Poster presentation at the “2nd PV Asia Scientific Conference, Asia Clean Energy Summit (ACES), Singapore Energy Week (SIEW) 2015”, Singapore, October 2015.

BAKER, R.S., BIERI, M., CHER, W.K., ZHANG, K., RÜTHER, R., REINDL, T., NOBRE, A.M. **National Solar Repository (NSR) – 5-year country-wide assessment of PV systems’ performance in Singapore.** Poster presentation at the “30th European Photovoltaic Solar Energy Conference & Exhibition (PVSEC)”, Hamburg, Germany, 14-18 September 2015, p. 2332-2334, <http://dx.doi.org/10.4229/EUPVSEC20152015-5BV.2.57>.

NOBRE, A.M., SEVERIANO JR. C.A., KUBIS, M., DU, H., KARTHIK, S., MARTINS, F.M., RÜTHER, R., REINDL, T. **A meteorological sensing network for improved short-term solar irradiance forecasting for PV applications in Singapore.** Oral presentation and conference proceedings at the “6th World Conference on Photovoltaic Energy Conversion, WCPEC-6 2014”, Kyoto, Japan, November 2014.

NOBRE, A.M., KUBIS, M., DU, H., PHUA, S., PYAE, S., YANG, D., REINDL, T. **First full 2D solar irradiation maps for Singapore based on a network of ground measurements.** Poster presentation at the “1st Photovoltaic Asia Scientific Conference (PVASC)”, Singapore, October 2014.

NOBRE, A.M., YANG, D., TAN, A.L., THOME, E.R., TAN, J., TAN, A.P., BARROT, J.M.O., ANTONIOLLI, A.F., RÜTHER, R., REINDL, T. **Large-area 2D mapping of PV systems performance.** Poster presentation and conference proceedings at the “29th European Photovoltaic Solar Energy Conference & Exhibition (PVSEC)”, Amsterdam, The Netherlands, 25-29 September 2014, p. 2858-2863, <http://dx.doi.org/10.4229/EUPVSEC20142014-5BV.2.16>.

6.2 OTHER PUBLISHED WORK

Published (in peer-reviewed journals)

VELDHUIS, A.J., NOBRE, A.M., PETERS, I.M., REINDL, T., RÜTHER, R., REINDERS, A.H.M.E. **An empirical model for rack-mounted PV module temperatures for Southeast Asian locations evaluated for minute time scales.** IEEE Journal of Photovoltaics, <http://dx.doi.org/10.1109/JPHOTOV.2015.2405762>.

Impact factor: 3.00

YANG, D., YE, Z., NOBRE, A.M., DU, H., WALSH, W.M., LIM, L.I., REINDL, T. **Bidirectional irradiance transposition based on the Perez model.** Solar Energy, v. 110, 2014, p. 768-780, <http://dx.doi.org/10.1016/j.solener.2014.10.006>.

Impact factor: 3.47

KHOO, Y.S., NOBRE, A., MALHOTRA, R., YANG, D., RÜTHER, R., REINDL, T., ABERLE, A.G. **Optimal orientation and tilt angle for maximizing in-plane solar irradiance for PV applications in Singapore.** IEEE Journal of Photovoltaics, <http://dx.doi.org/10.1109/JPHOTOV.2013.2292743>.

Impact factor: 3.00

YANG, D., DONG, Z., NOBRE, A., KHOO, Y.S., JIRITITIJAROEN, P., WALSH, W.M. **Evaluation of transposition and decomposition models for converting global solar irradiance from tilted surface to horizontal in tropical region.** Solar Energy, v. 97, 2013, p. 369-387, <http://dx.doi.org/10.1016/j.solener.2013.08.033>.

Impact factor: 3.47

ZOMER, C.D., NOBRE, A., CASSATELLA, P., REINDL, T., RÜTHER, R. **The balance between aesthetics and performance in building-integrated photovoltaics in the tropics.** Progress in Photovoltaics, 2013, <http://dx.doi.org/10.1002/pip.2430>.

Impact factor: 7.58

ZOMER, C.D., COSTA, M.R., NOBRE, A., RÜTHER, R. **Performance compromises of building-integrated and building-applied photovoltaics (BIPV and BAPV) in Brazilian airports.** Energy & Buildings, v. 66, 2013, p. 607-615, <http://dx.doi.org/10.1016/j.enbuild.2013.07.076>.

Impact factor: 2.88

YE, Z., NOBRE, A., REINDL, T., LUTHER, J., REISE, C. **On PV module temperatures in tropical regions.** Solar Energy, v. 88, 2013, p. 80-87, <http://dx.doi.org/10.1016/j.solener.2012.11.001>.

Impact factor: 3.47

Under revision by co-authors

BIERI, M., LIU, L., NOBRE, A.M., YANG, D., RIVAS, C., REINDL, T. **The impact of the declining oil price on the competitiveness of unsubsidized rooftop PV systems in Singapore.**

To be submitted to "Energy Policy".

Impact factor: 2.58

ZOMER, C.D., NOBRE, A.M., REINDL, T., RÜTHER, R. **Performance analysis for BIPV in high-rise, high-density cities: A case study in Singapore.**

To be submitted to "Renewable Energy".

Impact factor: 3.48

Published (in conference proceedings)

KARTHIK, S., ZHAO, L., NICHOLLS, A.D., PYAE, S., KUBIS, M., NOBRE, A.M. **Floating platform motion monitoring system for PV applications.** Poster presentation at the "2nd PV Asia Scientific Conference, Asia Clean Energy Summit (ACES), Singapore Energy Week (SIEW) 2015", Singapore, October 2015.

GUO, S., WU, C., DANNER, M., NOBRE, A., ABERLE, A.G., PETERS, I.M. **Modeling of an integrated standalone streetlamp PV system.** Poster presentation and conference proceedings at the "IEEE 42nd Photovoltaic Specialists Conference (PVSC)", New Orleans, LA, United States of America, 14-19 June 2015.

ABERLE, A., LIU, H., NOBRE, A.M., REN, Z., BUONASSISI, T., PETERS, I.M. **Design criteria of GaAs on silicon tandem solar cells for terrestrial applications.** Oral presentation and conference proceedings at the “Light, Energy and the Environment 2014”, Canberra, Australia, 2-5 December 2014, <http://dx.doi.org/10.1364/PV.2014.PTu3C.5>.

LIU, H., NOBRE, A.M., YANG, D., YE, J., MARTINS, F.R., RÜTHER, R., REINDL, T., ABERLE, A.G., PETERS, I.M. **The impact of haze on performance ratio and short-circuit current of PV systems in Singapore.** Poster presentation and conference proceedings at the “6th World Conference on Photovoltaic Energy Conversion, WCPEC-6 2014”, Kyoto, Japan, November 2014.

ZOMER, C.D., NOBRE, A.M., YANG, D., REINDL, T., RÜTHER, R. **Performance analysis for BIPV in high-rise, high-density cities: A case study in Singapore.** Oral presentation and conference proceedings at the “6th World Conference on Photovoltaic Energy Conversion, WCPEC-6 2014”, Kyoto, Japan, November 2014.

ANTONIOLLI, A.F., NOBRE, A.M., REINDL, T., RÜTHER, R. **A review on grid-connected PV systems in Brazil including system performance.** Poster presentation and conference proceedings at the “29th European Photovoltaic Solar Energy Conference & Exhibition (PVSEC)”, Amsterdam, The Netherlands, 25-29 September 2014, p. 2747-2752, <http://dx.doi.org/10.4229/EUPVSEC20142014-5BV.1.47>.

NOBRE, A., MALHOTRA, R., TANG, C.H., REISE, C., KIEFER, K., RÜTHER, R., REINDL, T. **Degradation analysis of photovoltaic systems in a tropical environment.** Oral presentation and conference proceedings at the “28th European Photovoltaic Solar Energy Conference & Exhibition (PVSEC)”, Paris, France, 30 Sep-4 Oct 2013, p. 3673-3677, <http://dx.doi.org/10.4229/28thEUPVSEC2013-5CO.5.4>.

ZOMER, C., NOBRE, A., CASSATELLA, P., REINDL, T., RÜTHER, R. **The balance between aesthetics and performance in building-integrated photovoltaics in the tropics.** Winner of one of seven student awards, oral presentation and conference proceedings at the “28th European Photovoltaic Solar Energy Conference & Exhibition (PVSEC)”, Paris, France, 30 Sep-4 Oct 2013, p. 3779-3787,

<http://dx.doi.org/10.4229/28thEUPVSEC2013-5DO.12.3>.

VELDHUIS, A.J., NOBRE, A., REINDL, T., RÜTHER, R., REINDERS, A.H.M.E. **The influence of wind on the temperature of PV modules in tropical environments, evaluated on an hourly basis.** Poster presentation at the “IEEE 39th Photovoltaic Specialists Conference (PVSC)”, Tampa, FL, United States of America, 16-21 June 2013, <http://dx.doi.org/10.1109/PVSC.2013.6744273>.

ZOMER, C., NOBRE, A., SOUZA, R., DU, H., REINDL, T., RÜTHER, R. **Environmental and performance issues in building-integrated and building-applied photovoltaics (BIPV and BPAV) in airports in tropical regions.** Poster presentation at the “2nd Photovoltaic Asia Pacific Conference (PVAP)”, Singapore, October 2012.

NOBRE, A., MONTENEGRO, A., YE, Z., REINDL, T., RÜTHER, R. **On PV module temperatures in tropical regions – a comparison between system locations in Singapore and Brazil.** Oral presentation and conference proceedings at the “IV Brazilian Solar Energy Congress and V Latin America Conference of the International Solar Energy Society (ISES)”, São Paulo, Brazil, 18-21 September 2012, http://www.acquaviva.com.br/CD_CBENS/trabalhos/T333.pdf#!

NOBRE, A., YE, Z., CHEETAMUN, H., REINDL, T., LUTHER, J., REISE, C. **High performing PV systems for tropical regions – optimization of system performance.** Oral presentation and conference proceedings at the “27th European Photovoltaic Solar Energy Conference & Exhibition (PVSEC)”, Frankfurt, Germany, 24-28 September 2012, p. 3763-3769, <http://dx.doi.org/10.4229/27thEUPVSEC2012-5CO.6.2>.

Technical papers

KUBIS, M., NOBRE, A. **Large-area real-time solar irradiance mapping for PV applications.** 2014 NI ASEAN Engineering Impact Awards, ASEAN Regional Contest, National Instruments.
Awarded “Best innovation in renewable energy”

YANG, D., NOBRE, A., BAKER, R., REINDL, T. **Large-area solar irradiance mapping.** Photovoltaics International, 24th Edition, p.91, May 2014, ISSN: 1757-1197

7. REFERENCES

AGEB. **Energieverbrauch in Deutschland im Jahr 2014**. A. E. E.V., 2014.

AIT. Preparing electricity grids for High-Penetration PV An Overview of the latest developments in Europe. In: PV Asia Pacific Conference, 2012. **Conference Proceedings**. Singapore: Austrian Institute of Technology, 2012.v.p.

ALMEIDA, M. P.; ZILLES, R.; LORENZO, E. Extreme overirradiance events in São Paulo, Brazil. **Solar Energy**. Issue 0, v.110, p.168-173, 2014.

AMERICA_DO_SOL. **Sistema solar instalado no Estádio de Pituacu**. Available at <http://www.americadosol.org/pituacu_solar/> Accessed on 24/Apr/2013.

ANEEL. **Resolução Normativa nº 482, de 17 de abril de 2012**. A. N. D. E. E. B. E. R. Agency) 2012.

ANTONIOLLI, A. F.; NOBRE, A. M.; REINDL, T.; RUTHER, R. A review on grid-connected PV systems in Brazil including system performance. In: European Photovoltaic Solar Energy Conference (EU PVSEC), 2014. **Conference Proceedings**. Amsterdam, 2014.v.p. 2747-2752.

ARYAPUTERA, A. W.; YANG, D.; WALSH, W. M. Day-Ahead Solar Irradiance Forecasting in a Tropical Environment. **Journal of Solar Energy Engineering**. 2015.

BADESCU, V. **Modeling Solar Radiation at the Earth's Surface**, 2008.

BIERI, M.; LIU, L.; NOBRE, A. M.; YANG, D.; RIVAS, C.; REINDL, T. The impact of the declining oil price on the competitiveness of unsubsidized rooftop PV systems in Singapore. **Energy Policy (in press)**. 2015.

BLOOMBERG. **Chinese Solar Billionaire Remains an Enigma After 47% Plunge**. Available at <<http://www.bloomberg.com/news/articles/2015-06-09/li-s-magical-thinking-leaves-hanergy-a-broken-empire>> Accessed on 11/6/2015.

BRAUER, M.; HISHAM-HASHIM, J. Peer Reviewed: Fires in Indonesia: Crisis and Reaction. **Environmental Science & Technology**. Issue 17, v.32, p.404A-407A, 1998.

BRAUN, M.; STETZ, T.; BRÜNDLINGER, R.; MAYR, C.; OGIMOTO, K.; HATTA, H.; KOBAYASHI, H.; KROPOSKI, B.; MATHER, B.; CODDINGTON, M.; LYNN, K.; GRADITI, G.; WOYTE, A.; MACGILL, I. Is the distribution grid ready to accept large-scale photovoltaic deployment? State of the art, progress, and future prospects. **Progress in Photovoltaics: Research and Applications**. Issue 6, v.20, p.681-697, 2012.

BSW. **Photovoltaik reift zur tragenden Säule der Energieversorgung**. Bundesverband Solarwirtschaft. Available at <http://www.solarwirtschaft.de/presse-mediathek/pressemeldungen/pressemeldungen-im-detail/news/photovoltaik-reift-zur-tragenden-saeule-der-energieversorgung.html> > Accessed on 1/May/2013.

_____. **Photovoltaics Report - Average price for PV rooftop systems in Germany**. Bundesverband Solarwirtschaft e.V. , 2014.

BURGER, B.; RÜTHER, R. Inverter sizing of grid-connected photovoltaic systems in the light of local solar resource distribution characteristics and temperature. **Solar Energy**. Issue 1, v.80, p.32-45, 2006.

CALINOIU, D.; PAULESCU, M.; IONEL, I.; STEFU, N.; POP, N.; BOATA, R.; PACURAR, A.; GRAVILA, P.; PAULESCU, E.; TRIFTORDAI, G. Influence of aerosols pollution on the amount of collectable solar energy. **Energy Conversion and Management**. Issue 0, v.70, p.76-82, 2013.

CAO, J. C.; CAO, S. H. Study of forecasting solar irradiance using neural networks with preprocessing sample data by wavelet analysis. **Energy**. Issue 15, v.31, p.3435-3445, 2006.

CEMIG. **CEMIG e governo estadual inauguram usina solar no Mineirão**. Available at <http://www.cemig.com.br/sites/Imprensa/pt-br/Paginas/Usina-Solar-do-Mineirao.aspx> > Accessed on

CHEN, C.; DUAN, S.; CAI, T.; LIU, B. Online 24-h solar power forecasting based on weather type classification using artificial neural network. **Solar Energy**. Issue 11, v.85, p.2856-2870, 2011.

CHEN, C. C. **Attenuation of Electromagnetic radiation by haze, fog, clouds, and rain**. U. S. a. F. P. Rand, 1975.

CHOW, C. W.; BELONGIE, S.; KLEISSL, J. Cloud motion and stability estimation for intra-hour solar forecasting. **Solar Energy**. v.115, p.645-655, 2015.

CHOW, C. W.; URQUHART, B.; LAVE, M.; DOMINGUEZ, A.; KLEISSL, J.; SHIELDS, J.; WASHOM, B. Intra-hour forecasting with a total sky imager at the UC San Diego solar energy testbed **Solar Energy**. Issue 11, v.85, p.2881-2893, 2011.

CHU, Y.; LI, M.; PEDRO, H. T. C.; COIMBRA, C. F. M. Real-time prediction intervals for intra-hour DNI forecasts. **Renewable Energy**. Issue 0, v.83, p.234-244, 2015.

CHU, Y.; PEDRO, H. T. C.; COIMBRA, C. F. M. Hybrid intra-hour DNI forecasts with sky image processing enhanced by stochastic learning. **Solar Energy**. v.98, Part C, p.592-603, 2013.

CHU, Y.; URQUHART, B.; GOHARI, S. M. I.; PEDRO, H. T. C.; KLEISSL, J.; COIMBRA, C. F. M. Short-term reforecasting of power output from a 48 MWe solar PV plant. **Solar Energy**. v.112, p.68-77, 2015.

CHUA, G. **Brighter days solar panel sales**. Straits Times Singapore: STS 2012.

CNA. **HDB calls for largest public solar tender to date**. Available at <<http://www.channelnewsasia.com/news/singapore/hdb-calls-for-largest/1894504.html?cid=TWTCNA>> Accessed on 5/Jun/2015.

DA SILVA FONSECA, J. G.; OOZEKI, T.; TAKASHIMA, T.; KOSHIMIZU, G.; UCHIDA, Y.; OGIMOTO, K. Use of support vector regression and numerically predicted cloudiness to forecast power output of a photovoltaic power plant in Kitakyushu, Japan. **Progress in Photovoltaics: Research and Applications**. Issue 7, v.20, p.874-882, 2012.

DGS. Planning and Installing Photovoltaic Systems - A guide for Installers, Architects and Engineers, 2008.

DIAGNE, M.; DAVID, M.; BOLAND, J.; SCHMUTZ, N.; LAURET, P. Post-processing of solar irradiance forecasts from WRF model at Reunion Island. **Solar Energy**. Issue 0, v.105, p.99-108, 2014.

DIRNBERGER, D.; BLACKBURN, G.; MÜLLER, B.; REISE, C. On the impact of solar spectral irradiance on the yield of different PV technologies. **Solar Energy Materials and Solar Cells**. Issue 0, v.132, p.431-442, 2015.

DO NASCIMENTO, L. R.; RUTHER, R. Fifteen years and counting: The reliable long-term performance of the first grid-connected, building-integrated, thin-film photovoltaic installation in Brazil. In: Photovoltaic Specialist Conference (PVSC), 2014 IEEE 40th, 2014. **Conference Proceedings**., 2014.v.p. 3372-3377.

DONG, Z.; YANG, D.; REINDL, T.; WALSH, W. M. Short-term solar irradiance forecasting using exponential smoothing state space model. **Energy**. Issue 0, v.55, p.1104-1113, 2013.

_____. Satellite image analysis and a hybrid ESSS/ANN model to forecast solar irradiance in the tropics. **Energy Conversion and Management**. Issue 0, v.79, p.66-73, 2014.

EISSA, Y.; MARPU, P. R.; GHERBOUDJ, I.; GHEDIRA, H.; OUARDA, T. B. M. J.; CHIESA, M. Artificial neural network based model for retrieval of the direct normal, diffuse horizontal and global horizontal irradiances using SEVIRI images. **Solar Energy**. Issue 0, v.89, p.1-16, 2013.

EMA. **Operation Statistics**. Energy Market Authority of Singapore (EMA). Available at <<http://www.ema.gov.sg/reports>> Accessed on 27/04/2013.

_____. **Energy Market Authority - Installed Capacity of Grid-Connected Solar Photovoltaic (PV) Systems, 2008 - 2Q 2014**. Disponível em. Acesso em:

_____. **Statistics, Monthly Peak System Demand**. Available at <http://www.ema.gov.sg/statistic.aspx?sta_sid=201408047htU7faVzLaZ> Accessed on 1/May/2015.

EMC. **Capacity for Registered Facilities**. Available at
 <<https://www.emcsg.com/marketdata/priceinformation#priceDataView>>
 Accessed on 1/May/2015.

EPE. **Balanço Energético Nacional 2014 - Ano base 2013 (Brazilian Energy Balance 2014 - Year 2013)**. E. D. P. E. B. E. R. Office), 2014.

ESTUPIÑÁN, J. G.; RAMAN, S.; CRESCENTI, G. H.; STREICHER, J. J.; BARNARD, W. F. Effects of clouds and haze on UV-B radiation. **Journal of Geophysical Research: Atmospheres**. Issue D11, v.101, p.16807-16816, 1996.

FAINE, P.; KURTZ, S. R.; RIORDAN, C.; OLSON, J. M. The influence of spectral solar irradiance variations on the performance of selected single-junction and multijunction solar cells. **Solar Cells**. Issue 3, v.31, p.259-278, 1991.

FAIRLEY, P. **Hawaii's Solar Push Strains the Grid**. MIT Technology Review. Available at
 <<http://www.technologyreview.com/news/534266/hawaiiis-solar-push-strains-the-grid/>> Accessed on

FAN, J. Investigation of solar energy for photovoltaic application in Singapore. In: The 8th International Power Engineering Conference, 2007. **Conference Proceedings**. Singapore, 2007.v.p. 86-89.

FERNÁNDEZ, E. F.; ALMONACID, F.; RUIZ-ARIAS, J. A.; SORIA-MOYA, A. Analysis of the spectral variations on the performance of high concentrator photovoltaic modules operating under different real climate conditions. **Solar Energy Materials and Solar Cells**. Issue 0, v.127, p.179-187, 2014.

FIELD, R. D.; VAN DER WERF, G. R.; SHEN, S. S. P. Human amplification of drought-induced biomass burning in Indonesia since 1960. **Nature Geoscience**. Issue 3, v.2, p.185-188, 2009.

FIRST_SOLAR. **Desert Sunlight Solar Farm**. Available at
 <<http://www.firstsolar.com/en/about-us/projects/desert-sunlight-solar-farm>>
 Accessed on 30/12/2013.

FONG, M. **The Weather and Climate of Singapore**: Meteorological Service Singapore. Singapore, 2012.

FONSECA JUNIOR, J. G. D. S.; OOZEKI, T.; OHTAKE, H.; TAKASHIMA, T.; OGIMOTO, K. Regional forecasts of photovoltaic power generation according to different data availability scenarios: a study of four methods. **Progress in Photovoltaics: Research and Applications**. p.n/a-n/a, 2014.

FONSECA_JR., J. G. D. S.; OOZEKI, T.; OHTAKE, H.; SHIMOSE, K.-I.; TAKASHIMA, T.; OGIMOTO, K. A comprehensive study of photovoltaic power generation forecasts in multiple locations in Japan. In: 28th European Photovoltaic Solar Energy Conference and Exhibition, 2013. **Conference Proceedings**. Paris, France, 2013.v.p. 3601 - 3606.

FRANKENBERG, E.; MCKEE, D.; THOMAS, D. Health Consequences of Forest Fires in Indonesia. **Demography**. Issue 1, v.42, p.109-129, 2005.

GAISMA. **Sunrise, sunset, dawn and dusk around the world**. Available at <www.gaisma.com> Accessed on 14/04/2013.

GOHARI, M. I.; URQUHART, B.; YANG, H.; KURTZ, B.; NGUYEN, D.; CHOW, C. W.; GHONIMA, M.; KLEISSL, J. Comparison of Solar Power Output Forecasting Performance of the Total Sky Imager and the University of California, San Diego Sky Imager. **Energy Procedia**. v.49, p.2340-2350, 2014.

GREEN, M. A.; EMERY, K.; HISHIKAWA, Y.; WARTA, W.; DUNLOP, E. D. Solar cell efficiency tables (Version 45). **Progress in Photovoltaics: Research and Applications**. Issue 1, v.23, p.1-9, 2015.

GUEYMARD, C. An anisotropic solar irradiance model for tilted surfaces and its comparison with selected engineering algorithms. **Solar Energy**. Issue 5, v.38, p.367-386, 1987.

GUEYMARD, C. A. The sun's total and spectral irradiance for solar energy applications and solar radiation models. **Solar Energy**. Issue 4, v.76, p.423-453, 2004.

_____. Temporal variability in direct and global irradiance at various time scales as affected by aerosols. **Solar Energy**. Issue 12, v.86, p.3544-3553, 2012.

H. QASEM, T. R. B., H. MÜLLEJANS, H. ALBUSAIRI, R. GOTTSCHALG. Effect of Dust Shading on Photovoltaic Modules. In: 26th

European Photovoltaic Solar Energy Conference and Exhibition, 2011.
Conference Proceedings. Hamburg, Germany, 2011.v.p. 3652 - 3656.

HAY, J. E.; DAVIES, J. A. Calculation of the solar radiation incident on an inclined surface. In: First Canadian Solar Radiation Workshop, 1980.
Conference Proceedings., 1980.v.p. 59-72.

HAYKIN, S. **Neural Networks - A Comprehensive Foundation:** Pearson Education. 1999.

HEYDENREICH, W.; MUELLER, B.; REISE, C. Describing the world with three parameters: a new approach to PV module power modelling. In: 23rd European Photovoltaic Solar Energy Conference and Exhibition (EU PVSEC), 2008. **Conference Proceedings.** Valencia, Spain, 2008.v.p. 2786-2789.

HEYDENREICH, W.; MÜLLER, B.; REISE, C. Describing the World With Three Parameters: A New Approach to PV Module Power Modelling. In: 23rd European Photovoltaic Solar Energy Conference and Exhibition, 2008. **Conference Proceedings.** Valencia, Spain, 2008.v.p.

HOFF, T. E.; PEREZ, R. Quantifying PV power Output Variability. **Solar Energy.** Issue 10, v.84, p.1782-1793, 2010.

HUMMON, M.; DENHOLM, P.; MARGOLIS, R. Impact of photovoltaic orientation on its relative economic value in wholesale energy markets. **Progress in Photovoltaics: Research and Applications.** p.n/a-n/a, 2012.

HUSSAIN, Z. **S'pore, Indonesia officials to meet.** The Straits Times. Singapore 2013.

HYNDMAN, R.; KOEHLER, A. B.; ORD, J. K.; SNYDER, R. D. **Forecasting with Exponential Smoothing:** Springer-Verlag Berlin Heidelberg. 2008.

HYNDMAN, R. J.; KHANDAKAR, Y. Automatic Time Series Forecasting: The forecast Package for R. **Journal of Statistical Software.** Issue 3, v.27, 2008.

IEA. **Task 14: High Penetration of PV Systems in Electricity Grids.** Available at <<http://www.iea-pvps.org/index.php?id=58#c92>> Accessed on 18/3/2013.

_____. **Key World Energy Statistics**. I. E. Agency, 2014a.

_____. **Technology Roadmap - Solar Photovoltaic Energy**. I. E. Agency, 2014b.

_____. **Trends 2014 in photovoltaic applications - Survey report of selected IEA countries between 1992 and 2013**. I. E. Agency, 2014c.

IEC. **Photovoltaic system performance monitoring – Guidelines for measurement, data exchange and analysis**: International Electrotechnical Commission. IEC 61724, Edition 1.0, 1998-04 1998.

_____. **Photovoltaic (PV) module performance testing and energy rating - Part 1: Irradiance and temperature performance measurements and power rating** International Electrotechnical Commission. IEC 61853-1:2011 2011.

INMAN, R. H.; PEDRO, H. T. C.; COIMBRA, C. F. M. Solar forecasting methods for renewable energy integration. **Progress in Energy and Combustion Science**. Issue 6, v.39, p.535-576, 2013.

ISE. **Photovoltaics Report (figure adapted from PSE AG)**. Fraunhofer Institute for Solar Energy Systems. Freiburg, Germany, 2014.

JAMROZIK, E.; MUSK, A. W. Respiratory health issues in the Asia-Pacific region: an overview. **Respirology**. Issue 1, v.16, p.3-12, 2011.

JIAYING, Y.; REINDL, T.; ABERLE, A. G.; WALSH, T. M. Effect of Solar Spectrum on the Performance of Various Thin-Film PV Module Technologies in Tropical Singapore. **Photovoltaics, IEEE Journal of**. Issue 5, v.4, p.1268-1274, 2014.

JORDAN, D. C.; KURTZ, S. R. Photovoltaic Degradation Rates-an Analytical Review. **Progress in Photovoltaics: Research and Applications**. Issue 1, v.21, p.12-29, 2013.

JORDAN, D. C.; SEKULIC, B.; MARION, B.; KURTZ, S. R. Performance and Aging of a 20-Year-Old Silicon PV System. **Photovoltaics, IEEE Journal of**. Issue 3, v.5, p.744-751, 2015.

JOURNÉE, M.; STÖCKLI, R.; BERTRAND, C. Sensitivity to spatio-temporal resolution of satellite-derived daily surface solar irradiation. **Remote Sensing Letters**. Issue 4, v.3, p.315-324, 2011.

K. KIEFER, D. D., B. MÜLLER, W. HEYDENREICH, A. KRÖGGER-VODDE. A degradation analysis of PV power plants. In: 25th European Photovoltaic Solar Energy Conference and Exhibition (PVSEC), 2010. **Conference Proceedings**. Valencia, Spain, 2010.v.p.

KHATIB, T.; MOHAMED, A.; MAHMOUD, M.; SOPIAN, K. A New Approach for Meteorological Variables Prediction at Kuala Lumpur, Malaysia, Using Artificial Neural Networks: Application for Sizing and Maintaining Photovoltaic Systems. **Journal of Solar Energy Engineering**. Issue 2, v.134, p.021005-021005, 2012.

KHOO, Y. S.; NOBRE, A.; MALHOTRA, R.; DAZHI, Y.; RUTHER, R.; REINDL, T.; ABERLE, A. G. Optimal Orientation and Tilt Angle for Maximizing in-Plane Solar Irradiation for PV Applications in Singapore. **Photovoltaics, IEEE Journal of**. Issue 2, v.4, p.647-653, 2014.

KHOO, Y. S.; SINGH, J. P.; WALSH, T. M.; ABERLE, A. G. Comparison of Angular Reflectance Losses Between PV Modules With Planar and Textured Glass Under Singapore Outdoor Conditions. **Photovoltaics, IEEE Journal of**. Issue 1, v.4, p.362-367, 2014.

KING, D. L.; BOYSON, W. E.; KRATOCHVILL, J. A. **Photovoltaic Array Performance Model**. S. N. Laboratories. Albuquerque, NM, USA, 2004.

KLEISSL, J. **Solar Energy Forecasting and Resource Assessment**: Elsevier Academic Press. 2013.

KLUCHER, T. M. Evaluation of models to predict insolation on tilted surfaces. **Solar Energy**. Issue 2, v.23, p.111-114, 1979.

LARA-FANEGO, V.; RUIZ-ARIAS, J. A.; POZO-VÁZQUEZ, D.; SANTOS-ALAMILLOS, F. J.; TOVAR-PESCADOR, J. Evaluation of the WRF model solar irradiance forecasts in Andalusia (southern Spain). **Solar Energy**. Issue 8, v.86, p.2200-2217, 2012.

LAVE, M.; KLEISSL, J.; STEIN, J. S. A Wavelet-Based Variability Model (WVM) for Solar PV Power Plants. **Sustainable Energy, IEEE Transactions on**. Issue 2, v.4, p.501-509, 2013.

LIMA, F. L.; MARTINS, F. R.; PEREIRA, E. B. Forecast of short-term solar irradiation in Brazil using numerical models and statistical postprocessing. In: EuroSun 2014, 2014. **Conference Proceedings**. Aux-les-Bains, 2014.v.p.

LIPPERHEIDE, M.; BOSCH, J. L.; KLEISSL, J. Embedded nowcasting method using cloud speed persistence for a photovoltaic power plant. **Solar Energy**. v.112, p.232-238, 2015.

LIU, B.; JORDAN, R. Daily insolation on surfaces tilted towards equator. **ASHRAERJ**. v.10, p.53-59, 1961.

LIU, H.; NOBRE, A. M.; YANG, D.; YE, J.; MARTINS, F. R.; RUTHER, R.; REINDL, T.; ABERLE, A. G.; PETERS, I. M. The effect of haze of current ratio of PV systems in Singapore. **IEEE Journal of Photovoltaics**. 2014a.

LIU, H.; NOBRE, A. M.; YANG, D.; YE, J. Y.; MARTINS, F. R.; RUTHER, R.; REINDL, T.; ABERLE, A. G.; PETERS, I. M. The Impact of Haze on Performance Ratio and Short-Circuit Current of PV Systems in Singapore. **Photovoltaics, IEEE Journal of**. Issue 6, v.4, p.1585-1592, 2014b.

LORENZ, E.; HEINEMANN, D.; KURZ, C. Local and regional photovoltaic power prediction for large scale grid integration: Assessment of a new algorithm for snow detection. **Progress in Photovoltaics: Research and Applications**. Issue 6, v.20, p.760-769, 2012.

LORENZ, E.; SCHEIDSTEGE, T.; HURKA, J.; HEINEMANN, D.; KURZ, C. Regional PV power prediction for improved grid integration. **Progress in Photovoltaics: Research and Applications**. Issue 7, v.19, p.757-771, 2011.

LTA. Land Transport Authority of Singapore (LTA). Land Transport Statistics in Brief - 2014. Available at <http://www.lta.gov.sg/content/dam/ltaweb/corp/PublicationsResearch/files/FactsandFigures/Statistics%20in%20Brief%202014.pdf> Accessed on

LUTHER, J. Grid parity drivers (figure) 2009.

LUTHER, J.; REINDL, T. **Solar Photovoltaic (PV) Roadmap for Singapore**. Singapore, p.77, 2013.

MARQUEZ, R.; COIMBRA, C. F. M. Forecasting of global and direct solar irradiance using stochastic learning methods, ground experiments and the NWS database. **Solar Energy**. Issue 5, v.85, p.746-756, 2011.

_____. Proposed metric for evaluation of solar forecasting models. **Journal of Solar Energy Engineering**. v.135, 2012.

_____. Intra-hour DNI forecasting based on cloud tracking image analysis. **Solar Energy**. Issue 0, v.91, p.327-336, 2013.

MARQUEZ, R.; PEDRO, H. T. C.; COIMBRA, C. F. M. Hybrid solar forecasting method uses satellite imaging and ground telemetry as inputs to ANNs. **Solar Energy**. Issue 0, v.92, p.176-188, 2013.

MARTINS, F. R.; PEREIRA, E. B.; GUARNIERI, R. A. Solar radiation forecast using artificial neural networks. **International Journal of Energy Science**. Issue 6, v.2, p.217-227, 2012.

MARTINS, F. R.; PEREIRA, E. B.; SILVA, S. A. B.; ABREU, S. L.; COLLE, S. Solar energy scenarios in Brazil, Part one: Resource assessment. **Energy Policy**. Issue 8, v.36, p.2853-2864, 2008.

MASA-BOTE, D.; CAAMAÑO-MARTÍN, E. Forecast of Energy Production for PV Systems 24 Hours Ahead. In: 25th European Photovoltaic Solar Energy Conference and Exhibition / 5th World Conference on Photovoltaic Energy Conversion, 2010. **Conference Proceedings**. Valencia, Spain, 2010.v.p. 4813 - 4819.

MATHIESEN, P.; COLLIER, C.; KLEISSL, J. A high-resolution, cloud-assimilating numerical weather prediction model for solar irradiance forecasting. **Solar Energy**. v.92, p.47-61, 2013.

MATHIESEN, P.; KLEISSL, J. Evaluation of numerical weather prediction for intra-day solar forecasting in the continental United States. **Solar Energy**. Issue 5, v.85, p.967-977, 2011.

MELLIT, A.; KALOGIROU, S. A. Artificial intelligence techniques for photovoltaic applications: A review. **Progress in Energy and Combustion Science**. Issue 5, v.34, p.574-632, 2008.

MELLIT, A.; PAVAN, A. M. A 24-h forecast of solar irradiance using artificial neural network: Application for performance prediction of a grid-connected PV plant at Trieste, Italy. **Solar Energy**. Issue 5, v.84, p.807-821, 2010.

METEONORM. **Irradiance data for Singapore**. Meteonorm_6.2 2013.

METEOTEST. **Meteonorm software**. Available at
<<http://meteonorm.com/>> Accessed on 24/Jun/2015.

MEWR. **A Lively & Liveable Singapore: Strategies for Sustainable Growth**. M. O. T. E. a. W. R. a. M. O. N. Development, 2009.

MIETTINEN, J.; LIEW, S. C. Burn-scar patterns and their effect on regional burnt-area mapping in insular South-East Asia. **International Journal of Wildland Fire**. Issue 7, v.18, p.837-847, 2009.

MONTENEGRO, A. **Analise economico-financeira da geracao de energia eletrica atraves de sistemas fotovoltaicos integrados a residencias unifamiliares urbanas no Brasil**. Civil Engineering, Universidade Federal de Santa Catarina, Florianopolis, SC, 2013.

MTI. **The SolarNova Programme**. Available at
<<http://www.mti.gov.sg/MTIInsights/SiteAssets/Pages/Budget-2014/SolarNova.pdf>> Accessed on

MÜLLER, B.; HARDT, L.; ARMBRUSTER, A.; KIEFER, K.; REISE, C. Yield predictions for photovoltaic power plants: empirical validation, recent advances and remaining uncertainties. **Progress in Photovoltaics: Research and Applications**. p.n/a-n/a, 2015.

NASA. **NASA surface meteorology and solar energy: global data sets**. Langley, USA 2013.

NCCS. **Singapore Announces Region's First Floating Photovoltaic Pilot Project at Solar Pioneer Awards Ceremony**. Available at
<<https://www.nccs.gov.sg/news/singapore-announces-regions-first-floating-photovoltaic-pilot-project-solar-pioneer-awards>> Accessed on 2/2/1012.

National Environment Agency of Singapore **Weatherwise Singapore**. 2009.

NEA. **Satellite image of Singapore:** Meteorological Services Division, NEA 2010.

_____. **Rain Areas Animation.** National Environment Agency (NEA). Available at <<http://www.nea.gov.sg/weather-climate/weather-information/rain-areas-animation>> Accessed on 20/12/2012.

_____. **Climate information and data of Singapore.** National Environment Agency. Available at <http://app2.nea.gov.sg/localclimate_climateinfo.aspx> Accessed on 20/4/2013.

_____. **Historical PSI readings.** Available at <<http://app2.nea.gov.sg/anti-pollution-radiation-protection/air-pollution-control/psi/historical-psi-readings/year/2013/month/6/day/22>> Accessed on

_____. **Air pollution control - haze.** National Environment Agency of Singapore (NEA). Available at <<http://app2.nea.gov.sg/anti-pollution-radiation-protection/air-pollution-control/haze>> Accessed on

_____. **Frequently asked questions on PSI.** National Environment Agency of Singapore (NEA). Available at <<http://app2.nea.gov.sg/anti-pollution-radiation-protection/air-pollution-control/psi/faqs-on-psi>> Accessed on

NETO, S. L. M. **Metodologia de Modelagem e Representacao Multivariada dos Padrões Atmosféricos Utilizando Cameras a Partir da Superfície.** Universidade Federal de Santa Catarina, UFSC, Brasil, Florianopolis, SC, 2010.

NGUYEN, D.; KLEISSL, J. Stereographic methods for cloud base height determination using two sky imagers. **Solar Energy**. v.107, p.495-509, 2014.

NICHOL, J. Smoke haze in Southeast Asia: A predictable recurrence. **Atmospheric Environment**. Issue 14–15, v.32, p.2715-2716, 1998.

NIKKEI. **'World's Largest' Floating Solar Plant Operates on Reservoir.** Available at <http://techon.nikkeibp.co.jp/english/NEWS_EN/20131117/316700/?ST=mbe> Accessed on 25/Mar/2014.

NOBRE, A.; MALHOTRA, R.; TANG, C. H.; REISE, C.; KIEFER, K.; RUTHER, R.; REINDL, T. Degradation analysis of photovoltaic systems in a tropical environment. In: 28th European Photovoltaic Solar Energy Conference & Exhibition, 2013. **Conference Proceedings**. Paris, France, 2013.v.p. 3673-3677.

NOBRE, A.; MONTENEGRO, A.; ZHEN, Y.; REINDL, T.; RUTHER, R. On PV module temperatures in tropical regions - a comparison between system locations in Singapore and Brazil. In: IV Brazilian Solar Energy Congress and V ISES Latin America Conference, 2012. **Conference Proceedings**. Sao Paulo, 2012.v.p.

NOBRE, A.; YE, Z.; CHEETAMUN, H.; REINDL, T.; LUTHER, J.; REISE, C. High Performing PV Systems for Tropical Regions - Optimization of Systems Performance. In: 27th European Photovoltaic Solar Energy Conference and Exhibition, 2012. **Conference Proceedings**. Frankfurt, Germany, 2012.v.p.

NOBRE, A. M.; KARTHIK, S.; LIU, H.; YANG, D.; MARTINS, F. R.; PEREIRA, E. B.; RUTHER, R.; REINDL, T.; PETERS, I. M. On the impact of haze on the yield of photovoltaic systems in Singapore. **Renewable Energy**. 2015 (submitted).

NOBRE, A. M.; SEVERIANO_JR., C. A.; KUBIS, M.; KARTHIK, S.; MARTINS, F. R.; RUTHER, R.; REINDL, T. A meteorological sensing network for improved short-term solar irradiance forecasting for PV applications in Singapore. In: 6th World Conference on Photovoltaic Energy Conversion, WCPEC-6 2014, 2014. **Conference Proceedings**. Kyoto, Japan, 2014.v.p.

NOBRE, A. M.; YANG, D.; TAN, A. L.; THOME, E. R.; TAN, J.; TAN, A. P.; BARROT, J. M. O.; ANTONIOLLI, A. F.; RUTHER, R.; REINDL, T. Large-area 2D mapping of systems performance. In: 29th European Photovoltaic Solar Energy Conference & Exhibition, 2014. **Conference Proceedings**. Amsterdam, The Netherlands, 2014.v.p. 2858-2863.

NONNENMACHER, L.; COIMBRA, C. F. M. Streamline-based method for intra-day solar forecasting through remote sensing. **Solar Energy**. Issue 0, v.108, p.447-459, 2014.

NSR. **About NSR**. National Solar Repository of Singapore. Available at <www.solar-repository.sg> Accessed on 12/4/2013.

_____. **Benchmark of PV systems in Singapore.** National Solar Repository of Singapore. Available at <www.solar-repository.sg> Accessed on 15/04/2013.

_____. **PV Systems in Singapore - Pictures.** Available at <<http://www.flickr.com/photos/55797564@N02/>> Accessed on 27/4/2013.

_____. **Installed PV capacity in Singapore: 2008-2012.** National Solar Repository of Singapore (NSR). Available at <www.solar-repository.sg> Accessed on 27/4/2015.

_____. **PV Systems Pictures.** National Solar Repository of Singapore (NSR). Available at <<http://www.solar-repository.sg/pv-systems-pictures>> Accessed on 27/4/2015.

_____. **Singapore photovoltaic market.** Available at <<http://www.solar-repository.sg/singapore-market>> Accessed on

_____. **Singapore PV systems benchmarking.** Available at <<http://www.solar-repository.sg/pv-systems-benchmarking>> Accessed on 15/May/2015.

_____. **Sky cameras.** Available at <<http://www.solar-repository.sg/sky-cameras>> Accessed on

PEDRO, H. T. C.; COIMBRA, C. F. M. Assessment of forecasting techniques for solar power production with no exogenous inputs. **Solar Energy**. Issue 7, v.86, p.2017-2028, 2012.

PEEL, M. C.; FINLAYSON, B. L.; MCMAHON, T. A. Updated world map of the Köppen-Geiger climate classification. **Hydrol. Earth Syst. Sci.** Issue 5, v.11, p.1633-1644, 2007.

PEREIRA, E. B.; MARTINS, F. R.; ABREU, S. L.; COUTO, P.; STUHLMANN, R.; COLLE, S. Effects of burning of biomass on satellite estimations of solar irradiation in Brazil. **Solar Energy**. Issue 1, v.68, p.91-107, 2000.

PEREIRA, E. B.; MARTINS, F. R.; ABREU, S. L.; RUTHER, R. **Atlas Brasileiro de Energia Solar - Brazilian Solar Energy Atlas:** Sao Jose dos Campos, SP, Brazil, 2006.

PEREIRA, E. B.; MARTINS, F. R.; ABREU, S. L. D.; RUTHER, R. **Atlas Brasileiro de Energia Solar**: Sao Jose dos Campos, SP, Brazil, 2006.

PEREZ, R.; INEICHEN, P.; SEALS, R.; MICHALSKY, J.; STEWART, R. Modeling daylight availability and irradiance components from direct and global irradiance. **Solar Energy**. Issue 5, v.44, p.271-289, 1990.

PEREZ, R.; KIVALOV, S.; SCHLEMMER, J.; JR., K. H.; RENNE, D.; HOFF, T. E. Validation of short and medium term operational solar radiation forecasts in the US. **Solar Energy**. Issue 12, v.84, p.2161-2172, 2010.

PEREZ, R.; LORENZ, E.; PELLAND, S.; BEAUHARNOIS, M.; VAN KNOWE, G.; HEMKER JR, K.; HEINEMANN, D.; REMUND, J.; MÜLLER, S. C.; TRAUNMÜLLER, W.; STEINMAUER, G.; POZO, D.; RUIZ-ARIAS, J. A.; LARA-FANEGO, V.; RAMIREZ-SANTIGOSA, L.; GASTON-ROMERO, M.; POMARES, L. M. Comparison of numerical weather prediction solar irradiance forecasts in the US, Canada and Europe. **Solar Energy**. Issue 0, v.94, p.305-326, 2013.

PEREZ, R.; MOORE, K.; WILCOX, S.; RENNE, D.; ZELENKA, A. Forecasting solar radiation - Preliminary evaluation of an approach based upon the national forecast database. **Solar Energy**. Issue 6, v.81, p.809-812, 2007.

PEREZ, R.; SEALS, R.; INEICHEN, P.; STEWART, R.; MENICUCCI, D. A new simplified version of the Perez diffuse irradiance model for tilted surfaces. **Solar Energy**. Issue 3, v.39, p.221-231, 1987.

PEREZ, R.; STEWART, R.; ARBOGAST, C.; SEALS, R.; SCOTT, J. An anisotropic hourly diffuse radiation model for sloping surfaces: Description, performance validation, site dependency evaluation. **Solar Energy**. Issue 6, v.36, p.481-497, 1986.

PIKE. **BIPV and BAPV: market drivers and challenges, technology issues, competitive landscape, and global market forecasts**. N. Consulting, 2012.

PINTO, A. F. D. C. **Qualificação e etiquetagem de inversores para sistemas fotovoltaicos conectados à rede**. Programa de Pós Graduação em Energia, Universidade de São PauloSão Paulo, 2012.

PMO. **A sustainable population for a dynamic Singapore - Population White Paper.** Prime Minister's Office, National Population and Talent Division. Singapore, 2013.

PV-TECH. **Bosch shuts down solar division; total loss amounts to €2.4 billion.** PV-Tech.org. Available at <http://www.pv-tech.org/news/bosch_shuts_down_solar_division_total_loss_amounts_to_2.4_billion> Accessed on 22/3/2013.

_____. **QA Solar launches second phase of 1GW Pakistan project.** Available at <http://www.pv-tech.org/news/qa_solar_launches_second_phase_of_1gw_pakistan_project> Accessed on

PV*SOL. **PV*SOL - software for photovoltaics.** The Solar Design Company. Available at <<http://www.solardesign.co.uk/pv.php>> Accessed on 1/5/2013.

PV_MAGAZINE. **First Solar raises bar for CdTe with 21.5% efficiency record.** Available at <http://www.pv-magazine.com/news/details/beitrag/first-solar-raises-bar-for-cdte-with-21.5-efficiency-record_100018069/#axzz3cfZZzID0> Accessed on 31/03/2015.

PVSYST. **PVsyst - Photovoltaic Software.** Available at <<http://www.pvsyst.com/en/>> Accessed on 1/5/2013.

QUAH, E. Transboundary Pollution in Southeast Asia: The Indonesian Fires. **World Development.** Issue 3, v.30, p.429-441, 2002.

REICH, N. H.; MUELLER, B.; ARMBRUSTER, A.; VAN SARK, W. G. J. H. M.; KIEFER, K.; REISE, C. Performance ratio revisited: is PR > 90% realistic? **Progress in Photovoltaics: Research and Applications.** Issue 6, v.20, p.717-726, 2012.

RENEWABLES_INTERNATIONAL. **Germany meets 75% of the domestic electricity demand with renewables.** Available at <<http://www.renewablesinternational.net/germany-meets-75-of-the-domestic-electricity-demand-with-renewables/150/407/81057/>> Accessed on 18/Mar/2015.

REUTERS. **Solar energy enjoys a glowing outlook.** Available at <<http://blogs.reuters.com/data-dive/2015/05/04/solar-energy-enjoys-a-growing-tailwind/>> Accessed on 1/Jun/15.

ROBERT, A.; KUMMERT, M. Designing net-zero energy buildings for the future climate, not for the past. **Building and Environment**. Issue 0, v.55, p.150-158, 2012.

ROSS, R. Interface design considerations for terrestrial solar cell modules. In: 12th IEEE Photovoltaic Specialists Conference, 1976. **Conference Proceedings**. Baton Rouge, LA, USA, 1976.v.p. 801-806.

ROTTMAN, G. The SORCE Mission. **Solar Physics**. Issue 1-2, v.230, p.7-25, 2005.

RÜTHER, R. **Edifícios Solares Fotovoltaicos**:. Florianopolis, SC, Brazil, 2004.

RÜTHER, R.; KLEISS, G.; REICHE, K. Spectral effects on amorphous silicon solar module fill factors. **Solar Energy Materials and Solar Cells**. Issue 3, v.71, p.375-385, 2002.

RÜTHER, R.; KNOB, P. J.; JARDIM, C. D. S.; REBECHI, S. H. Potential of building integrated photovoltaic solar energy generators in assisting daytime peaking feeders in urban areas in Brazil. **Energy Conversion and Management**. Issue 5, v.49, p.1074-1079, 2008.

RÜTHER, R.; LIVINGSTONE, J. Seasonal variations in amorphous silicon solar module outputs and thin film characteristics. **Solar Energy Materials and Solar Cells**. Issue 1, v.36, p.29-43, 1995.

RÜTHER, R.; NASCIMENTO, L.; JUNIOR, J. U.; PFITSCHER, P.; VIANA, T. Long-term performance of the first grid-connected, building integrated amorphous silicon PV installation in Brazil. In: 35th IEEE Photovoltaic Specialists Conference, 2010a. **Conference Proceedings**. Honolulu, HI, USA, 2010a.v.p.

_____. Performance assessment of a microcrystalline Si PV installation in a warm climate. In: 35th IEEE Photovoltaic Specialists Conference, 2010b. **Conference Proceedings**. Honolulu, HI, USA, 2010b.v.p.

RÜTHER, R.; ZILLES, R. Making the case for grid-connected photovoltaics in Brazil. **Energy Policy**. Issue 3, v.39, p.1027-1030, 2011.

SASTRY, N. Forest Fires, Air Pollution and Mortality in Southeast Asia. **Demography**. Issue 1, v.39, p.1-23, 2002.

Singapore Department of Statistics. **Population and Population Structure**. 2013.

SDS. **Population Trends 2014**. S. D. O. Statistics. Singapore, 2014.

SERIS. **SERIS Meteorological Station - Annual Report 2011**. Singapore 2011.

SHARMA, V.; YANG, D.; WALSH, W. M.; REINDL, T. A mixed wavelet neural network based short term solar irradiance forecasting for the tropics. **IEEE Transactions on Smart Grid**. v.In press, 2015 (in press).

SHELL. **New Lens Scenarios - A shift in perspective for a world in transition**. Royal Dutch Shell plc, 2013.

SMA. **Performance of Photovoltaics (PV) in Germany**. Available at <<http://www.sma.de/en/company/pv-electricity-produced-in-germany.html>> Accessed on 27/4/2013.

_____. **SUNNY TRIPOWER 10000TL / 12000TL / 15000TL / 17000TL**. SMA. Available at <<http://www.sma.de/en/products/solar-inverter-without-transformer/sunny-tripower-10000tl-12000tl-15000tl-17000tl.html#Technical-Data-9513>> Accessed on 27/4/2013.

_____. **Performance of Photovoltaics (PV) in Germany**. SMA. Available at <<http://www.sma.de/en/company/pv-electricity-produced-in-germany.html>> Accessed on 12/6/2015.

_____. **Sunny Tripower 60**. Available at <<http://www.sma.de/en/products/solarinverters/sunny-tripower-60.html#Downloads-109590>> Accessed on 14/Jul/2015.

SOLARBUZZ. **Retail Price Environment - Module Pricing**. Solarbuzz - Solar Market Research and Analysis. Available at <<http://www.solarbuzz.com/facts-and-figures/retail-price-environment/module-prices>> Accessed on 1/5/2013.

_____. **Understanding Solar Energy Systems - Technologies**. Solarbuzz - Solar Market Research and Analysis. Available at

<<http://www.solarbuzz.com/going-solar/understanding/technologies>>

Accessed on 1/5/2013.

SOLARGIS. Global Horizontal Irradiation - South and Southeast Asia: GeoModel Solar s.r.o 2012.

SOLMETRIC. SunEye tool from Solmetric. Available at

<<http://www.solmetric.com/>> Accessed on 27/4/2013.

SPB. Primeiro sistema solar fotovoltaico residencial conectado a rede da CEMIG em MG. Solar Power Brazil. Available at

<<http://solarpowerbrazil.com.br/geracao-de-energia/>> Accessed on 27/12/2012.

SPE. Global Market Outlook for Solar Power - 2015-2019. S. Europe, 2015.

STETZ, T.; KRAICZY, M.; DIWOLD, K.; BRAUN, M.; BLETTERIE, B.; MAYR, C.; BRÜNDLINGER, R.; NOONE, B.; BRUCE, A.; MACGILL, I.; MATHER, B.; OGIMOTO, K.; WASHIHARA, K.; UEDA, Y.; IARIA, A.; GATTI, A.; CIRIO, D.; REKINGER, M.; THEOLOGITIS, I. T.; BRABANDERE, K. D.; TSELEPIS, S.; BUCHER, C.; WANG, Y. High Penetration PV in Local Distribution Grids - Outcomes of the IEA PVPS Task 14 Subtask 2. In: 29th European Photovoltaic Solar Energy Conference and Exhibition, 2014. **Conference Proceedings**. Amsterdam, The Netherlands, 2014.v.p. 2176 - 2183.

STETZ, T.; VON APPEN, J.; NIEDERMEYER, F.; SCHEIBNER, G.; SIKORA, R.; BRAUN, M. Twilight of the Grids: The Impact of Distributed Solar on Germany's Energy Transition. **Power and Energy Magazine, IEEE**. Issue 2, v.13, p.50-61, 2015.

STRAITS_TIMES. Brighter days for solar panel sales. Straits Times. Singapore 2012.

TECHXPLORE. Japan has floating solar power plants in Hyogo Prefecture. Available at <<http://techxplore.com/news/2015-04-japan-solar-power-hyogo-prefecture.html>> Accessed on

TEMPS, R. C.; COULSON, K. L. Solar radiation incident upon slopes of different orientations. **Solar Energy**. Issue 2, v.19, p.179-184, 1977.

TEO, C. W. **Johor bears brunt of smoky air**. The Straits Times. Singapore 2013.

TODAY. Pilot projects using water sites to generate solar power launched. Available at <<http://www.todayonline.com/singapore/pilot-projects-using-water-sites-generate-solar-power-launched>> Accessed on 22/Nov/2014.

TRAPANI, K.; REDÓN SANTAFÉ, M. A review of floating photovoltaic installations: 2007–2013. **Progress in Photovoltaics: Research and Applications**. Issue 4, v.23, p.524-532, 2015.

UEDA, Y. Summary of lessons learned from Pal-town - Ota city PV demonstration project. In: IEA PVPS Workshop, 2010. **Conference Proceedings**. Valencia, Spain, 2010.v.p.

URQUHART, B.; KURTZ, B.; DAHLIN, E.; GHONIMA, M.; SHIELDS, J. E.; KLEISSL, J. Development of a sky imaging system for short-term solar power forecasting. **Atmos. Meas. Tech.** Issue 2, v.8, p.875-890, 2015.

VBEW. **Bayerische Windkraft und Photovoltaik legte auch in 2014 zu**. Verband der Bayerischen Energie- und Wasserwirtschaft e.V. (VBEW). Available at <http://www.vbew.de/index.php?id=518&tx_ttnews%5Btt_news%5D=201&cHash=2e344bea7ac8b9fde2d6cdfc08465ae9> Accessed on 31/May/2015.

VELASCO, E.; ROTH, M. Review of Singapore's air quality and greenhouse gas emissions: Current situation and opportunities. **Journal of the Air & Waste Management Association**. Issue 6, v.62, p.625-641, 2012.

VELDHUIS, A. J.; NOBRE, A.; REINDL, T.; RUTHER, R.; REINDERS, A. H. M. E. The influence of wind on the temperature of PV modules in tropical environments, evaluated on an hourly basis. In: Photovoltaic Specialists Conference (PVSC), 2013 IEEE 39th, 2013. **Conference Proceedings**., 2013.v.p. 0824-0829.

VELDHUIS, A. J.; NOBRE, A. M.; PETERS, I. M.; REINDL, T.; RUTHER, R.; REINDERS, A. H. M. E. An Empirical Model for Rack-Mounted PV Module Temperatures for Southeast Asian Locations Evaluated for Minute Time Scales. **Photovoltaics, IEEE Journal of**. Issue 3, v.5, p.774-782, 2015.

WALL_STREET_JOURNAL. **Yingli Green Loss Widens in First Quarter**. Available at <<http://www.wsj.com/articles/yingli-green-loss-widens-in-first-quarter-1433507260>> Accessed on 11/6/2015.

WEST, S. R.; ROWE, D.; SAYEEF, S.; BERRY, A. Short-term irradiance forecasting using skycams: Motivation and development. **Solar Energy**. v.110, p.188-207, 2014.

WILCOX, S.; MARION, W. **Users Manual for TMY3 Data Sets**. N. R. E. Laboratory, 2008.

WITTKOPF, S.; VALLIAPPAN, S.; LIU, L.; ANG, K. S.; CHENG, S. C. J. Analytical performance monitoring of a 142.5 kWp grid-connected rooftop BIPV system in Singapore. **Renewable Energy**. Issue 0, v.47, p.9-20, 2012.

WOYTE, A.; RICHTER, M.; MOSER, D.; REICH, N.; GREEN, M.; MAU, S.; BEYER, H. G. **Analytical Monitoring of Grid-connected Photovoltaic Systems: Good Practices for Monitoring and Performance Analysis**. I. E. Agency, 2014.

YANG, D.; DONG, Z.; NOBRE, A.; KHOO, Y. S.; JIRUTITIJAROEN, P.; WALSH, W. M. Evaluation of transposition and decomposition models for converting global solar irradiance from tilted surface to horizontal in tropical regions. **Solar Energy**. Issue 0, v.97, p.369-387, 2013.

YANG, D.; DONG, Z.; REINDL, T.; JIRUTITIJAROEN, P.; WALSH, W. M. Solar irradiance forecasting using spatio-temporal empirical kriging and vector autoregressive models with parameter shrinkage. **Solar Energy**. Issue 0, v.103, p.550-562, 2014.

YANG, D.; JIRUTITIJAROEN, P.; WALSH, W. M. Hourly solar irradiance time series forecasting using cloud cover index. **Solar Energy**. Issue 12, v.86, p.3531-3543, 2012.

YANG, D.; SHARMA, V.; YE, Z.; LIM, L. I.; ZHAO, L.; ARYAPUTERA, A. W. Forecasting of global horizontal irradiance by exponential smoothing, using decompositions. **Energy**. Issue 0, v.81, p.111-119, 2015.

YANG, D.; WALSH, W. M.; DONG, Z.; JIRUTITIJAROEN, P.; REINDL, T. G. Block Matching Algorithms: Their Applications and Limitations in

Solar Irradiance Forecasting. **Energy Procedia**. Issue 0, v.33, p.335-342, 2013.

YANG, D.; WALSH, W. M.; JIRUTITIJAROEN, P. Estimation and Applications of Clear Sky Global Horizontal Irradiance at the Equator. **Journal of Solar Energy Engineering**. Issue 3, v.136, p.034505-034505, 2014.

YANG, D.; YE, Z.; LIM, L. H. I.; DONG, Z. Very short term irradiance forecasting using the lasso. **Solar Energy**. Issue 0, v.114, p.314-326, 2015.

YANG, D.; YE, Z.; NOBRE, A. M.; DU, H.; WALSH, W. M.; LIM, L. I.; REINDL, T. Bidirectional irradiance transposition based on the Perez model. **Solar Energy**. Issue 0, v.110, p.768-780, 2014.

YANG, H.; KURTZ, B.; NGUYEN, D.; URQUHART, B.; CHOW, C. W.; GHONIMA, M.; KLEISSL, J. Solar irradiance forecasting using a ground-based sky imager developed at UC San Diego. **Solar Energy**. Issue 0, v.103, p.502-524, 2014.

YE, J.; REINDL, T.; ABERLE, A. G.; WALSH, T. M. Effect of solar spectrum on the performance of various thin-film PV module technologies in tropical Singapore. **IEEE Journal of Photovoltaics**. Issue 99, v.PP, p.1-7, 2014a.

_____. Performance Degradation of Various PV Module Technologies in Tropical Singapore. **Photovoltaics, IEEE Journal of**. Issue 5, v.4, p.1288-1294, 2014b.

YE, Z.; NOBRE, A.; REINDL, T.; LUTHER, J.; REISE, C. On PV module temperatures in tropical regions. **Solar Energy**. Issue 0, v.88, p.80-87, 2013.

ZAGOURAS, A.; PEDRO, H. T. C.; COIMBRA, C. F. M. On the role of lagged exogenous variables and spatio-temporal correlations in improving the accuracy of solar forecasting methods. **Renewable Energy**. Issue 0, v.78, p.203-218, 2015.

ZENGKUN, F. **Plans in place if haze worsens**. The Straits Times. Singapore 2013a.

_____. **S'pore calls on Jakarta to tackle haze**. The Straits Times. Singapore 2013b.

ZOMER, C.; COSTA, M.; NOBRE, A.; RUTHER, R. Performance compromises of building-integrated and building-applied photovoltaics (BIPV and BAPV) in Brazilian airports. **Energy & Buildings (submitted)**. 2013.

ZOMER, C.; NOBRE, A.; CASSATELLA, P.; REINDL, T.; RÜTHER, R. The balance between aesthetics and performance in building-integrated photovoltaics in the tropics. **Progress in Photovoltaics: Research and Applications**. Issue 7, v.22, p.744-756, 2014.